Connections between the Mass Balance, Ice Dynamics and Hypsometry of White Glacier, Axel Heiberg Island, Nunavut

Laura Irene Thomson

A thesis submitted to the
Faculty of Graduate and Postdoctoral Studies
in partial fulfillment of the requirements
for the Doctorate in Philosophy in Geography

Department of Geography, Environment and Geomatics
Faculty of Arts
University of Ottawa

© Laura Thomson, Ottawa, Canada, 2016

ABSTRACT

This thesis investigates how changing climate conditions have impacted the mass balance, dynamics and associated hypsometry (area-elevation distribution) of White Glacier, an alpine glacier on Axel Heiberg Island, Nunavut.

The first article describes the production of a new map of White Glacier from which changes in ice thickness and glacier hypsometry could be determined. A new digital elevation model (DEM) was created using >400 oblique air photos and Structure from Motion, a method built upon photogrammetry but with the advantage of automated image correlation analysis. The result of this work demonstrates that the method is able to overcome the challenges of optical remote sensing in snow-covered areas. The resulting DEM and orthoimage facilitated the production of a map with 5 m vertical accuracy in the style of earlier cartographic works.

The new map supported the calculation of the glacier's geodetic mass balance and provides an updated glacier hypsometry, which improves the accuracy of mass balance calculations. A modeled glacier hypsometry time-series was created to support a reanalysis of the mass balance record over the period 1960-2014, which through comparison of the geodetic and glaciological methods enables the detection of potential sources of error in the glaciological method. Comparison of the two approaches reveals that within the error margin no significant difference exists between the average annual glaciological mass balance (-213 ± 28 mm w.e. a^{-1}) and geodetic mass balance (-178 ± 16 mm w.e. a^{-1}).

To determine how ice dynamics have responded to ice thinning and negative mass balances, dual-frequency GPS observations of ice motion were compared to historic velocity measurements collected at three cross-sectional profiles along the glacier. Comparisons of annual and seasonal velocities indicate velocity decreases of 10–45% since the 1960s. However, increased summer velocities at the highest station suggests that increased delivery of surface meltwater to the glacier bed has initiated basal sliding at elevations that did not experience high levels of melt in earlier decades. Modeled balance fluxes demonstrate that observed fluxes, both historically and currently, are unsustainable under current climate conditions.

I don't know anything,

but I do know that everything is interesting

if you go into it deeply enough.

- Dr. Richard Feynman (1918-1988)

TABLE OF CONTENTS

LIST OF FIGURES

LIST OF TABLES

ACKNOWLEDGEMENTS

This thesis has been possible through the guidance, encouragement, and support of many mentors, friends, relatives, and organizations. First, I would like to thank my supervisor Dr. Luke Copland for his guidance through my studies, for the countless opportunities and experiences I have had as a student in the LCR, and for providing me with the freedom, independence, and encouragement to pursue a project very close to my heart. I also would like to acknowledge my thesis committee, Drs. Denis Lacelle, Michael Sawada, and David Burgess for their advice and support though my studies. Thank you to the Department of Geography, Environment, and Geomatics, which has been my academic home at University of Ottawa these past few years.

I gratefully acknowledge my co-authors on the second article (Chapter 3). I will be forever thankful for the opportunity to work with Dr. Michael Zemp at the World Glacier Monitoring Service and for the chance to connect with many of the kindred spirits who have worked in the Expedition Fiord Area of Axel Heiberg Island (including Drs. Juerg Alean, Atsumu Ohmura, Heinz Blatter, Koni Steffan, Martin Funk, and Gordon Young). I would specifically like to thank Dr. Graham Cogley for his assistance with, and insights into, the White Glacier mass balance record and for his thorough and comprehensive documentation of the studies at White Glacier during the Trent years. Additionally, I thank Wayne Pollard for his efforts toward making the McGill Arctic Research Station the modern basecamp it is today, which makes our fieldwork possible. A great big thanks go to Abby Dalton, Mike Hackett, Dorota Medrzycka, and Adrienne White who have helped me carry heavy things for long distances in the field, and for making that task more enjoyable with laughter, music, and memorable conversations. To the rest of the LCR lab, it has been a pleasure getting to know each of you, and I wish you all the best in your future endeavours.

To Miles Ecclestone, this thesis would not have been possible without your guidance on White Glacier and your lessons on life and glacier stewardship. To Christopher Omelon, your support in the field and beyond inspires me to continue on this Arctic journey for years to come. Finally, to my dear family and friends, both far and near, your love and support through this adventure has kept me smiling and laughing (often at myself); thank you. *Piqsiq*, we did it!

This project has resulted from the generous support of several agencies and organizations including: the Association of Canadian Universities for Northern Studies; the Garfield Weston Foundation; the Natural Sciences and Engineering Research Council of Canada Canadian Graduate Scholarship; the Ontario Graduate Scholarship; Esri Canada; the International Arctic Science Committee – Network on Arctic Glaciology; the International Association of Cryospheric Sciences – Cryosphere Working Group; Stability and Variations of Arctic Land Ice (SVALI) - Nordic Centre of Excellence; Glacio-Ex Norwegian/Canadian/American Partnership Program; the World Glacier Monitoring Service; ArcticNet; the University Centre in Svalbard; the Northern Scientific Training Program; Canadian Polar Commission - Polar Continental Shelf Program; the Canada Foundation for Innovation; the Ontario Research Fund; the Natural Sciences and Engineering Research Council of Canada Discovery Grant; the Faculty of Graduate and Post-Doctoral Studies (University of Ottawa); the Department of Geography, Environment and Geomatics (University of Ottawa); and the University of Ottawa.

CHAPTER 1: INTRODUCTION

1.1 BACKGROUND AND MOTIVATION

Excluding the ice sheets and their peripheral ice masses, the glaciers and ice caps of Canada, Russia, and Svalbard contain 39% of the global land ice area and are reported to have an average mass budget of -76 ± 14 Gt a^{-1} between 2003-2009 [*Gardner et al.*, 2013]. Compared to all glaciated areas outside of the ice sheets, the Canadian Arctic Archipelago (CAA) has been the largest recent contributor to global sea level rise and of these Arctic regions it holds the greatest capacity to contribute to future sea level rise. This region is generally characterized by continental conditions with low levels of accumulation (<500 mm w.e. a^{-1}). Glacier surface mass balance, defined as the annual difference of mass gained by the accumulation of snow and mass lost by the ablation of ice, is primarily controlled by summer temperatures that show significantly higher interannual variability than winter accumulation [*Braithwaite*, 2005; *Koerner*, 2005]. In recent decades the negative mass balance trend of glaciers in the CAA has accelerated [*Sharp et al.*, 2011] and estimates derived from the Gravity Recovery and Climate Experiment (GRACE) indicate that glaciers of the Queen Elizabeth Islands continue to lose mass at an accelerating rate with the 2003-2013 average being -38 ± 2 Gt a^{-1} [*Harig and Simons*, 2016].

This negative mass balance trend is linked to Arctic Amplification, the observed augmented warming of the Arctic compared to the Northern hemisphere mean [*AMAP*, 2011]. This phenomenon is caused by a positive feedback that is primarily driven by the loss of high albedo surface features such as sea ice and snow cover, leading to a subsequent rise in ocean and surface temperatures [*Screen and Simmonds*, 2010]. For glaciers in the CAA, increasingly warmer summer surface air temperatures are highly correlated (explaining >90% of the variance) with increasingly negative mass balances [*Gardner and Sharp*, 2007]. Increased melt rates at the summit of several Canadian ice caps, inferred from an increase in the melt fraction of ice cores [*Fisher et al.*, 2012], indicates that warming in the Canadian Arctic is occurring at both high and low elevations. While an increase in evaporation from the Arctic Ocean and a heightened capacity of a warmer lower troposphere to hold water vapour will likely lead to an increase in precipitation, as observed by a 10% increase at Eureka weather station over the period 1954-2007 [*Lesins et al.*, 2010], there has

yet to be a significant trend in precipitation levels across the Arctic [*AMAP*, 2011]. Moreover, modeled mass balance sensitivities for the CAA show that despite a predicted increase in accumulation with temperature (18.5 mm $^{\circ}C^{-1}$), this potential gain is more than offset by the significantly greater increase in ablation as a result of rising temperatures (-119 mm $^{\circ}C^{-1}$) [*Oerlemans et al.*, 2005].

The physical response of a glacier to a new mass balance regime may not manifest itself as simply an advance or retreat of the terminus. Changing mass balance can also invoke changes in ice thickness, the surface gradient, and the nature of mass transfer from the accumulation area to the ablation area, which together modify glacier hypsometry (the distribution of area with elevation). The variation in this response of glaciers to changes in climate is a function of both: 1) static characteristics linked to local topography including the range of elevations, surface gradients, conditions at the glacier bed, and distribution of accumulation and ablation regions; and 2) dynamic processes including changing glacier geometry (size and hypsometry) and mass turnover rates [*Furbish and Andrews*, 1984]. The feedback cycle depicted in Figure 1.1 illustrates that mass balance and ice dynamics together play a role in modifying glacier hypsometry, and subsequently that glacier hypsometry dictates future mass balance conditions for a glacier. Mass balance controls on hypsometry comprise elevation gain due to snowfall in the accumulation area, and elevation loss due to surface melt in the ablation area. In an idealized case with stable climate conditions, the transfer of mass (flux) from the accumulation area to the ablation area by ice motion will compensate for these changes in elevation (via the continuity equation; *Cuffey and Paterson* [2010]).

With a stepwise change in climate the glacier geometry should be expected to adjust, by the mechanisms of ice motion, to a new state that is stable (in balance) in the new climate regime [*Cuffey and Paterson*, 2010; *Elsberg et al.*, 2001; *Harrison et al.*, 2009]. The dynamics of ice motion are, however, controlled by many internal and external factors that may lead to mass transfers that exceed, or fail to meet, the mass flux required for a stable response of the glacier to changes in climate. For example, on multi-decadal timescales changes in mass balance can invoke changes in ice thickness and the surface gradient that together factor into the force balance equation that explains the driving force behind ice motion. Conversely, short-term (hourly-daily) fluctuations in ice motion are closely linked with the meteorologically controlled input of surface melt water, the conditions at the glacier bed, the structure of the subglacial hydrological system

and the efficiency at which water leaves the system [*Bartholomaus et al.*, 2008; *Bingham et al.*, 2006; *Cuffey and Paterson*, 2010; *Sundal et al.*, 2011]. These long- and short-term processes can lead to ice fluxes that exceed the balance flux and, as a result, ice will be conveyed to lower elevations at a rate that is unsustainable in the present climate. This augmented mass transfer will cause the accumulation area to descend into lower elevations with increasingly negative mass balance regimes. The future stability of a glacier is therefore determined by the nature of the glacier response to changes in climate [*Harrison et al.*, 2009]. Examples of recently observed unstable glacier response to climate warming are Yakutat and Brady glaciers in southeast Alaska, where significant ice thinning at higher elevations has ultimately removed the accumulation areas of these glaciers and resulted in unsustainable hypsometries for glacier mass balance [*Harrison et al.*, 2009].

While previous studies have used energy balance models to predict future mass balance conditions [*Lenaerts et al.*, 2013; *Oerlemans et al.*, 2005], the stability of the physical response of Arctic mountain glaciers to accelerating climate warming has yet to be investigated. Recent climate and mass balance modeling results predict an irreversible mass loss for glaciers in the Canadian Arctic under future climate projections [*Lenaerts et al.*, 2013]. However, if these glaciers assume new hypsometries that are stable in the contemporary climate, the findings of *Lenaerts et al.* [2013] do not necessarily imply that these glaciers are destined to disappear. This distinction is important to note because while the projected warming would force Arctic glaciers into high elevation basins following significant volume losses, the persistence of small ice masses throughout the year would hold important implications for sustained streamflow in these watersheds through the summer months and for the riparian ecosystems that depend of them. The future of Arctic glaciers therefore depends on their ability to dynamically adjust their geometries to elevations and extents that are sustainable under projected climate conditions.

Since early mapping campaigns in the CAA during the 1950s and 1960s, the response of glacier and ice cap geometry to the decreasing mass balance trend has been one of retreat and varying degrees of thinning, particularly on small stagnating glaciers and ice caps [*Braun et al.*, 2004a; *Papasodoro et al.*, 2015; *Thomson et al.*, 2011]. Thinning due to ablation is known as downwasting, whereas dynamic thinning occurs as a result of a positive flux divergence, where more ice flows out of a given region than flows in [*Cogley et al.*, 2011b]. Thinning can also occur in the accumulation area as a result of changes to the amount and form of precipitation [*Screen*

and Simmonds, 2012], as well as the rate of snow densification [*Morris and Wingham*, 2011]. Processes of thinning that cause glaciers to assume a hypsometry with more area at lower elevations will likely initiate a positive feedback as more of the glacier area is lowered into negative mass balance conditions (Figure 1.1). By understanding the relative contribution to changes in glacier geometry from each of these processes, it may be possible to improve predictions of the future response of Arctic mountain glaciers.

1.2 FOCUS AND OBJECTIVES

This thesis investigates how climate conditions over the past half-century have impacted the response of White Glacier, an alpine glacier on Axel Heiberg Island in the Canadian High Arctic. White Glacier is currently the only mountain glacier (i.e., not an ice cap or outlet glacier) in the CAA with *in situ* measurements of mass balance and ice dynamics spanning multiple decades. While mountain glaciers generally comprise a minority of glacier-covered area in the CAA (e.g. 26% on Axel Heiberg Island), they demonstrate a greater sensitivity to climate warming both in terms of area change and mass balance [*Dowdeswell et al.*, 1997; *Paul*, 2004; *Thomson et al.*, 2011]. Therefore, this study of White Glacier's mass balance and dynamics serves as an indicator of how glaciers in the alpine environment are responding to Arctic amplification in the CAA. Using historic datasets dating back to 1960, this work presents a multi-decadal assessment of mass balance, dynamics, and hypsometry of the glacier through comparison of early and contemporary glaciological datasets including large-scale maps, a 56-year mass balance record, englacial temperature measurements, local climate observations, and measurements of seasonal and annual ice velocities from 1960–1970 and 2012–2016.

The first objective of this thesis is to produce an updated map of White Glacier from which changes in ice thickness and glacier hypsometry can be determined. Using >400 oblique aerial photographs collected in July 2014, a new digital elevation model (DEM) was created using Structure from Motion techniques, a method built upon traditional photogrammetry but with the advantage of automated image correlation analysis. The result of this work demonstrates that the Structure from Motion method is able to overcome the challenges of optical remote sensing in low-contrast, snow-covered areas due to the high resolution of the photographs and their subsequent detection of small features at the surface. The resulting DEM and orthoimage

facilitated the production of a new 1:10,000 topographic map with 5 m vertical accuracy in the style of earlier cartographic works of White Glacier dating back to 1960.

The second objective is to assess how changing glacier geometry (hypsometry and extent) impacts the calculation of glacier mass balance. The impact of glacier thinning and glacier retreat have contrasting impacts on the calculation of glacier mass balance; the former promotes increasingly negative mass balance as more mass is exposed to warmer temperatures at lower elevations, whereas the latter results in the removal of the portion of the glacier where the most extreme loss is experienced, resulting a less negative mass balance overall. The new map created in the first part of the thesis enabled calculation of the glacier's geodetic mass balance (mass change determined from ice volume change) and provides an updated glacier hypsometry that improves the accuracy of contemporary mass balance calculations. A modeled glacier hypsometry time series was created to support a reanalysis of the mass balance record [*Zemp et al.*, 2013], which through comparison of the geodetic and glaciological methods enabled the estimation of generic differences (i.e. discrepancies between total and surface mass balance) and potential sources of error in the glaciological method.

The third objective of this thesis is to provide a determination of how ice dynamics have responded to a trend of ice thinning and increasingly negative mass balance conditions at White Glacier. To address this objective, dual-frequency GPS (dGPS) stations were installed at the centre of three cross-sectional profiles to continuously monitor ice motion from 2012–2016. These sites were the focus of previous surface velocity measurements from 1960–1970 [*Iken*, 1974; *Müller and Iken*, 1973]. Post-processing of the dGPS data following the approach of the earlier observations, which enables comparison of annual, winter and summer velocities at each of the three stations. Modeling of expected glacier velocities using theoretical balance velocities and Glen's flow law are used to assess the relative roles of mass balance and hypsometry changes (i.e. ice thinning) in the observed changes in glacier velocity.

1.3 STUDY LOCATION AND REGIONAL CLIMATE

White Glacier (79.4º N, 90.6º W) is a 14 km long mountain glacier extending from approximately 100 to 1800 m a.s.l. in the region of Expedition Fiord on western Axel Heiberg Island in the Queen Elizabeth Islands of the Canadian High Arctic (Figure 1.2). The glacier has a

5 km wide accumulation area and flows southeast into a narrow 0.8-1.1 km wide valley. Over the period of observation (1960–2015), the average equilibrium line altitude was 1075 m a.s.l. and the mean accumulation area ratio (accumulation area divided by the total area) was 0.55. The glacier area in 1960 was 41.07 km^2, which decreased to 38.54 km^2 by 2014 [*Thomson and Copland*, 2016]. White Glacier terminates at a junction with Thompson Glacier, a major outlet glacier of the Müller Ice Cap.

The glaciers on Axel Heiberg Island, numbering 1108 in 1960 [*Ommanney, 1969*], range from large outlet glaciers (>100 km^2) to small mountain and niche-type ice masses observed to have decreased in area by 50-80% between 1960 and 2000 [*Thomson et al.*, 2011]. The two major ice caps on the island are the Müller Ice Cap, located 50 km northeast of Expedition Fiord (maximum elevation 2210 m a.s.l. at Outlook Peak) and the Steacie Ice Cap on the southern half of the island, approximately 70 km south of White Glacier. The Müller Ice Cap was named in honour of Dr. Fritz Müller of McGill University who initiated the glacier monitoring activities in the Expedition Fiord regions, and who founded the McGill Arctic Research Station as part of the Jacobsen-McGill Arctic Research Expedition 1959-1962.

The region experiences mean annual temperatures of approximately –20°C and annual precipitation ranging from 58 mm a^{-1} at sea level (as measured at Eureka, 125 km to the northeast) to 370 mm a^{-1} at 2120 m a.s.l. as measured in a 41-year snowpit record of annual accumulation on the Müller Ice Cap [*Cogley et al.*, 1996]. There are no continuous measurements of local climate conditions in the Expedition Fiord region, although several early studies based at the McGill Arctic Research Station include periodic climate data (e.g. *Andrews*, 1964; *Havens et al.*, 1965). A significant amount of climate data is also available in *Ohmura* [1981], which presents the first detailed energy balance model of the high-arctic that accounts for the interactions between glaciers, tundra, and sea ice [*Cogley et al.*, 1996].

The closest weather stations with near-continuous climate data are the Eureka Weather Station, located approximately 125 km to the northeast on Ellesmere Island, and Isachsen station situated 275 km to the southwest on Ellef Ringnes Island. An analysis of the long-term climate record at Eureka (1954-2007) by Lesins et al. [2010] shows that mean annual surface temperatures have risen there by 3.2°C since 1972 and that the most significant warming has occurred during the winter months. A 10% increase in total annual precipitation, predominantly during the spring, summer and autumn months, was also observed over the period of record. Figure 1.3 presents the

mean annual air temperature and precipitation data for Eureka and Isachsen, acquired from Environment Canada's Historical Climate Data pages: www.climate.weather.gc.ca/historical_data

From these records, a period of cooling temperatures in the 1970s is apparent at both stations, which may correlate with increasing precipitation at the Isachsen station. Since the 1970s, the Eureka temperature data follow the warming trend indicated by Lesins et al. [2010]. A warming trend also appears likely in the Isachsen record given contemporary measurements, despite a gap in the data between 1978 and 2003. Given these observations at stations to the east and west of Axel Heiberg Island, it is likely that the region of Expedition Fiord has experienced similar warming since the 1970s and that this warming explains the increasingly negative mass balance conditions observed in recent decades (Figure 3.2). While an increase in precipitation has occurred at Eureka, mass balance records show no apparent increase in accumulation rates on White Glacier over the period of record (1960-2015). This is potentially related to the difference in elevation between the Eureka observing station (~10 m a.s.l.) and the accumulation area of White Glacier (~1200-1800 m a.s.l.), as well as distance from moisture sources such as the Arctic Ocean.

1.4 THESIS FORMAT

The thesis follows a manuscript-style format in which three articles are developed. An introductory chapter (Chapter 1) synthesizes the scientific literature that has motivated this work and presents the thesis objectives. Chapters 2-4 (the articles) open with an attestation statement indicating the individual contributions of coauthors and the current status of the article in the publication process. A certain degree of repetition is present between the three papers in the sections concerning previous studies and description of the study site. At the end of each chapter the associated tables and figures are provided. Chapter 5 presents the combined findings of these articles. It highlights overall implications for the stability of the response of White Glacier under the current climate and places these findings in the context of other studies relating to glacier mass balance and ice dynamics. The references for all chapters are provided together in Chapter 6.

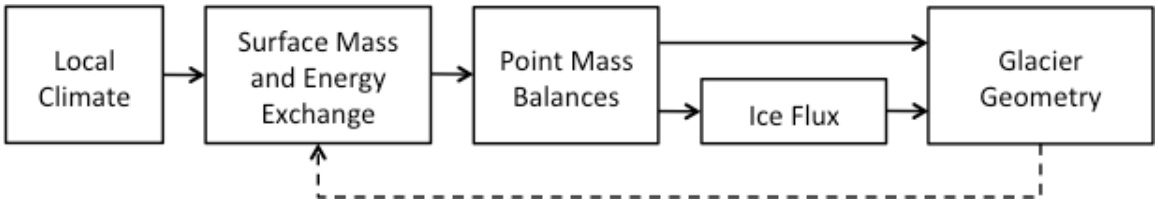

Figure 1.1. Processes and forcings leading to the evolution of glacier geometry. The dashed line indicates the feedback of glacier geometry into the future distribution of mass (via snowfall) and energy (causing melt) at the surface. Adapted from Cuffey and Paterson, 2010, p.93.

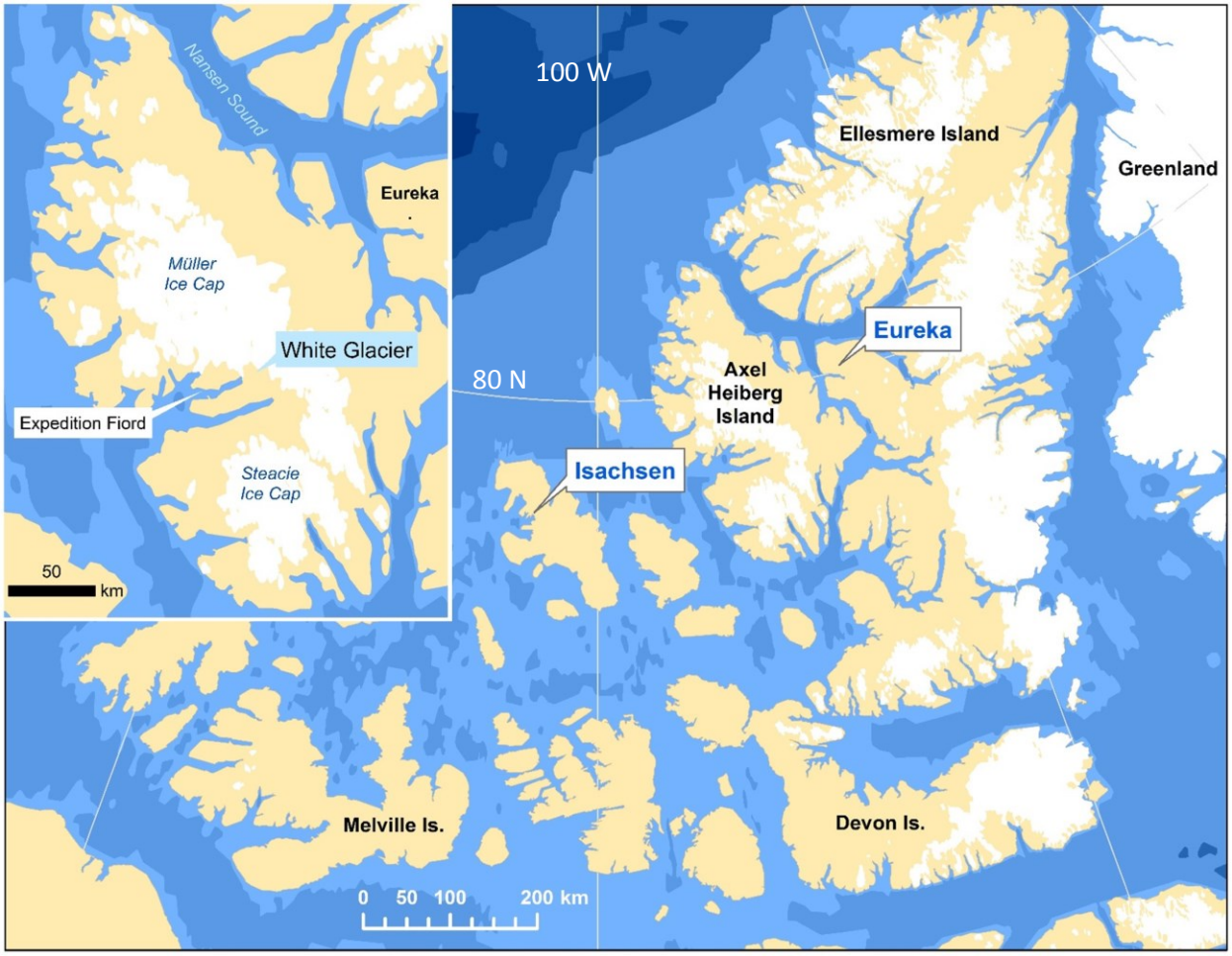

Figure 1.2. Regional map of the Queen Elizabeth Islands, including the locations of the Eureka and Isachsen weather stations, respectively 125 km northeast and 275 km southwest of Expedition Fiord on Axel Heiberg Island (shown in the inset map).

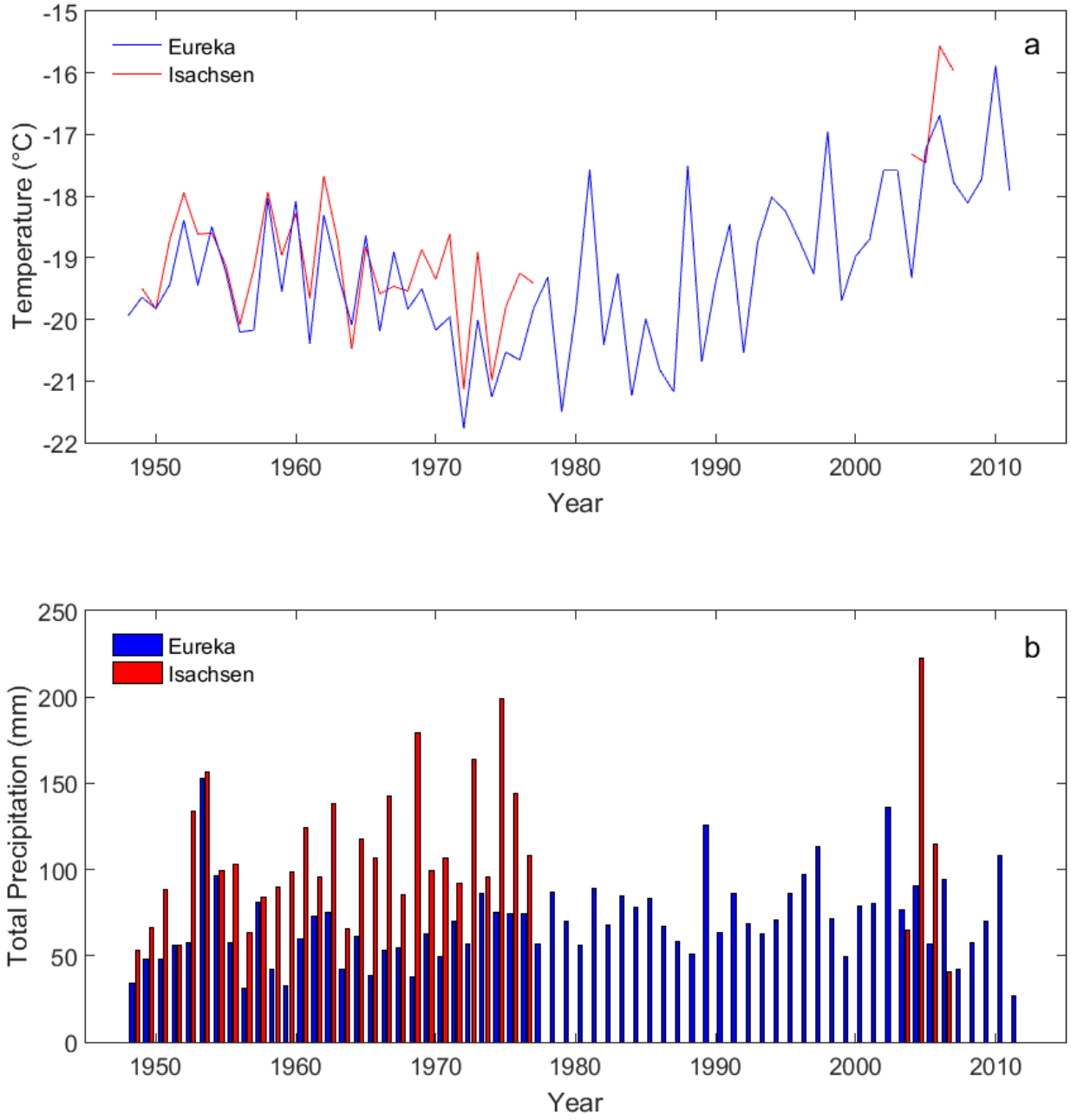

Figure 1.3. Mean annual air temperature (°C) and total annual precipitation (mm) for the Eureka and Isachsen Environment Canada weather stations.

CHAPTER 2: GLACIER MAPPING USING STRUCTURE FROM MOTION

2.1 ARTICLE 1 SUMMARY AND ATTESTATION

We use Structure from Motion software to generate a new digital elevation model (DEM) of White Glacier, Axel Heiberg Island, Nunavut, using >400 oblique aerial photographs collected in July 2014. Spatially and radiometrically high-resolution imagery, optimized camera settings, low angle lighting conditions, and image post-processing methods together supported the detection of small but distinct features on the surface of the snowpack and enabled feature matching during the image correlation process. The resulting DEM and orthoimage facilitated the production of a new 1:10,000 topographic map with 5 m vertical accuracy in the style of earlier cartographic works of White Glacier dating back to 1960. The new map of White Glacier will support calculation of the glacier's geodetic mass balance (mass change determined from ice volume change over the past 54 years) and provides an updated glacier hypsometry (area-elevation distribution) that will improve the accuracy of future mass balance calculations.

Laura Thomson and Luke Copland, respectively, co-authored an article entitled "White Glacier 2014, Axel Heiberg Island, Nunavut: mapped using Structure from Motion methods" based on this chapter. Laura Thomson was responsible for the data collection, post-processing, topographic model building, map development, and initial authorship of this article. Luke Copland, along with three reviewers from the Journal of Maps, provided helpful revisions that have resulted in the following publication:

Thomson, L. and Copland, L. 2016. White Glacier 2014, Axel Heiberg Island, Nunavut: mapped using Structure from Motion methods. Journal of Maps. doi: 10.1080/17445647.2015.1124057.

2.2 INTRODUCTION

White Glacier (79.45° N, 90.67° W, Figure 2.1) on Axel Heiberg Island, Nunavut, has been the subject of glaciological studies in Canada's north since 1959 and today hosts the longest mass balance record for an alpine glacier in the Canadian Arctic (55 years). It is one of 37 official reference glaciers within the Global Terrestrial Network for Glaciers through the United Nations Framework Convention on Climate Change. These observations, submitted annually to the World

Glacier Monitoring Service (e.g. *WGMS* [2013] and previous issues), are used with others to calculate a worldwide glacier mass balance index, which is regularly published in climate change assessment reports [*WGMS*, 2008]. Since the onset of the mass balance programme, yearly measurements of snow accumulation and ice melt have been extrapolated across the White Glacier basin at its 1960 hypsometry and extent to calculate annual mass balance, save for an update to the hypsometry below 400 m a.s.l. in 2003 [*Hember et al.*, 2003]. By producing a new map of the White Glacier basin and updating the hypsometry we can (1) improve the accuracy of future mass balance measurements and (2) reanalyze the historic record of observations using modelled estimates of hypsometry as it changed from 1960 to present [*Zemp et al.*, 2013]. A new map will also enable the calculation of geodetic mass balance, which is derived from ice volume change. This independent measure of mass change will allow us to assess quality of the historic mass balance record based on the consistency, or discrepancy, between the two methods.

Airborne and ground-based surveying and mapping were important in the foundation and development of glaciological work at White Glacier. Early aerial photograph surveys by the Royal Canadian Air Force in the summer of 1960 enabled the photogrammetric production of a series of six topographic maps of the Expedition Fiord area on Axel Heiberg Island. The esthetic quality and cartographic caliber of the Expedition Fiord map series, including the 1:10,000 scale map of White Glacier by *Haumann and Honegger* [1964], pictured in Figure 2.2, are considered unprecedented in the Canadian Arctic for their era or indeed any time since [*McKortel*, 1963; *Wheate et al.*, 2001]. Recently, digital versions of these six maps have been made available through the World Glacier Monitoring Service map database "Fluctuation of Glaciers Maps" (http://www.wgms.ch/fog_maps.html), along with supporting texts describing the cartographic and photogrammetric methods of *Haumann* [1961], *Haumann* [1963], *Blachut* [1961], and *Blachut* [1963] used during these campaigns. Later surveys of ice elevations, conducted in 1969-1970 by *Arnold* [1981] to determine ablation rates and ice emergence velocities and in 2002-2003 by *Hember et al.* [2003] to determine the volume change of White Glacier below 400 m a.s.l., were restricted to the lower 4 km of the White Glacier terminus.

Now more than fifty years since the foundation of glaciological studies on Axel Heiberg Island, we present a new topographic map of White Glacier based on 2014 oblique aerial photography. The topographic model for this map was produced using Agisoft's PhotoScan (version 1.1.0) Structure from Motion software (SfM), which uses the principles of classical

photogrammetry and takes advantage of computer automated image correlation analysis [*Jebara et al.*, 1999]. In recognition of the merit of the first 1:10,000 scale map of White Glacier by *Haumann and Honegger* [1964] we have strived to mimic the design features and quality of the original in our own map, while accepting the fundamental differences between hand-drawn and digital cartographic methods.

2.3 METHODS

2.3.1 AERIAL PHOTOGRAPH SURVEY AND IMAGE POST-PROCESSING

A Canon EOS 6D digital SLR camera equipped with an EF 24-105mm f4 L IS USM lens (set to a fixed focal length of 24 mm) was used to collect >500 oblique photographs of White Glacier from the open window of a Bell 206L helicopter on July 10, 2014. At an average flying height of 1645 m above sea level (a.s.l.) (~5400 ft.), and a maximum altitude of 1990 m a.s.l. (~6525 ft.) over the accumulation area, the camera achieved ground resolutions ranging from 0.05 to 0.52 m based on photographs with a resolution of 3648 x 5472 pixels (20 Megapixels). An automatic intervalometer programmed to capture images every 3 seconds enabled 80% image overlap along-track and 60% across-track at an average flying speed of ~150 km hr^{-1}, as recommended in AgiSoft PhotoScan (hereafter, PhotoScan) User Manual and by Dr. Matt Nolan (personal communication, 2014).

At the start of the survey, a reconnaissance flight was conducted over the Crusoe Glacier accumulation area (Figure 2.3a) to adjust the camera to settings that could detect features from the brightest part of the image (i.e., snow under direct sunshine). On the camera screen we were able to view the image exposure and RGB histograms on test photographs; through trial and error we found that camera settings of F-stop=F/10, ISO=100 and a fixed shutter speed of 1/2500 allowed for maximum contrast and detection of snow features across the accumulation area. These features included ripple marks (Figure 2.3b) and sastrugi, which were enhanced by high-elevation surface melt and low angle lighting, as well as small slush avalanches and meltwater streams originating near nunataks. The low exposure camera settings resulted in good definition in the accumulation area at the expense of under exposure in other locations, particularly in shadowed areas in the western tributary basins of White Glacier. However, the 14-bit radiometric resolution of the Canon EOS 6D enables over 16,000 tones to be uniquely identified, which supported the detection of

subtle features in both snow-covered and shadowed regions. Using Canon Digital Photo Professional (version 3.12.51.2) photo editing software, the image brightness was increased by 30%, maintaining definition in the accumulation area while enhancing contrast in the shadowed regions of the glacier (Figure 2.3c). Batch post-processing was applied to ensure continuity in lighting throughout the photo series.

2.3.2 Model Building

The Structure from Motion approach used by PhotoScan differs from traditional digital photogrammetry in that the image correlation analysis is used not only to derive three-dimensional structure from measureable feature offsets between images (i.e. parallax), but also to infer the camera position and calibration parameters of each photograph. This reduces the processing time required and enables projects to involve hundreds of photographs. Construction of a topographic model in PhotoScan is a multi-step process, as illustrated in Figure 2.4. Several iterations of model building for White Glacier were run before the final results were achieved; here, we describe the parameter settings and method used to produce the final product.

With the reference projection defined as NAD27, the post-processed photographs were imported into PhotoScan and inspected for image coverage and quality, resulting in 473 photographs that were used to build the final model. Manually delineated image masks were applied to the photos to exclude features such as clouds and distant terrain outside the White Glacier basin that would interfere with photo alignment. In PhotoScan, photo alignment refers to the process in which a user-defined number of tie-points, detected by correlation analysis between two photos, and camera orientation and positions are determined in 3D space using a bundle adjustment (PhotoScan User Manual). The resulting 3D point cloud calculated for a pair of images is referred to as a depth map, and PhotoScan amalgamates these depth maps to produce sparse point cloud for the entire 3D structure to be modelled (PhotoScan User Manual). The most intensive and iterative phase of model building was adjusting and improving the photo alignment by the manual addition and removal of tie points and ground control points (discussed in Section 2.4) and the deletion of erroneous points with high reprojection errors. In PhotoScan, reprojection error is a measure of localization accuracy in pixels. The standard assumption is that an "*average reprojection error higher than 0.8 pix indicates quite inaccurate solution. Whereas reprojection error less than 0.5 is almost perfect*" (Agisoft Technical Support). The final sparse point cloud

produced for White Glacier was reduced from over 3 million to approximately 2.5 million points, resulting in a final average reprojection error of 0.55 pixels.

With the derived camera positions resulting from the photo alignment (Figure 2.5a), a dense 3D point cloud was generated from depth maps created for each image pair, this time with the maximum number of tie points possible. The dense point cloud contained >200 million points over an area of approximately 100 km^2 (>2 points per m^2). An internal tool within PhotoScan ("Classify Ground Points") was used to iteratively identify and filter out anomalous points that exceeded a 10 m radius and 45° inclination within a 100 m cell. These parameters were determined by trial and error and allowed for the preservation of topographic features while removing erroneous points resulting from image correlation mismatches.

From the filtered dense point cloud, a 3D model was reconstructed using the Build Mesh function with the maximum number of model faces possible (>31 million) and interpolation of model voids enabled. Finally a textured surface model, based on the Build Texture function, was produced using the average value of the pixels from individual photographs upon each model face. Figure 2.6 illustrates the intermediate and final products of PhotoScan model building near the White Glacier icefall, which features both ice and rock surfaces with varying degrees of complexity and slope.

2.3.3 Ground Control and Marker Errors

Ground control points (GCPs), referred to as "Markers" in PhotoScan, were selected from prominent features identifiable in both the 1960 White Glacier map and 2014 photographs. Fifteen GCPs and 38 tie points, amounting to 53 Markers, were used in the final photo alignment for the White Glacier basin following the iterative phase of Photo Alignment in PhotoScan (Figure 2.5b). The number of Marker projections (i.e. number of photographs where each Marker was manually identified) ranged from 4 to 95, with more than 50% of markers being detected in over 40 photographs.

Marker errors, defined as the discrepancy between defined and modeled GCP positions, ranged from 6.5 m to 45.1 m (combined horizontal and vertical error), with an average error of 23.9 m. Marker errors increased for GCPs with high numbers of projections selected from photographs showing the target at distances exceeding 3-4 km, which resulted in the target feature

being at a compromised resolution. However, we believed it to be important to incorporate as many projections as possible for each GCP to ensure continuity in the model.

2.3.4 Model Results

We found that the SfM model construction generally performed well across the White Glacier basin, and surprisingly so across the accumulation area. The combination of low exposure settings, high spatial and radiometric-resolution photography, low angle lighting, and the onset of summer surface melt generally resulted in successful feature matching and model construction throughout the snow-covered regions.

Erroneous sections of the model were found to be associated primarily with failures in survey design and photo coverage, rather than issues with the model building process. For example, two basins in the northeastern accumulation area of the glacier returned "pitted" results, i.e., regions of elevations significantly below (up to 100 m) the actual surface. In this case, image coverage of these basins was compromised by the eclipsing effect of ridges in the foreground of the oblique photographs. In another example, we found that along the western margin of the glacier trunk the model had difficulty transitioning smoothly from illuminated to shadowed lighting conditions, resulting in an artificial terrace in this region. Significant efforts were made to remedy this issue, including (1) adjusting the brightness and contrast parameters, (2) the inclusion of tie points, and (3) adjusting the selection parameters for ground points, but these proved to be ineffective. These two cases exemplify the most extreme and extensive model errors, yet together they comprise only 3% of the mapped basin area. Smaller isolated instances of "pitting" on the scale of 50-400 m in length appear primarily in the accumulation area, and in some cases appear to be associated with variable cloud coverage between photographs. Our approach to managing these issues is addressed in Section 2.4.2, which describes contour construction and design.

The resulting 3D model and textured surface were exported as a DEM and orthophoto, respectively. The default model export cell size provided by Agisoft was 0.769 m, but we chose to export the DEM at a resolution of 5 m to reduce the impact of small-scale noise and variability on contour construction. The orthophoto was exported at a resolution of 1 m to facilitate the detailed mapping of small-scale features such as supraglacial streams and crevasses.

2.4 MAP CONSTRUCTION AND DESIGN

The White Glacier 2014 1:10,000 map (Appendix 1) was produced entirely in Esri's ArcMap 10.1 from a combination of manually digitized features as well as data products generated by a variety of ArcMap tools. In this section we describe the steps taken to produce the map and the accuracy of the final product. We have endeavored to mirror the original 1960 map by *Haumann* [1961] in terms of both style and structure while updating the extent, hypsometry, and surface features of White Glacier.

2.4.1 Coordinate system and layout

The final data products (DEM and orthophoto) from PhotoScan were produced and exported to ArcMap with NAD27 geographic coordinates and reprojected into the local planar coordinate system used by *Haumann and Honegger* [1964]. This system follows a Mercator projection with a central meridian of 269.2571944° E and latitude of origin of 79.4100306° N and respective false easting and northing values of 3000 m and 60000 m. The map is oriented to geographic north with a grid overlay divided into 1 km intervals. The extent of the final map extends from 25000 m E, 61000 m N in the southwest, to 32780 m E, 75000 m N in the northeast (-90.987° E, 79.419° N; -90.605° E, 79.544° N). An interesting feature of the original map that we have maintained is the overflow of the northwestern-most basin of White Glacier 1.5 km beyond the western boundary of the neatline. We also chose to reproduce the two identical scale bars presented on the 1960 map, presumably because the original map was produced in two sheets that were divided latitudinally at 69000 m N.

2.4.2 Contours

The Contour tool in ArcMap's Spatial Analysis toolbox was used to create 10 m contours from the imported PhotoScan DEM (raw contours shown in Figure 2.7a). These contours were then clipped to the contour extent of the 1960 map and smoothed using a PAEK (Polynomial Approximation with Exponential Kernel) filter with a 25 m threshold, which will interpolate along line paths of 25 m length (Figure 2.7b). Next, regions of model errors (i.e. voids) were identified and the erroneous contours produced in these regions were extracted using the Clip tool. We

manually interpolated across these voids and in some cases used the contours of the 1960 map as a visual guide for the topographic structure of the area (Figure 2.7c). The final contours were coloured according to land classification (rock=brown or ice=blue) with 100 m contours being represented with thicker line weights. Formlines, represented as dashed contour lines, indicate the areas where contours were interpolated across voids.

2.4.3 Relief Shading

At the time of production, select maps in the 1960 Expedition Fiord map series were considered novel in North America for their inclusion of both relief shading and rock drawings [*McKortel*, 1963]. Today, relief shading (also known as hill shading) is a common feature of topographic maps known to aid and accelerate map interpretation [*Castner and Wheate*, 1979]. Using the Hillshade tool in ArcMap's Spatial Analysis toolbox, we produced separate relief shading products for rock and ice regions using an aspect of 280° and angle of 50°, which together achieved illumination and shading effects similar to those on the White Glacier 1960 map.

2.4.4 Glacial and proglacial features

Elements of the glacier surface and forefield were manually digitized in ArcMap as either polygon (p) or line (l) features. These include proglacial and supraglacial streams (l), crevasses (p), transverse and longitudinal ice structures (e.g. faults) (l), surface debris (p), and moraine materials (p). At this phase of map production, the fundamental differences between hand- and digitally-produced cartography were obvious. Whereas the *Haumann and Honegger* [1964] map illustrated in great detail examples of rock-fall and debris cover, with individual rocks and boulders being depicted, we instead resorted to coarse and generic representations of surface debris and moraine material, accepting the futility of manually outlining such transitory small scale features. Similar to the earlier map, we were unable to confidently represent the topography of particularly steep cliffs on the western margin of the glacier trunk and have therefore purposefully left these regions as blank voids labeled "Rock Wall". However, the PhotoScan model did perform well in the eastern "Rock Wall" region depicted in the 1960 map and we are therefore able to present the topography of that area for the first time. For historical context, we have also included a simple

representation of the extent of the glacier terminus in 1960, as shown in the *Haumann and Honegger* [1964] map.

2.4.5 Survey cairns, spot elevations, and reference prisms

Ground surveys which provided ground control for the 1960 photogrammetry project made use of signal plates and a network of cairns, many of which were created in pairs to form survey baselines (e.g. I.C.B.N. and I.C.B.S., which we assume to signify Ice Cave Baseline North and South). We have chosen to include these reference points, as well as spot elevations, from the *Haumann and Honegger* [1964] map in our own, making it clear in the legend that these points are accurate as of their year of survey, 1960. It should be noted that the elevations of the 1960 spot elevations on the ice surface will have changed as a result of ice thinning or, in the case of Signal cairns W.G.F.4 and W.G.F.5, by the advance of Thompson Glacier into the White Glacier Forefield (W.G.F.) from the east. Several of the signal cairns that remain were resurveyed using a dual-frequency GPS (dGPS) system between 2011 and 2014. We include the point elevations of these contemporary surveys with a separate symbology. In all cases, our dGPS measurements of off-ice markers returned elevations within 1 m of those reported in *Haumann and Honegger* [1964], attesting to the high precision of the early work by the Swiss and Canadian surveyors on Axel Heiberg Island. We have added three new spot elevations at the sites of permanent reference prisms installed for our own total station surveys (R1-R3) and two spot elevations at historic markers we found that post-date the *Haumann and Honegger* [1964] map, including a meteorological station on the White Glacier Outwash Plain 'W.G.O.P.' used by Atsumu Ohmura in 1969 [*Ohmura*, 1981].

2.4.6 Map accuracy

As recommended by Agisoft, the standard rule of thumb for determining DEM accuracy from ground sampling distance (GSD) is 2x GSD in the horizontal and 4x in the vertical. Therefore, our GSD of 0.38 m (average ground resolution as calculated by PhotoScan) returns a horizontal accuracy of 0.76 m and vertical accuracy of 1.52 m. However, we believe this to be overly optimistic and more likely a reflection of DEM precision, not accuracy. The reported marker errors of the PhotoScan DEM product, which reflect the discrepancy between user defined and modeled

GCPs, indicate average horizontal errors in longitude and latitude of 14.1 m and 16.3 m, respectively, and an average elevation error of 10.5 m. These values, on the other hand, are subject to the unknown errors associated with the local plane coordinate system, which is poorly defined [*Cogley and Jung-Rothenhäusler*, 2002], thereby introducing further errors in the geolocation of the model.

The majority of ground control validation in the model was acquired from off-ice survey points and peaks with established elevations during the 1960 ground surveys. However, for the purposes of future glaciological studies, including comparison of historic and contemporary surfaces to determine glacier volume change, it is important to have on-ice validation of glacier surface elevations. We used a dGPS profile collected by snow-mobile in the spring of 2014 as on-ice validation for the 2014 DEM. Comparison of 286 point elevations acquired along the dGPS track with the 2014 SfM DEM (Figure 2.8 a-b) show that, on average, the DEM is 1.30 m lower than the dGPS elevations and exhibits a normal distribution (Figure 2.8 c). Scatter plots comparing the elevation discrepancies suggest that the 2014 DEM tends to overestimate elevation at lower elevations near the terminus and at higher elevations in the accumulation area (Figure 2.8 d-e). One possible explanation for this pattern is that the dGPS measurements were collected during the spring months (prior to the onset of summer 2014 melt) and would therefore reflect pre-melt elevations at the terminus, and pre-summer lowering of the accumulated winter snow (densification driven by melt and refreezing in the snowpack). It is also possible that there is a warping of the model near the model edges at the glacier terminus and upper accumulation area, however it is difficult to know how this effect might be introduced or quantified.

Ultimately, map accuracy can be considered as "the degree of conformity with a standard" [*Thompson*, 1988]. To determine how well our DEM conforms to our standard, the *Haumann and Honegger* [1964] map, we used the universal co-registration method developed by *Nuth and Kääb* [2011] and found that the standard deviation of elevation differences over stable terrain between our DEM and the 1960 map was 5.08 m following horizontal shifts on the order of 10-15 m. The necessity for these shifts is likely associated with the uncertainty in the estimated parameters of the local plane coordinate system and not inaccuracies in the DEM, considering the low reprojection error of 0.55 pixels that we were able to achieve in PhotoScan. With these considerations, we believe a reasonable generalization for the accuracy of the map to be 10 m vertically and 5 m horizontally.

2.5 CONCLUSIONS

Through the use of SfM photogrammetry methods applied to >400 oblique air photos, we have produced a DEM and orthoimage that together provide the foundation for a new 1:10,000 topographic map of White Glacier. Image correlation over the snow-covered areas of the glacier was possible due to the low-exposure camera settings, favorable lighting conditions, and melt season survey that enabled the detection of small-scale snow-surface features. Challenges faced in the process, which resulted in some localized model errors, were largely associated with flight survey design and uncertainties in the local plane coordinate system. Provided the opportunity to apply this technique in the future, nadir-oriented photography acquired from a greater flying height would resolve the issue of eclipsed regions, and map accuracy could be improved by the placement of more photo-identifiable GCPs. The co-registration technique developed by *Nuth and Kääb* [2011] provides an important tool in overcoming the coordinate system uncertainties of the *Haumann and Honegger* [1964] map as we move forward in calculating the volume change of White Glacier between 1960 and 2014 in future studies.

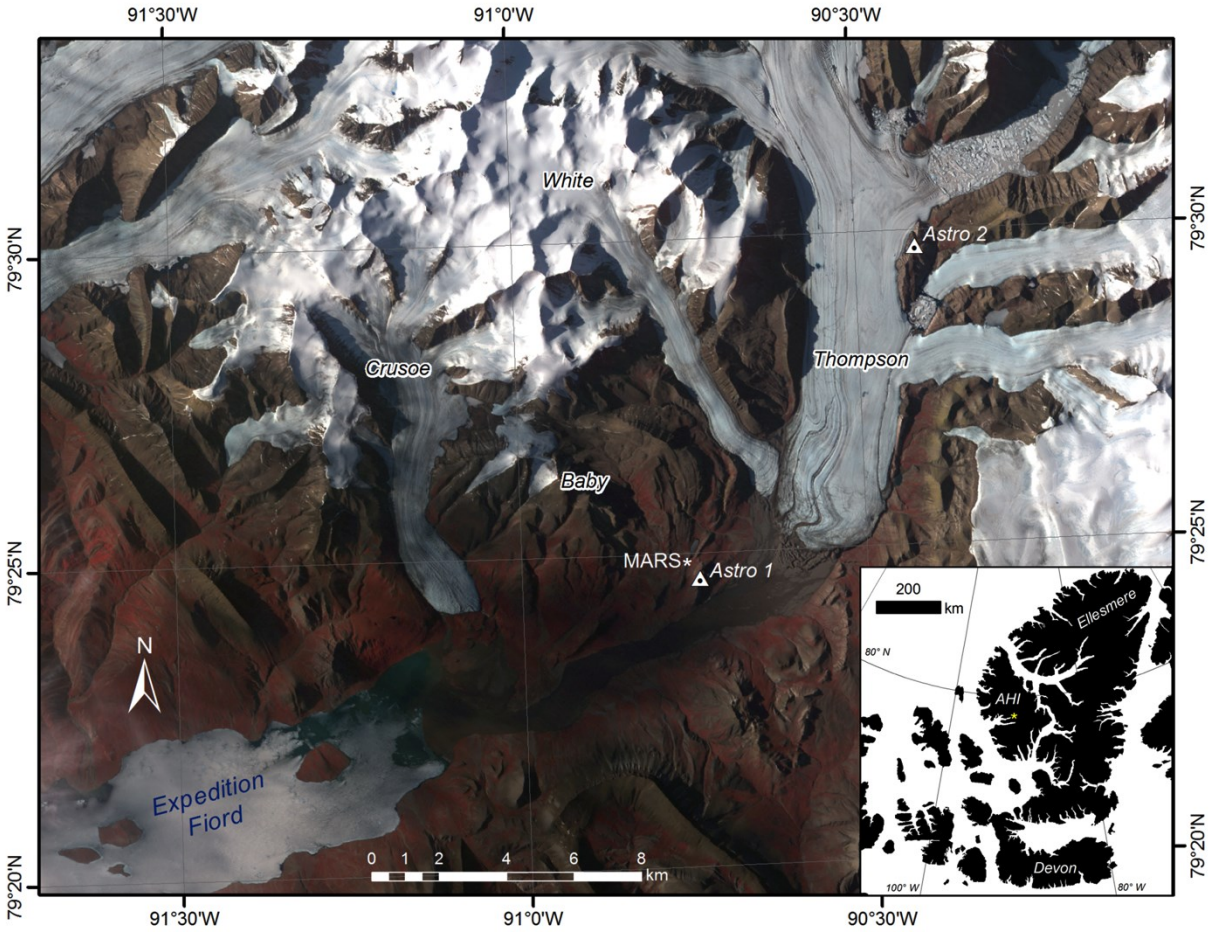

Figure 2.1: Location of White, Crusoe, Thompson, and Baby glaciers in the region of Expedition Fiord, Axel Heiberg Island (AHI). Survey baseline points Astro 1 and Astro 2 are indicated, as is the location of the McGill Arctic Research Station (MARS). Background image: ASTER L1B composite, July 5, 2010.

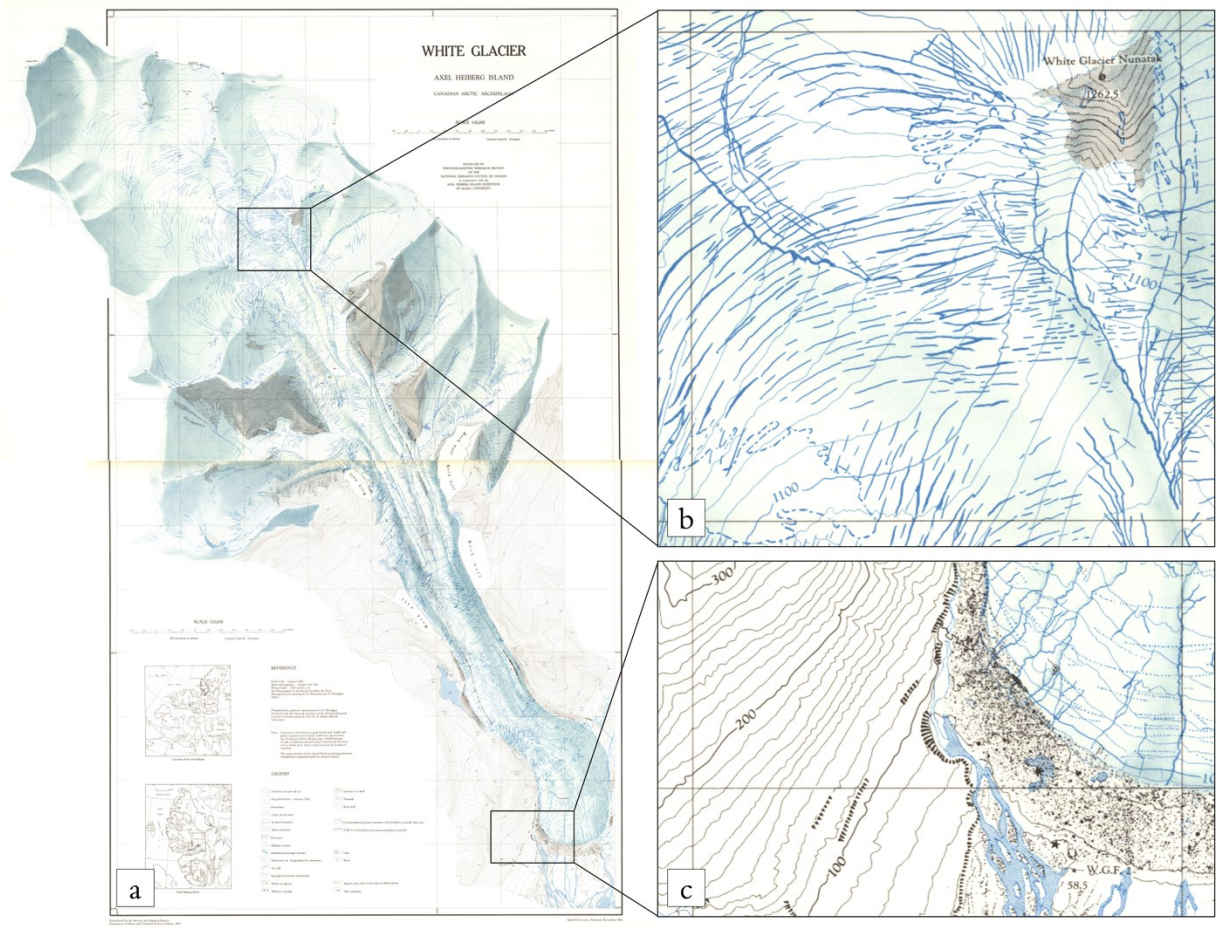

Figure 2.2: (a) Overview of White Glacier 1:10,000 [*Haumann and Honegger*, 1964], mapped in 1960 from ground surveys and photogrammetric techniques with examples of (b) detailed glacial features including supraglacial streams, crevasses, and the perennial snowline, and (c) the glacier terminus showing fault lines, proglacial streams and ponds, moraine and surface debris material, and survey cairns. Grid dimensions are 1 km x 1 km.

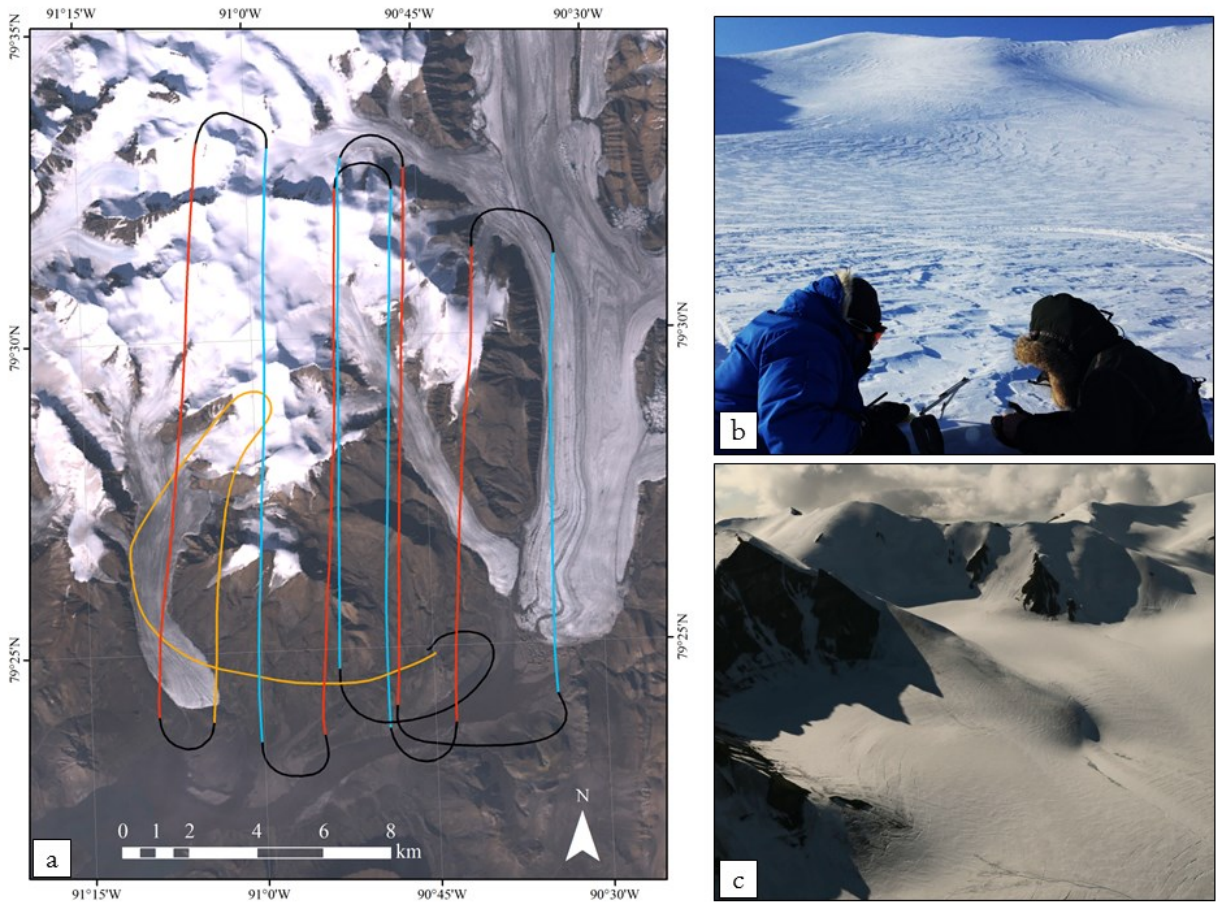

Figure 2.3: (a) Survey path on July 10, 2014, illustrating northbound flights in red, southbound flights in blue, and reconnaissance flight indicated in orange. (b) Example of sastrugi present in the accumulation of White Glacier with field team conducting snow pit analysis in foreground. (c) Provides an example survey photo demonstrating the detail and contrast possible from the accumulation area in both snow covered and shadowed regions.

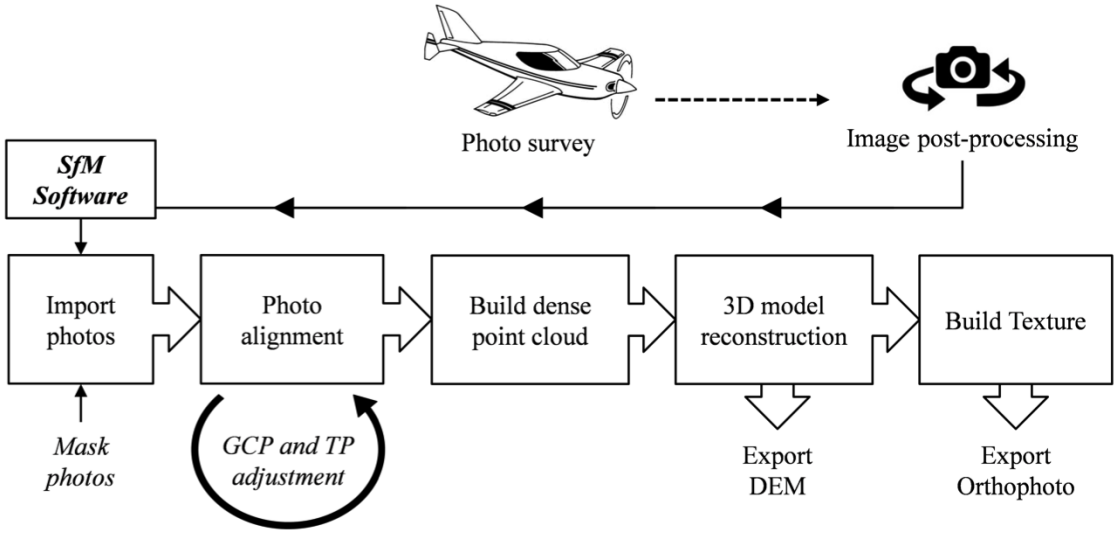

Figure 2.4: Workflow for the White Glacier model construction using Agisoft PhotoScan Structure from Motion Software.

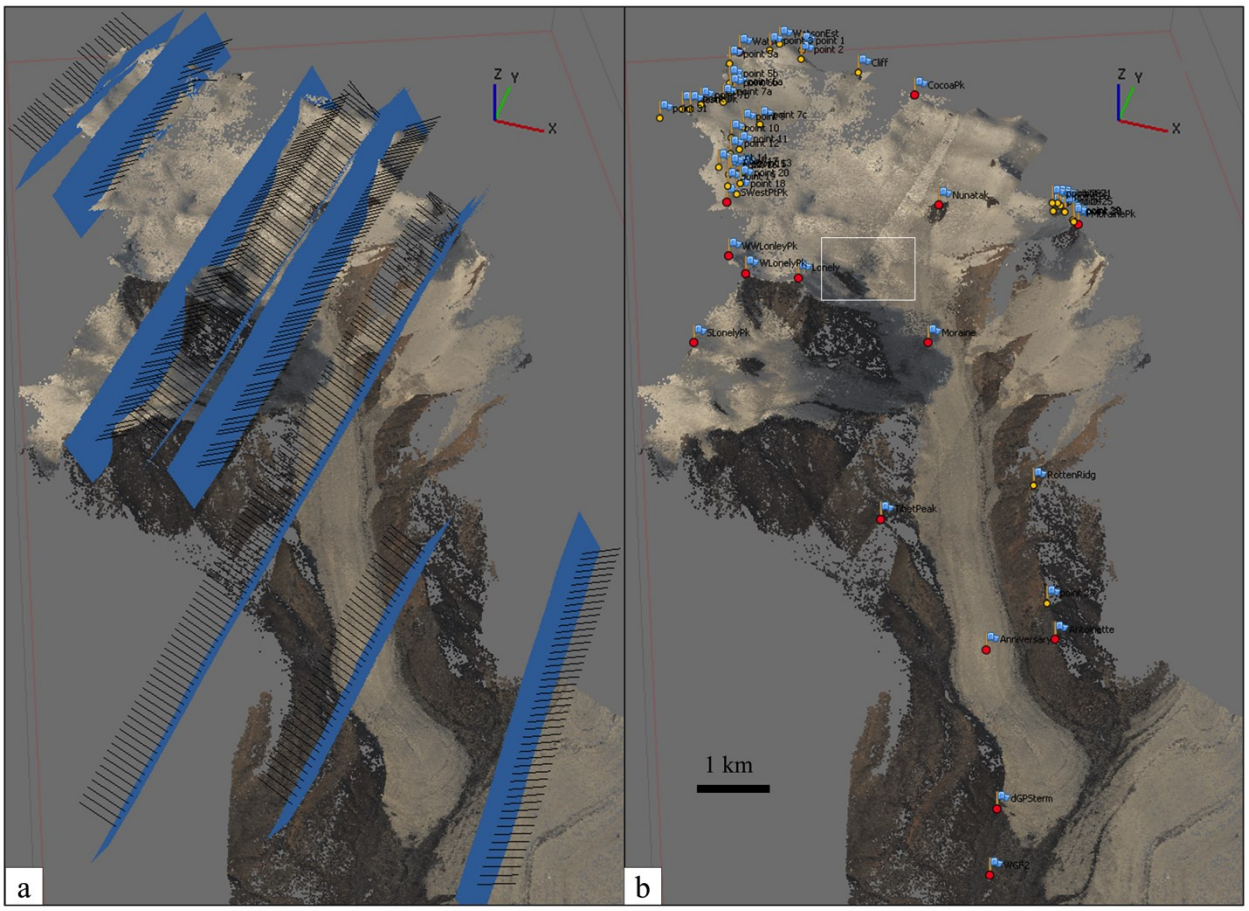

Figure 2.5: (a) Camera positions derived from the Photo Alignment bundle adjustment phase in Agisoft PhotoScan. Black lines indicate camera pointing direction and blue represents the camera faces. The Y-axis indicates geographic north. (b) Markers used to aid in Photo Alignment with red Markers indicating GCPs and yellow markers indicating TPs. The white box indicates the location of the White Glacier icefall shown in Figure 2.6.

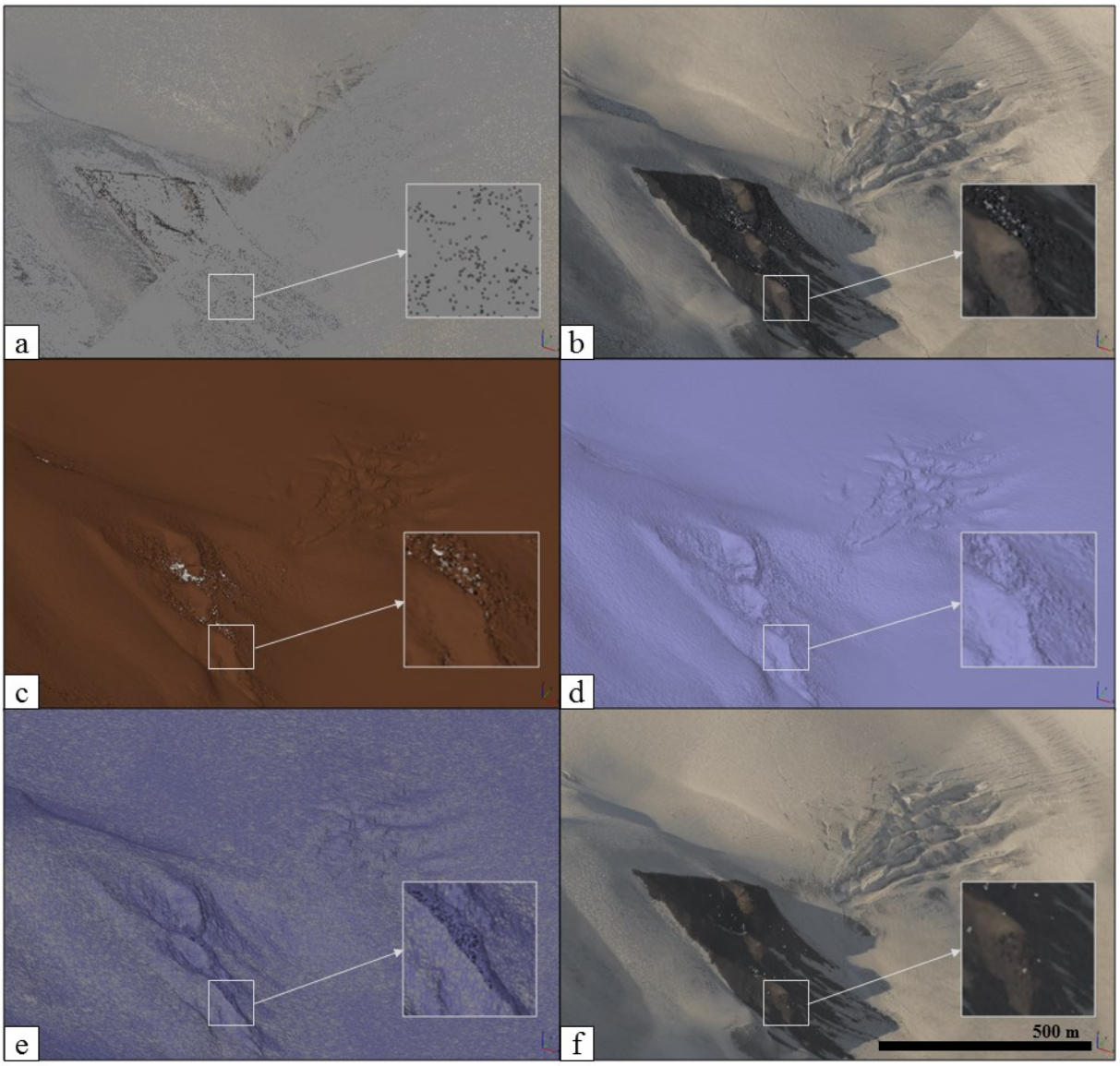

Figure 2.6: Progression of intermediate products from PhotoScan including: (a) Sparse point cloud; (b) Dense point cloud; (c) Classified points (brown = ground points, white = unclassified; (d) Solid surface model; (e) Wireframe model; (f) Textured model (Orthophoto).

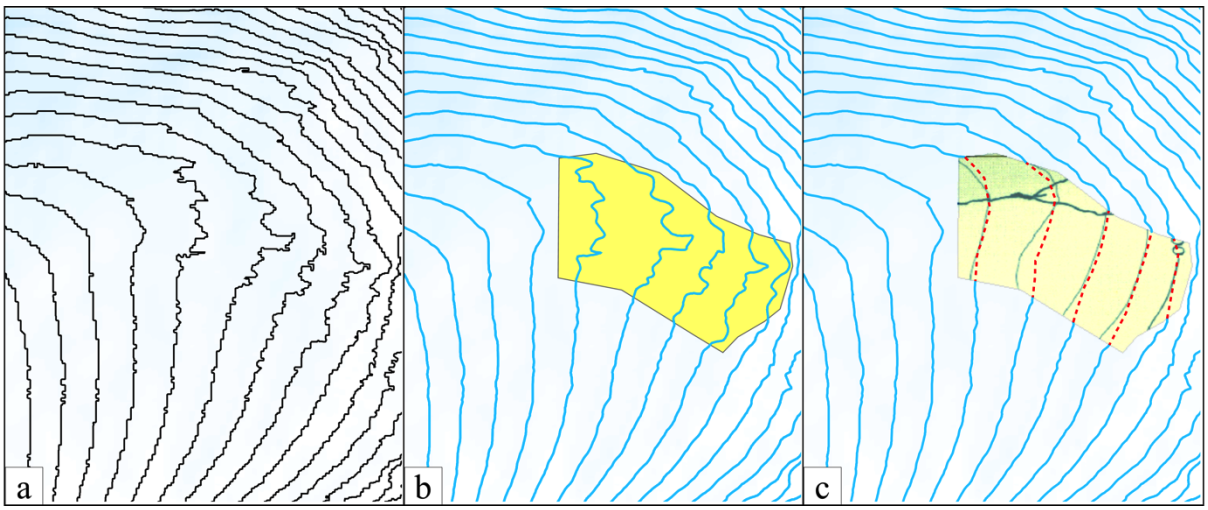

Figure 2.7: (a) Raw contours shown in black (10 m interval); (b) Smoothed contours with region of model errors highlighted in yellow; (c) Manually interpolated contours shown as red dashed lines overlaid on an inset of the Haumann and Honegger (1964) map in the region of error. Contour interval = 10 m.

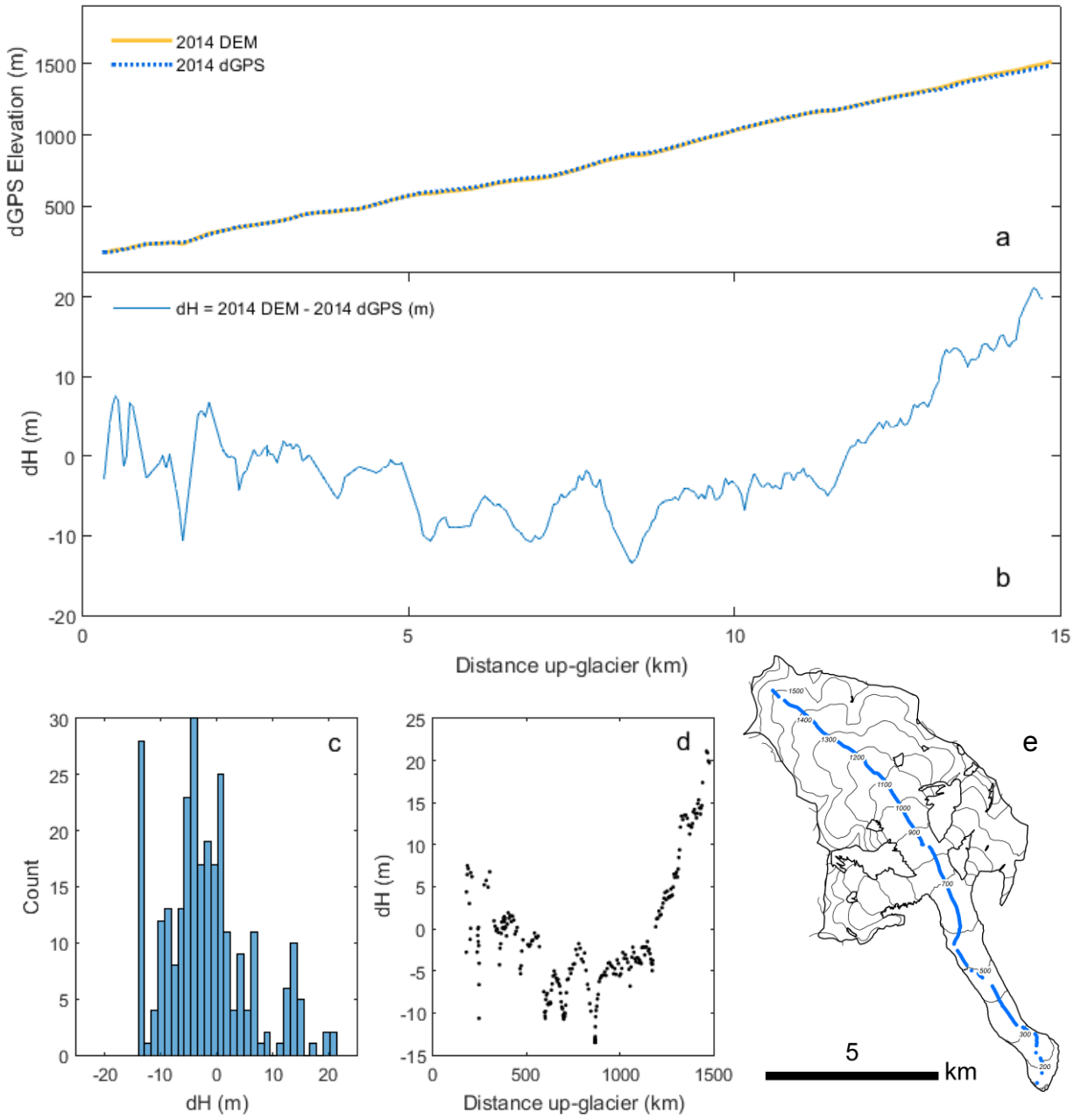

Figure 2.8: (a) Elevations along a glacier centreline profile derived from the summer 2014 SfM DEM (yellow) and the spring 2014 dGPS observations and (b) discrepancies (dH) along the glacier centreline derived from differencing the 2014 DEM and dGPS measurements. The distribution of dH values shows a normal distribution with a mean of -1.30 m. Scatter plot (d) indicates the pattern of dH with elevation. (e) Location dGPS measurements along White Glacier, collected in April 2014.

CHAPTER 3: MASS BALANCE REANALYSIS

3.1 ARTICLE 2 SUMMARY AND ATTESTATION

This study presents the first reanalysis of a long-term glacier mass balance record in the Canadian Arctic. The reanalysis is accomplished through comparison of the 1960-2014 glaciological mass balance record of White Glacier, Axel Heiberg Island, Nunavut, with a geodetically derived mass change over the same period. The corrections required to homogenize the two datasets, including adjusting for changes in hypsometry over the period of record and the generic differences between methods, are discussed along with the associated systematic and random errors of the two forms of mass-balance estimation. Statistical comparison of the two datasets reveals that within the error margin there is no significant difference between the average annual glaciological balance (–213 ± 28 mm w.e. a^{-1}) and geodetic balance (–178 ± 16 mm w.e. a^{-1}) at White Glacier over the 54-year record. The validity of this result, and the assumptions made in implementing the glaciological method, are critically assessed.

The following chapter forms the basis for an article coauthored by Laura Thomson (University of Ottawa), Michael Zemp (World Glacier Monitoring Service), Luke Copland (University of Ottawa), Graham Cogley (Trent University), and Miles Ecclestone (Trent University). The mass balance record at White Glacier, spanning 56 years (as of 2016), results from the efforts of many field scientists including those who worked under the leadership of Fritz Müller from 1960 to 1980, members of the Trent University Geography department from 1983 to present, and participants from the University of Ottawa (L. Thomson, L. Copland, and M. Hackett) in recent years. The reanalysis presented here was conducted by Laura Thomson under the mentorship of Michael Zemp during a 5-month internship at the World Glacier Monitoring Service at the University of Zurich (Zurich, Switzerland). Helpful revisions of the initial manuscript written by L. Thomson were provided by the co-authors, as well as by E. Thibert and an anonymous reviewer for the Journal of Glaciology.

Thomson, L. I., M. Zemp, L. Copland, J. G. Cogley, and M. A. Ecclestone (2016), Comparison of Geodetic and Glaciological Mass Budgets for White Glacier, Axel Heiberg Island, NU, Journal of Glaciology, accepted Aug. 2016..

3.2 INTRODUCTION

The Canadian Arctic Archipelago (CAA) hosts the largest volume of ice outside of the ice sheets [*Pfeffer et al.*, 2014] and occupies latitudes that are currently experiencing some of the greatest rates of climate warming [*Sharp et al.*, 2011; *Sharp et al.*, 2015], a tendency that is predicted to continue well into the future [*Kirtman et al.*, 2013; *Lenaerts et al.*, 2013]. A recent analysis of the CAA *in situ* surface mass balance records indicates that the average glacier mass balance between 2005 and 2009 was five times more negative than the average from 1963 to 2004 [*Sharp et al.*, 2011]. Through modelling and remote sensing, *Gardner et al.* [2011] showed that 92% of the mass loss from the CAA can be explained by increased melt, while only 8% is attributable to frontal ablation (i.e. calving) between 2004 and 2009.

In terms of estimating glacier mass balance in alpine basins, there are two primary methods: the glaciological method (also often referred to as the direct method) involves interpolation between *in situ* measurements of accumulation and ablation at stakes drilled into the glacier surface. These stakes are typically located along the glacier centreline, and interpolation across the glacier basin is undertaken either by assuming that mass balance varies only with elevation (the profile method) or by mapping accumulation and ablation patterns (the contour method) [*Østrem and Brugman*, 1991].

The geodetic method differences elevation models to determine changes in ice volume over time. Estimates of the density of the ice/snowpack are then used to convert this volume change to mass loss or gain. At the present day, these elevation models are often derived from airborne or satellite remote sensing. Laser altimeter data from ICESat have provided a valuable resource to determine recent ice volume changes in the CAA [*Gardner et al.*, 2011]. However, such data does not work well for relatively small alpine glaciers. Mass changes can also be determined using the gravimetric method over large ice caps and ice sheets (e.g., using data from the Gravity Recovery and Climate Experiment; *Sharp et al.* [2011]), but these measurements lack sufficient spatial resolution to detect changes at the scale of alpine glacier basins.

Remote sensing methods are promising for future glacier mass balance monitoring, but to detect and understand climatic trends in context we require earlier datasets for comparison. Surface mass balance estimates using the glaciological method began in 1959 across the Queen Elizabeth Islands (QEI) of the northern CAA and primarily focused on two smaller ice caps (Melville and

Meighen), two outlet basins of larger ice caps (Devon and Agassiz), and two mountain glaciers (White and Baby, Axel Heiberg Island). Intermittent observations were also conducted for many years on Ward Hunt Ice Rise and Ice Shelf on northern Ellesmere Island and Prince of Wales Icefield on SE Ellesmere Island [*Braun et al.*, 2004b; *Hattersley-Smith and Serson*, 1970; *Koerner*, 2005; *Mair et al.*, 2009]. Those records submitted to the World Glacier Monitoring Service (WGMS) and exceeding 10 years in length are shown in Figure 3.1a. Due to the large area of ice in the QEI (~104000 km^2; *Sharp et al.* [2014]) and logistical barriers, the CAA is comparatively under-sampled in contrast to some other Arctic regions (e.g. Iceland, Svalbard, northern Scandinavia; *Sharp et al.* [2011]). As such, it is particularly important to periodically assess the validity of these key measurements, which have served as *in situ* constraints for numerous other studies, through periodic reanalysis of the glaciological mass balance datasets [*Zemp et al.*, 2013].

The comparison of mass-balance data series obtained by the glaciological method with independently derived estimates of mass change offers insight into the completeness and accuracy of the measurements [*Cogley*, 2009; *Østrem and Haakensen*, 1999; *Zemp et al.*, 2013]. While the glaciological method excels in capturing the large temporal and spatial variability of climate–glacier processes, the method is also subject to biases that might be small on an annual basis but can compound to cause significant errors over multi-decadal records. Whereas random errors rise proportionally to the square root of the number of years, systematic biases sum linearly from year to year. The biases are associated with the inherent limitations of the glaciological method, primarily the challenge of measuring superimposed ice and internal accumulation, and are often undetectable within the random error margin that is approximated to be 200 mm w.e. a^{-1} (w.e., water equivalent) for most glaciological balance measurements [*Cogley and Adams*, 1998]. As the biases build over many years, however, they can be detected by multi-year geodetic balance observations. For example, the Norwegian maritime glacier Ålfotbreen was observed to have a positive glaciological balance of +3.4 m w.e. over a 20 year period, while the geodetic balance determined from map comparison was found to be –5.8 m w.e. [*Østrem and Haakensen*, 1999]. The discrepancy was primarily assigned to uncertainties in the glaciological method associated with high accumulation rates (sinking stakes), and overestimation of accumulation by snow-probe measurements. As such, a reanalysis of mass balance data should not only reveal how well a glaciological measurement programme is performing, but may also indicate the magnitude and extent to which specific processes have impacted the cumulative data series and the corrections

that can be imposed to reconcile the geodetic and glaciological mass balance measurements [*Andreassen et al.*, 2015; *Zemp et al.*, 2013].

This study presents the first reanalysis of a surface mass balance record in the CAA for White Glacier, Axel Heiberg Island. The cumulative record of glaciological mass balance observations is compared to a geodetic balance calculated from elevation data spanning 1960 to 2014 using an approach that strives to ensure consistency between the datasets before comparison [*Zemp et al.*, 2013].

3.3 STUDY SITE AND PREVIOUS RESEARCH

White Glacier (79.50° N, 90.84° W) is a 14 km long alpine glacier extending from 80 to 1782 m a.s.l. in the region of Expedition Fiord on Axel Heiberg Island, Nunavut, Canada (Figure 3.1a). The glacier has a 5 km wide accumulation area and flows southeast into a narrow 0.8-1.1 km wide valley, terminating at a junction with Thompson Glacier (Figure 3.1b). The glacier area in 1960 was 41.07 km^2, which decreased to 38.54 km^2 by 2014 [*Thomson and Copland*, 2016]. The region experiences mean annual temperatures of approximately –20°C and annual precipitation ranging from 58 mm a^{-1} at sea level (as measured at Eureka, 120 km to the northeast) to 370 mm a^{-1} at 2120 m a.s.l. as measured in a 41-year snowpit record of annual accumulation on the Müller Ice Cap [*Cogley et al.*, 1996]. Over the period of observation (1960–2015), the average equilibrium line altitude was 1075 m a.s.l. and the mean accumulation area ratio (accumulation area divided by the total area) was 0.55.

The mass balance programme at White Glacier was initiated in 1959 and brought about several years of intensive glaciological studies, all of which were based at the nearby McGill Arctic Research Station (79.42° N, 90.75° W). Studies that included snow accumulation processes [*Andrews*, 1964; *Havens et al.*, 1965], glacier facies [*Müller*, 1962], ice velocity fluctuations [*Iken*, 1974], and polythermal regime [*Blatter*, 1987a] were led by Dr. Fritz Müller of McGill University from 1960 to 1980. Dr. Müller, for whom Müller Ice Cap on central Axel Heiberg Island was named, passed away in July 1980 resulting in a 3-year gap in the mass balance record until Trent University re-established the mass balance monitoring programme in 1983. Since this time, studies at White Glacier have focused on mass balance and remote sensing techniques [*Cogley and Adams*, 2000; *Cogley et al.*, 2011a; *Cogley et al.*, 1996]. In 2014, University of Ottawa undertook

responsibility for the White Glacier mass balance monitoring programme. As a result of these combined efforts, today White Glacier has the longest mass balance record for an alpine glacier in the Canadian Arctic (55 years) and is one of 37 reference glaciers within the Global Terrestrial Network for Glaciers through the United Nations Framework Convention on Climate Change. These observations, submitted annually to WGMS (e.g. *WGMS* [2015] and previous issues), are used with observations from 40 other glaciers to calculate a worldwide glacier mass balance index [*WGMS*, 2008].

3.4 METHODS AND DATA

In the following sections we present the measurement methods used to calculate the White Glacier glaciological and geodetic mass balances and describe the approaches taken to homogenize the data. Data homogenization refers to corrections for "*artefacts and biases that are not natural variations of the signal itself but originate from changes in instrumentation or changes in observational or analytical practice*" [*Cogley et al.*, 2011b]. We discuss the systematic and random errors associated with these datasets and address the differences between the mass balance processes captured by each of the methods. In this case, while the geodetic method is considered to measure surface, internal, and basal mass balance [*Zemp et al.*, 2013], the glaciological method only captures surface processes (i.e. accumulation by snowfall and ablation by surface melt and sublimation). We use estimates of the internal and basal mass balance in an attempt to correct for these generic differences, allowing for comparison of results obtained with the two methods. Finally, the homogenized and corrected balances over the period of record (PoR, 1960–2014) are compared and the discrepancy between them is assessed statistically to determine whether the glaciological series requires calibration.

3.4.1 Glaciological Balance Measurements and Calculation

Owing to logistical and financial constraints, field measurements at White Glacier are conducted once per year in the spring (typically late April to early May) and as such the measurements do not allow for differentiation between winter and summer balances. The stratigraphic year generally starts and ends in September (at the end of the melt season) and is identified by the year in which the ablation season ends [*Cogley et al.*, 1996]; e.g., the 2014 balance

year combines accumulation from winter 2013–2014 and ablation from summer 2014. Winter accumulation of the current balance year is measured in snow pits at stakes located above the lower limit of the equilibrium line (~900 m a.s.l.) and the previous summer surface is commonly identifiable as a compact and slightly dirty layer overlain by well-developed depth hoar and cup-shaped ice crystals [*Müller*, 1961]. Stake readings below the equilibrium line (identifiable by glacier ice at the base of snow pits) indicate the summer ablation of the previous balance year by the change in height of the stake above the ice surface. The full record of mass balance stake measurements from 1960 to 2015, excluding the 3-year gap from 1980 to 1982, as well as further details on the field measurements and calculation of the annual mass balance are provided in Appendix 2.

Annual surface mass balance (B) is calculated using a modified version of the profile method [*Cogley et al.*, 1996; *Østrem and Brugman*, 1991]. A polynomial regression (order k=3) through b, the annual stake balances, at measured elevations along the glacier centreline is used to describe the mass balance gradient, which is then extrapolated across the glacier hypsometry in 25 m elevation bands where $s(h,t)$ is the area of the elevation band with midpoint elevation h in year t, and t is 0 in 1960. The reasoning behind using a third order polynomial relates to the desire to better represent the differing slope of the mass balance gradient above and below the ELA, which becomes less steep at higher elevations. Statistically, the third order polynomial fit on average returns a better R^2 value (0.93) than a linear (n=1) fit where $R^2 = 0.88$. However, the overall impact of using a third order polynomial versus a linear regression is ultimately negligible in the scope of this reanalysis. Examples of the polynomial fit in 10-year intervals since the onset of measurements in 1960 are provided in Appendix 2. The elevation band balances $b(h,t)$ are calculated from the regression equation at the elevation band midpoints and the annual specific balance (i.e. normalized by $S(t)$, the glacier area) is calculated as follows:

$$B_t = \frac{\sum s(h,t)b(h,t)}{S(t)} \qquad \text{(Eq. 1)}$$

From 1960-2003, B_t was calculated using the 1960 glacier hypsometry $s(h,0)$, which was derived from the topographic map of *Haumann and Honegger* [1964]. In 2003, a mapping campaign by *Hember et al.* [2003] allowed for an update to the hypsometry below 400 m a.s.l. and thereafter calculations of B have used the 1960 hypsometry above 400 m, and the updated 2003 hypsometry

from 400 m down to the terminus. In 2014 a new digital elevation model (DEM) of White Glacier, described below and in *Thomson and Copland* [2016], was produced and will serve as the new hypsometry for mass balance calculations until the next mapping campaign and reanalysis.

A detailed history of mass balance measurements at White Glacier is provided by *Cogley et al.* [1996], along with a discussion of the mass balance record from 1960-1991 and an assessment of errors. The two most negative pentadal averages of mass balance occurred within the last decade (2005–2014) and this has been accompanied by increasing equilibrium line altitudes and decreasing accumulation area ratios (Figure 3.2a-c). The stake network at White Glacier has evolved from a dense network of >100 stakes in the 1960s, to 30–40 stakes in recent years (Figure 3.1b, 3.2d), resulting in an approximate coverage of 1 stake per km^2. The 39 stakes measured in the last reported balance year (2014) ranged from 122 to 1519 m a.s.l. (about 97% of the area of the glacier), with stake balances (b) from –2884 to +138 mm w.e.

3.4.2 Conventional Balances

An advantage of calculating glacier-wide mass balance over a historic reference surface is that it results in mass balance values that exclusively reflect changes in glacier-climate interactions [*Cogley et al.*, 2011b; *Elsberg et al.*, 2001]. However, this *reference-surface balance* does not reflect the actual mass change in a given year but rather the mass change that would have resulted from using a constant reference topography for which the glacier hypsometry (i.e. the *s(h,t)* and *S(t)* terms) remained unchanged through time. Therefore, a cumulative glaciological balance data series that would be equivalent to the geodetic balance would use *conventional balances* [*Elsberg et al.*, 2001] that are calculated from glacier hypsometries that are concurrent in time with the mass balance measurements. However, annual measurements of glacier hypsometry are impractical and nonexistent for most glaciers.

Conventional balances were calculated for the White Glacier mass balance series using a linear regression that updates the glacier hypsometry annually between 1960 to 2014, the two years with complete topographic coverage based on the 1:10,000 map by *Haumann and Honegger* [1964] and the new 2014 DEM of White Glacier [*Thomson and Copland*, 2016]. The time-series of 25 m elevation band areas was calculated from the linear relationship:

$$s(h,t) = s(h,0) + t \times \left(\frac{s(h,n) - s(h,0)}{n}\right) \quad \text{(Eq. 2)}$$

where *s(h,0)* is the band area in the first year (1960) and *t* increases from 0 in unit steps over the *n* years in the record. These interpolated *s(h,t)* values were used to calculate the conventional balance using Eq. 1. The reference and conventional balances, with associated equilibrium line elevations and accumulation area ratios, are provided in Table 3.1. While the long-term record illustrates that changes to mass balance have not been linear over the period of record at White Glacier (Figure 3.2) and elsewhere in the Canadian Arctic [*Gardner et al.*, 2011], a linear interpolation of the glacier hypsometry is used given the lack of geodetic data over the glacier between 1960 and 2014. To test the potential impact of assuming a constant linear change in hypsometry from 1960 to 2014 a simple sensitivity analysis, based on calculations of conventional balances using a constant glacier hypsometry from 1960 to 2000 followed by a linear change in hypsometry from 2000 to 2014, revealed that the resulting impact on the cumulative glaciological balance was insignificant within the errors of the glaciological measurements.

3.4.3 Geodetic Balance

A 54-year geodetic balance of White Glacier was calculated by differencing the earliest large-scale map of White Glacier (1:10,000) based on 1960 aerial photography [*Haumann and Honegger*, 1964], with a new DEM produced using Structure from Motion techniques from >400 oblique air photos collected in July 2014 [*Thomson and Copland*, 2016]. The 1960 White Glacier 1:10,000 map is available through the WGMS "Fluctuations of Glaciers Maps" (http://wgms.ch/products_fog_maps/), along with supporting documentation that summarizes the field surveys, photogrammetry and plotting techniques used to produce it [*Blachut*, 1961; 1963; *Cogley and Jung-Rothenhäusler*, 2002; *Haumann*, 1961; 1963]. The 10 m contours of the 1960 map were manually digitized at a working scale of 1:2,000 and converted into a 5 x 5 m DEM using the Esri ArcGIS 10.1 'Topo to Raster' tool, which is based on the ANUDEM software developed by *Hutchinson* [1988]. The DEM was produced without drainage enforcement (i.e. no sinks in the DEM were filled), with a discretization error factor of one, and a vertical standard error of 0, which ensured that no systematic bias was introduced when converting the 1960 contours to a raster surface.

The 2014 DEM was originally produced at 1 m resolution in NAD27. The surface was then down-sampled to 5 m resolution to allow direct comparison with the 1960 DEM and reprojected into a local planar coordinate system used to define the original 1960 map. A coregistration of the

two DEMs was finally performed to minimize the error in the observed volume change. To determine the glacier-wide average change in height, the geodetic balance was calculated as the sum of observed changes in elevation, pixel by pixel, within the 1960 White Glacier extent, divided by the mean area between 1960 and 2014 to arrive at the glacier-wide average change in height [*Zemp et al.*, 2013]. Specific details of the 2014 DEM production, projection systems, the application of ground control, coregistration techniques, and error analysis can be found in *Thomson and Copland* [2016].

3.4.4 DEM Coregistration

Coregistration, guided by minimization of the elevation differences between DEMs over areas of stable terrain near the glacier, can be considered as a means of homogenizing the geodetic datasets [*Zemp et al.*, 2013]. The universal co-registration method [*Nuth and Kääb*, 2011] exploits the relationship between elevation differences (d*h*), terrain slope and aspect, and was applied here to identify the translational offsets between the geodetic DEMs. The full details of the coregistration process, including parameters and error analysis are provided in *Thomson and Copland* [2016]. This was assessed over three regions of stable terrain, together covering 4.5 km^2 and with a slope range of 5–30° and elevation range of 50-1410 m a.s.l (Figure 3.3a). Introducing a small rotation correction before using the Nuth and Kääb (2011) method significantly improved the co-registration results (Table 3.2). The rotation correction, about the z-axis, was determined using Horn's absolute orientation solution [*Horn*, 1987], which produces a least-squares fit between the coordinates of common points between the 2014 DEM (source points) and 1960 DEM (target points).

Rotation and translation parameters that resulted in the minimum average d*h* and standard deviation σ_{dh} over stable terrain were applied to the 2014 DEM, from which the 1960 DEM was then subtracted to produce a d*h* map (Figure 3.3a). Small voids in the 2014 DEM, consisting of <3% of the basin area, were treated by assigning the void space a *dh* value equal to the average d*h* of its 25 m elevation band. For example, if a void were judged to lie within the 1000-1025 m a.s.l. elevation band, it would be assigned the average of all d*h* values found within that band. The same method was applied in the area where Thompson Glacier has advanced since 1960 into the area previously occupied by White Glacier (Figure 3.3a). The distribution of d*h* across the glacier hypsometry is shown in Figure 3.3b.

3.5 RANDOM AND SYSTEMATIC ERRORS

Uncertainties of the glaciological method are associated with point measurements in the field and the extrapolation of these measurements across elevation bands [*Cogley and Adams*, 1998]. Regarding the latter, the longitudinal design of the stake network limits the extent to which we can observe and assess variability of mass balance in the glacier basin. For the 1960-1962 balance years, Young (1972) conducted a parameterization of surface mass balance as a function of elevation, slope, aspect and curvature across the White Glacier basin and found that the parameterization resulted in slightly higher estimates of melt, which differed from an elevation-only parameterization by –0.10 ± 0.04 m w.e. a^{-1}. At the same time, studies of spatial variability in the ablation area at three cross-profiles ranging from 250-850 m a.s.l. showed a standard deviation in stake balances of 0.196 m w.e. a^{-1} [*Adams*, 1966]. The variability of the stake balances with elevation (Figure 3.4) has not changed measurably over the PoR and the polynomial regression (k=3) used to estimate band balances each year has an average R^2=0.93. As has been predicted (e.g. [*Dyurgerov and Dwyer*, 2000]) we do observe a slight (though not statistically significant) steepening of the linear mass balance gradient towards the present day, as well as a shift towards more negative mass balance values, which corresponds with increasing equilibrium line altitudes over the PoR (Figure 3.4b). From the above studies and previous literature concerning the errors associated with the glaciological method [*Adams*, 1966; *Cogley et al.*, 1996], we take 0.250 m w.e. a^{-1} to be the random error associated with the glaciological record ($\sigma_{glac.a}$), which incorporates 0.20 m w.e. a^{-1} as the random sampling error and an estimated 0.050 m w.e. a^{-1} to account for unquantified systematic errors.

For the geodetic balance, the coregistration results over stable terrain are taken to define errors associated with the DEM comparison. The bias in the geodetic balance over the PoR, $\varepsilon_{geod.PoR}$ = 0.663 ± 0.047 m w.e., is derived from the average d*h* over stable terrain (0.78 m) and an assumed density of 850 ± 60 kg m^{-3}, as described below. The random error in the geodetic balance, $\sigma_{geod.PoR}$ = 0.866 m w.e., is taken from the DEM standard error and the uncertainty in the density conversion. The DEM standard error is calculated to be twice the standard deviation of *dh* over stable terrain (2 × 5.08 m) divided by the root of the sample size. Given the spatial autocorrelation between pixels of a DEM derived from contours (as is the case for the 1960 DEM), we approximate the sample size to be 319, based on the number of individual contour lines over glacier ice in the 1960

map. This is likely a conservative estimate for the degrees of freedom considering that it would also be reasonable to use the number of photographs used to produce the 2014 DEM (507) as a proxy for the independent sample size, which would reduce $\sigma_{geod.PoR}$ to 0.814 m w.e. In both the glaciological and geodetic balance calculations, we consider random uncertainties to have a normal error distribution and to be uncorrelated when combined (i.e. in the calculation of geodetic balance errors).

3.6 CORRECTIONS OF GENERIC DIFFERENCES

3.6.1 Density Conversion

One of the generic differences between glaciological and geodetic mass balance estimates is that the former are derived from well constrained *in situ* density measurements, whereas the latter are seated in volume change measurements, which require conversion to mass by an estimated density for the material lost or gained. While density conversion is a significant issue (e.g. *Moholdt et al.* [2010]), this study follows the recommended approximation for density conversion of 850 ± 60 kg m^{-3} developed by *Huss* [2013] which, through modelling of synthetic and monitored glaciers, incorporates elements of densification, internal refreezing, and changing volume of the firn. The approximation is suitable for White Glacier, which meets the requirements of *Huss* [2013] that the geodetic observations span more than 5 years, and that the glacier demonstrates relatively stable mass balance gradients, non-negligible changes in volume, and an established and stable region of firn. It also enables consistent comparison with other mass balance reanalysis studies [*Zemp et al.*, 2013].

3.6.2 Survey Differences

Temporal differences between the geodetic and glaciological observations need to be addressed because the geodetic observations span the air photo survey dates of August 2, 1960, to July 10, 2014, rather than the end-of-summer dates in each of these years. To align the geodetic dates with the stratigraphic year used for the glaciological mass balance measurements, a simple degree-day model (eq. 3 of *Zemp et al.* [2010]) was used to estimate melt between the observation dates in 1960 and 2014 and the ends of their respective stratigraphic years, which were taken to be

September 1, 1960, and September 8, 2014, the dates on which temperatures near the terminus dropped below 0°C. Temperature data for August and September 1960 were acquired from *Andrews* [1964] at "Lower Ice Station", and from a Campbell Scientific automatic weather station at the White Glacier end moraine (500 m southwest of the terminus) for the same months in 2014. From the results of Braithwaite and Raper (2007) who assessed mass balance sensitivity to +1°K warming using an empirical relationship between glacier mass balance and the estimated temperature at the ELA, we assumed a degree-day factor for ice of 7.0 mm w.e. d^{-1} K^{-1} (their 'Medium" assumption) to estimate mass balance corrections of +0.095 m w.e for 1960 and –0.197 m w.e. for 2014 that were applied as corrections to the geodetic balance, as shown in Figure 3.5. The gap in the mass-balance record (1980-1982) was filled by *Glenday* [1989] using a multivariate regression of glaciological balance values from 1970-1980 with temperature and shortwave radiation data available from the nearest weather station, at Eureka, Nunavut, approximately 125 km northeast of White Glacier. The parameterization returned balances of –0.178, –0.175, and –0.092 m w.e. for 1980, 1981, and 1982, respectively. Unfortunately, information on the uncertainty of this parameterization is not available, so we estimate the uncertainty to be the standard deviation of the 51 years with observations (0.320 m w.e. a^{-1}).

3.6.3 Internal and Basal Mass Balance

The glaciological method measures surface mass balance, and is unable to capture internal and basal accumulation and ablation. Here, simple estimates of these processes are considered and applied to the glaciological balances to allow comparison with the geodetic balance. In temperate glaciers, potential energy loss by the transfer of mass downslope leads to internal strain heating and frictional warming at the bed. Considering that White Glacier is comprised of cold ice (–15 to –5°C for the majority of the ice volume; *Blatter* [1987a]), we assume that any strain or frictional energy will go towards only slightly warming this cold ice, rather than promoting melt. Internal ablation due to the loss of potential energy (A_{PE}) of englacial and subglacial runoff was estimated using

$$A_{PE} = \frac{mhg}{L_f \rho S} \quad \text{(Eq. 3),}$$

where m is the mass of flowing water, g is acceleration due to gravity, h is the elevation loss, L_f is the latent heat of fusion, ρ is the density of water, and S is the glacier area (average between 1960 and 2014). The cumulative measured surface ablation over the 54 year record was used to estimate the mean annual discharge, and subsequently m, to be 1.4×10^{10} kg a^{-1}. The elevation loss was approximated by assuming that on average meltwater originates at half the vertical distance from the terminus to the average equilibrium-line altitude, h = (1070–50)/2 = 510 m. Together, these resulted in a calculation of A_{PE} = 0.274 m w.e. over the PoR (i.e., 5.1 mm w.e. a^{-1}). We have assumed no melting by turbulent transfer of energy from the flowing water to the ice, but have also assumed that all the meltwater loses all its potential energy to internal ablation and none to warming of the bedrock. With these assumptions we are neglecting biases of the same order as our estimate of A_{PE}, and they will tend to cancel.

Internal accumulation by surface melt and refreezing in the firn does not lead to a bias in glaciological balance measurements at White Glacier because the snow accumulation measurements, made in the spring, are presumed to be representative of winter accumulation and therefore are unlikely to have been affected by melting. However, summer accumulation is not necessarily negligible and may constitute a bias such that reported annual balances are too negative. At other monitored glaciers in the CAA, summer accumulation (excluding that by rainfall that freezes) gained between April-May mass balance measurements and the end of the melt season has been determined by the use of records from automatic weather stations [*Koerner*, 2005]. Currently the only snow-depth sounder installed at White Glacier is situated in the ablation area to monitor the onset and duration of surface melt. Instead, photography from a time-lapse camera located on a nunatak of White Glacier (white square in Figure 3.1b) with a field of view covering elevations between ~900-1400 m a.s.l. was used to detect the occurrence of snowfall in the accumulation area between April 2013 and July 2015. These observations indicate that between 1-3 snowfall events have occurred each year in the period following spring mass balance measurements and before the melt season begins. Together, these events amount to < 20 cm of snow accumulation in each year on average (<22 mm w.e. using $\rho_{\text{fresh snow}}$ = 108 kg m^{-3}; *Metcalfe et al.* [1994]). This contribution to the total mass balance of the glacier is considered negligible because it comprises the first layers of snow that are exposed at the onset of summer melt and therefore the first mass to melt and run off. During the melt season only one snowfall event per year was observed by the time-lapse camera in 2013 and 2014, and these events resulted in

snowfall accumulations of 5 cm (<6 mm w.e.), which rapidly melted at lower elevations and likely upper elevations as well (given observations of "glazing" of the snowpack surface within a day or two of snowfall).

Basal ablation from geothermal heating was estimated for the area of White Glacier where the bed is known to be temperate along the centreline of the glacier trunk, which totals approximately 5 km^2, or 12.5% of the total glacier area [*Blatter*, 1987a]. Basal ablation by geothermal melt (A_{GT}) was estimated to be 0.015 m w.e. over the PoR when calculated using

$$A_{GT} = \frac{qt}{L_f \rho} \qquad \text{(Eq. 4)}$$

where the geothermal heat flux q is taken to be 0.023 W m^{-2} [*Blatter*, 1987b], and t is the time elapsed (in seconds) over the PoR. Basal accumulation can be considered negligible for non-tidewater glaciers [*AMAP*, 2011].

3.7 RESULTS AND DISCUSSION

In the glaciological record, a +0.445 m w.e. correction was applied to convert the cumulative reference-surface balance (–11.214 m w.e.) to a conventional balance (–10.769 m w.e.) using a linear interpolation of changing hypsometry over the 51 years with observations. Figure 3.6 illustrates the difference in balances calculated from the reference surface (1960) and conventional surfaces (interpolated). The conversion from reference to conventional balances incorporates two scenarios that present contrasting effects: (1) as the glacier terminus retreats, the glacier loses area in the region of most strongly negative balance resulting in a net positive influence on the glacier-average balance, and (2) as the glacier thins, its surface lowers, which exerts a net negative influence on the mass balance because ablation is stronger at lower altitudes. The positive correction applied to arrive at our reference-surface balance would suggest that the former process dominates over the latter. Investigating the relative roles of these processes requires calculating and comparing mass change related to a fixed elevation with varying area (B_{HdS} for scenario 1), and the mass change resulting from elevation change (generally ice thinning) assuming a constant area (B_{SdH}, for scenario 2). For this approach it is necessary to work with total water

equivalent mass change rather than specific balances to remove the second area term (denominator in equation 1). We find that B_{ref} = –486321 kt and B_{con} = –447206 kt, requiring that a correction C of +39115 kt be applied to B_{ref} to arrive at B_{con}. This correction is the sum of the positive B_{HdS} and the negative B_{SdH}. From the geodetic balance calculations, we calculate B_{SdH} using

$$B_{SdH} = \rho \sum(\overline{dh}\, s(h_0)) \qquad \text{(Eq. 5)}$$

where dh is the average elevation change observed over the PoR across a given elevation band, s is the band area according to 1960 hypsometry, and ρ is the assumed density (850 ± 60 kg m^{-3}). Consequently, if $C = B_{SdH} + B_{HdS}$ we find that with B_{SdH} = –386423 kt from equation 5, B_{HdS} therefore equals 425538 kt. The greater absolute magnitude of B_{SdH} therefore indicates that glacier retreat has a greater impact than glacier thinning on the mass balance of White Glacier.

The remaining corrections to the glaciological record, including estimates of mass balance during the gap years (1980-1982) and melt induced by the loss of potential energy and by geothermal heating, together lead to a more negative corrected glaciological balance by –0.445, –0.274, and –0.015 m w.e., respectively, over the PoR (Figure 3.5a). The final estimate of the glaciological cumulative balance is –11.503 ± 2.037 m w.e. between 1960 and 2014.

For the geodetic record, the average dh across the 1960 hypsometry shows that glacier thinning (maximum –30 m) was prominent from the terminus up to elevations of approximately 1400 m, and that moderate thickening (maximum 15 m) was observed at the highest elevations (Figure 3.3). The average elevation change across the mean glacier extent (39.81 km^2) was –11.97 m over the 1960-2014 PoR. When the elevation change is multiplied by density, the resulting initial geodetic estimate of mass balance is –10.17 ± 0.866 m w.e., with an estimated error of 0.72 m w.e. Corrections to the geodetic balance (Figure 3.5b) include accounting for the observed non-zero elevation change over stable terrain after coregistration, which increased the geodetic balance by 0.663 ± 0.047 m w.e. over the PoR. The geodetic balance also required small adjustments of +0.095 and –0.197 m w.e. to account for melt between the geodetic survey dates and the end of the respective 1960 and 2014 stratigraphic years. We cannot estimate the uncertainty of these modelled adjustments but we assume that they are small.

The random errors (σ) in the two methods are significantly different due to the way in which they propagate over time. Over n years,

$$\sigma_{glac.a} = \frac{\sigma_{glac.PoR}}{\sqrt{n}} \quad \text{(Eq. 6)}$$

and

$$\sigma_{geod.a} = \frac{\sigma_{geod.PoR}}{n} \quad \text{(Eq. 7)}$$

such that $\sigma_{glac.a}$ = 0.277 m w.e. a^{-1} (2.037 m w.e. over PoR) determined from the combined 0.250 m w.e. a^{-1} error for the 51 years with observations in the glaciological record and 0.320 m w.e. a^{-1} for the parameterized gap years. For the geodetic balance, $\sigma_{geod.a}$ = 0.016 m w.e. a^{-1} (0.866 m w.e. over PoR), which incorporates errors associated with the density conversion (0.718 m w.e. over PoR) and the standard error in the elevation change observation (0.484 m w.e. over PoR). In this study the geodetic balance is therefore taken to be the standard against which the glaciological balance is compared, owing to its lower random error.

Figure 3.5 illustrates the original glaciological and geodetic balances and the corrections applied to homogenize the data. The resulting glaciological and geodetic balances over the PoR, determined over the average of the 1960 and 2014 glacier extents, are –11.50 m w.e. and –9.61 m w.e., respectively. Note that the corrections of biases did not reduce the ~1 m w.e. difference between the uncorrected balances, but rather they almost doubled the difference, from 1.04 to 1.89 m w.e. The statistical significance of the difference between balances is determined from the reduced discrepancy,

$$\delta = \frac{\Delta_{PoR}}{\sigma_{common\ PoR}} \quad \text{(Eq. 8),}$$

where Δ_{PoR} is the difference between the corrected glaciological and geodetic balances (–1.89 m w.e.) and $\sigma_{\text{common.PoR}}$ is the common variance (2.21 m w.e.), which describes the combined random errors of the glaciological and geodetic balances [*Zemp et al.*, 2013]. As the reduced discrepancy (δ = –0.85) falls within the 95% confidence interval (–1.96 < δ < 1.96), the balances can be deemed statistically equivalent. Therefore, the glaciological method can be considered to have accurately captured the long-term mass changes at White Glacier when compared against the geodetic balance. However, it is not possible to statistically identify any biases that might explain the observed –1.89 m w.e. discrepancy over the PoR. From the common variance it is also possible to calculate the smallest bias that could theoretically be detected in the glaciological record within

this 54 year period [*Zemp et al.*, 2013]; the bias calculated at the 5% risk limit, which can be of either sign, is 0.148 m w.e. a^{-1} and well below the random error of 0.250 m w.e. a^{-1} in the glaciological balance measurements.

In determining the geodetic mass balance for this study, DEM coregistration combined with rotation was an important step considering the challenges of working with the 1960 map, for which there is limited information about the map projection and datum [*Cogley and Jung-Rothenhäusler*, 2004]. The coregistration method of *Nuth and Kääb* [2011] enabled alignment of the DEMs independent of georeferencing difficulties and reduced the random error and biases between the DEMs. In fact, DEM alignment without coregistration would have resulted in a positive geodetic balance of 1.63 m w.e. over the PoR. Coregistration by translation alone was found to decrease the random error by 14% and, when combined with rotation, to reduce it by 39%.

While the observed discrepancy (–1.89 m w.e.) the glaciological and geodetic balances is not statistically significant, it is possible to explore the parameter space in which certain parameters vary. Of particular note is the uncertainty associated with density applied in the calculation of the geodetic balance [*Huss*, 2013; *Moholdt et al.*, 2010]. Holding all other parameters fixed, we find that allowing the density to vary within 850 ± 60 kg m^{-3} results in a maximum possible discrepancy of –2.27 m w.e. over the PoR when density equals 790 kg m^{-3}. The resulting delta value of this discrepancy is –1.11 m w.e., which still falls within the 95% confidence interval ($-1.96 < \delta < 1.96$). A similar test was conducted by holding all parameters fixed and allowing the modeled mass balance for each of the three gap years to fluctuate within the observed variance of the mass balance record. The resulting possible glaciological balances ranged from –10.86 to –11.57 m w.e., the latter of which produced a discrepancy of –2.34 m w.e. and a delta value also within the 95% confidence interval. If both density and the modeled balances over the gap years are combined the maximum discrepancy is –2.34 m w.e. with a delta value of –1.29, which still remains within $-1.96 < \delta < 1.96$.

It is possible that the more negative balance observed from the glaciological record is attributable to the assumption that summer snowfall is negligible; however the lack of observational data limits our ability to estimate the impact of this assumption. Similarly, while internal refreezing below the summer snowpack has been shown to impact glaciological (i.e.

summer mass balance) and geodetic measurements in other studies (e.g. [*Bolch et al.*, 2013; *Huss*, 2013] we are unable to treat it quantitatively. Another possible explanation for the more negative glaciological balance is the missed contribution of mass from superimposed ice originating from snowmelt off nunataks. In theory superimposed ice, recognized as such, does not impact mass balance measurements because it is a redistribution of mass within the system. However, snow originating on nunataks, which is not included in the mass balance calculation, regularly melts and runs off during the summer months and could refreeze in the accumulation area if the nunatak is above the ELA, or may freeze as superimposed ice. At present, nunataks comprise 6% of the White Glacier basin above 1000 m a.s.l. (the approximate average ELA) and including their area in the glacier hypsometry and subsequent mass balance calculations would only lead to a small increase (<1%) in the calculated balance. However, as nunataks expand with increasing melt, as we observed by an increase in the overall nunatak area by 2% from comparison of the White Glacier 1:10,000 maps by *Haumann and Honegger* [1964] and *Thomson and Copland* [2016], this proposed effect may impact mass balance measurements in future years.

3.8 CONCLUSIONS

Reanalysis of the White Glacier mass balance record from 1960-2014 indicates that, in comparison to the observed geodetic balance, the glaciological method successfully captures the long-term mass change and does not require correction or calibration. This finding suggests that the assumptions made in the glaciological method, including that summer accumulation is negligible at White Glacier, are reasonable for the PoR. One of the more significant findings of this study was the importance of employing the coregistration techniques of *Nuth and Kääb* [2011], and in this case DEM rotation as well, before calculating the geodetic balance. Indeed, failure to do so would have resulted in a positive geodetic balance over the 54 year period of record, as opposed to the measured -9.61 m w.e. loss. Homogenization of the glaciological record by conversion to conventional balances reduced the discrepancy with the geodetic balance by approximately 0.5 m w.e. More detailed analysis of the individual roles of glacier retreat and thinning suggests that glacier thinning impacts calculated mass balance to a lesser extent than glacier retreat, such that loss of significantly negative mass balance regions presents a buffering effect under the negative mass balance conditions. Corrections applied to address processes that

define the generic difference between the glaciological and geodetic balances (i.e. internal and basal ablation) were found to increase the difference. This may suggest that the surface mass balance is a reasonable approximation to the total (climatic–basal) mass balance for land-terminating glaciers in the CAA, which is perhaps not surprising considering the short summer season at high latitudes during which internal and basal melt might occur.

		Previous WGMS published version			Recommended mass balance series		
Year	**Stakes**	**B_{ref}**	**ELA_{ref}**	**AAR_{ref}**	**B_{con}**	**ELA_{con}**	**AAR_{con}**
1960	71	-408	1261	0.40	-425	1265	0.37
1960	71	-408	1261	0.40	-425	1265	0.37
1961	85	17	931	0.74	19	933	0.74
1962	115	-781	1371	0.20	-782	1373	0.20
1963	80	-155	1172	0.50	-160	1165	0.51
1964	31	349	481	0.91	358	492	0.91
1965	28	-12	886	0.77	-4	889	0.77
1966	51	-25	996	0.69	-13	984	0.70
1967	29	119	828	0.80	137	820	0.81
1968	50	-408	1226	0.44	-405	1222	0.44
1969	76	72	908	0.75	82	905	0.75
1970	68	-4	953	0.73	-9	964	0.72
1971	51	-183	1107	0.60	-194	1114	0.58
1972	91	118	659	0.85	116	672	0.86
1973	49	191	746	0.82	195	761	0.82
1974	48	-44	997	0.69	-48	999	0.68
1975	63	251	800	0.81	250	812	0.81
1976	65	114	832	0.80	120	837	0.80
1977	76	-370	1093	0.60	-388	1117	0.58
1978	23	-131	1018	0.67	-144	1037	0.66
1979	63	-87	1011	0.69	-89	1025	0.66
	-	-	-	-	-	-	-
1983	26	-76	980	0.71	-98	991	0.70
1984	27	-44	1009	0.69	-67	1026	0.66
1985	28	1	897	0.76	0	854	0.78
1986	33	-242	1072	0.63	-283	1089	0.61
1987	31	-595	1444	0.10	-626	1442	0.10
1988	25	141	470	0.91	144	457	0.92
1989	31	40	511	0.91	38	505	0.91
1990	27	-431	1395	0.17	-457	1405	0.13
1991	27	-160	1168	0.51	-183	1188	0.47
1992	23	-274	1387	0.21	-286	1396	0.17
1993	23	-423	1376	0.21	-444	1385	0.17
1994	24	-276	1328	0.29	-284	1348	0.25
1995	29	-347	1199	0.47	-381	1222	0.44
1996	32	50	759	0.83	44	754	0.82
1997	45	-38	1055	0.66	-43	1048	0.66
1998	46	-201	1061	0.66	-212	1053	0.64
1999	44	-471	1249	0.41	-484	1247	0.41
2000	51	-405	1299	0.33	-416	1292	0.33
2001	55	-151	1167	0.51	-156	1156	0.51
2002	52	32	848	0.80	27	847	0.80
2003	46	-106	1120	0.58	-114	1112	0.58
2004	55	37	921	0.75	29	918	0.75
2005	33	-612	1291	0.33	-616	1278	0.33
2006	46	-93	1097	0.61	-100	1085	0.61
2007	35	-817	1347	0.25	-843	1347	0.25
2008	43	-806	1397	0.17	-823	1406	0.14
2009	41	-586	1338	0.25	-630	1355	0.21
2010	38	-194	1141	0.55	-216	1156	0.51
2011	28	-987	1428	0.13	-1012	1440	0.11
2012	39	-951	1442	0.10	-974	1458	0.09
2013	28	45	858	0.80	73	857	0.78
2014	39	-	-	-	-417	1329	0.25

Table 3.1: Surface mass balance values and attributes calculated using the reference (ref) and conventional (con) hypsometry matrices, which are recommended as an update to the previous WGMS published versions. Mass balance (B) is provided in mm w.e., ELA is the equilibrium line altitude in meters, and AAR refers to the accumulation area ratio.

	Translation (m)			**Stable terrain *dh* (m)**	
	E	N	Z	Avg. *dh*	σ_{dh}
No rotation; no translation	0	0	0	12.95	8.28
No rotation; translation	–12.2	19.5	10.4	–1.32	7.15
Rotation (0.412° (ccw); no translation	0	0	0	4.82	6.69
Rotation (0.412° (ccw); translation	**10.7**	**–16.5**	**–9.4**	**–0.78**	**5.08**

Table 3.2: Coregistration parameters for homogenization of 1960 and 2014 DEM areas over stable terrain using rotation and translation, where ccw indicates counter clockwise rotation. Final parameters applied to the full DEMs are in bold.

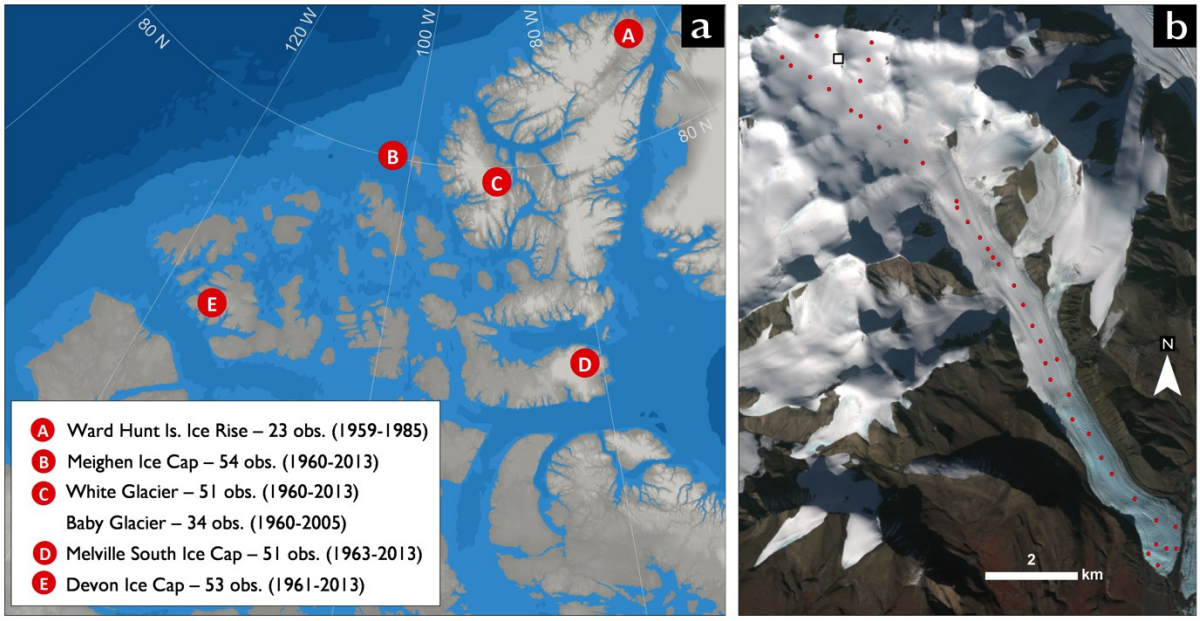

Figure 3.1: (a) Locations of glaciers in the CAA with published mass balance records exceeding 10 years in duration. "Obs." refers to the number of years of observations. (b) SPOT 5 composite image of White Glacier, August 29, 2008. Mass balance stakes measured in 2014 are indicated in red and the white box notes the location of the nunatak time-lapse camera.

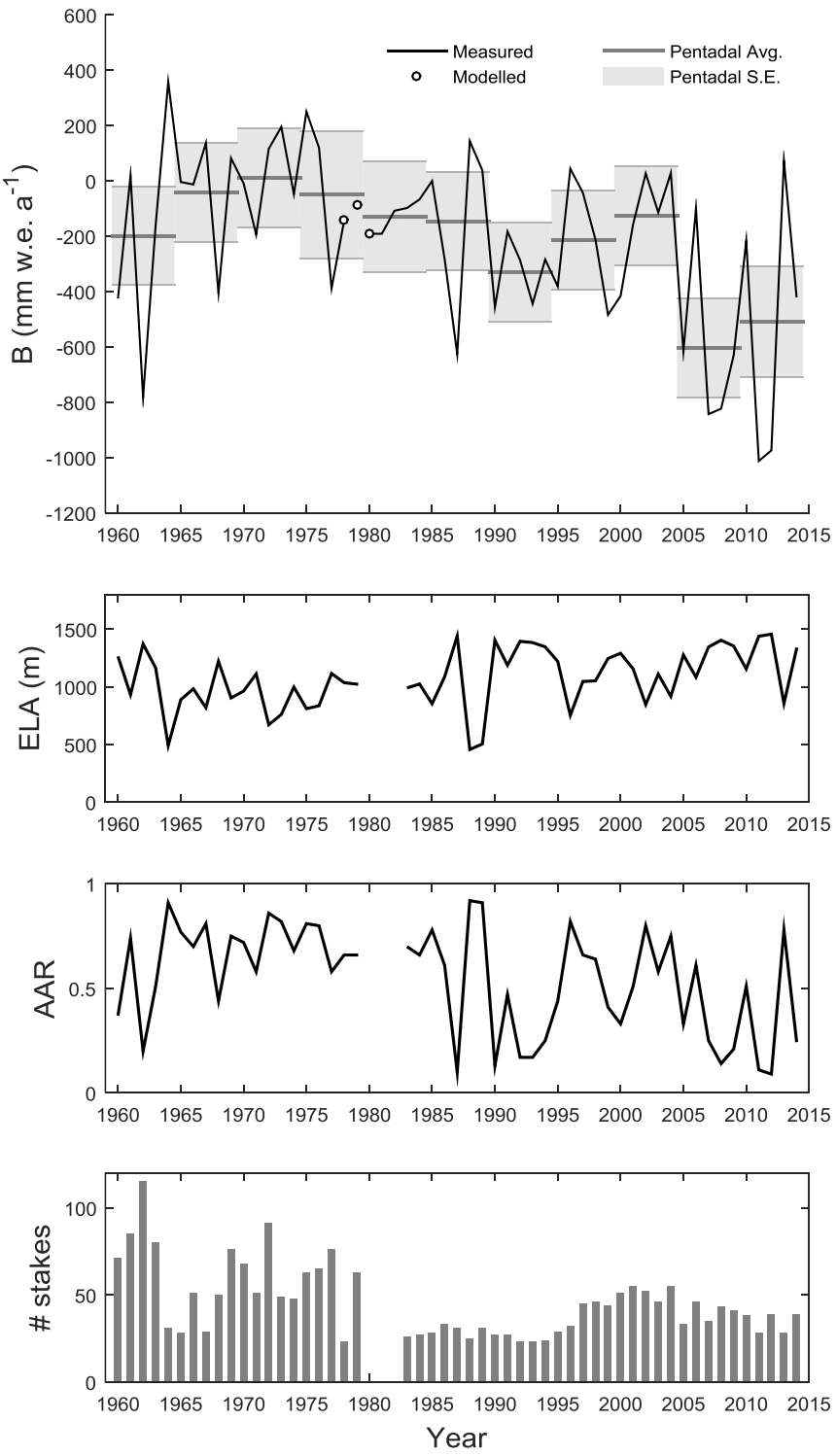

Figure 3.2: (a) The 55 year record of glaciological mass balance (*B*) with pentadal averages and standard errors; (b) Equilibrium line altitudes (ELA); (c) Accumulation area ratios (AAR); and (d) number of mass balance stakes in network.

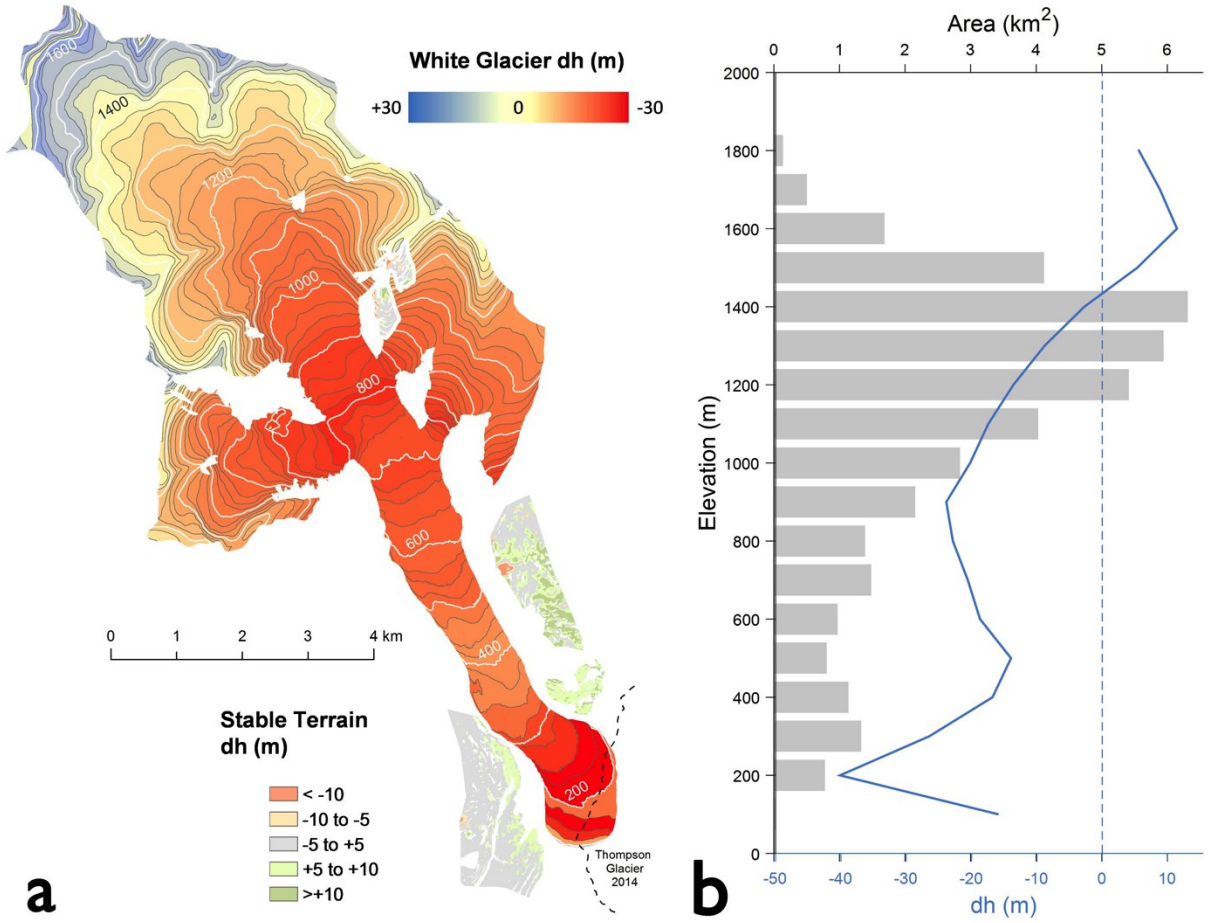

Figure 3.3: (a) Average change in elevation (*dh*) between 1960 and 2014 observed in each 25 m hypsometric band (1960 hypsometry and extent shown). The upper right legend refers to elevation changes over ice, while the lower left legend indicates elevation differences over stable terrain following the DEM coregistration. The position of the Thompson Glacier terminus as of 2014 is illustrated in the lower right. (b) White Glacier hypsometry (1960; grey bars) and observed elevation changes (blue line) over PoR for 100 m elevation bands.

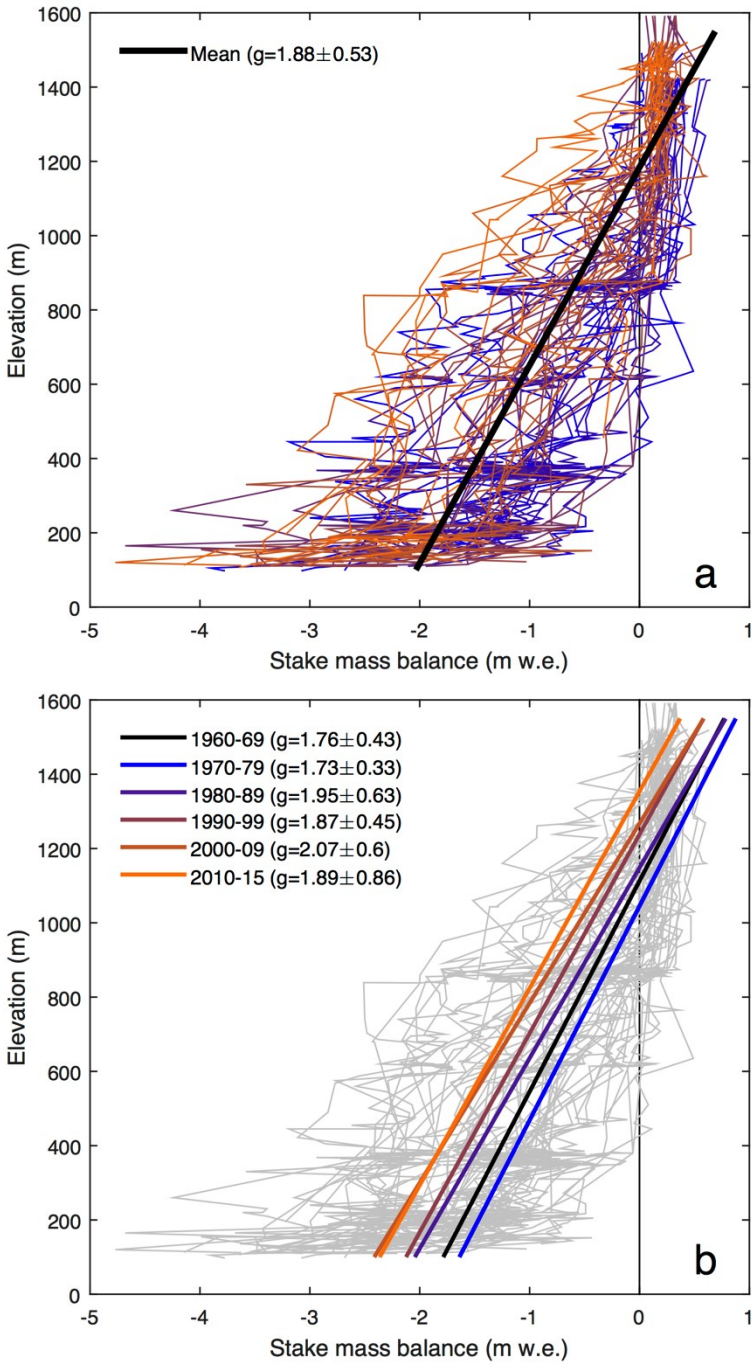

Figure 3.4: (a) Stake mass balances for 1960-2014 tending from blue to orange colours over the PoR. The overlying black line indicates the average linear mass balance gradient. (b) Progression of the decadal mass balance gradients from 1960-2014, ending with the 2010-2014 pentadal gradient. Mass balance gradients are in m w.e. km^{-1}.

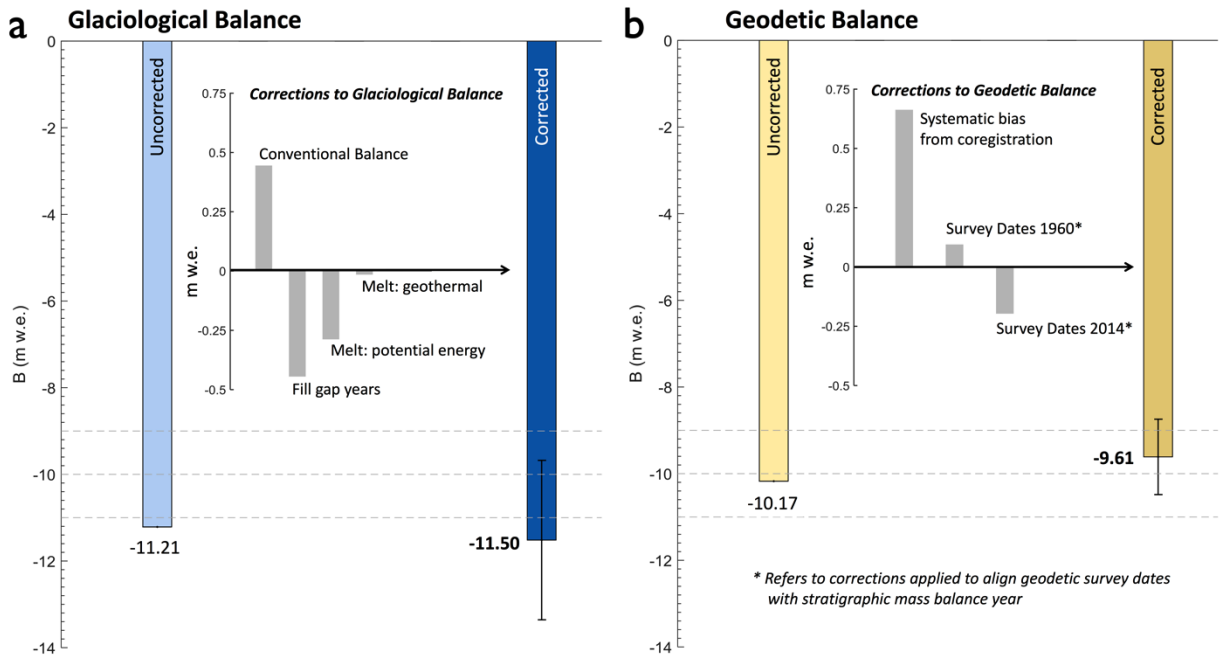

Figure 3.5: Uncorrected and corrected balances from (a) the glaciological method and (b) the geodetic method. A breakdown of the corrections applied to each method to homogenize the balances is shown as inset graphs.

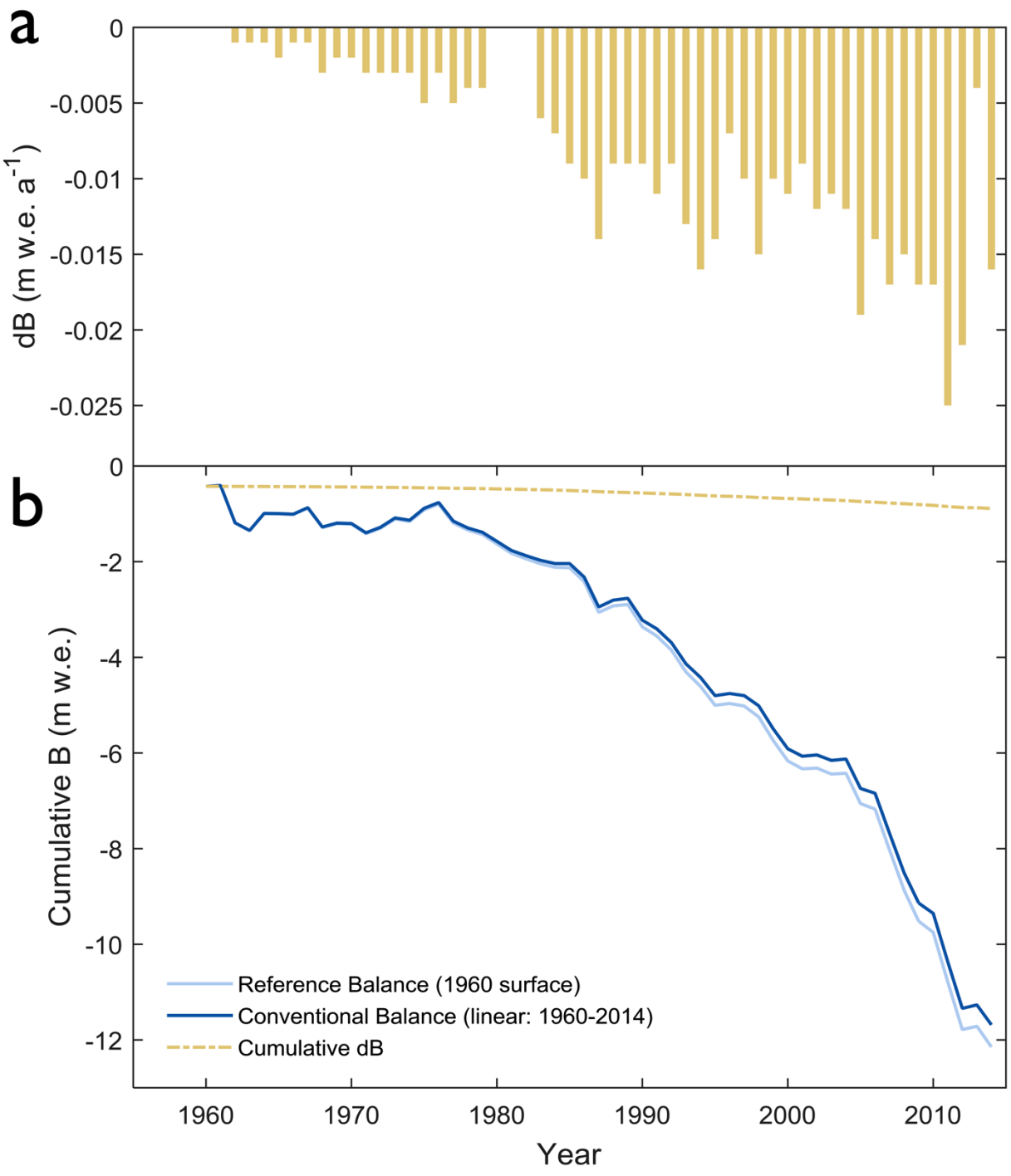

Figure 3.6: (a) Difference (*dB*) between the reference (measured) and conventional (modelled based on a linear change in hypsometry) glaciological balances from 1960 to 2014. (b) Cumulative balances over the 55-year period with the cumulative difference (*dB*) plotted above.

CHAPTER 4: OBSERVATIONS OF MULTI-DECADAL VELOCITY FLUCTUATIONS AND MECHANISMS DRIVING LONG-TERM SLOWDOWN

4.1. ARTICLE 3 SUMMARY AND ATTESTATION

Annual and seasonal surface velocities measured continuously from 1960-1970 at White Glacier provide the most comprehensive historical record of ice dynamics in the Canadian Arctic. Comparison with dual-frequency GPS-derived velocity data spanning 2012-2016 reveals a general trend of decreasing ice motion of 10–45%, particularly towards the glacier terminus. However, an observed increase in summer velocities at high elevations suggests that increased surface-melt and delivery of this water to the glacier bed through moulins has initiated basal sliding in a zone that was not subject to significant melt or sliding in earlier decades. The long-term decrease in ice motion in the lower ablation area of the glacier can be explained by both decreases in internal deformation driven by reductions in ice thickness of ~15-20 m since the 1960s, and by reduced basal motion. Despite the long-term slowdown, comparison with theoretical balance velocities indicates that the flow regime of White Glacier over the period of record is unsustainable with the current climate.

This study was conducted by Laura Thomson with contributions from Luke Copland. Laura Thomson was responsible for the compilation of historic data [*Iken*, 1974; *Müller and Iken*, 1973] and the collection, post-processing, analysis, and interpretation of contemporary velocity measurements. An article based on the following chapter was submitted to *Journal of Glaciology* in July 2016 under the title "Long-term reduction in velocities glacier and mechanisms driving deceleration at polythermal White Glacier, Arctic Canada" and was coauthored by Laura Thomson and Luke Copland.

4.2 INTRODUCTION

With a change in climate, glaciers can be expected to adjust their extent, thickness, and flow dynamics to a configuration that is in 'steady state' with the new climate [*Benn and Evans*, 2010]. Glacier mass balance determines the rate of mass transfer required for a glacier to maintain a geometry in 'steady state', such that mass gains at higher elevations are transferred down-glacier

at a rate that compensates mass and elevation losses at lower elevations [*Nye*, 1960]. This rate of mass movement should define a glacier's overall velocity structure, although local velocity patterns are complicated by the variety of mechanisms and processes that define glacier motion. The mechanics of ice flow are attributable to three primary processes: the deformation of ice (creep) under gravity [*Glen*, 1955]; basal motion associated with sliding at the bed [*Fowler*, 2010]; and basal motion associated with the deformation of the bed [*Van der Meer et al.*, 2003]. For a given ice thickness, ice deformation rates are strongly related to ice temperature, and basal sliding and basal sediment deformation are believed to only occur where water is present at the glacier bed where the ice reaches the pressure melting point.

Under a changing climate, the mechanisms of ice motion might be expected to change due to changes in ice thickness, ice temperature, and the presence of basal water, but there is currently considerable uncertainty concerning the direction and magnitude of these changes. For example, it has been suggested that the speedup of Jakobshavn Isbrae and other outlet glaciers on the western coast of Greenland are driven by enhanced surface melt at increasingly higher elevations, prompting increased water pressure at the bed and acceleration of the glacier, thus inducing a potential positive-feedback cycle whereby dynamic thinning as acceleration draws down high-elevation ice to lower, warmer elevations [*Zwally et al.*, 2002]. In contrast, other studies suggest a buffering to this "Zwally effect" in which efficient drainage systems at the glacier bed are able to develop under high and continuous melt conditions, thus rapidly removing water from the bed and ultimately reducing the basal water pressures and leading to a slowing of the ice [*Schoof*, 2010; *Sundal et al.*, 2011].

There are limited measurements of multi-decadal changes in glacier velocities. One of the few studies used repeat optical feature-tracking of satellite imagery across several glaciated regions to indicate that the majority of ice masses have decelerated over time periods spanning up to 50 years [*Heid and Kääb*, 2012]. This observed slow-down was mainly attributed to reduced ice flux as a result of negative mass balance conditions. Other studies of velocity fluctuations of land-terminating glaciers over several decades show periods of acceleration and deceleration associated with corresponding increases or decreases in mass balance and ice thickness [*Vincent et al.*, 2009]. However, since 2000 consistent deceleration appears to be the dominant response, particularly towards glacier termini [*Kaufmann et al.*, 2015; *Tedstone et al.*, 2015; *Waechter et al.*, 2015]. In the Canadian Arctic Archipelago (CAA), which is currently responsible for the largest

glacier mass losses outside of the ice sheets [*Gardner et al.*, 2013; *Harig and Simons*, 2016], multi-decadal changes in ice motion are poorly constrained. Comparison of velocity maps from 2000 and 2011-2015 [*Van Wychen et al.*, 2016] identified that out of 117 large outlet glaciers on Ellesmere and Axel Heiberg Islands, 7% had slowed by >20 m a^{-1}, 2% had accelerated, and 5% showed periods of both acceleration and deceleration. No velocity changes were detectable on the remaining 86% of glaciers, which were generally all slower moving ice masses (<50 m a^{-1}).

Most previous measurements of changes in glacier velocity have focused on large ice caps and outlet glaciers, meaning that the long-term velocity changes of slow moving ice masses (<100 m a^{-1}) remain relatively unknown. While mountain and valley glaciers comprise a minority of glacier-covered area in the CAA (e.g. 26% on Axel Heiberg Island), they demonstrate a greater sensitivity to climate warming both in terms of area change and mass balance [*Dowdeswell et al.*, 1997; *Paul*, 2004; *Thomson et al.*, 2011]. One location where it is possible to study detailed patterns of short- and long-term changes in surface velocities is White Glacier, Axel Heiberg Island, where Almut Iken conducted her first pioneering studies showing that surface meltwater was both able to reach the glacier bed and lead to enhanced subglacial water pressures that facilitated basal sliding [*Flowers*, 2010; *Iken*, 1974]. These observations were corroborated by measurements of englacial ice temperature gradients that supported the existence of a temperate basal ice zone below the equilibrium line [*Blatter*, 1987a]. The record of ice velocities at White Glacier, dating from 1960-1973, is unprecedented in the Canadian Arctic and provides a unique opportunity to observe changes to the flow regime of polythermal mountain glaciers in the CAA. This study focuses on a comparison of annual and seasonal velocity observations measured on White Glacier from 1960-1970 [*Iken*, 1974; *Müller and Iken*, 1973] with contemporary measurements collected between 2012 and 2016 at the same geographic locations. Observed changes in glacier velocities are investigated in terms of the mechanical processes driving ice motion and their variability in a changing climate, including changes to glacier mass balance, ice thickness, and englacial temperatures. While limited observational data is available about the subglacial conditions at White Glacier, a comparison of observed and theoretical surface velocities enable us to infer the extent of basal sliding and estimate the dynamic response time of the glacier.

4.3 STUDY LOCATION

White Glacier is a 40 km^2 mountain glacier measuring ~14 km in length, located on Axel Heiberg Island in the Canadian Arctic Archipelago (Fig. 4.1). It is characterized by a ~5 km wide accumulation area which feeds into a narrow (~1 km wide, 9 km long) valley. Elevations range from 1782 m a.s.l. in accumulation area to 100 m a.s.l. at the glacier terminus. The region experiences mean annual temperatures of approximately -20°C and annual precipitation ranges from 58 mm a^{-1} at sea level (as measured at Eureka, 125 km to the northeast) to 370 mm a^{-1} at 2120 m a.s.l. [*Cogley et al.*, 1996].

Between 1960 and 1980, White Glacier was the focus of numerous glaciological studies, including mapping campaigns [*Haumann and Honegger*, 1964], englacial temperature measurements [*Blatter*, 1987a], and velocity surveys at glacier cross-sectional profiles [*Iken*, 1974; *Müller and Iken*, 1973]. Together, these early studies provide important baseline information for this study, as well as a 55-year mass balance record. Surface mass balance measurements have continued on a near annual basis since 1959 and the observed balance has become increasingly negative since 2005 [*Cogley et al.*, 2011a; *Thomson et al.*, 2016], a trend that was not statistically significant between 1960 and 1991 [*Cogley et al.*, 1996]. There is good agreement between the cumulative annual surface balance measurements (–213 ± 28 mm w.e. a^{-1}) and the geodetic balance (–178 ± 16 mm w.e. a^{-1}) calculated over the period 1960-2014. The geodetic data indicates that thinning has occurred along the length of the glacier below 1400 m a.s.l. since 1960, with losses exceeding 50 m near the terminus.

The historic (1960-70) and recent (2012-16) velocity measurements were collected at three profiles located 8.5 km, 5.5 km, and 3.2 km from the glacier terminus (Figure 4.1). The upper profile (historically referred to as 'Moraine Profile') is at 870 m a.s.l. and was located near the mean equilibrium line observed during the 1960s, while the middle ('Wind Profile', 580 m a.s.l.) and lower ('Anniversary Profile', 370 m a.s.l.) profiles are well within the ablation zone since the onset of measurements at White Glacier. The average equilibrium line altitude (ELA) at the time of early velocity observations (1960-70) was 990 ± 160 m a.s.l. and located approximately 2 km up-glacier of the upper profile, but has since risen to 1270 ± 190 m a.s.l. in the last decade (2005-2015), which equates to approximately 3.5 km up-glacier [*Thomson et al.*, 2016].

4.4 METHODS

4.4.1 Velocity observations 1960-1970

Between 1960 and 1968 surveys of annual (v_a), winter (v_w), and summer (v_s) velocities were compiled in *Müller and Iken* [1973], along with calculations of the mean increase in v_s over v_a (Δv), melt season duration (s), movement increment during the melt season (Δd), and ablation (a). Glacier velocities were observed at the upper and lower profiles from repeat stake positions measured by theodolite surveys of baseline cairns setup along the margins of the glacier [*Müller and Iken*, 1973]. These velocity measurements motivated later detailed studies of daily to seasonal velocity fluctuations by Almut Iken from 1968-1970 as part of her PhD dissertation [*Iken*, 1974]; this study therefore extends beyond the *Müller and Iken* [1973] dataset for the upper and lower profiles by incorporating the velocity data recorded at the middle profile by *Iken* [1974].

The survey timing at the onset and end of each melt season enabled the calculation of mean annual and seasonal glacier velocities, with v_a being defined as the total displacement observed over one winter season and the following summer melt season (e.g. late-summer 1960 to late-summer 1961). Velocity errors were calculated from "*repeated and 180° reversed readings from the two ends of a base line*" and range from 0.01 to 1.48 cm d^{-1} [*Müller and Iken*, 1973]. For each station, the duration of the melt period (s) was defined by the number of days for which the 5-day mean daily temperatures surpassed 0°C. These measurements were collected using thermographs and recorders maintained by members of the research expedition at each of the three stations [*Müller*, 1963]. Ablation at each profile was approximated from the mean annual ablation measured at 5-10 stakes installed across the profile. When *in situ* observations of ablation or temperature (for the calculation of s) were not available, estimates were made by interpolation between the highest and lowest observation sites, or in a few cases extrapolated from climate data at the Eureka weather station on Ellesmere Island, 125 km northeast of White Glacier (Fig. 4.1a; see Environment Canada Archive: http://climate.weather.gc.ca/). The errors in s and a (Table 4.1) consequently reflect the uncertainties associated with extrapolated climate and ablation data. The applicability of Eureka climate data for conditions at White Glacier in the early studies (1960-70) is currently unknown, although comparison s derived from summer temperatures at Eureka and temperatures recorded at an automatic weather station located at the White Glacier terminus from

2012 to 2015 indicate that the average difference in mean daily temperatures is <1°C and maximum residuals do not exceed 5°C (Figure 4.2).

4.4.2 Velocity observations 2012-2016

In 2012, velocity measurements were re-initiated on White Glacier with three Trimble R7 dual-frequency GPS (dGPS) units that were installed at the middle profile in April 2012, at the upper profile in April 2013, and at the lower profile in July 2013. The dGPS antennae were mounted on steel poles drilled ~3.5 m into the ice and powered using 50-75 amp hour 12 V batteries connected to 20 W solar panels. In 2012 the middle dGPS was initially configured to collect positions every 15 s for 1 hour between 12h00 and 13h00 local time daily, in an effort to prolong the operating period into the winter months. However, starting in spring 2013 all of the dGPS units were operated continuously every spring/summer with a 15 s sampling frequency. Post-processing of dual-frequency GPS data utilized the Precise Point Positioning (PPP) tool provided by Natural Resources Canada (http://webapp.geod.nrcan.gc.ca/geod/tools-outils/ppp.php), in which the signal timing between ground stations and receiving satellites, alongside well-constrained satellite orbital positions, are used to generate baselines for trilateration and positioning. PPP analysis was conducted using the precise satellite orbits, which are released ~10 days after data acquisition. This provides three-dimensional (x, y, z) accuracies of approximately ± 2 cm for an observation period of 1 hour. Appendix 3 provides the daily station coordinates through the duration of this study.

For comparison with the *Müller and Iken* [1973] and *Iken* [1974] datasets, it was first necessary to define the span of the melt season (*s*) within which v_s would be calculated, and the final day of the melt period that defines the start of the v_w and v_a sample period. As in the earlier studies, *s* was defined as the period in which the 5-day mean daily temperature surpassed 0°C. Shielded HOBO-U23 temperature/relative humidity loggers mounted on poles 1-3 m above the ice at each dGPS station were used to calculate *s*, and data gaps were filled by modelled temperatures using daily temperature lapse-rates derived from two automatic weather stations (AWS) at the glacier terminus and an upper nunatak (Figure 4.1). Annual ablation (*a*) was modelled for each station using the annual mass balance gradient determined from stake measurements along the glacier centreline. The goodness of fit of the polynomial (n=3) expression of mass balance gradient that is used to calculate glacier-wide surface mass balance shows an R^2 greater than 0.9 for >90% of the 55 years with observations, and a fit greater than 0.95 for >65% of the record. The mean

summer velocity (v_s) is determined from displacement between the daily mean positions of the first and last days of *s*, divided by *s*. Errors in dGPS derived velocities are based on a calculation of the RMSE incorporating the standard deviation of the daily positions divided by the duration of *s*.

4.4.3 Surface elevations

The 1:10,000 map of White Glacier by *Haumann and Honegger* [1964] was used as the primary source of ice surface elevations between 1960-70. This map, plotted in a local planar coordinate system with 10 m contours (vertical accuracy considered to be 5 m) was created using a combination of field-based surveying and photogrammetry methods. A summary of the mapping techniques for *Haumann and Honegger* [1964] and associated references are provided in the World Glacier Monitoring Service's Fluctuations of Glaciers Maps data archive (http://wgms.ch/products_fog_maps/). A digital elevation model derived from this map was used to extract point elevations along the cross-sectional velocity profiles [*Thomson and Copland*, 2016]. Contemporary surface elevations, based on measurements made in 2014, were derived from kinematic dGPS measurements collected with a Trimble R7 system mounted on a skidoo and post-processed with the same online PPP tool as the aforementioned dGPS stations. A 1:10,000 map of White Glacier produced using >400 oblique air photos and Structure from Motion photogrammetry methods supported determination of elevations near the glacier margins where dGPS measurements were not possible [*Thomson and Copland*, 2016]. This map, with a 5 m vertical accuracy, was also valuable in assessing the amplitude and spatial variability of ice thinning along the trunk of White Glacier. The 1960 and 2014 DEMs were used to derive glacier surface slope at each of the three velocity profiles over an along-glacier distance of 2 km (Figure 4.3).

4.4.4 Ice thickness

Cross-sectional ice depth profiles for the three stations were collected in 2014 using a 10 MHz ice penetrating radar system equipped with GPS, as described by *Mingo and Flowers* [2010]. Assuming a radar wave speed in ice of 1.68×10^8 m s^{-1}, the glacier bed was clearly identifiable at the lower and middle profiles with an estimated vertical error of <10 m [*Wilson*, 2012]. At the upper profile, challenges in interpreting radar returns due to steep rock walls adjacent to the profile

resulted in only a single successful measurement of ice thickness, located near the glacier centreline at the site of the dGPS station. A polynomial regression through the observations was used to estimate the glacier bed in regions where surface conditions restricted radar measurements (primarily close to the glacier margins). A parabolic curve best described the measured basal profiles at the lower and middle sites, with R^2 values exceeding 0.9. It was assumed that the bed profile at the upper profile exhibited a similar parabolic profile to the two lower stations, so the cross-sectional area of this profile was estimated by fitting a polynomial (n=2) regression through the single measured ice thickness near the glacier centre and 0 m ice thickness at the glacier margins (Figure 4.4). The results of the ice radar measurements show reasonable agreement (± 50 m) with early seismic and gravity-based observations of ice thickness conducted in 1961-1962 [*Müller*, 1963].

Given the superior accuracy of ice surface elevation measurements, changes in ice thickness were derived from changes in surface height between 1960-70 and 2014 (described above), rather than comparison of present ice thickness measurements with historic gravity and seismic observations collected between 1970-1980 [*Müller*, 1963]. This approach assumes that basal erosion processes are negligible.

4.5 RESULTS

Annual, winter and summer glacier velocities were calculated for 2012-2016 at the upper, middle, and lower profiles following the criteria of *Müller and Iken* [1973] and are shown with the 1960-70 measurements in Figure 4.5. Comparing the historic and contemporary observations, mean annual velocities decreased at the middle profile from 10.53 cm d^{-1} to 7.31 cm d^{-1} (down 31%) and from 8.64 cm d^{-1} to 5.40 cm d^{-1} (down 38%) at the lower profile. Mean annual velocities at the upper station do not show a statistically significant change within their combined errors (0.82 cm d^{-1}). Mean winter velocities showed a similar trend to the annual velocities with decreases of 31% (9.62 cm d^{-1} to 6.72 cm d^{-1}) and 45% (8.08 cm d^{-1} to 4.45 cm d^{-1}) at the middle and lower profiles, respectively, and a smaller decrease at the upper profile (3.5%) that is not statistically significant. The summer patterns are somewhat different; the middle and lower sites exhibited decreased mean summer velocities by 12% (11.73 cm d^{-1} to 10.38 cm d^{-1}) and 35% (11.97 cm d^{-1} to 7.75 cm d^{-1}), respectively, but the upper station exhibited a 12% increase (11.49 cm d^{-1} to 13.37

cm d^{-1}) in mean summer velocity since 1960-70. The detailed velocity time series, including information on the length of the summer period (*s*), ablation (*a*), and associated errors are given in Table 4.1, which builds upon the record presented in *Müller and Iken* [1973]. At the upper and lower profiles, where the historic record of measurements spans 10 years, we find that the percent contribution of summer motion to annual velocity has increased from 2% to 8% at the upper profile over the period of record, and from 8% to 15% at the lower profile. We also find that the difference between winter and annual velocities has increased. In the 1960s, winter velocities were 2% and 8% slower than annual velocities at the upper and lower profiles, respectively, whereas presently they are 6% and 14% slower.

The longitudinal pattern of ice velocities has also changed from the 1960-70 observations of *Müller and Iken* [1973], who observed that v_a decreased from the upper to middle profiles and then showed a slight increase to the lower profile, after which the velocity declined steeply towards the terminus. Our new results indicate a continuous decrease in annual velocity from the upper profile towards the terminus, with no increase near the lower profile.

The average duration of the summer melt period (*s*) has increased across the glacier between the 1960s and today, with the largest change at the upper profile where melt conditions prevail for 18 days longer per year (Figure 4.6). This corresponds to a 53% increase in melt at the upper profile in recent years (2011-2015) in comparison to the mean ablation observed from 1960-70. The increase in *s* is not as large at the lower profile, only 15 days longer than the 1960-70 average of 65 days, although the increase in ablation is greater than at the upper station with a 73% increase in melt being observed since the observations of *Müller and Iken* [1973].

4.6 DISCUSSION

To investigate the potential causes of the observed long-term slowdown in the lower parts of White Glacier, and lack thereof at the upper profile, we consider how the primary influences on glacier motion may have changed over time, including internal deformation, basal motion, and surface mass balance. Additionally, we assess how changes in ice thickness, duration of the melt period, ablation, and potential changes in englacial temperatures have impacted the processes controlling ice velocities.

4.6.1 Internal deformation

Following from Glen's [1955] flow law and the formulations of *Nye* [1965], which describes the role of the glacier bed profile on ice deformation at the glacier centreline, we applied the method of *Nolan et al.* [1995] to calculate the surface motion due to ice deformation at the three velocity profiles using:

$$U_d = 2A(n+1)^{-1}\,(\rho g H \sin\alpha)^n\, H^{n+1}\, f^n \qquad \text{(Eq. 1).}$$

Here U_d refers to the centreline velocity due to ice deformation and is a function of the rate factor (A), the flow-law exponent (n=3), basal shear stress, which is the product of ice density (ρ = 900 kg m^{-3}), gravity (g = 9.8 m s^{-2}), ice thickness (H), surface slope (α), and the shape factor (f). Surface slope α was determined by a linear regression through a 2 km longitudinal transect of surface elevations centered on each station using the 1960 and 2014 topographic models of the glacier [*Thomson and Copland*, 2016] and are shown in Figure 4.3. The ice radar results (Figure 4.4) indicate that the glacier cross-section is approximately parabolic in the study areas, and thus we utilize the parameterization of Nye's [1965] parabolic shape factor values by *Nolan et al.* [1995], which calculates f based upon the ratio between the glacier half-width and ice thickness at the centreline.

In many studies the rate factor A is commonly stated as a constant, which is a reasonable assumption for temperate glaciers where ice temperatures are generally homogeneous and at or very near the pressure melting point. However, with englacial temperatures ranging from -15°C to very near 0°C in White Glacier [*Blatter*, 1987a], it is less clear how one should define A. The rate factor changes as a function of temperature according to the Arrhenius relation:

$$A = A_o \exp(-Q/RT) \qquad \text{(Eq. 2)}$$

where A_o = 2.95 x 10^{-9} (independent of temperature), the activation energy of creep Q = 7.88 x 10^4 [*Weertman*, 1983], R = 8.31 J mol^{-1} K^{-1} is the universal gas constant, and T is the ice temperature. Using temperature profiles from boreholes drilled at each of the three velocity profiles between 1976 and 1981, we apply a discretization to account for the variability of ice temperature with depth and the subsequent impact on A and U_d. Starting from the glacier bed, the mean temperature

of 50 m thick segments was calculated for the upper, middle, and lower profiles using englacial temperature profiles from the boreholes '3/81', '4/80', and '1/76' of *Blatter* [1987a], respectively (Figure 4.7a-c). It should be noted that the borehole at the upper station was roughly 100 m short of the glacier bed, so a linear regression through the lower portion of the profile was used to estimate the temperatures between the deepest drill depth of 260 m and the bed. From the mean temperature ($\bar{T}$) of each 50 m layer, A was calculated using Eq. 2 and the resulting velocity of each layer attributable to ice deformation (U_d) was determined from Eq. 1. The sum of U_d values from each layer thus provides the expected surface velocity attributable to ice deformation at the centreline (Figure 4.7d-f).

As Eq. 1 indicates, decreases in ice thickness H induce exponential decreases in U_d. For each station, contemporary ice thickness measurements were determined using the radar methods and elevation data described in Section 4.4.4. Changes in ice thickness (dH) between 1960 and 2014 at the three stations were: dH_{upper} = -23 m, dH_{middle} = -19.5 m, and dH_{lower} = -19 m. The slightly smaller ice thinning at the middle and lower stations is likely attributable to shadowing effects at these sites, where the glacier is narrower and confined by steep valley walls. It is also possible that dynamic thinning is occurring due to flux-divergence at the upper station, notably the only station that did not demonstrate a statistically significant decrease in v_a between the 1960s and present day.

Arguments exist that support both increases and decreases in englacial temperatures under a warming climate and thinning glacier, with the outcome depending on the dominant processes taking place [*Wilson and Flowers*, 2013]. For example, heat delivered from supraglacial meltwaters to the glacier bed followed by refreezing and the release of latent heat has been presented as a mechanism for warming and softening the base of the Greenland Ice Sheet [*Bell et al.*, 2014]. Conversely, for smaller ice masses it has been demonstrated that the loss of ice thickness reduces englacial strain heating and the capacity for reaching pressure melting point with decreased overburden pressure [*Rippin et al.*, 2011]. A 3°C warming of annual air temperatures over the past 60 years has been observed at Eureka station [*Lesins et al.*, 2010], but without concrete evidence of how englacial temperatures might be changing at White Glacier we investigate the possibility of both ice warming and cooling in this analysis.

Considering the observed changes in ice thickness and potential changes in englacial temperatures over the past several decades, the above methodology was applied to estimate the centreline velocity attributable to ice deformation under the following scenarios:

(1) Historic (1960-70) ice thickness (H) and $\bar{T}$ values (denoted as $U_{1960\text{-}70}$);

(2) Changing ice thickness (dH, 1960 to 2014) and historic $\bar{T}$ values (U_{dH});

(3) Changing ice thickness (dH) and a -1°C change to historic $\bar{T}$ values ($U_{dH\,-1°C}$);

(4) Changing ice thickness (dH) and a +1°C change to historic $\bar{T}$ values ($U_{dH\,+1°C}$).

In scenario 4, if the temperature increase led to temperatures >0°C these layers were assigned a maximum temperature of -0.1°C.

From these scenarios (Figure 4.7d-f), we see that changes in ice thickness alone decrease deformation rates by 29%, 27%, and 37% respectively at the upper, middle, and lower stations. A 1°C decrease in temperature along the entire temperature profile would theoretically lead to a further 10-15% decrease in deformation rates at each profile, whereas 1°C of englacial warming results in ice deformation rates approaching (or exceeding, in the case of the lower profile) those modeled from 1960-70. The consequences of changing englacial temperatures are most significant at the lower station, which has the warmest temperature profile. This is likely because deformation rates are particularly sensitive at temperatures approaching the pressure melting point (~0°C), where ice deforms at a rate >100 times faster than ice at -20°C [*Hambrey*, 1994]. We also find that the proportion of net motion attributable to the deformation of the deepest 50 m of ice increases from the upper (63%) to the middle (77%) and lower (86%) stations as englacial temperatures near the bed also increase. Additionally, we find that the modeled depth-averaged velocities, based on the profiles in Figure 4.7, are very close to the modeled surface velocities (95-96%) and varied by <1% between stations.

4.6.2 Basal motion

Where the modeled deformation rates fail to meet the observed surface velocities, it is generally accepted that the residual motion is due to basal sliding or deformation of the bed [*Copland et al.*, 2003b; *Hubbard et al.*, 1998; *Minchew et al.*, 2015]. We are unable to discriminate between the relative importance of basal sliding vs. bed deformation processes at the bed of White Glacier, so from hereon we refer to any motion at the bed simply as basal motion.

4.6.2.1 Winter basal motion

The findings of Iken (1974) provided the first evidence that basal motion was able to occur beneath mostly-cold polythermal Arctic glaciers during the melt season. More recent studies have indicated that basal motion can also continue through the winter months on polythermal glaciers, as has been observed at John Evans Glacier on Ellesmere Island [*Bingham et al.*, 2003; *Copland et al.*, 2003a] and McCall Glacier, Alaska [*Rabus and Echelmeyer*, 1997].

From the ice deformation model results in scenario 1, with historic ice thickness and englacial temperature conditions ($U_{1960\text{-}70}$), we find that ice deformation fully accounts for observed winter velocities at the upper station, but that basal motion is required to explain 47% of the observed wintertime motion at the middle profile, and 15% at the lower profile (Figure 4.8). This finding agrees with the suggestion of *Blatter* [1987a], based on observed ice thicknesses and temperature profiles, that basal sliding begins just down-glacier of the upper profile where englacial temperatures closest to the bed transition from approximately -6°C to >-1°C.

For contemporary velocities (2012-16) reductions in H alone (scenario 2; U_{dH}) have led to a decrease in deformation rates at all stations since 1960-70 (Figure 4.8). Of particular note is the observed onset of wintertime basal motion that appears to have occurred at the upper profile since 1960-70. This essentially offsets the decrease in ice deformation in that region, such that the overall changes in v_w at the upper profile are negligible. Downstream of the upper profile, the proportion of wintertime basal motion has decreased since 1960-70, particularly at the lower profile where internal deformation now accounts for >95% of v_w (assuming no changes in englacial temperatures; U_{dH} = scenario 2). If englacial temperatures have decreased since the observations of *Blatter* [1987a], scenario 3 ($U_{dH\ -1°C}$) indicates that ice deformation rates would have declined correspondingly, and increased basal motion is required to reach contemporary winter velocities at all stations. The converse is true for an increase in englacial temperatures (scenario 4; $U_{dH\ +1°C}$), in which warmer, softer ice will deform more readily.

4.6.2.2 Summer basal motion

The relationship between meltwater delivery to the glacier bed and the resulting magnitude of basal motion is dependent on the efficiency of the subglacial hydrological network [*Flowers*, 2015] and its capacity to maintain basal water pressures that reduce friction at the glacier bed [*Bartholomaus et al.*, 2008]. Glacier speed-up events occur when subglacial water pressures are

high and the subglacial hydrological network is unable to efficiently convey water out of the system, with this behavior observed at both temperate [*Iken and Binschadler*, 1986; *Iken et al.*, 1983] and polythermal glaciers [*Bingham et al.*, 2003; *Copland et al.*, 2003b; *Iken*, 1974]. If the subglacial hydrological network evolves into a system of large conduits that can efficiently drain the system and reduce water pressures at the glacier bed, then even high levels of surface melt and delivery of that water to the bed may not result in glacier speedup, as has been observed and modeled at locations in Greenland [*Schoof*, 2010; *Sundal et al.*, 2011] and the Canadian Arctic [*Copland et al.*, 2003a].

While detailed information about the nature of the subglacial hydrological network at White Glacier is not available, we can make inferences based on the relationships between ablation and summer velocities at the upper and lower stations, where the greatest number of historic observations are available. A weak positive correlation between annual (i.e., summer) ablation and summer velocity at the upper profile, both historically and recently, suggests that basal motion occurs in the summer as a result of an inefficient drainage network that supports high basal water pressures (Figure 4.9). The marked increase in v_s at this profile between the 1960s and present day suggests that over the past half-century the upper profile has shifted flow regimes from being driven exclusively by ice deformation to a combination of ice deformation and basal motion.

A possible mechanism for the increase in v_s at the upper profile relates to the prolonging of s and a rise of the mean ELA from 1000 to 1270 m a.s.l. (± 160 m) since the 1960-70 mean, thereby increasing the area of the up-glacier catchment where meltwater can be produced. The occurrence of many crevasses in this region, some indicative of being the precursors of moulins given supraglacial streamflow into them, suggest that this meltwater is reaching the bed and facilitating basal motion in the past decade.

In contrast to the upper profile, a weak negative correlation was found between annual ablation and v_s at the lower profile from 1960-70, suggesting that an efficient subglacial drainage system was in place over the lower ablation area during this time. Evidence for the presence of a sustained subglacial drainage system down-glacier of the middle profile includes: (1) the occurrence of several large active moulins in locations that have remained stable since the mid-1960s to present; (2) the continued presence of an ice cave that directs a marginal stream beneath the glacier 1 km down-glacier of the lower profile (first reported in the early 1960s by *Maag* [1969]); (3) the recent exposure of very large subglacial and englacial drainage conduits near the

glacier terminus following the collapse of the glacier surface between White Glacier and the adjacent Thompson Glacier in ~2010; (4) the presence of a temperate bed extending from ~200-700 m a.s.l. [*Blatter*, 1987a]. Recent observations hint at a possible positive correlation between v_s and ablation at the lower profile, but with only two observations this is not statistically significant.

4.6.3 Role of mass balance

Over long time periods ice velocities are dictated by glacier mass balance, meaning that the ice mass passing through a flux gate ought to be equal to the net mass input (i.e. cumulative mass balance) of the upstream basin [*Cuffey and Paterson*, 2010]. This theoretical mass turnover is known as the balance flux, and can be used to calculate the balance velocity when divided by the cross-sectional area of a flux gate. For each 25 m elevation band (h) on White Glacier, we calculate the theoretical balance flux (Q_b) for each year of the 55 year mass balance record using:

$$Q_{b(h,t)} = \sum_{i=h}^{h_0} b(i,t)\, s(i,t) \qquad \text{(Eq. 3)}$$

where i ranges from h, a given 25 m elevation band, up to h_0, the maximum elevation, b is the observed elevation band mass balance, s is the area of the elevation band in year t (updated annually by linear interpolation from 1960-2014 in *Thomson et al.* [2016], where t is 0 in 1960).

Plotting the annual and decadal mean balance flux profiles illustrates a nearly constant decline in fluxes towards the present day, with the exception the 1970s (Figure 4.10a). The elevation at which the balance flux profile intersects Q_b=0 indicates the theoretical balance terminus and is the threshold at which ice flux can be sustained by the cumulative mass balance conditions upglacier. The decadal mean profiles suggest that the hypsometry of White Glacier (Figure 4.10b) was dynamically in balance with the climate conditions of the 1970s, the only recent decade in which Q_b=0 at the elevation of the present terminus (~100 m a.s.l.) and for which the decadal mean glacier wide mass balance was ~0 m w.e.. In all other decades, the elevation of the balance terminus is well above the present glacier terminus and since 1990 it has risen above the upper velocity profile (870 m a.s.l), to reach a maximum elevation of 1190 m a.s.l. in 2010-2015.

Observed mass flux (Q_{obs}) through the three velocity profiles, calculated from the product of the depth averaged velocity (~95% of the observed surface velocity; Section 4.6.1) and the

cross-sectional area of the profiles, show that mass fluxes have decreased at all three profiles since the 1960s (Figure 4.10a). At the upper profile, this decline (-16.4 Mt) is entirely attributable to the reduction in the cross-sectional area of the profile as a result of ice thinning, while at the middle and lower profiles both ice thinning and decreased ice velocities have led to the reduced fluxes. For the main glacier trunk below the middle profile, the cumulative decline in mass flux between 1960 and 2014 has reduced the dynamic replenishment of ice mass by 81.5 Mt below the middle profile, and 68.2 Mt below the lower profile. These reductions in mass delivery explain only a small percentage (~2.5%) of the observed mass loss along the glacier terminus below the middle profile (-3427 Mt) and lower profile (-3043 Mt) based on geodetic mass balance (volume-derived) mass changes between 1960 and 2014 [*Thomson et al.*, 2016]. This indicates that the observed ~15 m thinning along the main trunk of White Glacier since 1960 is primarily due to down-wasting (melt), rather than reductions in dynamic mass input. Should ice fluxes along the glacier trunk continue to decline at a linear rate similar to that observed over 1960-2014, stagnant ice conditions (Q_{obs}=0) would hypothetically occur within ~80 years at the lower profile, within 110 years at the middle profile, and within 750 years at the upper profile.

We also find that the dynamic equilibrium line altitude (DELA), defined here as the elevation at which the maximum flux is expected, is consistently above the ELA that is based on the mass balance gradient. This observation contradicts general theory [*Benn and Evans*, 2010; *Cuffey and Paterson*, 2010], which suggests that, for a glacier in steady state, maximum mass turnover (flux) should occur at the ELA. This discrepancy is related to the hypsometry of White Glacier, which the DELA incorporates, but which the mass balance ELA does not because this is defined simply as the elevation at which the mass balance gradient intersects $b(h)$=0. The observed discrepancy between the DELA and ELA therefore emphasizes the importance of basin geometry in the stability of glacier response. The hypsometry of the White Glacier basin reaches its maximum area at elevations of 1300-1500 m a.s.l., meaning that this zone presents an important threshold. Should the long-term mass balance ELA exceed this elevation range, the glacier will likely be reduced to a small cirque-type ice mass, which *Harrison et al.* [2009] characterize as an 'unstable' glacier response. Based on the mass balance record the observed ELA has risen by an average rate of +6 m a^{-1} over the past 55 years, increasing to a rate of +9 m a^{-1} over the past 30 years. If the trend persists, then the average ELA will exceed the 1500 m a.s.l. threshold sometime between ~2040 and 2060.

4.7 CONCLUSIONS

Long-term ice velocities are decreasing at White Glacier with the observed decline being greatest towards the glacier terminus; this result is consistent with studies elsewhere in the Arctic [*Heid and Kääb,* 2012]. One exception is the upper station, which showed an increase in summer velocities suspected to be associated with an increase in meltwater reaching the bed and inducing basal motion that persists beyond the summer melt period. In agreement with *Van Wychen et al.* [2016], we find in our contemporary velocity measurements that winter velocities are ~6-13% slower than annual velocities, an increase in comparison to earlier velocity measurements [*Müller and Iken*, 1973] in which winter velocities were 1-7% lower than annual velocities. Vertical ice deformation profiles modeled using rate parameters based on historic englacial temperature measurements [*Blatter*, 1987a] indicate that ice deformation alone cannot explain contemporary surface velocities. It is therefore highly likely that basal motion occurs at White Glacier through the winter, possibly by means of transient water storage at the glacier bed through the winter months as has been observed at Kennicott Glacier, Alaska [*Bartholomaus et al.*, 2008].

Observed declines in ice flux have not, however, contributed significantly (<2.5%) to observed mass loss along the glacier trunk from 1960-2014. The observed thinning at low elevations is therefore primarily associated with high ablation rates and not reduced dynamic contributions over the past 55 years. It is worthwhile noting that the majority of mass lost between 1960 and 2014 is associated with retreat of the terminus, rather than ice thinning, which acts to buffer the glacier system by removing ice from low elevations where the largest melt rates occur. Therefore, with regard to changes in hypsometry, White Glacier is presently exhibiting a stable response to recent warming. Balance velocities modeled using annual mass balance observations and glacier hypsometry reveal that the current flow regime is unsustainable and that the observed mass fluxes through three cross-sectional profiles currently exceed balance fluxes by >200%. While contemporary ice fluxes appear to be in-sync with mass balance conditions in the 1970s, possibly suggesting a response time of ~50 years, calculation of response time based on the ratio between maximum ice thickness (350-400 m) and the average mass balance at the terminus over the period of record (-2500 mm w.e.) [*Benn and Evans*, 2010], suggests that White Glacier's response time is in fact on the order of 135-155 years. It is expected that ice within the primary

glacier trunk below 400 m a.s.l. will become stagnant within the next ~80 years and within the next 120 years at elevations near 600 m a.s.l. if contemporary deceleration rates continue into the future.

Year	v_a cm d^{-1}	v_w cm d^{-1}	v_s cm d^{-1}	Δv %	s d	Δd cm	a cm w.e.
Upper (Moraine) Profile: 870 m a.s.l.; 8.5 km from terminus; 1.3 km wide.							
1960-61	10.10	10.10 ± 0.2	10.1 ± 0.2	0.2 ± 4	43 ± 5	0	25 ± 4
61-62	10.53	10.15 ± 0.15	13.00 ± 0.5	28 ± 7	49 ± 4	1.40 ± 0.4	143 ± 11
62-63	9.93	-	-	-	38 ± 5	-	54 ± 5
63-64	10.25	-	-	-	-	-	-36
64-65	9.93	-	-	-	-	-	45
65-66	9.99	9.89	11.13 ± 0.5	9 ± 5	28 ± 8	0.35	39 ± 9
66-67	10.23	10.20	11.40 ± 0.4	10 ± 5	10 ± 4	0.12	6 ± 2
67-68	10.43 ± 1.0	10.28	11.73 ± 0.2	15 ± 5	44 ± 6	0.64	98 ± 12
68-69	10.75 ± 1.1	10.53 ± 1.03	11.56 ± 1.16	-	-	-	9 ± 15
69-70	-	11.16 ± 1.05	-	-	-	-	17 ± 15
2011-12	-	-	-	-	-	-	157 ± 0.9
12-13	-	-	12.16 ± 0.13	-	38	-	2 ± 2.6
13-14	10.79 ± 0.10	10.25 ± 0.19	13.93 ± 0.13	39 ± 5	54	2.76	73 ± 0.5
14-15	10.53 ± 0.10	9.70 ± 0.05	14.01 ± 0.10	42 ± 2	68	2.93	128 ± 2.4
15-16	-	9.98 ± 0.08	-	-	-	-	-
Middle (Wind) Profile: 580 m a.s.l.; 5.7 km from terminus; 1.2 km wide.							
1968-69	10.53 ± 1.05	9.62 ± 0.96	11.73 ± 1.17	-	-	-	154± 10
2011-12	-	-	-	-	-	-	208 ± 3
12-13	-	5.72 ± 0.07	10.82 ± 0.05	43	91	2.16	24 ± 1
13-14	6.34 ± 0.04	7.28 ± 0.05	9.32 ± 0.11	-	59	-	126 ± 4
14-15	-	-	11.01 ± 0.03	-	92	-	190 ± 9
15-16	-	7.17 ± 0.04	-	-	83	-	-
Lower (Anniversary) Profile: 370 m a.s.l.; 3.2 km from terminus; 1.0 km wide.							
1960-61	8.29	7.78 ± 0.18	12 ± 1.41	49 ± 18	56 ± 4	2.22 ± 0.67	95 ± 5
61-62	8.86	8.28 ± 0.16	11.41 ± 0.67	46 ± 9	69 ± 5	2.47 ± 0.30	245 ± 7
62-63	7.91	7.38 ± 0.01	11.93 ± 1.48	57 ± 21	56 ± 4	2.41 ± 0.84	139 ± 13
63-64	7.89	-	-	-	-	-	30 ± 7
64-65	8.53	-	-	-	68 ± 7	-	122 ± 4
65-66	8.81	8.25 ± 0.01	11.19 ± 0.39	38 ± 5	68 ± 4	2.09 ± 0.07	123 ± 3
66-67	8.84	7.99 ± 0.01	12.82 ± 0.70	58 ± 10	65 ± 6	3.06 ± 0.13	95 ± 8
67-68	8.81	8.24 ± 0.06	11.09 ± 0.10	36 ± 5	74 ± 4	2.15 ± 0.11	201 ± 8
68-69	9.66 ± 0.96	8.60 ± 0.86	12.90 ± 1.29	-	-	-	127 ± 7
69-70	8.76 ± 0.88	8.08 ± 0.81	12.40 ± 1.24	-	-	-	106 ± 7
2011-12	-	-	-	-	-	-	250 ± 4
12-13	-	-	-	-	55	-	46 ± 1
13-14	5.27 ± 0.02	4.62 ± 0.02	7.37 ± 0.02	58 ± 3	92	2.55 ± 0.04	171 ± 6
14-15	5.52 ± 0.02	4.68 ± 0.02	8.12 ± 0.02	86 ± 3	93	3.20 ± 0.04	230 ± 11
15-16	-	4.04 ± 0.05	-	-	-	-	-

Table 4.1: Annual and seasonal velocity changes in the ablation area of White Glacier where: v_a = mean annual surface velocity; v_w = mean winter surface velocity; v_s = mean summer surface velocity; Δv = mean increase of v_s over average of preceding and succeeding v_w; s = length of "summer" (melt period); Δd = movement increment during melt period = $s(v_s - v_w)$; a = ablation. Observations from 1960-1968 and 1968-1970 originate from Müller and Iken (1973) and Iken (1974), respectively, while observations from 2012-16 result from dGPS measurements conducted in this study.

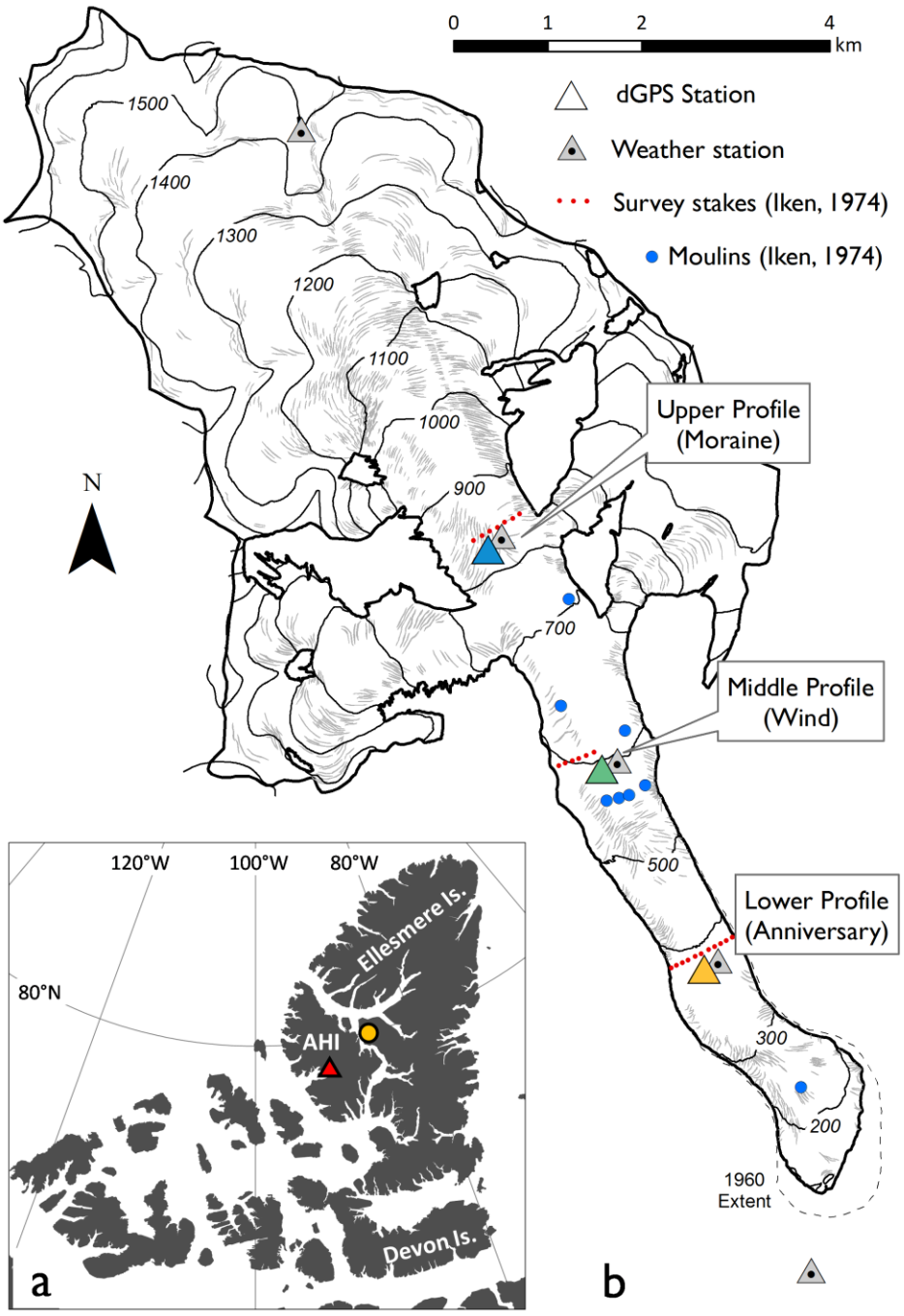

Figure 4.1: (a) Location of White Glacier on Axel Heiberg Island (red triangle) and the Eureka weather station (yellow circle). (b) Map of White Glacier showing the location of 3 cross-sectional profiles and the location of crevasses (light grey lines) and moulins (blue circles) identified in Iken (1974) that are still present as of 2014 Field observations suggest a new moulin has formed within 100 m southeast of the upper profile, but it is not confirmed if it is regularly active.

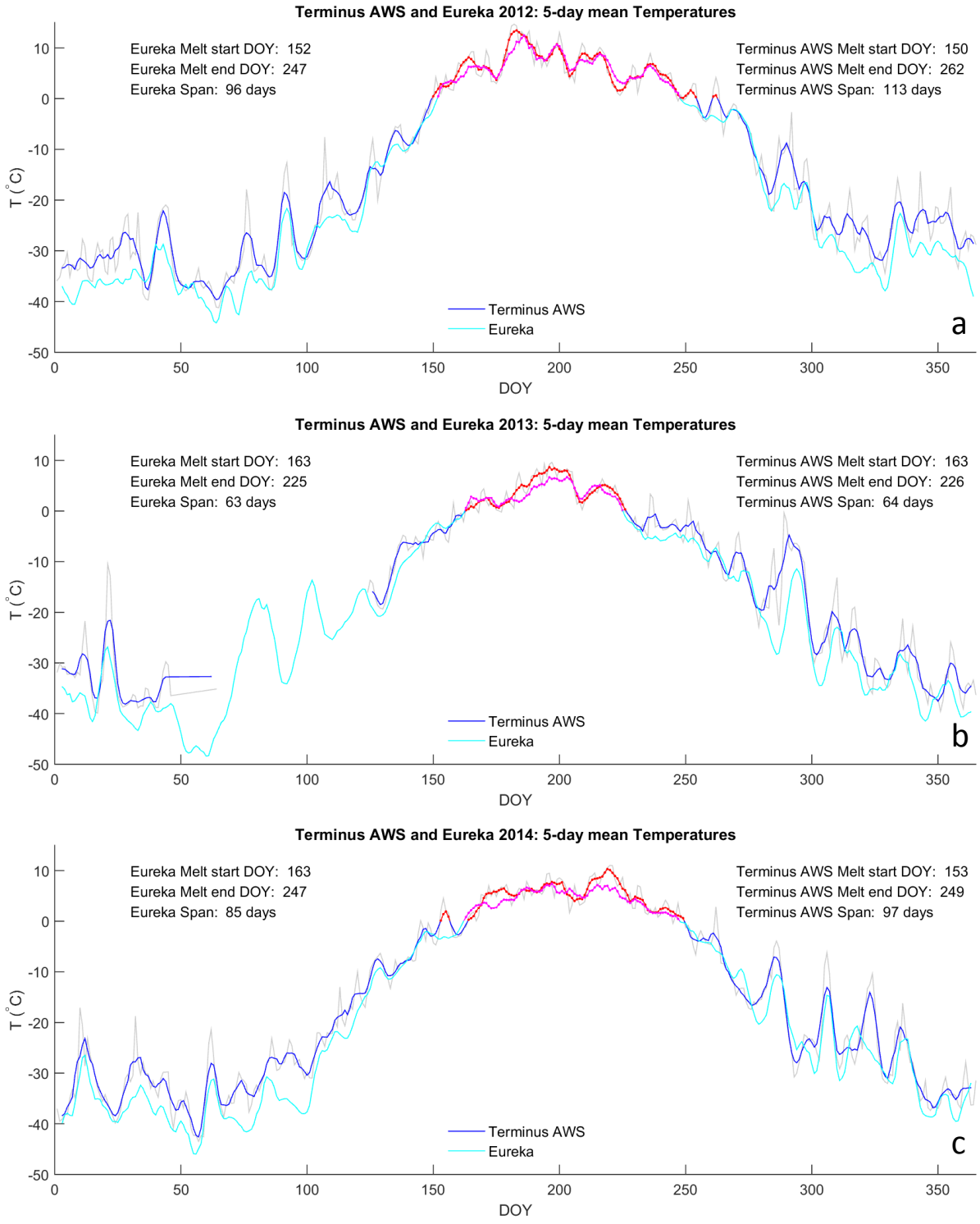

Figure 4.2: Comparison of daily mean temperatures observed at the Environment Canada Eureka weather station and at an automatic weather station (AWS) located at the terminus of White Glacier in (a) 2012, (b) 2013, and (c) 2014.

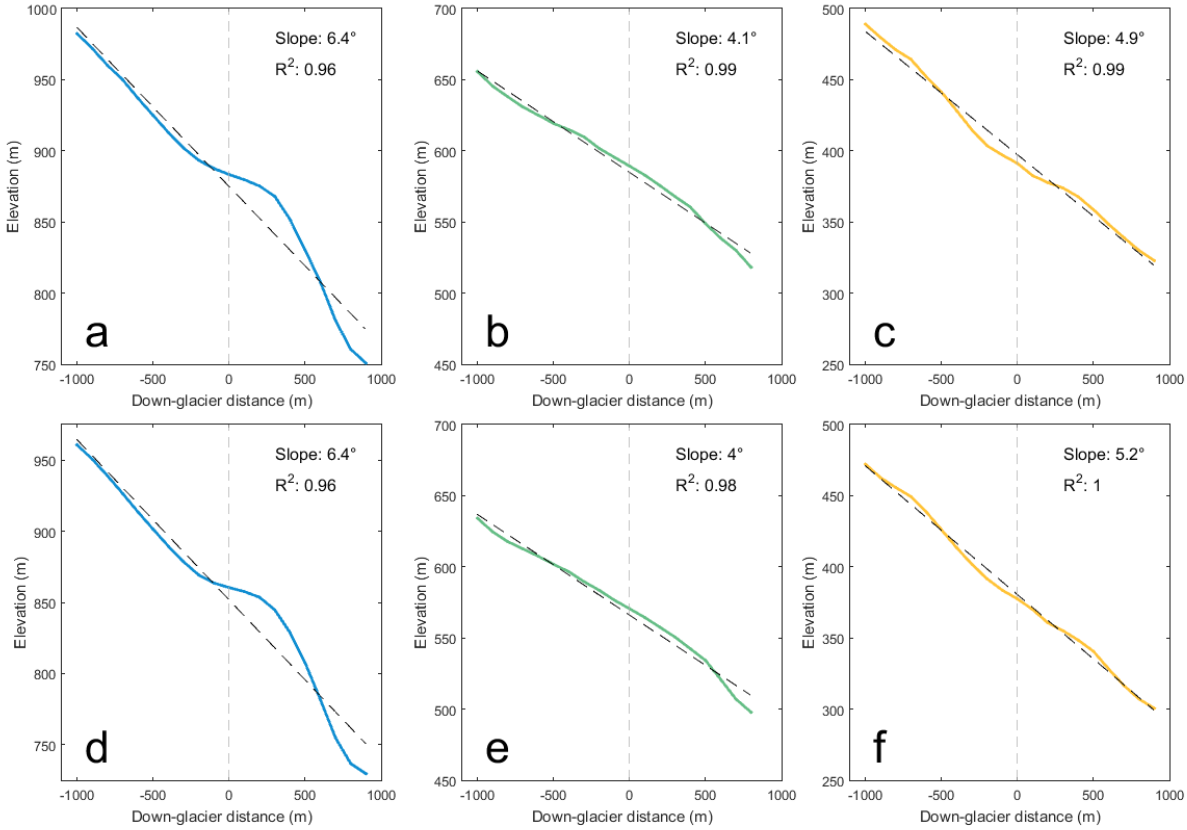

Figure 4.3: Surface slope profiles in 1960 (a, b, c) and in 2014 (d, e, f) at the upper, middle, and lower profiles, respectively.

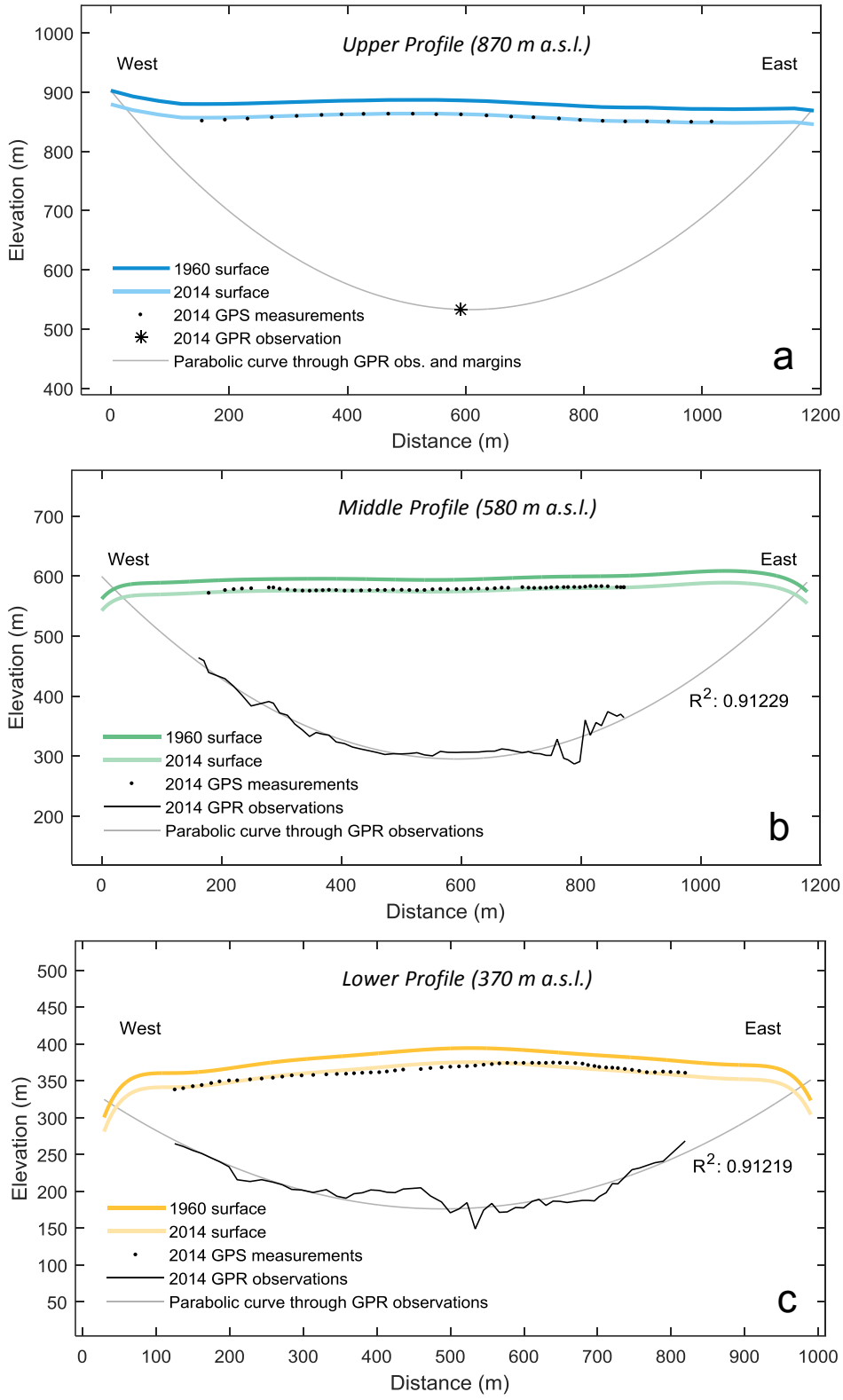

Figure 4.4: Cross sectional depth and elevation profiles based on 10 MHz ice penetrating radar measurements at the (a) upper, (b) middle, and (c) lower velocity profiles.

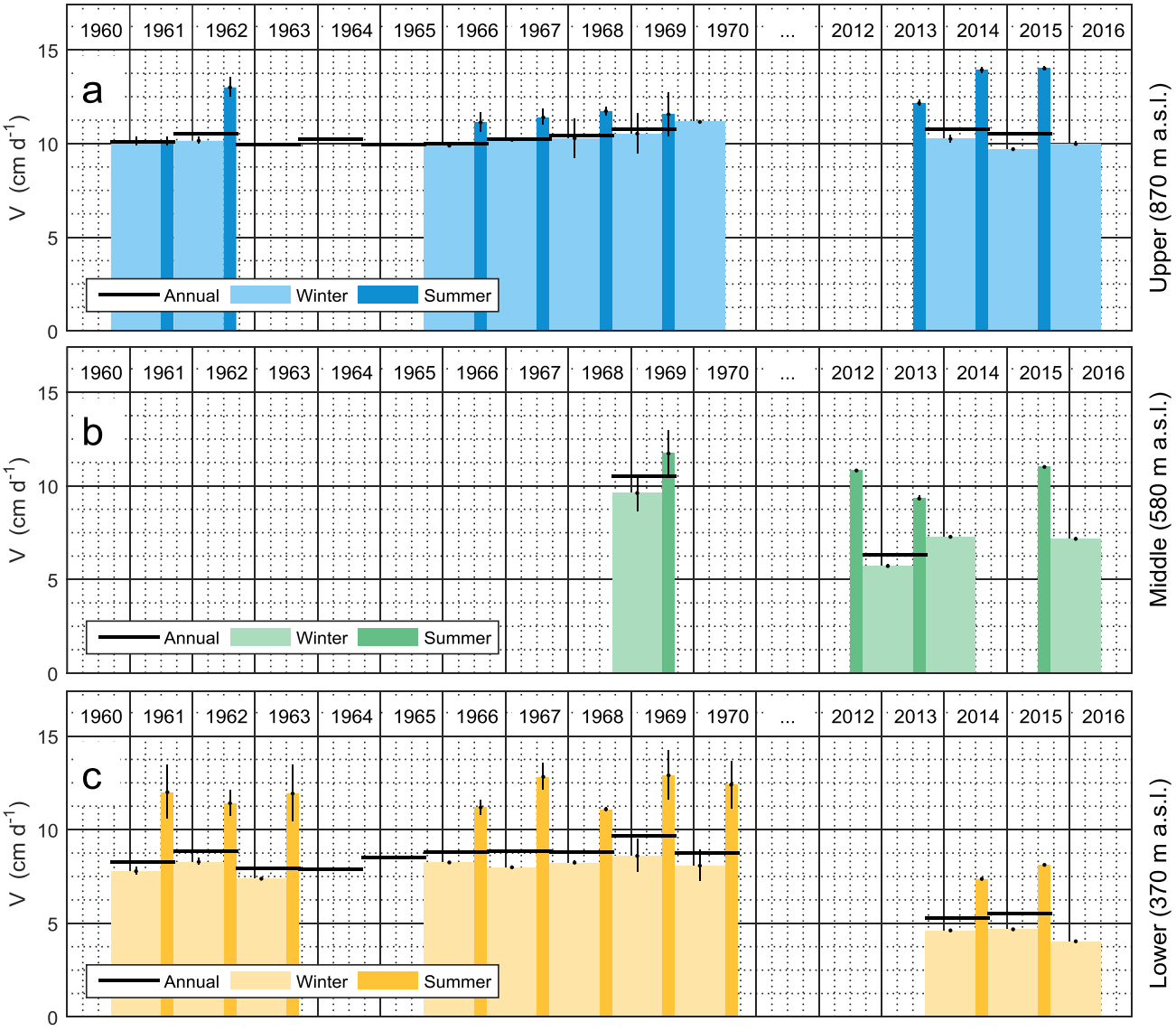

Figure 4.5: Variations in annual, winter, and summer velocities between 1960-70 [*Müller and Iken*, 1973] and 2012-2016 (this study) at the (a) upper, (b) middle, and (c) lower velocity profiles. Summer and winter errors are indicated as vertical lines on the summer and winter velocities.

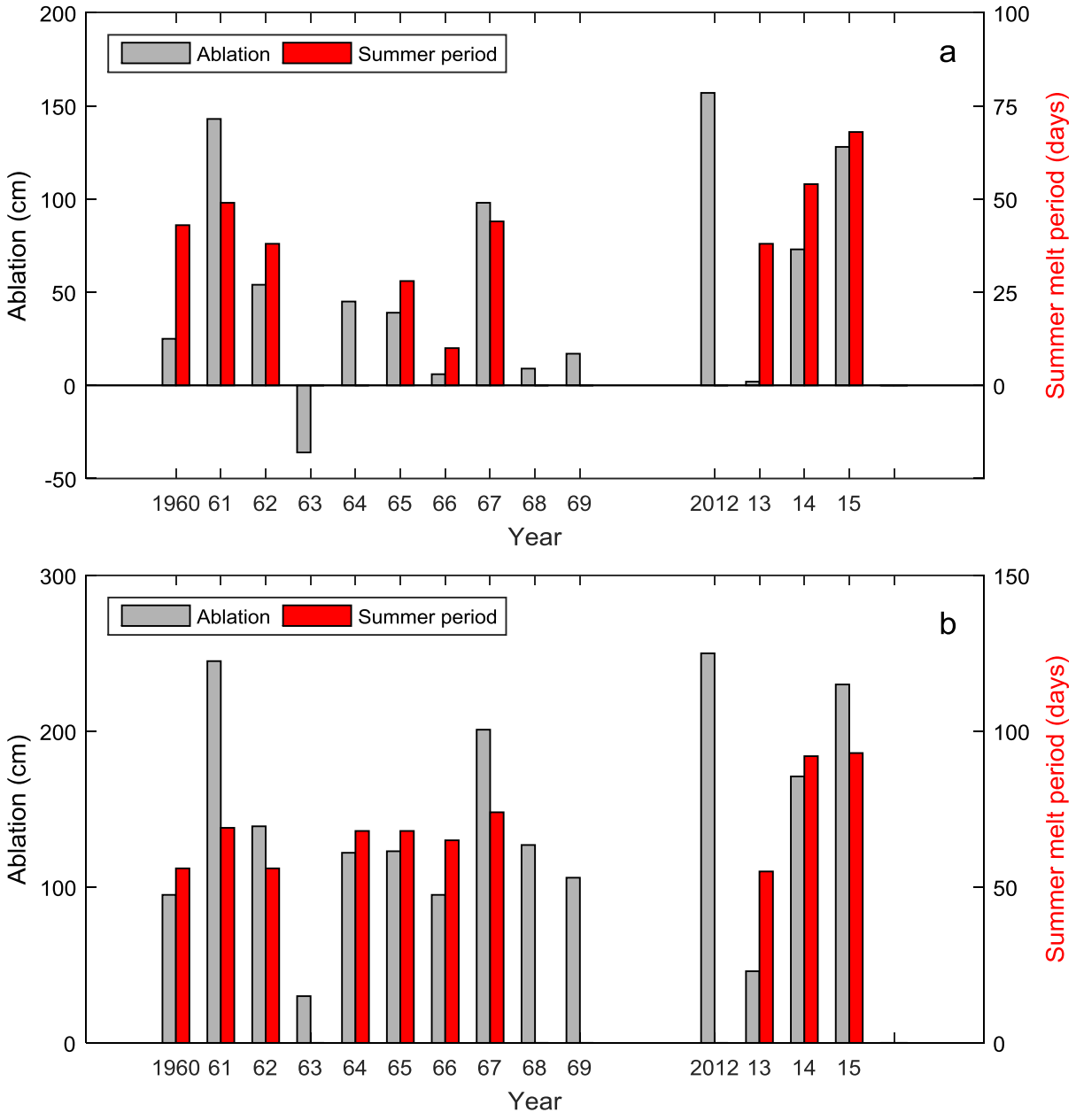

Figure 4.6: Annual ablation (*a*) derived from mass balance measurements and duration of the melt period (*s*) for the: (a) upper, and (b) lower profiles. Negative ablation values indicate that the profile was in the accumulation area (e.g. in 1963). Missing *s* values refer to years where meteorological data was not available for the given profile.

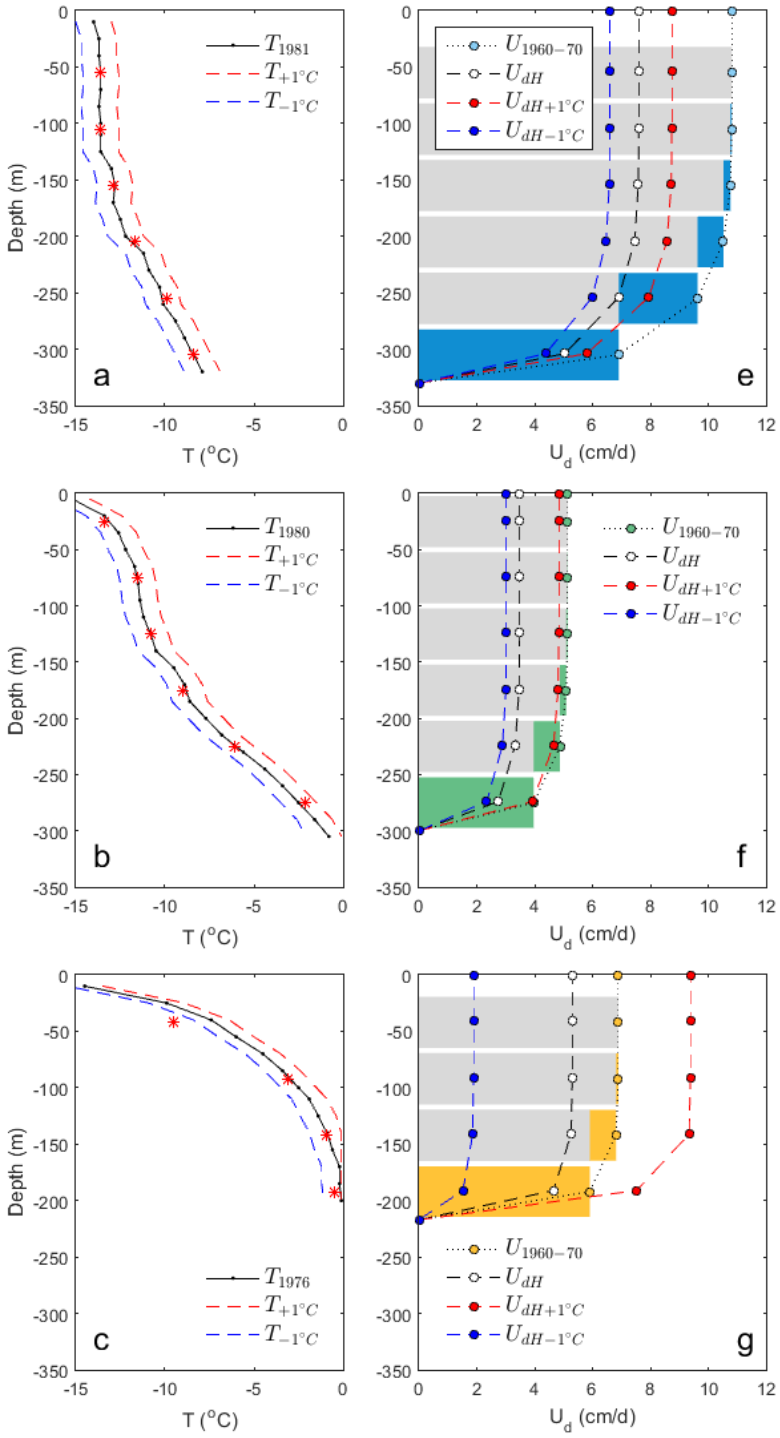

Figure 4.7: Englacial temperature measurements at the (a) upper, (b) middle, and (c) lower velocity profiles with 50 m mean temperatures indicated by red stars [*Blatter*, 1987a], and modeled vertical deformation profiles (d,e,f) for each profile within scenarios 1-4 as described in section 4.6.1., where $U_{1960\text{-}70}$ refers to modeled deformation using ice thickness and temperature conditions during the 1960-70s, while U_{dH} applies the thickness change (dH) observed between 1960-2014 with no temperature change, or with a +1°C warming ($U_{dH+1°C}$) or with 1°C cooling ($U_{dH-1°C}$).

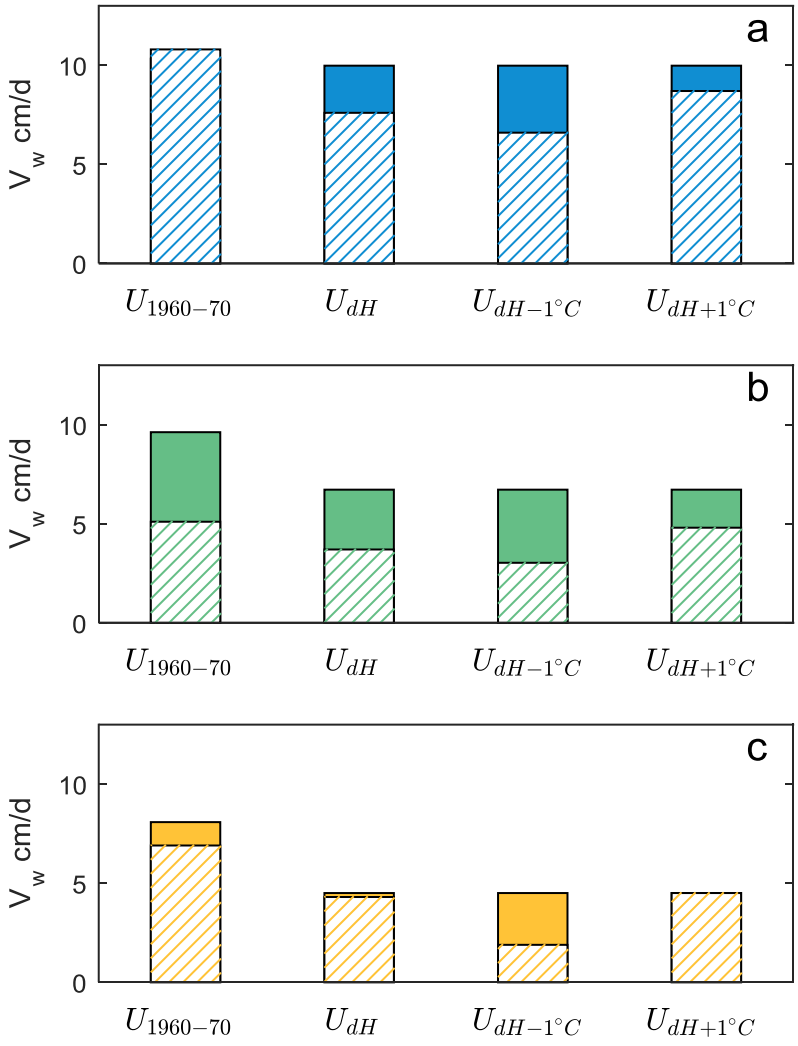

Figure 4.8: Component of winter surface velocity attributable to deformation (hatched pattern) and basal motion (solid colour) at the (a) upper, (b) middle, and (c) lower velocity profiles for scenarios 1-4 described in section 4.6.1., where $U_{1960\text{-}70}$ refers to modeled deformation using ice thickness and temperature conditions during the 1960-70s, while U_{dH} applies the thickness change (*dH*) observed between 1960-2014 with no temperature change, or with a +1°C warming ($U_{dH\,+\,1°C}$) or with 1°C cooling ($U_{dH\,-\,1°C}$).

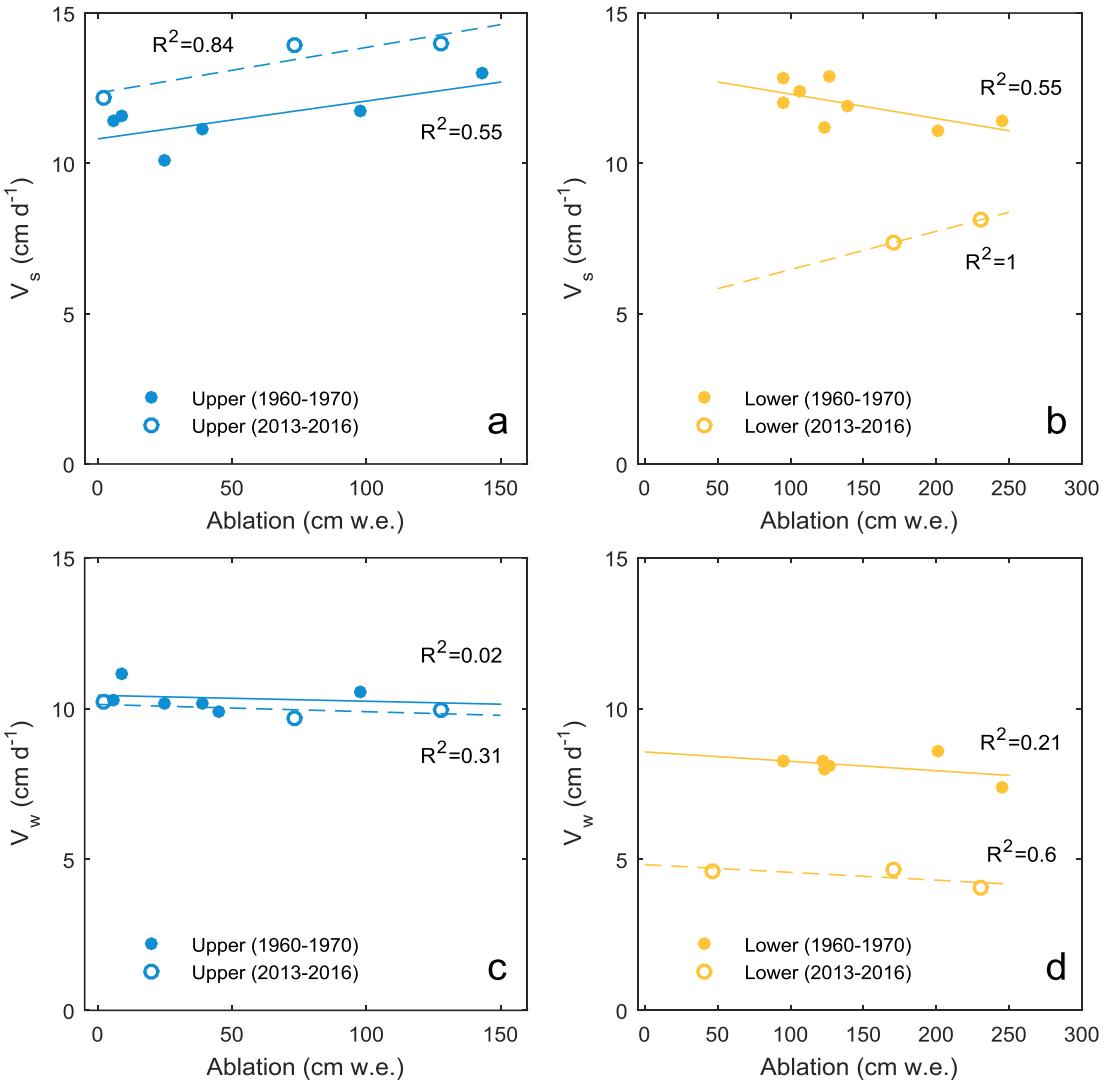

Figure 4.9: Relationship between annual ablation and summer velocities (v_s) at the (a) upper and (b) lower profiles, and on velocities the following winter (v_w) at the (c) upper and (d) lower profiles.

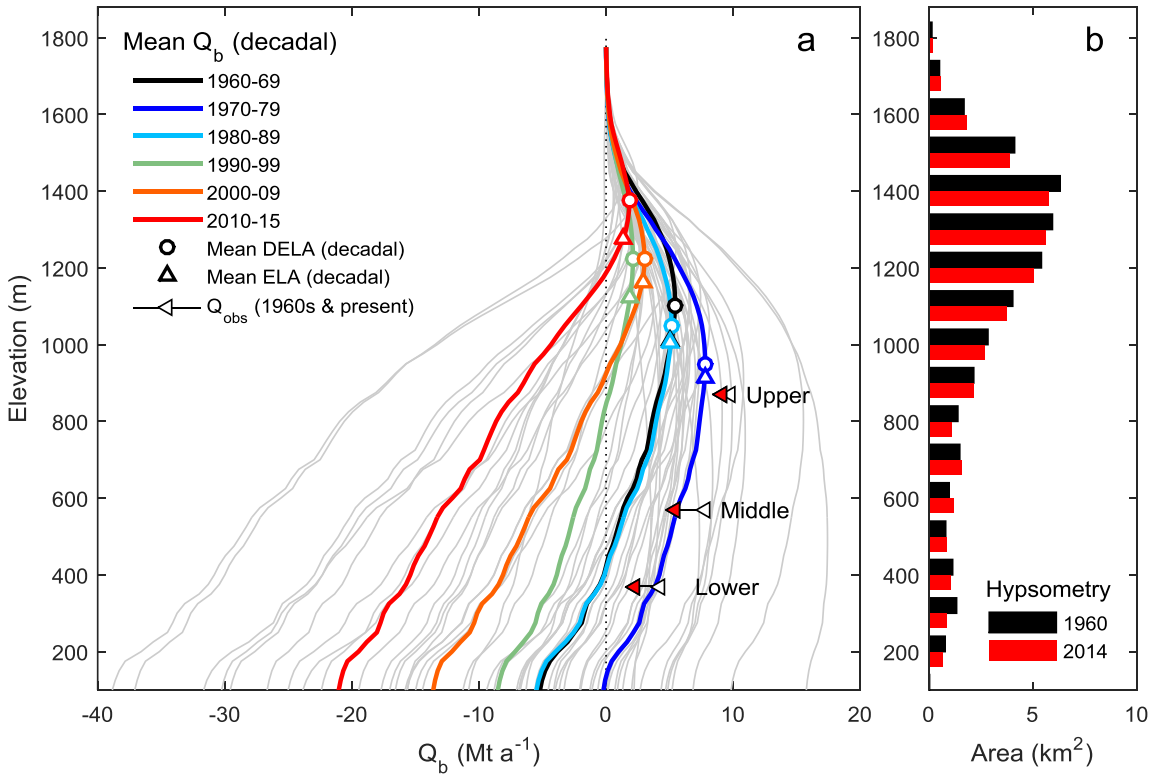

Figure 4.10: (a) Annual (grey) and decadal mean (coloured) balance flux (Q_b) profiles based upon the 55-year mass balance record at White Glacier. Also plotted are the observed fluxes (Q_{obs}) derived from 1960-70 velocities (white triangles) and 2012-16 velocities (red triangles). Coloured circles and triangles respectively refer to the dynamic ELA where maximum flux occurs, and the corresponding ELA based on surface mass balance data. (b) Glacier hypsometry in 1960 (black) based upon *Haumann and Honegger* [1964] and 2014 (red) from *Thomson and Copland* [2016b].

CHAPTER 5: CONCLUSIONS AND FUTURE WORK

5.1. SUMMARY AND SYNTHESIS

Building upon the rich archive of early glaciological studies at White Glacier, Axel Heiberg Island, Nunavut, this thesis has: (1) quantified changes to the glacier hypsometry (area-elevation distribution), mass balance, and ice dynamics since 1960, (2) sought to elucidate the primary processes driving the observed changes, (3) makes simple predictions about the glacier's future.

5.1.1 Summary of primary findings

The first requirement of this study was to create an updated map of White Glacier from which changes in ice thickness and glacier hypsometry could be determined. Using >400 oblique aerial photographs collected in July 2014, a new digital elevation model (DEM) was created using Structure from Motion techniques, a method built upon traditional photogrammetry but with the advantage of automated image correlation analysis [*Fonstad et al.*, 2013]. The outcome of this work demonstrated that, with careful camera setup, the Structure from Motion method is able to overcome the challenges of optical remote sensing in low-contrast, snow-covered areas due to the high resolution of the photographs and their ability to detect of small features at the surface. The resulting DEM and orthoimage facilitated the production of a new 1:10,000 topographic map of White Glacier with 5 m vertical accuracy in the style of earlier cartographic works dating back to 1960 [*Haumann and Honegger*, 1964].

The new map supported the calculation of the glacier's geodetic mass balance (mass change determined from ice volume change) and provided an updated glacier hypsometry that improves the accuracy of contemporary mass balance calculations. A modeled glacier hypsometry time series was created to support a reanalysis of the mass balance record, from which comparison of the geodetic and glaciological methods enabled the detection of generic differences and potential sources of error in the glaciological method [*Zemp et al.*, 2013]. Statistical comparison of the two approaches revealed that, within error margins, there was no significant difference between the average annual glaciological mass balance (–213 ± 28 mm w.e. a^{-1}) and geodetic mass balance (–178 ± 16 mm w.e. a^{-1}) of White Glacier between 1960 and 2014.

To determine how ice dynamics have responded to a long-term trend of ice thinning and increasingly negative mass balance conditions, dual-frequency GPS stations were installed at the centre of three cross-sectional profiles on White Glacier to continuously monitor ice motion from 2012–2016. These sites were the focus of surface velocity measurements from 1960–1970 [*Iken*, 1974; *Müller and Iken*, 1973]. Comparison of annual, winter, and summer velocities indicated decreasing ice motion of ~10–45%, with biggest reductions towards the glacier terminus. However, an observed increase in summer velocities at the highest station suggested that increased surface melt and delivery of this water to the glacier bed through moulins has initiated basal sliding in a zone that was not subject to this effect in earlier decades. The component of surface velocity attributable to ice deformation was modeled using Glen's [1955] flow law applied with site-specific enhancement factors derived from earlier englacial temperature observations. These calculations enabled the estimation of historic and contemporary basal sliding velocities for each station and indicate that for the stations below 600 m a.s.l., basal sliding has diminished while internal deformation rates have remained constant, or may have increased in response to an increasing annual air temperature of ~3°C [*Lesins et al.*, 2010]. Comparison of observed fluxes through cross-sections at the three velocity profiles with balance fluxes modeled from the long-term mass balance record indicated that the current flow regime of White Glacier is not sustainable.

5.1.2 Synthesis

The combined results provide some insight into the stability of the post-1960 response of White Glacier since early observations in 1960 which coincided with the onset of contemporary amplified warming in the Arctic [*Screen and Simmonds*, 2010]. Foremost, negative mass balance conditions have continued to increase since the last detailed assessments of the data [*Cogley et al.*, 2011a; *Cogley et al.*, 1996], with 8 of the 10 most negative mass balance years being observed in the last 15 years. It has been well established in previous studies that the mass balance of glaciers in the CAA is primarily attributable (>90%) to summer surface air temperatures, rather than variability in accumulation [*Koerner*, 2005; *Sharp et al.*, 2011]. While predictions that precipitation will increase with diminishing Arctic sea ice [e.g. *Kopec et al.*, 2016] have proven true in some parts of the northern hemisphere and particularly over Siberia [*Cohen and Cherry*, 2012; *Ghatak*, 2012], no statistically significant changes have been observed in the accumulation area of White Glacier since the 1960s. Similarly, the suggestion that mass balance gradients should

steepen, due to the potential shift from continental- to maritime-type climates with decreasing sea ice [*Dyurgerov and Dwyer*, 2000], has not been detected either (see Chapter 3, Figure 3.4).

Changes in the elevation and extent of White Glacier, through comparison of the new 2014 1:10,000 map [*Thomson and Copland*, 2016b] and the original 1960 map [*Haumann and Honegger*, 1964], reflect a dominant trend of ice thinning with >20 m of elevation loss having occurred below 1000 m a.s.l. (see Chapter 3, Figure 3.3), and a retreat of the terminus by ~1 km. Decreases in hypsometry at higher elevations (1000-1400 m a.s.l.) are also attributable to the increasing size of nunataks as high elevation ice thins, thereby exposing more of the bedrock below. Elevation losses along the main trunk of the glacier below ~700 m a.s.l. are primarily due to increased ablation (>97%) rather than reductions in the dynamic contribution of mass towards the terminus as the glacier slows down. Although thinning has negative repercussions for glacier mass balance by shifting more ice to lower, warmer elevations, it was found that the magnitude of this effect was more than offset by the positive response of glacier retreat, which acts to remove ice from elevations where the maximum potential for melt occurs. This suggests that the glacier, in regard to changes in hypsometry, is presently exhibiting a stable response to current warming. However, if the observed rate of thinning persists into the future and continues to impact higher elevations, as has been modeled for Yakutat Glacier in southeast Alaska [*Trüssel et al.*, 2015], a threshold will pass at which the retreat response will no longer have the capacity to offset enhanced melt at higher elevations.

5.2 KEY CONTRIBUTIONS

This thesis presents several new contributions to Canadian Arctic glaciology by reporting the first multi-decadal observations of changes to mountain glacier hypsometry and dynamics, and by demonstrating new methods of analysis that reflect the stability of glacier response.

As demonstrated by the scientific value of the original 1960 1:10,000 map of White Glacier [*Haumann and Honegger*, 1964], the new map produced using Structure from Motion techniques (Chapter 2) contributes an important baseline of the glacier extent and elevation for future research. In addition to providing an updated hypsometry that improves the accuracy of mass balance calculations in the future, the new map also presents a record of surface features on the glacier (e.g. crevasses, surface streams, terminus collapse feature) that reflect the contemporary dynamics

and supraglacial hydrological system. The new White Glacier map (2014; Appendix 1), as well as the entire collection of large-scale Expedition Fiord maps produced in the 1960s, have now been submitted to the World Glacier Monitoring Service's 'Fluctuations of Glaciers – Maps' digital archive (www.wgms.ch/products_fog_maps) to ensure that they are properly archived and accessible in the future.

This thesis also provides the first reanalysis of a high-Arctic glacier mass balance record in the Canadian Arctic. Through rigorous statistical analysis it confirms, for the first time, that the fundamental assumptions made in the glaciological method applied at White Glacier (e.g. that summer accumulation is negligible) are reliable and do not impose any statistically significant biases into the record spanning 1960-2014. New analysis of the individual roles of glacier retreat and thinning provided the first evidence that glacier thinning impacts calculated mass balance to a lesser extent than glacier retreat, such that loss of strongly negative mass balance regions presents a buffering effect under negative mass balance conditions. However, it is not yet possible to say whether this response is occurring at other mountain glaciers in the CAA.

Ice velocity measurements presented in this thesis show the first observations of glacier deceleration in the CAA occurring over the span of more than 50 years. These measurements also revealed that the contribution of summer movement to annual motion has increased significantly since the 1960s at all stations. A new method of modeling internal deformation rates, in which the flow rate parameter was allowed to vary with depth according to englacial temperatures, showed good agreement at high elevations where historically all ice motion was attributable to creep processes. It was also discovered that basal motion (by sliding or deformation of the bed) is likely now occurring at higher elevations where historically surface velocities were entirely explainable by ice deformation.

The broader impact of this research concerns the provision of *in situ* observations and interpretation of glacier-climate interactions in a region where most glacier monitoring is dominated by large-scale remote sensing endeavors with limited ground-based validation. At present, the data in this thesis comprise the only contemporary field measurements of a mountain glacier in the Canadian Arctic despite a majority of CAA glaciers (according to number, rather than area), and those with the most significant evidence of retreat, being classified as alpine type [*Oerlemans and Fortuin*, 1992; *Thomson et al.*, 2011].

5.3 FUTURE WORK

This thesis demonstrates the value of long-term glacier monitoring programs and the scientific opportunity provided by comprehensive and well documented baseline studies. Therefore, future work at White Glacier should foremost ensure the continuation of the annual glaciological mass balance measurements and continued submission of this data to the World Glacier Monitoring Service. As a follow-up to the reanalysis of the mass balance record (Chapter 3), the White Glacier record held at WGMS will be updated to reflect the conventional mass balance between 1960 and 2014, calculated using a linear interpolation of hypsometry between those years. Future calculations of glaciological mass balance will use the new 2014 hypsometry until another topographic survey is conducted. While the assumption that summer accumulation is negligible holds true following the reanalysis findings presented here, this may not be so in the future. We have therefore established a new automated snow-depth sounder at the highest mass balance stake on White Glacier (1480 m a.s.l.) to monitor snowfall patterns through the year.

The intention is to continue monitoring ice velocities on White Glacier at the upper, middle, and lower profiles, alongside the mass balance measurements, as a means of determining whether the observed deceleration will persist. An important question is whether this slowdown will occur at a constant rate, or whether the glacier will behave in a non-linear fashion, which might be expected given that deformation rates decrease exponentially with decreasing ice thickness [*Glen*, 1955]. With the observation that the contribution of summer motion to annual velocities has more than doubled at lower elevations, and quadrupled at the upper station, it is essential to monitor this behaviour into the future to determine if and when it is no longer appropriate to assume that winter motion is representative of annual motion in remote sensing studies of ice dynamics.

A new project will begin in the fall of 2016 to investigate the evolution of englacial temperatures, which in Chapter 4 are shown to have a significant impact on the rate of ice deformation. This work will repeat early field measurements of englacial temperatures [*Blatter*, 1987a] in the upper 15-20 m of the glacier and will integrate the historic and contemporary measurements as boundary conditions into a thermodynamical model of ice temperatures through time [*Wilson and Flowers*, 2013]. The goal of this work is to elucidate how englacial temperatures impact the dynamic processes (including ice deformation, basal motion, and the supra- and subglacial hydrological networks) of mostly-cold polythermal glaciers, a thermal-state considered

to describe the majority of ice masses in the CAA, and what the long-term effects will be on glacier response.

In closing, this thesis highlights the admirable quality of the early glaciological studies conducted in the Expedition Fiord region of Axel Heiberg, and demonstrates the scientific potential that exists for countless more future studies built upon the foundation of research established there.

CHAPTER 6: REFERENCES

Adams, W. P. (1966), Ablation and run-off on the White Glacier. Axel Heiberg Island, Canadian Arctic Archipelago., *Axel Heiberg Island Research Reports*, *Glaciology, No. 1*, pp. 84.

AMAP (2011), *Snow, Water, Ice and Permafrost in the Arctic (SWIPA): Climate Change and the Cryosphere*, Oslo, Norway.

Andreassen, L. M., H. Elvehøy, B. Kjøllmoen, and R. V. Engeset (2015), Glaciological and geodetic mass balance of ten long-term glaciers in Norway, *The Cryosphere Discuss.*, *9*(6), 6581-6626, doi:10.5194/tcd-9-6581-2015.

Andrews, R. H. (1964), Meteorology and heat balance of the ablation area, White Glacier. Canadian Arctic Archipelago - Summer 1960., *Axel Heiberg Island Research Reports*, *Meteorology, No.1*, 116 pp.

Arnold, K. C. (1981), Ice ablation measured by stakes and terrestrial photogrammetry - a comparison on the lower part of the White Glacier. Axel Heiberg Island, Canadian Arctic Archipelago., *Axel Heiberg Island Research Reports*, *Glaciology, No.2*, pp. 106.

Bartholomaus, T. C., R. S. Anderson, and S. P. Anderson (2008), Response of glacier basal motion to transient water storage, *Nature Geoscience*, *1*, 33-37.

Bell, R. E., K. Tinto, I. Das, M. Wolovick, W. Chu, T. T. Creyts, N. Frearson, A. Abdi, and J. D. Paden (2014), Deformation, warming and softening of Greenland's ice by refreezing meltwater, *Nature Geosci*, *7*(7), 497-502, doi:10.1038/ngeo2179

Benn, D. I., and D. J. A. Evans (2010), *Glaciers and Glaciation*, Hodder Education.

Bingham, R. G., P. W. Nienow, M. Sharp, and L. Copland (2006), Hydrology and dynamics of a polythermal (mostly cold) High Arctic glacier, *Earth Surface Processes and Landforms*, *31*, 1463-1479.

Bingham, R. G., P. W. Nienow, and M. J. Sharp (2003), Intra-annual and intra-seasonal flow dynamics of a High Arctic polythermal valley glacier, *Annals of Glaciology*, *37*(1), 181-188, doi:10.3189/172756403781815762.

Blachut, T. J. (1961), Participation of the Photogrammetric Research Section of the N.R.C., in *Preliminary Report of 1959-60, Jacobsen-McGill Arctic Research Expedition to Axel*

Heiberg Island, Queen Elizabeth Islands, edited by B. S. Müller, pp. 27-33, McGill University, Montreal.

Blachut, T. J. (1963), Photogrammetric and cartographic results of the Axel Heiberg Island expedition, *Canadian Surveyor*, *17*(2), 79-80.

Blatter, H. (1987a), On the thermal regime of an Arctic valley glacier: a study of White Glacier, Axel Heiberg Island, N.W.T., Canada, *Journal of Glaciology*, *33*(114), 200-211.

Blatter, H. (1987b), Stagnant ice at the bed of White Glacier, Axel Heiberg Island, N.W.T., Canada, *Annals of Glaciology*, *9*, 35-38.

Bolch, T., L. Sandberg Sørensen, S. B. Simonsen, N. Mölg, H. Machguth, P. Rastner, and F. Paul (2013), Mass loss of Greenland's glaciers and ice caps 2003–2008 revealed from ICESat laser altimetry data, *Geophysical Research Letters*, *40*(5), 875-881, doi:10.1002/grl.50270.

Braithwaite, R. J. (2005), Mass-balance characteristics of arctic glaciers, *Annals of Glaciology*, *42*(1), 225-229, doi:10.3189/172756405781812899.

Braithwaite, R. J., and S. C. B. Raper (2007), Glaciological conditions in seven contrasting regions estimated with the degree-day model, *Annals of Glaciology, 46*, 297-302.

Braun, C., D. R. Hardy, and R. S. Bradley (2004a), Mass balance and area change of four High Arctic plateau ice caps, *Geografiska Annaler*, *86A*, 43-52.

Braun, C., D. R. Hardy, R. S. Bradley, and V. Sahanatien (2004b), Surface mass balance of the Ward Hunt Ice Rise and Ice Shelf, Ellesmere Island, Nunavut, Canada, *Journal of Geophysical Research*, *109*(D22110), doi:10.1029/2004JD004560.

Burgess, D. O., M. J. Sharp, D. W. F. Mair, J. A. Dowdeswell, and T. J. Benham (2005), Flow dynamics and iceberg calving rates of Devon Ice Cap, Nunavut, Canada, *Journal of Glaciology*, *51*(173), 219-230, doi:10.3189/172756505781829430.

Castner, H. W., and R. Wheate (1979), Re-assessing the role played by shaded relief on topographic scale maps, *The Cartographic Journal*, *16*(2), 77-85.

Cogley, J. G. (2009), Geodetic and direct mass-balance measurements: comparison and joint analysis, *Annals of Glaciology*, *50*, 96-100.

Cogley, J. G., and W. P. Adams (1998), Mass balance of glaciers other than the ice sheets, *Journal of Glaciology*, *44*(147), 315-325, doi:10.3189/172756409787769744.

Cogley, J. G., and W. P. Adams (2000), Remote-sensing resources for monitoring glacier fluctuations on Axel Heiberg Island, *Arctic*, *53*(3), 248-259, doi:10.3189/172756409787769744.

Cogley, J. G., W. P. Adams, and M. A. Ecclestone (2011a), Half a century of measurements of glaciers on Axel Heiberg Island, Nunavut, Canada, *Arctic*, *64*(3), 371-375, doi:10.14430/arctic4127.

Cogley, J. G., W. P. Adams, M. A. Ecclestone, F. Jung-Rothenhäusler, and C. S. Ommanney (1996), Mass balance of White Glacier, Axel Heiberg Island, N.W.T., 1960-1991, *Journal of Glaciology*, *42*(142), 548-563.

Cogley, J. G., et al. (2011b), Glossary of Glacier Mass Balance and Related Terms, in *IHP-VII Technical Documents in Hydrology No. 86, IACS Contribution No. 2*, edited by UNESCO-IHP, pp. 114, Paris.

Cogley, J. G., and F. Jung-Rothenhäusler (2002), Digital Elevation Models of Axel Heiberg Island Glaciers, *Rep.*, pp. 46, Department of Geography, Trent University, Peterborough, Canada.

Cogley, J. G., and F. Jung-Rothenhäusler (2004), Uncertainty in digital elevation models of Axel Heiberg Island, Arctic Canada, *Arctic, Antarctic, and Alpine Research*, *36*(2), 249-260.

Cohen, J. L., J. C., Furtado, M. A. Barlow, V. A. Alexeev, and J. E. Cherry (2012), Arctic warming, increasing snow cover and widespread boreal winter cooling, *Environmental Research Letters*, *7*(1), 014007.

Copland, L., M. Sharp, and P. W. Nienow (2003a), Links between short-term velocity variations and the subglacial hydrology of a predominantly cold polythermal glacier, *Journal of Glaciology*, *49*(166), 337-348.

Copland, L., M. J. Sharp, P. Nienow, and R. G. Bingham (2003b), The distribution of basal motion beneath a High Arctic polythermal glacier, *Journal of Glaciology*, *49*(166), 407-414, doi:10.3189/172756503781830511.

Cuffey, K. M., and W. S. B. Paterson (2010), *The Physics of Glaciers*, Fourth ed., Elsevier, Amsterdam.

Dowdeswell, J. A., et al. (1997), The Mass Balance of Circum-Arctic Glaciers and Recent Climate Change, *Quaternary Research*, *48*(1), 1-14, doi:http://dx.doi.org/10.1006/qres.1997.1900.

Dyurgerov, M. B., and J. Dwyer (2000), The steepening of glacier mass balance gradients with Northern Hemisphere warming, *Zeitschrift für Gletscherkunde und Glazialgeologie*, *36*, 107-118.

Elsberg, D. H., W. D. Harrison, K. A. Echelmeyer, and R. M. Krimmel (2001), Quantifying the effects of climate and surface change on glacier mass balance, *Journal of Glaciology*, *47*(159), 649-658, doi:10.3189/172756501781831783.

Fisher, D., J. Zheng, D. O. Burgess, C. Zdanowicz, C. Kinnard, M. Sharp, and J. Bourgeois (2012), Recent melt rates of Canadian arctic ice caps are the highest in four millennia, *Global and Planetary Change*, *84-85*, 3-7.

Flowers, G. E. (2010), Glacier hydromechanics: early insights and the lasting legacy of three works by Iken and colleagues, *Journal of Glaciology*, *56*(200), 1069-1078, doi:10.3189/002214311796406103.

Flowers, G. E. (2015), Modelling water flow under glaciers and ice sheets, *Proceedings of the Royal Society of London A: Mathematical, Physical and Engineering Sciences*, *471*(2176), doi:10.1098/rspa.2014.0907.

Fonstad, M. A., J. T. Dietrich, B. C. Courville, J. L. Jensen, and P. E. Carbonneau (2013), Topographic structure from motion: a new development in photogrammetric measurement, *Earth Surface Processes and Landforms*, *38*(4), 421-430, doi:10.1002/esp.3366.

Fowler, A. C. (2010), Weertman, Lliboutry and the development of sliding theory, *Journal of Glaciology*, *56*(200), 965-972.

Furbish, D. J., and J. T. Andrews (1984), The use of hypsometry to indicate long-term stability and response of valley glaciers to changes in mass transfer, *Journal of Glaciology*, *30*(105), 199-211.

Gardner, A., et al. (2013), A Reconciled Estimate of Glacier Contributions to Sea Level Rise: 2003-2009, *Science*, *340*, 852-857.

Gardner, A., G. Moholdt, B. Wouters, G. J. Wolken, D. O. Burgess, M. Sharp, J. G. Cogley, C. Braun, and C. Labine (2011), Sharply increased mass loss from glaciers and ice caps in the Canadian Arctic Archipelago, *Nature*, *473*, 357-360.

Gardner, A., and M. Sharp (2007), Influence of the Arctic Circumpolar Vortex on the Mass Balance of Canadian High Arctic Glaciers, *Journal of Climate*, *20*, 4586-4598, doi:10.1175/JCLI4268.1.

Ghatak, D., C. Deser, A. Frei, G. Gong, A. Phillips, D. A. Robinson, and J. Stroeve (2012), Simulated Siberian snow cover response to observed Arctic sea ice loss, 1979–2008, *Journal of Geophysical Research: Atmospheres*, *117* (D23108), doi:10.1029/2012JD018047.

Glen, J. W. (1955), The Creep of Polycrystalline Ice, *Proceedings of the Royal Society of London A: Mathematical, Physical and Engineering Sciences*, *228* (1175), 519-538, doi:10.1098/rspa.1955.0066.

Glenday, P. J. (1989), Mass balance parameterization. White Glacier, Axel Heiberg Island, N. W. T., 1970-1980., Department of Geography, Trent University, Peterborough, ON, Canada.

Hambrey, M. (1994), *Glacial Environments*, Taylor & Francis.

Harig, C., and F. J. Simons (2016), Ice mass loss in Greenland, the Gulf of Alaska, and the Canadian Archipelago: Seasonal cycles and decadal trends, *Geophysical Research Letters*, *43*(7), 3150-3159, doi:10.1002/2016GL067759.

Harrison, W. D., L. H. Cox, R. Hock, R. S. March, and E. C. Pettit (2009), Implications for the dynamic health of a glacier from comparison of conventional and reference-surface balances, *Annals of Glaciology*, *50*(50), 25-30, doi:10.3189/172756409787769654.

Hattersley-Smith, G., and H. Serson (1970), Mass balance of the Ward Hunt Ice Rise and Ice Shelf: A 10 year record, *Journal of Glaciology*, *9* (56), 247-252.

Haumann, D. (1961), Co-ordinates of ground control points determined in 1960, in *Preliminary Report of 1959-60, Jacobsen-McGill Arctic Research Expedition to Axel Heiberg Island, Queen Elizabeth Islands*, edited by B. S. Muller, pp. 35-42, McGill University, Montreal.

Haumann, D. (1963), Surveying glaciers in Axel Heiberg Island, *Canadian Surveyor*, *17*(2), 81-93.

Haumann, D., and D. Honegger (1964), White Glacier, Axel Heiberg Island, Canadian Arctic Archipelago, *1:10,000*, McGill University, Photogrammetric Research Section, National Research Council of Canada.

Havens, J. M., F. Müller, and G. C. Wilmot (1965), Comparative meteorological survey and a short-term heat balance study of the White Glacier. Canadian Arctic Archipelago - Summer 1962, *Axel Heiberg Island Research Reports*, *Meteorology, No.4*, 76.

Heid, T., and A. Kääb (2012), Repeat optical satellite images reveal widespread and long term decrease in land-terminating glacier speeds, *The Cryosphere*, *6*, 467-479.

Hember, R. A., J. G. Cogley, and M. A. Ecclestone (2003), Volume balance of White Glacier terminus, Axel Heiberg Island, Nunavut, 1961-2003, in *Eastern Snow Conference Proceedings*, edited, p. 11.

Horn, B. K. P. (1987), Closed-form solution of absolute orientation using unit quaternions, *Journal of the Optical Society of America A*, *4*(4), 629-642, doi:10.1364/JOSAA.4.000629.

Hubbard, A., H. Blatter, P. Nienow, D. Mair, and B. Hubbard (1998), Comparison of a three-dimensional model for glacier flow with field data from Haut Glacier d'Arolla, Switzerland, *Journal of Glaciology*, *44*(147), 368-378, doi:10.3198/1998JoG44-147-368-378.

Huss, M. (2013), Density assumptions for converting geodetic glacier volume change to mass change, *The Cryosphere*, *7*(3), 877-887, doi:10.5194/tc-7-877-2013.

Hutchinson, M. F. (1988), Calculation of hydrologically sound digital elevation models, paper presented at Proceedings of the Third International Symposium on Spatial Data Handling, August 17-19, International Geographical Union, Columbus, Ohio, Sydney, Australia.

Iken, A. (1974), Velocity fluctuations of an arctic valley glacier, A study of the White Glacier, Axel Heiberg Island, Canadian Arctic Archipelago., *Axel Heiberg Island Research Reports*, *Glaciology, No. 5*, 123.

Iken, A., and R. A. Binschadler (1986), Combined measurements of subglacial water pressure and surface velocity of Findelengletscher, Switzerland: conclusions about drainage system and sliding mechanism, *Journal of Glaciology*, *32*(110), 101-119.

Iken, A., H. Rothlisberger, A. Flotron, and W. Haeberli (1983), The uplift of Unteraargletcher at the beginning of the melt season - a consequnce of water storage at the bed?, *Journal of Glaciology*, *29*(101), 28-47.

Jebara, T., A. Azarbayejani, and A. Pentland (1999), 3D structure from 2D motion, *IEEE Signal Processing Magazine*, *16*(3), 66-84.

Kaufmann, V., A. Kellerer-Pirklbauer, G. K. Lieb, H. Slupetzky, and M. Avian (2015), Glaciological Studies at Pasterze Glacier (Austria) Based on Aerial Photographs, in *Monitoring and Modeling of Global Changes: A Geomatics Perspective*, edited by J. Li and X. Yang, pp. 173-198, Springer Netherlands, Dordrecht, doi:10.1007/978-94-017-9813-6_9.

Kirtman, B., et al. (2013), Near-term climate change: projections and predictability, in *Climate Change 2013: The Physical Science Basis. Contribution of Working Group I to the Fifth Assessment Report of the Intergovernmental Panel on Climate Change*, edited by T. F. Stocker, D. Qin, G.-K. Plattner, M. Tignor, S. K. Allen, J. Boschung, A. Nauels, Y. Xia, V. Bex and P. M. Midgley, pp. 953–1028, Cambridge University Press, Cambridge, United Kingdom and New York, NY, USA, doi:10.1017/CBO9781107415324.023.

Koerner, R. M. (2005), Mass balance of glaciers in the Queen Elizabeth Islands, Nunavut, Canada, *Annals of Glaciology*, *42*(1), 417-423, doi:10.3189/172756405781813122.

Kopec, B. G., X. Feng, F. A. Michel, and E. S. Posmentier (2016), Influence of sea ice on Arctic precipitation, *Proceedings of the National Academy of Sciences*, *113*(1), 46-51.

Lenaerts, J. T. M., J. H. van Angelen, M. R. van den Broeke, A. S. Gardner, B. Wouters, and E. van Meijgaard (2013), Irreversible mass loss of Canadian Arctic Archipelago glaciers, *Geophysical Research Letters*, *40*(5), 870-874, doi:10.1002/grl.50214.

Lesins, G., T. J. Duck, and J. R. Drummond (2010), Climate trends at Eureka in the Canadian high arctic, *Atmosphere-Ocean*, *48*(2), 59-80, doi:10.3137/ao1103.2010.

Maag, H. U. (1969), Ice-dammed lakes and marginal glacial drainage on Axel Heiberg Island, Canadian Arctic Archipelalgo. *Rep.*, McGill University, Montreal.

Mair, D., D. Burgess, M. Sharp, J. A. Dowdeswell, T. Benham, S. Marshall, and F. Cawkwell (2009), Mass balance of the Prince of Wales Icefield, Ellesmere Island, Nunavut, Canada, *Journal of Geophysical Research: Earth Surface*, *114*(F2), F02011, doi:10.1029/2008JF001082.

McKortel, T. A. (1963), The reproduction of the Thompson Glacier map, *Canadian Surveyor*, *17*(2), 93-95.

Metcalfe, J. R., S. Ishida, and B. E. Goodison (1994), A corrected precipitation archive for the Northwest Territories, *Environment Canada - Mackenzie Basin Impact Study*, *Interim Report #2*, 110-117.

Minchew, B., M. Simons, S. Hensley, H. Björnsson, and F. Pálsson (2015), Early melt season velocity fields of Langjökull and Hofsjökull, central Iceland, *Journal of Glaciology*, *61*(226), 253-266, doi:10.3189/2015JoG14J023.

Mingo, L., and G. Flowers (2010), Instruments and Methods: An integrated lightweight ice-penetrating radar system, *Journal of Glaciology*, *56*(198), 709-714.

Moholdt, G., C. Nuth, J. O. Hagen, and J. Kohler (2010), Recent elevation changes of Svalbard glaciers derived from ICESat laser altimetry, *Remote Sensing of Environment*, *114*(11), 2756-2767, doi:http://dx.doi.org/10.1016/j.rse.2010.06.008.

Morris, E. M., and D. J. Wingham (2011), The effect of fluctuations in surface density, accumulation and compaction on elevation change rates along the EGIG line, central Greenland, *Journal of Glaciology*, *57*(203), 416-430.

Müller, F. (1961), *Preliminary Report of 1959-60, Jacobsen-McGill Arctic Research Expedition to Axel Heiberg Island, Queen Elizabeth Islands*, McGill University, Montreal.

Müller, F. (1962), Zonation of the accumulation area of the glaciers of Axel Heiberg Island, N.W.T., *Journal of Glaciology*, *4*, 302-311.

Müller, F. (1963), *Preliminary Report 1961-1962*, 257 pp., McGill University, Montreal, Quebec, Canada.

Müller, F., and A. Iken (1973), Velocity fluctuations and water regime of Arctic valley glaciers, paper presented at Symposium on the Hydrology of Glaciers, de I'Association Internationale d'Hydrologie Scientifique, Cambridge, 7-13 September 1969.

Nolan, M., R. J. Motkya, K. Echelmyer, and D. C. Trabant (1995), Ice-thickness measurements of Taku Glacier, Alaska, U.S.A., and their relevance to its recent behavior, *Journal of Glaciology*, *41*(139), 541-553.

Nuth, C., and A. Kääb (2011), Co-registration and bias corrections of satellite elevation data sets for quantifying glacier thickness change, *The Cryosphere*, *5*(1), 271-290, doi:10.5194/tc-5-271-2011.

Nye, J. F. (1960), The Response of Glaciers and Ice-Sheets to Seasonal and Climatic Changes, *Proceedings of the Royal Society of London A: Mathematical, Physical and Engineering Sciences*, *256*(1287), 559-584.

Nye, J. F. (1965), The flow of a glacier in a channel of rectangular, elliptic or parabolic cross-section, *Journal of Glaciology*, *5*(41), 661-690.

Oerlemans, J., R. P. Bassford, W. Chapman, J. A. Dowdeswell, A. F. Glazovsky, J. O. Hagen, K. Melvold, M. de Ruyter de Wildt, and R. S. W. van de Wal (2005), Estimating the contribution of Arctic glaciers to sea-level change in the next 100 years, *Annals of Glaciology*, *42*(1), 230-236, doi:10.3189/172756405781812745.

Oerlemans, J., and J. P. F. Fortuin (1992), Sensitivity of Glaciers and Small Ice Caps to Greenhouse Warming, *Science*, *258*(5079), 115-117, doi:10.1126/science.258.5079.115.

Ohmura, A. (1981), Climate and Energy Balance on Arctic Tundra, *Axel Heiberg Island Research Reports*, pp. 448.

Østrem, G., and M. Brugman (1991), *Glacier mass balance measurements: a manual for field and office work*, Saskatoon, SK, Environment Canada. National Hydrology Research Institute.

Østrem, G., and N. Haakensen (1999), Map comparison or traditional mass-balance measurements: which method is better?, *Geografiska Annaler*, *81*, 703-711.

Papasodoro, C., E. Berthier, A. Royer, C. Zdanowicz, and A. Langlois (2015), Area, elevation and mass changes of the two southernmost ice caps of the Canadian Arctic Archipelago between 1952 and 2014, *The Cryosphere*, *9*(4), 1535-1550, doi:10.5194/tc-9-1535-2015.

Paul, F., A. Kääb, M. Maisch, T. Kellenberger, and W. Haeberli (2004), Rapid disintegration of Alpine glaciers observed with satellite data, *Geophysical Research Letters*, *31*(L21402), doi:10.1029/2004GL020816.

Pfeffer, W. T., et al. (2014), The Randolph Glacier Inventory: a globally complete inventory of glaciers, *Journal of Glaciology*, *60*(221), 537-552, doi:10.3189/2014JoG13J176.

Rabus, B. T., and K. A. Echelmeyer (1997), The flow of a polythermal glacier: Mccall Glacier, Alaska, U.S.A, *Journal of Glaciology*, *43*(145), 522-536, doi:10.3198/1997JoG43-145-522-536.

Rippin, D. M., J. L. Carrivick, and C. Williams (2011), Evidence towards a thermal lag in the response of Ka˚rsaglaciären, northern Sweden, to climate change, *Journal of Glaciology*, *57*(205), 895-903, doi:10.3189/002214311798043672.

Schoof, C. (2010), Ice-sheet acceleration driven by melt supply variability, *Nature*, *468*, 803-806.

Screen, J. A., and I. Simmonds (2010), The central role of diminishing sea ice in recent Arctic temperature amplification, *Nature*, *464*, 1334-1337.

Screen, J. A., and I. Simmonds (2012), Declining summer snowfall in the Arctic: causes, impacts and feedbacks, *Climate Dynamics*, *28*, 2243-2256.

Sharp, M., et al. (2014), Remote sensing of recent glacier changes in the Canadian Arctic, in *Global Land Ice Measurements from Space*, edited by J. S. Kargel, G. J. Leonard, M. P. Bishop, A. Kääb and B. H. Raup, pp. 205-228, Praxis-Springer, doi:10.1007/978-3-540-79818-7_9.

Sharp, M., D. O. Burgess, J. G. Cogley, M. A. Ecclestone, C. Labine, and G. J. Wolken (2011), Extreme melt on Canada's Arctic ice caps in the 21st century, *Geophysical Research Letters*, *38*(L11501).

Sharp, M., et al. (2015), Glaciers and ice caps outside Greenland [in State of the Climate in 2014], *Bulletin of the American Meteorological Society*, *96*(7), 135-137.

Sundal, A. V., A. Shepherd, P. W. Nienow, E. Hanna, S. Palmer, and P. Huybrechts (2011), Melt-induced speed-up of Greenland ice sheet offset by efficient subglacial drainage, *Nature*, *469*(4), 521-524.

Tedstone, A. J., P. W. Nienow, N. Gourmelen, A. Dehecq, D. Goldberg, and E. Hanna (2015), Decadal slowdown of a land-terminating sector of the Greenland Ice Sheet despite warming, *Nature*, *526*(7575), 692-695, doi:10.1038/nature15722

Thompson, M. M. (1988), *Maps for America - Cartographic products of the U.S. Geological Survey and others*, 3rd ed., 265 pp., U.S. Government Printing Office, Washington, D.C.

Thomson, L. I., and L. Copland (2016), White Glacier 2014, Axel Heiberg Island, Nunavut: Mapped using Structure from Motion methods, *Journal of Maps*, doi:10.1080/17445647.2015.1124057.

Thomson, L. I., G. R. L. Osinski, and C. S. Ommanney (2011), Glacier change on Axel Heiberg Island, Nunavut, Canada, *Journal of Glaciology*, *57*(206), 1079-1086.

Thomson, L. I., M. Zemp, L. Copland, J. G. Cogley, and M. A. Ecclestone (2016), Comparison of Geodetic and Glaciological Mass Budgets for White Glacier, Axel Heiberg Island, NU, *Journal of Glaciology*, *Submitted*.

Trüssel, B. L., M. Truffer, R. Hock, R. J. Motyka, M. Huss, and J. Zhang (2015), Runaway thinning of the low-elevation Yakutat Glacier, Alaska, and its sensitivity to climate change, *Journal of Glaciology*, *61*(225), 65-75, doi:10.3189/2015JoG14J125.

Van der Meer, J., J. Menzies, and J. Rose (2003), Subglacial till: the deforming glacier bed, *Quaternary Science Reviews*, *22*(15–17), 1659-1685, doi:http://dx.doi.org/10.1016/S0277-3791(03)00141-0.

Van Wychen, W., D. O. Burgess, A. L. Gray, L. Copland, M. Sharp, J. Dowdeswell, and T. J. Benham (2014), Glacier velocities and dynamic ice discharge from the Queen Elizabeth Islands, Nunavut, Canada, *Geophysical Research Letters*, *41*(2), 484-490.

Van Wychen, W., J. Davis, D. Burgess, L. Copland, L. Gray, M. Sharp, and C. Mortimer (2016), Characterizing interannual variability of glacier dynamics and dynamic discharge (1999–2015) for the ice masses of Ellesmere and Axel Heiberg Islands, Nunavut, Canada, *Journal of Geophysical Research: Earth Surface*, *121*(1), 39-63, doi:10.1002/2015JF003708.

Vincent, C., A. Soruco, D. Six, and E. Le Meur (2009), Glacier thickening and decay analysis from 50 years of glaciological observations performed on Glacier d'Argentière, Mont Blanc area, France, *Annals of Glaciology*, *50*(50), 73-79, doi:10.3189/172756409787769500.

Waechter, A., L. Copland, and E. Herdes (2015), Modern glacier velocities across the Icefield Ranges, St Elias Mountains, and variability at selected glaciers from 1959 to 2012, *Journal of Glaciology*, *61*(228), 624-634, doi:10.3189/2015JoG14J147.

Weertman, J. (1983), Creep deformation of ice, *Annual Reviews Earth and Planetary Sciences*, *11*, 215-240.

WGMS (2008), *Global Glacier Changes: facts and figures*, 88 pp., UNEP, World Glacier Monitoring Service, Zurich, Switzerland.

WGMS (2013), Glacier Mass Balance Bulletin No. 12 (2010-2011)*Rep.*, ICSU(WDS)/IUGG(IACS)/UNEP/UNESCO/WMO, World Glacier Monitoring Service, Zurich, Switzerland.

WGMS (2015), Global Glacier Change Bulletin No. 1 (2012-2013)*Rep.*, 230 pp, World Glacier Monitoring Service, Zurich, Switzerland.

Wheate, R., N. Alexander, M. Fisher, and D. Mouafo (2001), A brief history and progress of mountain cartography in Canada, *Cartographica: The International Journal for Geographic Information and Geovisualization*, *38*(1-2), 31-39, doi:10.3138/N3L6-1874-5R18-118V.

Wilson, N. (2012), Characterization and Interpretation of Polythermal Structure in Two Subarctic Glaciers, 239 pp, MSc Thesis, Simon Fraser University, Vancouver, British Columbia, Canada.

Wilson, N., and G. Flowers (2013), Environmental controls on the thermal structure of alpine glaciers, *The Cryosphere*, *7*, 167-182.

Zemp, M., P. Jansson, P. Holmlund, I. Gärtner-Roer, T. Koblet, P. Thee, and W. Haeberli (2010), Reanalysis of multi-temporal aerial images of Storglaciären, Sweden (1959-99) - Part 2: Comparison of glaciological and volumetric mass balances, *The Cryosphere*, *4*(3), 345-357, doi:10.5194/tc-4-345-2010.

Zemp, M., et al. (2013), Reanalysing glacier mass balance measurement series, *The Cryosphere*, *7*, 1227-1245.

Zwally, H. J., W. Abdalati, T. Herring, K. Larson, J. Saba, and K. Steffen (2002), Surface melt-induced acceleration of Greenland Ice-Sheet flow, *Science*, *297*, 218-222.

APPENDIX 1: 2014 MAP OF WHITE GLACIER, 1:10,000

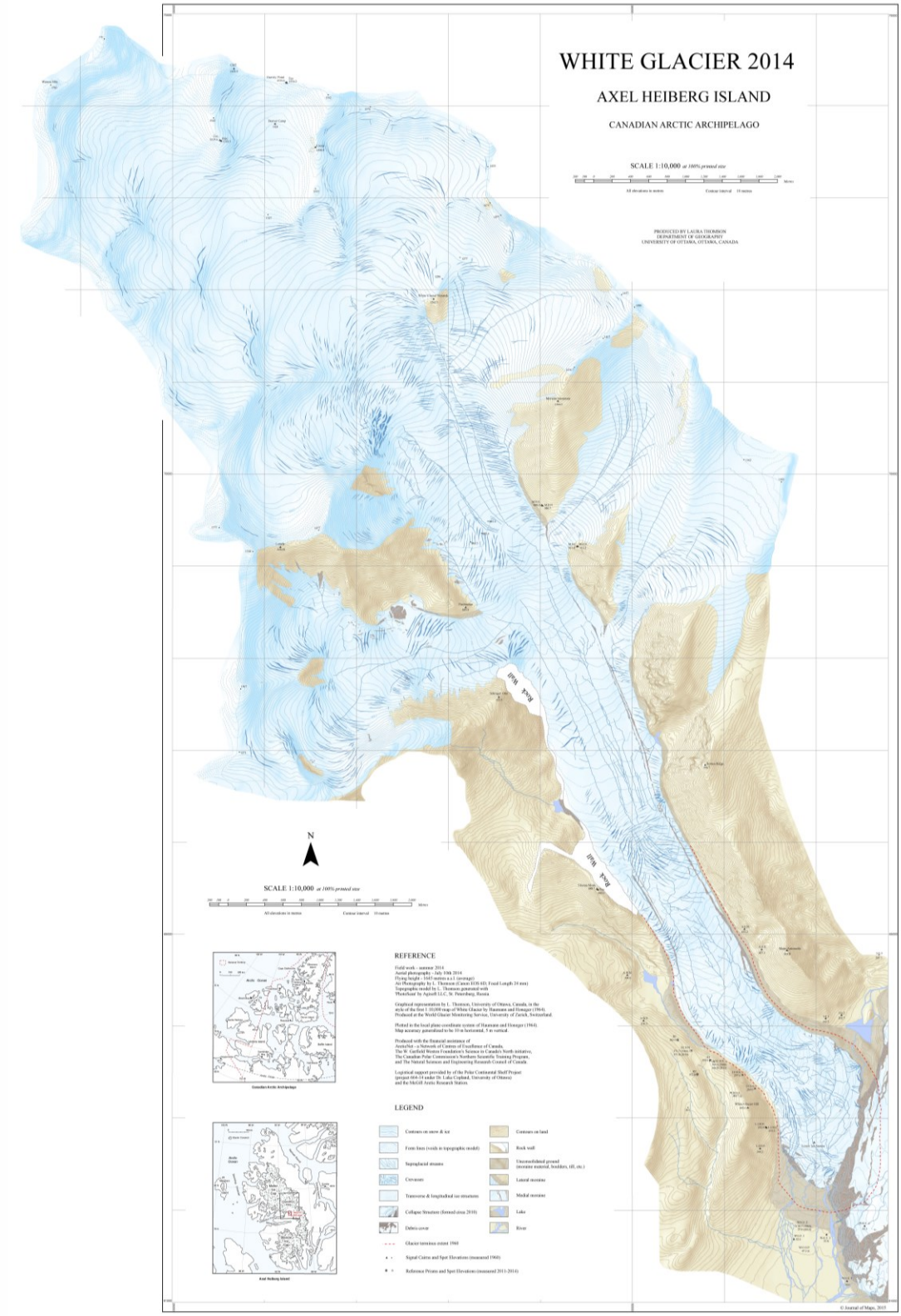

To view a full-scale version of the map, please refer to the supplementary material in *Thomson and Copland* [2016], available at: http://dx.doi.org/10.6084/m9.figshare.1632760.v1

APPENDIX 2: MASS BALANCE MEASUREMENT AND CALCULATION

Annual estimates of glacier mass balance at White Glacier were initiated in 1959, with the first full year of observations being completed in 1960. These studies have continued on a yearly basis to the present day (2016), with the exception of a three year gap from 1980-1982. Stake measurements are made during the spring field season in April/May. In the last decade (2005-2015) the number mass balance stake measurements located primarily along the glacier centreline (Figure 3.1, Chapter 3) has been close to 40, which amounts to a sampling density of approximately one stake per square kilometer. However, between 1960 and 1980, the number of stakes often exceeded 60, with a record number of 115 mass balance measurements in 1962. These observations occurred at the height of the Jacobsen-McGill Arctic Research Expedition and maintaining this number of stakes was possible only because members of the research expedition camped on the glacier at a number of sites (e.g. at Moraine Camp and Lower Ice Station) through the months of April to August in 1960-1962 (Miles Ecclestone and Peter Adams, personal communication). These measurements supported early studies of spatial variability in the accumulation and ablation zones [*Andrews*, 1964; *Havens et al.*, 1965, *Adams*, 1966] and glacier facies [*Müller*, 1962].

Stake measurement methods

Snow accumulation measurements use the stratigraphic method in which the internal layers of snow pits are characterized by thickness, hardness, crystal size and structure, and density that is acquired by measuring with a spring-scale the mass of a cylinder (having a known volume and weight) containing a snow sample from a given stratigraphic layer in a snow pit. At times it is necessary to estimate the density of a layer when it is particularly thin and/or hard (e.g. for an ice lens in the snowpack). The accumulation in a layer (in mm w.e.) is calculated from the product of the layer thickness and density. The total accumulation, noted as positive balance, for a specific stake is then calculated by summing the accumulation of all layers. It is possible to recognize the previous summer surface (which should define the bottom of the snow pit) by a layer of well-developed hoar frost and cup-shaped crystals [*Müller*, 1961] overlaying firn or glacier ice. The elevation at which the base of the snow pit transitions from firn to glacier ice is indicative of transition from accumulation to ablation conditions with decreasing elevation, and therefore is useful in identifying the equilibrium zone of the previous year. Ablation measurements are

conducted by measuring the increased exposure of stakes drilled into the glacier surface in previous years. The thickness of ice loss multiplied by the density of ice (900 kg m^3) gives the ablation in water equivalent at a given stake. Melt rates on White Glacier range from 10s of cm a^{-1} near the equilibrium zone to >500 cm a^{-1} near the terminus in high melt years. The ablation stakes used at White Glacier typically measure >3 m in length, so at high elevations it is possible to use stakes for several years before having to install a new stake, whereas near the terminus it is necessary to install replacement stakes every year. Stake elevations are updated on a near-annual basis through the use of hand-held GPS units with a vertical accuracy of ~ ±5 m, and a horizontal accuracy of ±2-3 m.

Compilation of annual balance records

At White Glacier, the stratigraphic year generally starts and ends in September (at the end of the melt season) and is identified by the year in which the ablation season ends [*Cogley et al., 1996*]; e.g., the 2014 balance year combines accumulation from winter 2013–2014 and ablation from summer 2014. However, stake observations conducted during a given year (e.g. in spring 2014) include the snow accumulation for the current mass balance year (for winter 2013-2014) and the melt of the previous summer (2013). Therefore, as illustrated in A2; Figure 1, the stake measurements used to calculate annual glacier-wide mass balance for 2014 must combine field measurements from two consecutive years; the first provides the accumulation over the winter of 2013-2014 (measured in spring 2014), and the second gives the ablation over the summer of 2014 (measured in spring 2015). The full series of annual records follow at the end of this appendix.

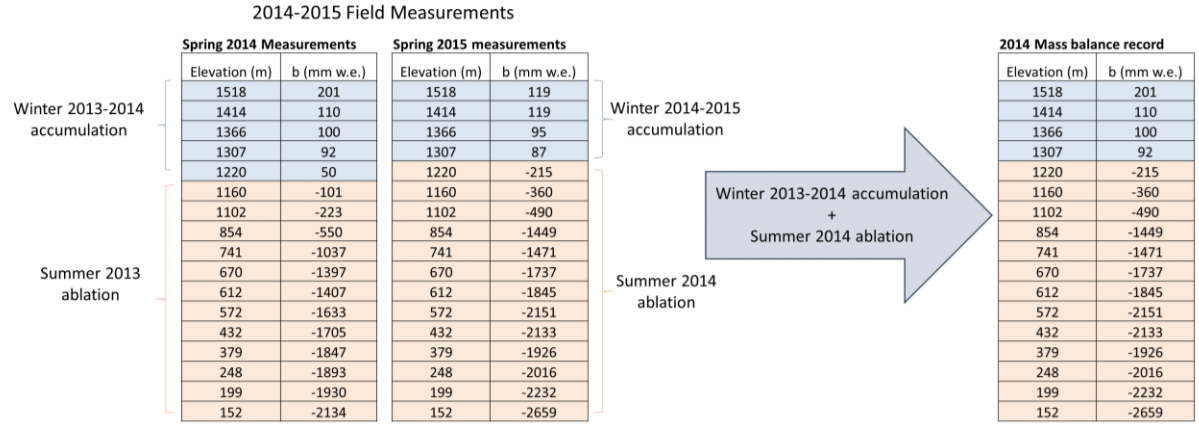

A2; Figure 1. Example of compilation of spring field observations from two years (left) to produce an annual mass balance record (right) using the stratigraphic system. Note that values given in table are just an example and do not reflect the actual field measurements in 2014 or 2015, or the final 2014 mass balance record.

Mass balance calculation

The glacier-wide estimate of mass balance calculation is based on the traditional profile method [*Østrem and Brugman*, 1991], however rather than taking the average of observed stake balances within a given elevation band to be the band balance (variable *b(h,t)* in Eq. 1, Chapter 3), a third-order polynomial curve is fit through the entire series of measured stakes (A2; Figure 2) and the balance for each 25 m elevation band midpoint is extracted from the polynomial relation between the point balances and their elevations. The product of the elevation band midpoint balance and the elevation band area gives the mass balance for that elevation band. Summing all elevation band balances gives the glacier-wide mass balance that, if divided by the total glacier area, gives the specific glacier-wide balance in mm w.e. The argument for applying a third-order polynomial is both physical, as a means of aiming to capture the signature of the mass balance gradient above and below the ELA (it becomes less steep at higher elevations) and historical, as a means of maintaining consistency with previous submissions of the White Glacier mass balance estimates to World Glacier Monitoring Service. Figure A2; Figure 2 demonstrates consistency between the methods used in this study (using a Matlab script written by L. Thomson) and previous glaciological mass balance estimates using Fortran code developed by Dr. J. G. Cogley [e.g. *Cogley et al.*, 1996].

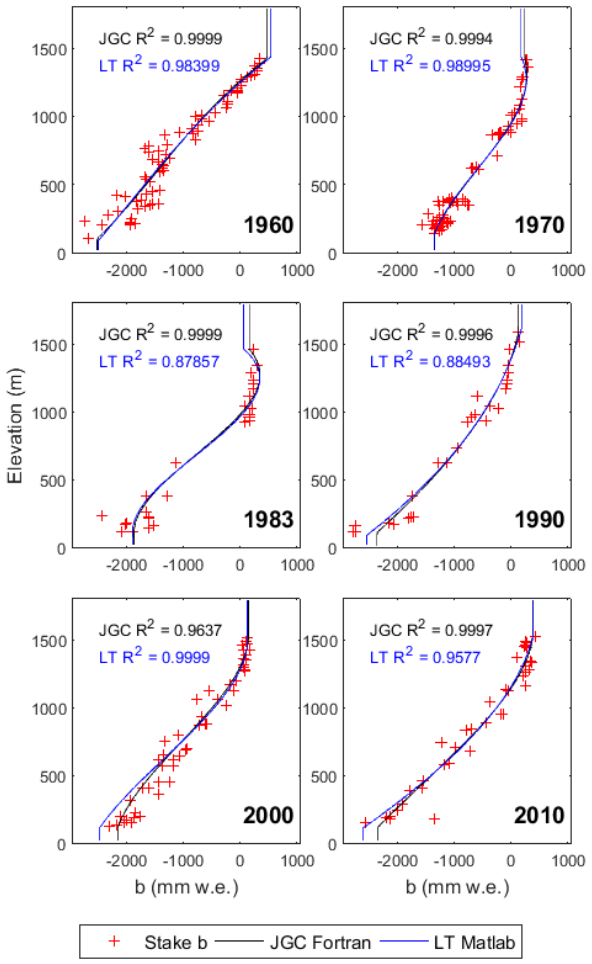

A2; Figure 2: Examples comparing polynomial fitting through observed stake balances (red crosses).

The following pages provide the mass balance stake observations for the 1960 to 2015 mass balance years. For each year of observation, provided in tables below, the first column refers to the measured stake balance (mm w.e.), the second is the stake elevation (m a.s.l.), and third provides the stake name. Those entries noted with an asterisk (*) denote estimated balance values, based upon a regression against stake CWGD. These estimates were necessary due to stakes melting out of the glacier under high-melt conditions in 2007.

1960

350	1425	L1
340	1390	L2
250	1370	L3
300	1350	L4
300	1330	L5
250	1310	L6
200	1300	L7
120	1290	L8
20	1270	L9
20	1250	L10
20	1230	L11
-50	1210	L12
-50	1190	L13
-50	1180	L14
-150	1185	Cxpf
-50	1170	L15
-290	1150	L16
-220	1110	L17
-220	1090	L18
-250	1060	L19
-450	1030	L20
-680	1010	L21
-780	1000	L22
-680	980	L23
-550	960	L24
-750	940	L25
-850	910	L26
-750	890	L27
-1080	880	L28
-820	870	Mxpf
-1320	860	L29
-780	830	Dxpf
-1290	790	L32
-1620	780	L33
-1680	765	L34
-1450	750	L35
-1620	735	L36
-1300	715	L37
-1250	695	L38
-1550	680	L39
-1450	665	L40
-1380	650	L41
-1360	635	L42
-1370	620	L43
-1360	605	L44
-1420	590	L45
-1680	560	L46
-1650	540	L47
-1600	520	L48
-1420	460	L49
-1550	450	L50
-1650	430	L51
-2180	420	L52
-2020	410	L53
-1750	380	L54
-1820	375	Axpf
-1550	360	L55
-1450	355	L56
-1600	350	L57
-1680	335	L58
-1800	320	L59
-2150	305	L60
-2320	280	L61
-1920	250	L63
-2750	235	L64
-1950	220	L65
-1950	210	L66
-1850	210	LIxpf
-1950	205	L67
-2450	200	L68
-2680	100	h

1961

390	1490	B0
190	1425	L1
360	1415	B2
320	1390	B4
160	1390	L2
160	1370	L3

1961 (cont.)

350	1360	B24
300	1360	B6
160	1350	L4
310	1340	B8
220	1330	L5
440	1330	B22
200	1330	B10
300	1320	B12
250	1310	L6
360	1300	L7
310	1300	B20
320	1295	B16
300	1290	B18
330	1290	L8
220	1270	L9
190	1250	L10
220	1230	L11
300	1210	L12
280	1190	L13
300	1180	L14
0	1170	L15
-30	1150	L16
-30	1110	L17
0	1090	L18
330	1060	L19
500	1030	L20
0	1010	L21
190	1000	L22
390	980	L23
360	960	L24
140	940	L25
-80	910	L26
-60	890	L27
-140	880	L28
-60	870	Mxpf
-410	860	L29
-80	830	Dxpf
-580	810	L30
-60	800	L31
0	790	L32
30	780	L33
360	765	L34
-360	750	L35
-380	735	L36
-440	715	L37
-600	695	L38
-550	680	L39
-580	665	L40
-440	650	L41
-520	635	L42
-500	620	L43
-1020	605	L44
-1130	590	L45
-800	560	L46
-630	540	L47
-600	520	L48
-550	460	L49
-660	450	L50
-880	430	L51
-1100	420	L52
-1320	410	L53
-1080	380	L54
-910	375	Axpf
-630	350	L55
-850	355	L56
-770	350	L57
-720	335	L58
-990	320	L59
-1380	305	L60
-1020	280	L61
-990	270	L62
-1160	250	L63
-1290	235	L64
-1100	220	L65
-940	210	L66
-1160	210	LIxpf
-1380	205	L67
-990	200	L68

1962

20	1490	B0
40	1425	L1
40	1421	B2
10	1390	B4
30	1390	L2
40	1370	L3
20	1360	B6
-80	1360	B24
40	1350	L4
10	1340	B8
20	1330	B10
-180	1330	B22
40	1330	L5
20	1320	B12
-40	1310	L6
-60	1305	62001
-50	1300	L7
-100	1300	62002
-230	1300	B20
-50	1300	B14
-260	1295	B16
-140	1290	B18
-250	1290	L8
-60	1290	62003
-180	1280	62004
-240	1275	62005
-260	1275	62006
-230	1270	L9
-240	1265	62007
-200	1250	L10
-220	1230	L11
-280	1210	L12
-250	1190	L13
-340	1180	L14
-620	1175	L14A
-340	1170	L15
-380	1160	62Cxp
-690	1150	L16
-610	1110	L17
-670	1090	L18
-660	1060	L19
-1000	1055	62022
-900	1040	62023
-780	1015	62024
-1060	990	62025
-1060	960	62026
-960	945	62027
-1210	920	62028
-1080	900	62029
-1430	890	62030
-1410	885	62031
-1810	875	62032
-1280	860	62033
-1940	855	62034
-1820	810	62035
-1810	780	62036
-1660	755	62037
-2190	740	62038
-1960	710	62039
-1770	700	62040
-2080	695	62041
-2120	685	62042
-2120	675	62043
-1910	645	62044
-2360	620	62045
-1900	615	62046
-1700	605	62047
-1920	595	62048
-2220	590	62049
-2580	560	62050
-2300	545	62051
-2070	510	62052
-2040	475	62053
-2120	460	62054
-2620	455	62055
-2240	445	62056
-3190	445	62057
-2860	405	62058
-1990	386	A5
-1990	382	A4

1962 (cont.)

-1940	379	A6
-2090	376	A3
-2460	375	A2
-2330	371	A1
-2320	370	62059
-2380	366	A7
-2020	365	62060
-1930	359	A8
-2020	350	62062
-2300	349	A9
-2480	347	A10
-2240	345	62063
-2220	340	62064
-2770	338	A11
-2310	320	62065
-2580	310	62066
-2430	280	62067
-2050	255	62068
-3000	240	62069
-2080	220	62070
-2000	205	62071
-2220	200	62072
-2260	198	62073
-2380	195	62074
-2320	180	62075
-2390	175	62076
-2400	165	62077
-2790	165	62078
-2860	160	62079
-2720	145	62080
-2780	140	62081
-3000	125	62082
-3500	110	62083
-3900	105	62084
-3780	98	62085

1963

270	1421	B2
290	1419	L1
260	1294	L7
290	1269	B20
60	1185	CP
150	1165	L15
-40	1147	L16
10	1108	L17
-250	1085	L18
-160	1057	L19
-230	1031	L20
-70	1009	L21
-300	997	L22
50	978	L23
0	958	L24
-100	936	L25
-110	910	L26
-10	890	L27
-70	880	L28
-720	875	M8
-400	875	M7
-240	874	M9
40	871	M10
-100	869	M13
-440	869	M6
-50	867	M12
30	867	M11
-550	862	M5
-600	860	L29
-700	859	M2
-650	859	M1
-380	857	M4
-610	855	M3
-460	847	MD
-460	830	L30
-360	795	L31
-500	760	L34
-190	745	L35
-740	720	L36
-790	700	L37
-970	680	L38
-800	660	L39

1963 (cont.)

-770	635	L41
-820	605	L43
-1240	585	L44
-1240	510	L48
-1020	460	L49
-930	445	L50
-1110	386	A5
-1130	382	A4
-1280	379	A6
-1190	376	A3
-1700	375	A2
-1380	371	A1
-1300	366	A7
-1450	365	L54
-1020	360	L55
-1240	359	A8
-1550	348	A9
-1110	346	L57
-1660	338	A11
-1030	315	L59
-1700	274	L61
-1360	250	L63
-1440	217	L65
-1440	207	L66
-1740	206	LD
-1330	205	L67
-2060	199	L68
-1450	183	L69
-1580	170	L70
-2090	162	L71
-1710	155	L72
-1750	146	L73
-1880	138	L74
-2260	130	L75
-2470	122	L76
-2620	114	L77
-2950	106	L78
-3070	98	L79

1964

590	1421	B2
550	1419	L1
480	1293	L7
600	1269	B20
190	844	MD
490	635	L41
180	605	L43
-40	585	L44
80	510	L48
-50	460	L49
110	445	L50
-260	384	A5
-210	382	A4
-410	377	A6
-270	376	A3
-450	376	A2
-130	358	A8
-180	349	A9
-440	347	A10
-410	338	A11
-690	272	L61
-490	243	L63
-490	217	L65
-870	206	LD
-420	205	L66
-790	197	L68
-710	181	L69
-840	168	L70
-840	162	L71
-620	144	L73
-890	136	L74

1965

190	1421	B2
200	1419	L1
250	1292	L7
220	1269	B20
-110	840	MD

1965 (cont.)

-280	697	L37
-300	677	L38
-300	657	L39
-270	632	L41
-150	602	L43
-670	508	L48
-610	458	L49
-930	440	L50
-790	384	A5
-1020	384	A6c
-790	381	A4
-1200	379	A3c
-940	376	A3
-1060	371	A1
-820	361	A7
-870	357	A8
-940	350	A9c
-830	349	A9
-1020	324	L57
-1110	302	L59
-1450	205	30mc
-1870	204	Cc
-1480	160	L71c

1966

360	1421	B2
330	1418	L1
310	1291	L7
300	1269	B20
10	871	M7
0	863	M6
-520	859	M1
-420	857	M2
-200	853	M5
-130	848	M4
-140	848	M3
-160	837	MD
-490	695	L37
-690	675	L38
-830	655	L39
-750	630	L41
-660	600	L43
-1020	381	A5
-1010	379	A4
-1200	378	A6c
-1290	378	A3c
-1180	376	A3
-1220	371	A1
-1250	368	L54
-1110	358	A7
-990	355	A8
-1230	350	L55
-1200	349	A9c
-1280	349	A9
-1350	332	L56
-1030	321	L57
-1300	303	L58
-1300	295	L59
-1580	276	L115
-1430	268	L114
-1370	260	L113
-1510	244	L112
-1710	228	L108
-1160	226	L107
-1370	225	L106
-1560	214	L105
-1490	204	L100
-1480	204	30mc
-1540	203	Cc
-1720	202	L109
-1550	188	L101
-1780	179	L110
-1440	164	L102
-1520	160	L71c
-1660	154	L111
-1800	148	L103

1967

320	1421	B2
360	1418	L1
410	1290	L7
330	1270	B20
250	868	M13
-90	868	M7
300	865	M12
40	865	M9
240	860	M10
50	860	M6
20	856	M2
-20	849	M5
-20	845	M4
90	845	M3
40	835	MD
-80	815	L30
-130	790	L31
-490	505	L48
-470	455	L49
-760	432	L122
-900	378	A3c
-830	375	A6c
-910	350	L118
-1030	276	L115
-1250	268	L114
-970	225	L106
-1240	204	30mc
-1540	202	Cc
-1220	158	L71c

1968

100	1421	B2
160	1417	L1
110	1289	L7
150	1270	B20
-270	1037	L19
-410	1012	L20
-560	989	L21
-420	975	L22
-350	953	L23
-410	931	L24
-520	910	L25
-660	894	L26
-640	875	L28
-950	856	M6
-1410	856	M2
-970	845	M5
-1390	843	M3
-1120	840	M4
-1000	795	L30
-1590	630	W6
-1540	630	W5
-1650	627	W4
-1500	623	W3
-1020	614	W2
-1510	607	W1
-2200	390	a5
-1880	387	a6
-1860	386	a4
-2210	380	a3
-1810	377	A3c
-2090	376	a2
-1790	373	a7
-1680	371	A6c
-1910	362	a8
-1810	348	A9c
-2310	276	L115
-2410	269	K6
-1980	264	L114
-2340	255	L113
-2380	239	K5
-2000	238	L112
-2200	225	L107
-1930	223	L106
-2300	213	K1
-1990	211	L105
-2480	203	L100
-1840	203	30mc
-2360	182	K2

1968 (cont.)

-2110	158	L71
-2660	148	L103

1969

420	1420	B2
390	1417	L1
410	1288	L7
400	1271	B20
370	1130	L16
300	1085	L17
270	968	L22
200	947	L23
150	925	L24
130	903	L25
130	888	L26
-220	881	L27
-310	880	m8
-300	878	m7
-100	874	m6
-50	867	m5
-160	864	m4
-250	863	m2
-240	862	m3
-540	852	M6
-240	842	M5
-90	841	M3
-320	795	L30
-720	630	W6
-800	630	W5
-800	628	L40
-640	627	W4
-530	622	W3
-890	615	W2
-820	614	L41
-880	601	L42
-700	500	L48
-1070	409	L122
-1750	396	L121
-1240	390	a5
-1400	387	a6
-1290	382	a4
-1190	379	a3
-1540	376	a2
-1370	376	A3c
-970	376	A4
-1070	376	A3
-1340	374	a1
-1490	374	A2
-1460	373	A1
-1360	373	A5
-1400	372	a7
-1320	368	A6c
-1380	363	A6
-1290	362	a8
-1340	354	A8
-1210	353	A7
-1060	350	A9
-1570	349	a10
-1390	348	a9
-1440	348	A9c
-1610	285	L116
-1640	276	L115
-1400	260	L114
-1620	259	K6
-1570	251	L113
-1570	238	K5
-1540	227	C3
-1710	222	L107
-1440	220	L106
-1390	216	C2
-1530	212	K1
-1470	209	L105
-1580	203	L100
-1830	201	K2
-1730	193	KX
-1770	186	KY
-1680	182	K3
-1750	171	C1
-1730	160	K4
-1830	145	L103

1970

280	1420	B2
260	1418	L1
300	1363	L4
210	1288	L7
200	1271	B20
170	1213	L11
190	1128	L16
170	1082	L17
150	1050	L18
60	1030	L19
20	1007	L20
190	983	L21
200	965	L22
110	946	L23
-40	923	L24
-40	902	L25
-210	885	L26
-180	880	m8
-10	880	m7
-230	877	L27
-180	873	m6
-220	865	m5
-330	863	m2
-190	862	m4
-330	860	m3
-250	710	L35
-620	625	W6
-690	624	W5
-690	624	W4
-670	621	W3
-570	615	W2
-1040	407	L122
-1090	395	L121
-850	389	a5
-1100	385	a6
-1020	378	a4
-970	376	A4
-1190	376	A3
-1280	375	a2
-1210	373	A1
-800	372	A5
-1060	370	a7
-930	351	A9
-740	351	A8
-1270	348	a10
-770	348	a9
-1470	285	L116
-1210	277	L115
-1260	260	L114
-1210	260	K6
-1170	251	L113
-1300	238	K5
-1080	233	L112
-1370	227	C3
-1110	224	L107
-1130	220	L106
-1110	216	C2
-1210	212	K1
-1240	209	L105
-1390	205	K2
-1570	204	L100
-1220	191	KX
-1270	186	KY
-1320	183	K3
-1350	178	P
-1230	170	C1
-1270	160	K4
-1350	144	L103

1971

340	1420	B2
270	1418	L1
210	1287	L7
230	1271	B20
180	1126	L16
150	1078	L17
120	1046	L18
0	1026	L19
-60	1003	L20

1971 (cont.)

-250	979	L21
-220	961	L22
-430	941	L23
-390	918	L24
-480	899	L25
-540	883	L26
-850	878	m8
-710	877	m7
-560	870	m6
-850	862	m5
-850	859	m4
-1180	857	m3
-1140	736	L34
-1030	709	L35
-1130	620	W
-1560	471	L48
-1580	461	L126
-1490	456	L125
-1500	443	L124
-1550	428	L123
-1480	405	L122
-1690	387	a5
-1650	382	a6
-1480	373	a1
-1630	370	a5
-1610	359	a8
-1470	359	a6
-1440	353	a7
-1540	350	a9
-1180	350	a8
-1790	348	a10
-1750	348	a9
-1740	276	L115
-1410	259	L114
-1750	250	K5
-1640	220	L106
-1680	209	L105
-1990	205	K2
-2190	183	K3
-2140	170	C1
-1910	160	K4
-2310	144	L103

1972

300	1420	B2
320	1419	L1
270	1360	L4
210	1285	L7
210	1270	B20
260	1210	L11
250	1123	L16
200	1074	L17
200	1042	L18
210	1001	L20
140	974	L21
230	956	L22
340	936	L23
320	913	L24
160	884	L25
120	880	L26
40	876	m8
-30	874	m7
150	872	L27
110	867	m6
110	859	m5
180	859	m2
150	856	m4
140	855	m3
100	849	mD
80	733	L34
190	708	L35
120	691	L36
-30	672	L37
-70	651	L38
90	637	L39
-30	624	L40
140	621	W6
120	620	W5
100	620	W4

1972 (cont.)

120	619	W3
40	616	W2
-320	477	L47
-110	470	L48
-550	459	L126
-400	454	L125
-710	441	L124
-820	426	L123
-580	403	L122
-720	392	L121
-500	385	a5
-850	379	a6
-490	378	a3
-710	377	a2
-800	375	A2
-760	373	A3
-920	373	A1
-560	373	a4
-290	373	a1
-420	372	A4
-490	368	A5
-570	366	a7
-730	360	a8
-510	357	A6
-430	352	A7
-820	349	A9
-410	349	A8
-1140	348	a10
-330	348	a9
-920	311	L118
-970	283	L116
-840	275	L115
-920	260	K6
-970	258	L114
-1030	250	L113
-890	238	K5
-1000	232	L112
-940	227	C3
-1110	224	L107
-1200	220	L106
-1210	216	C2
-1030	212	K1
-1210	209	L105
-1460	205	K2
-1500	204	L100
-1220	201	L111
-1290	191	KX
-1170	190	KZ
-1010	186	KY
-1300	183	K3
-1250	170	C1
-1340	160	K4
-1350	152	L104
-1580	144	L103
-1530	129	L101
-1930	112	L102

1973

350	1420	B2
450	1418	L1
300	1284	L7
410	1270	B20
330	1210	L11
350	1120	L16
370	1070	L17
340	1001	L20
330	891	L25
310	881	L26
360	874	m8
150	871	m7
120	869	L27
150	863	m6
250	856	m5
40	856	m2
90	852	m3
120	852	m4
-80	845	mD
180	729	L34
110	706	L35

1973 (cont.)

-130	690	L36
-330	668	L37
-290	648	L38
-240	634	L39
-210	619	W6
-200	619	W3
-180	618	W5
-270	618	W4
-330	616	W2
-580	474	L47
-400	467	L48
-860	414	L123
-930	399	L122
-1070	395	Drill
-710	380	a5
-540	376	a3
-850	374	L121
-710	373	a1
-980	371	a6
-1170	370	A3
-830	369	a4
-790	357	a8
-720	350	A7
-690	349	A9
-750	347	a9
-630	346	A8
-790	304	L118
-1100	184	KY

1974

210	1419	B2
190	1417	L1
200	1283	L7
200	1270	B20
170	1118	L16
150	1068	L17
-180	992	L20
10	947	L22
-90	927	L23
-70	905	L24
-190	888	L25
-280	879	L26
-310	872	m8
-270	869	m7
-250	866	L27
-230	862	m6
-510	854	m2
-150	853	m5
-220	850	m3
-280	848	m4
-300	841	mD
-400	726	L34
-290	703	L35
-400	685	L36
-470	665	L37
-570	645	L38
-540	631	L39
-650	618	W3
-730	616	W6
-630	616	W5
-730	615	W2
-840	350	A7
-920	345	A8
-1080	304	L116
-1120	282	L115
-1140	271	L114
-1170	255	K5
-1340	253	L113
-1210	240	L112
-1180	220	L111
-1220	220	K1
-1400	208	L107
-1570	205	C2
-1140	205	L106
-1300	202	L100
-1380	184	KY
-1360	171	C1
-1660	160	L103

1975

640	1419	B2
610	1417	L1
490	1282	L7
530	1279	B20
410	1116	L16
470	1063	L17
190	988	L20
360	962	L21
250	899	L24
120	877	L26
230	872	m12
0	866	m7
100	859	m6
10	850	m5
-60	847	m3
100	845	m4
-10	838	mD
-50	722	L34
-190	701	L35
-230	682	L36
-290	662	L37
-310	642	L38
-240	629	L39
-330	617	W3
-360	615	W4
-330	615	W2
-240	614	W6
-220	614	W5
-940	466	L48
-750	454	L126
-940	432	L124
-1030	397	L122
-1090	378	a5
-1040	378	a4
-910	375	a3
-1160	372	L121
-1350	368	A3
-940	368	a6
-1180	362	A5
-740	358	a7
-1110	355	a8
-970	352	A6
-1000	349	A7
-940	347	a9
-780	345	A8
-1120	328	L118
-970	312	L117
-1150	301	L116
-1300	280	L115
-1430	269	L114
-1170	253	K5
-1250	250	L113
-1330	235	L112
-1380	218	K1
-1230	216	L111
-1480	204	L107
-1250	202	L106
-1500	198	L100
-1210	189	KZ
-1490	183	KY
-1570	168	C1
-1570	159	L104
-1670	156	L103

1976

330	1419	B2
290	1416	L1
340	1281	L7
340	1278	B20
180	897	L24
170	882	L25
90	875	L26
-150	865	m8
0	860	m7
10	855	m6
0	845	m5
-220	843	m4
-80	832	mD
-30	698	L35

1976 (cont.)

-120	676	L36
-200	659	L37
-120	640	L38
-270	628	L39
-130	616	W3
-230	614	W4
10	614	W2
-170	613	W6
-380	613	W5
-1020	465	L48
-820	448	L126
-950	428	L124
-820	376	a4
-610	375	a5
-860	374	a3
-1040	370	a1
-800	370	L121
-1060	368	A1
-1150	365	a6
-720	365	A3
-930	360	A5
-730	356	a7
-560	353	a8
-480	350	A8
-720	350	A6
-740	346	a9
-570	345	A7
-1130	325	L118
-1080	298	L116
-930	280	L115
-1150	268	L114
-1040	250	K5
-1130	245	L113
-1030	238	K3
-1020	230	L112
-1110	220	L109
-1150	216	K1
-1140	211	L111
-1090	210	L108
-930	201	L107
-1020	198	L106
-1210	195	L110
-1190	195	L100
-1050	180	L105
-1210	175	KY
-1250	165	C1
-1140	160	KX
-1300	155	L104
-1130	150	L102
-1500	130	L103
-1570	130	L101

1977

120	1418	B2
150	1415	L1
130	1280	L7
100	1277	B20
90	1112	L16
-150	955	L21
-260	935	L22
-450	915	L23
-490	893	L24
-570	879	L25
-1300	850	m6
-1360	849	m2
-970	842	m3
-1080	841	m5
-1010	840	m4
-1030	828	mD
-1070	760	L32
-1230	726	L33
-1530	705	L34
-1430	694	L35
-1720	672	L36
-1800	656	L37
-1740	626	L39
-1730	613	W9
-1840	613	W3
-1700	612	W2

1977 (cont.)

-1770	611	W8
-1860	611	W4
-1700	609	W7
-1800	609	W5
-1700	608	W11
-1790	608	W6
-2460	501	L44
-2200	481	L45
-2060	474	L46
-2200	463	L48
-2270	444	L126
-2240	423	L124
-2240	393	L122
-2020	373	a4
-2340	373	a3
-2540	369	a1
-2090	368	L121
-2940	368	A1
-2380	365	A4
-2720	365	A3
-2050	362	a6
-2390	357	A5
-1860	353	a7
-1970	350	a8
-2140	349	A8
-2170	347	A6
-2300	345	a9
-2200	342	A7
-2410	322	L118
-2310	295	L116
-2370	278	L115
-2290	267	L114
-2390	248	K5
-2430	241	L113
-2290	227	L112
-2490	219	L109
-2220	215	K1
-2370	210	L111
-2560	208	L108
-2480	201	L107
-2260	197	L106
-2730	194	L100
-2360	192	L110
-2530	172	KY
-2450	163	C1
-2420	157	KX
-2330	153	L104
-2470	147	L102
-2790	127	L103
-2730	127	L101

1978

240	1415	L1
260	1280	L7
200	1277	B20
250	1109	L16
-90	952	L21
-170	932	L22
-130	912	L23
-70	890	L24
-400	876	L25
-890	839	m3
-630	838	m5
-700	837	m4
-1060	653	L37
-1110	636	L38
-1030	624	L39
-1010	612	W2
-1140	612	W3
-1100	610	W11
-1130	608	W4
-1110	608	W8
-1130	605	W5
-1130	605	W6
-1820	160	C1

1979

200	1418	B2
180	1415	L1
200	1279	L7
200	1276	B20
180	1165	L12
200	1106	L16
80	975	L20
30	950	L21
-30	930	L22
-80	910	L23
-250	874	L25
-200	835	m5
-630	835	m4
-660	760	L32
-580	725	L33
-670	695	L34
-670	652	L37
-890	635	L38
-850	622	L39
-820	611	W11
-1040	610	W10
-690	610	W2
-1000	608	W3
-850	602	W4
-1020	601	W9
-770	597	W5
-860	596	W8
-910	594	W7
-690	594	W6
-1080	580	L41
-1090	466	L47
-1300	425	L124
-1440	385	L122
-1030	372	a4
-1240	370	a3
-1490	370	a1
-1030	369	a5
-1050	365	L121
-1430	360	A3
-950	360	a6
-1230	360	L120
-1230	355	A9
-940	355	a8
-1030	353	a9
-1000	352	A8
-1210	348	A5
-1000	340	L119
-1300	320	L118
-1250	299	L116
-1300	280	L115
-1750	270	L114
-1350	265	78-1
-1600	260	78-2
-1320	238	K3
-1230	220	78-4
-1490	210	78-5
-1370	210	L106
-1450	195	78-9
-1410	190	78-8
-1320	175	KZ
-1550	160	KX
-1360	155	L102
-1650	130	78-12

1983

230	1460	Extra
290	1340	L1
190	1285	?
240	1235	Blue
230	1205	M2
240	1165	L16
180	1110	L17
90	1045	L18
220	1020	L19
170	975	L20
160	955	L21
160	935	L22
80	925	L23
-1140	620	CWGH

1983 (cont.)

-1660	380	CWGF
-1280	380	CWGF1
-1660	260	CWGE
-2440	230	OWPA1
-1610	220	CWGD
-1620	210	WG4
-2000	180	CWGB
-2020	165	CWGA
-1520	155	WG3
-1620	140	OWPA2
-1890	115	WG1
-2100	110	WG2

1984

260	1590	CJA1
530	1460	Extra
230	1340	L1
200	1285	?
230	1235	Blue
190	1205	M2
230	1165	L16
40	1110	L17
40	1045	L18
190	1020	L19
80	975	L20
90	955	L21
40	935	L22
50	925	L23
-1140	620	CWGH
-1050	380	CWGF
-1130	380	CWGF1
-1570	260	CWGE
-1420	230	OWPA1
-1610	220	CWGD
-1040	210	WG4
-1660	180	CWGB
-1750	165	CWGA
-2100	155	WG3
-2700	140	OWPA2
-2480	115	WG1
-2760	110	WG2

1985

260	1590	CJA1
370	1510	DCP1
210	1460	Extra
430	1340	L1
210	1285	?
200	1235	Blue
150	1205	M2
210	1165	L16
30	1110	L17
20	1045	L18
140	1020	L19
50	975	L20
70	955	L21
70	935	L22
50	925	L23
-1050	380	CWGF
-1130	380	CWGF1
-1570	260	CWGE
-1430	230	OWPA1
-1620	220	WG5
-1610	220	CWGD
-1040	210	WG4
-1660	180	CWGB
-1750	165	CWGA
-1990	155	WG3
-2460	140	OWPA2
-1980	115	WG1
-2760	110	WG2

1986

320	1590	CJA1
350	1510	DCP1
260	1460	Extra
230	1340	L1

1986 (cont.)

190	1285	?
240	1235	Blue
240	1205	M2
170	1165	L16
140	1110	L17
70	1045	L18
140	1020	L19
50	975	L20
90	955	L21
80	935	L22
100	925	L23
-1360	735	CWGEx
-2080	625	CWGG
-1860	620	CWGK
-2190	620	CWGH
-1740	615	CWGL
-1890	380	CWGF
-2030	380	CWGF1
-3140	260	CWGE
-2660	230	OWPA1
-2270	220	CWGD
-2920	220	WG5
-1870	210	WG4
-2990	180	CWGB
-3120	165	CWGA
-3390	155	WG3
-3480	140	OWPA2
-3400	115	WG1
-3070	110	WG2

1987

60	1590	CJA1
90	1510	DCP1
70	1460	Extra
-240	1340	L1
-330	1285	?
-290	1235	Blue
-370	1205	M2
-540	1165	L16
360	1110	L17
-500	1045	L18
-490	975	L20
-380	955	L21
170	935	L22
-560	925	L23
-1360	735	CWGEx
-1740	620	CWGK
-1740	620	CWGH
-2090	615	CWGL
-1800	380	CWGF
-2260	380	CWGF1
-4240	260	CWGE
-3390	230	OWPA1
-3430	220	WG5
-3610	220	CWGD
-3390	210	WG4
-3000	180	CWGB
-4680	165	CWGA
-3500	155	WG3
-3480	140	OWPA2
-3480	115	WG1
-3480	110	WG2

1988

330	1590	CJA1
300	1510	DCP1
210	1460	Extra
220	1340	L1
280	1285	?
230	1235	Blue
240	1205	M2
260	1165	L16
110	1110	L17
160	1045	L18
10	975	L20
240	955	L21
240	935	L22
120	925	L23

1986 (cont.)

-60	380	CWGF
-280	380	CWGF1
-820	230	OWPA1
-900	220	CWGD
-550	220	WG5
-760	210	WG4
-970	180	CWGB
-1170	165	CWGA
-1430	155	WG3
-1280	140	OWPA2
-1570	115	WG1

1989

280	1590	CJA1
250	1510	DCP1
130	1460	Extra
100	1340	L1
120	1285	?
200	1235	Blue
130	1205	M2
190	1165	L16
-30	1110	L17
30	1045	L18
20	1020	L19
20	975	L20
70	955	L21
120	935	L22
20	925	L23
-150	625	CWGG
40	620	CWGK
40	620	CWGH
-110	615	CWGL
-60	380	CWGF
-630	260	CWGE
-840	230	OWPA1
-650	220	CWGD
-550	220	WG5
-840	210	WG4
-770	180	CWGB
-720	165	CWGA
-1380	155	WG3
-1580	140	OWPA2
-1560	115	WG1
-1940	110	WG2

1990

120	1590	CJA1
150	1510	DCP1
-20	1460	Extra
-40	1340	L1
-50	1285	?
-70	1235	Blue
-80	1205	M2
-90	1165	L16
-590	1110	L17
-370	1045	L18
-230	1020	L19
-630	975	L20
-700	955	L21
-450	935	L22
-770	925	L23
-930	735	CWGEx
-1130	625	CWGG
-1280	620	CWGK
-1740	380	CWGF1
-1760	220	CWGD
-1720	220	WG5
-1800	210	WG4
-2160	180	CWGB
-2060	165	CWGA
-2740	155	WG3
-2790	115	WG1
-2740	110	WG2

1991

320	1590	CJA1
250	1510	DCP1

1991 (cont.)

160	1460	Extra
150	1340	L1
80	1285	?
80	1235	Blue
40	1205	M2
80	1165	L16
0	1110	L17
0	1045	L18
40	1020	L19
-170	975	L20
-170	955	L21
-140	935	L22
-370	925	L23
-620	735	CWGEx
-950	625	CWGG
-780	620	CWGK
-890	380	CWGF
-1470	220	CWGD
-1500	220	WG5
-2370	210	WG4
-1870	180	CWGB
-1650	165	CWGA
-2130	155	WG3
-3160	115	WG1
-2660	110	WG2

1992

140	1590	CJA1
150	1510	DCP1
90	1460	Extra
50	1340	L1
-100	1285	?
-120	1235	Blue
-150	1205	M2
-70	1165	L16
-300	1110	L17
-370	1045	L18
-240	955	L21
-340	935	L22
-820	735	CWGEx
-950	380	CWGF1
-810	380	CWGF
-800	220	WG5
-920	220	CWGD
-1390	210	WG4
-1610	180	CWGB
-1210	165	CWGA
-1510	155	WG3
-2380	115	WG1
-2330	110	WG2

1993

230	1590	CJA1
200	1510	DCP1
110	1460	Extra
120	1340	L1
-160	1285	?
-190	1235	Blue
-230	1205	M2
-110	1165	L16
-450	1110	L17
-550	1045	L18
-370	955	L21
-510	935	L22
-1230	735	CWGEx
-1430	380	CWGF1
-1450	380	CWGF
-1710	220	WG5
-1390	220	CWGD
-2500	210	WG4
-2420	180	CWGB
-2630	165	CWGA
-2470	155	WG3
-2370	115	WG1
-3510	110	WG2

1994

330	1590	CJA1
240	1510	DCP1
120	1460	Extra
100	1340	L1
120	1285	?
80	1235	Blue
-70	1165	L16
-140	1110	L17
-450	1045	L18
-260	955	L21
-560	770	WG8
-920	745	WG7
-1630	380	CWGF1
-1320	380	CWGF
-1210	375	WG6
-2260	220	CWGD
-1660	220	WG5
-670	210	WG4
-1890	180	CWGB
-3680	165	CWGA
-2130	155	WG3
-3990	155	WG0
-3100	115	WG1
-2400	110	WG2

1995

330	1590	CJA1
350	1510	DCP1
260	1460	Extra
180	1340	L1
70	1285	?
-180	1235	Blue
-50	1205	M2
-100	1165	L16
-330	1110	L17
-50	1045	L18
-300	1020	L19
-470	1020	L19A
-450	955	L21
-450	935	L22
-680	830	WG9
-860	770	WG8
-1080	735	CWGEx
-1320	660	WG7
-2460	380	CWGF1
-2160	380	CWGF
-2230	220	WG5
-2200	220	CWGD
-2840	210	WG4
-2470	180	CWGB
-2390	165	CWGA
-2760	155	WG3
-3540	115	WG1
-2760	110	WG2
-2210	110	WG0

1996

224	1485	CJA1
200	1463	LP2
267	1421	DCP1
82	1348	Extra
153	1258	L1
163	1197	?
162	1165	Blue
30	1070	L16
63	1018	L17
108	959	L18
36	934	L19
144	920	L19A
57	877	L21
-90	869	L22
27	793	WG9
18	698	WG8
-36	658	CWGEx
-99	614	WG7
-306	462	LP8
-297	421	WG6
-333	373	LP9

1996 (cont.)

-891	310	CWGF1
-504	310	CWGF
-558	228	WG5
-580	211	CWGD
-652	193	WG4
-684	191	LP10
-1020	159	WG3
-1440	152	WG0
-756	142	CWGA
-1570	127	WG2
-1035	122	WG1

1997

472	1485	CJA1
374	1473	WPA1
329	1463	LP2
334	1437	WPA2
399	1421	DCP1
349	1381	LP4
256	1355	WPA3
328	1348	Extra
296	1325	JGC2
289	1292	WPA4
288	1275	WPA5
177	1258	L1
287	1197	?
285	1165	Blue
345	1135	M2A
220	1070	L16
-53	1018	L17
-198	959	L18
-189	934	L19
-198	920	L19A
-459	877	L21
-144	877	L21A
-207	869	L22
-634	793	WG9
-717	750	LP5
-682	698	WG8
-639	658	CWGEx
-942	614	WG7
-1203	570	LP6
-792	462	LP8
-1143	421	WG6
-1170	372	LP9
-1260	315	CWGF
-1008	310	CWGF1
-1413	228	WG5
-891	211	CWGD
-1867	192	WG4
-1309	191	LP10
-1557	189	CWGB
-2151	159	WG3
-2268	152	WG0
-2142	152	WG0A
-1775	142	CWGA
-2592	127	WG2
-2007	121	WG1

1998

137	1525	JGC1
227	1485	CJA1
159	1473	WPA1
177	1463	LP2
159	1437	WPA2
209	1421	DCP1
115	1381	LP4
284	1355	WPA3
232	1348	Extra
172	1325	JGC2
210	1292	WPA4
232	1275	WPA5
198	1258	L1
170	1197	?
104	1165	Blue
162	1135	M2A
91	1070	L16
-153	1018	L17

1998 (cont.)

-99	959	L18
-243	934	L19
-180	920	L19A
-297	900	L20
-369	877	L21
-315	877	L21A
-675	869	L22
-540	793	WG9
-864	750	LP5
-891	698	WG8
-873	658	CWGEx
-846	614	WG7
-855	570	LP6
-1575	462	LP8
-2016	421	WG6
-1741	372	LP9
-2376	315	CWGF
-2484	310	CWGF1
-2304	228	WG5
-2610	211	CWGD
-2749	192	WG4
-2196	191	LP10
-2189	189	CWGB
-2601	159	WG3
-3384	152	WG0
-2070	142	CWGA
-3366	127	WG2
-2133	121	WG1

1999

212	1525	JGC1
200	1485	CJA1
193	1473	WPA1
185	1463	LP2
96	1437	WPA2
203	1421	DCP1
207	1381	LP4
153	1355	WPA3
184	1348	Extra
178	1325	JGC2
169	1292	WPA4
272	1275	WPA5
184	1258	L1
134	1197	?
96	1165	Blue
-72	1135	M2A
-532	1070	L16
-783	1018	L17
-882	959	L18
-1125	934	L19
-1008	920	L19A
-819	900	L20
-1435	793	WG9
-1755	750	LP5
-1512	698	WG8
-1575	665	CWGS
-1692	658	CWGEx
-1786	614	WG7
-1917	570	LP6
-1872	462	LP8
-1962	421	WG6
-2043	372	LP9
-2385	315	CWGF
-2667	310	CWGF1
-2142	228	WG5
-1908	211	CWGD
-2574	192	WG4
-2304	191	LP10
-2142	189	CWGB
-2232	159	WG3
-2457	152	WG0
-2277	142	CWGA
-3132	127	WG2
-2700	121	WG1

2000

130	1518	JGC1
99	1489	CJA1
45	1455	WPA1
117	1468	LP2
66	1421	WPA2
163	1423	DCP1
94	1384	LP4
71	1355	WPA3
105	1348	Extra
50	1317	JGC2
60	1291	WPA4
91	1278	WPA5
91	1266	L1
-63	1192	?
-180	1165	Blue
-108	1120	M2
-540	1120	M2A
-774	1063	L16
-405	1063	L16A
-252	1018	L17
-675	934	L19
-594	879	L20
-621	877	L21
-720	864	L22
-1089	793	WG9
-1332	747	LP5
-936	698	WG8
-963	690	CWGT
-1350	648	CWGS
-1071	643	CWGEx
-1449	614	WG7
-1179	614	WG7A
-1188	570	LP6
-1368	570	LP6A
-1431	449	LP8
-1242	449	LP8A
-1711	403	WG6
-1611	403	WG6A
-1431	363	LP9
-3582	330	CWGF
-1944	315	CWGF1
-1854	224	WG5
-1773	196	CWGD
-2106	192	WG4
-1876	190	LP10
-1917	152	CWGB
-1998	171	WG3
-2052	152	WG0
-2187	136	CWGA
-2304	127	WG2
-3042	121	WG1

2001

242	1518	JGC1
179	1489	CJA1
186	1455	WPA1
291	1468	LP2
125	1421	WPA2
154	1423	DCP1
214	1384	LP4
144	1355	WPA3
159	1348	Extra
76	1317	JGC2
98	1291	WPA4
183	1278	WPA5
153	1266	L1
170	1192	?
-9	1165	Blue
103	1160	Blue2
-36	1120	M2
36	1135	M2A
-126	1063	L16
-342	1065	L16A
-153	1018	L17
-333	950	L18
-108	934	L19
-301	879	L20
-297	877	L21
-360	864	L22

2001 (cont.)

-711	793	WG9
-864	747	LP5
-648	698	WG8
-630	698	WG8A
-409	690	CWGT
-567	648	CWGS
-864	643	CWGEx
-688	614	WG7
-774	570	LP6
-877	449	LP8
-1215	403	WG6A
-1201	363	LP9
-1305	315	CWGF1
-1165	251	ST4
-1219	224	WG5A
-1089	228	WG5
-1350	196	CWGD
-1210	192	WG4
-1269	192	WG4A
-1507	190	LP10
-1505	190	LP10A
-1440	152	CWGB
-1422	171	WG3
-1489	171	WG3A
-1701	152	WG0
-1377	152	WG0A
-1485	136	CWGA
-1831	127	WG2
-1813	121	WG1

2002

194	1518	JGC1
147	1489	CJA1
302	1455	WPA1
176	1468	LP2
173	1421	WPA2
168	1423	DCP1
126	1384	LP4
308	1355	WPA3
130	1348	Extra
137	1317	JGC2
263	1291	WPA4
175	1278	WPA5
243	1266	L1
-90	1192	?
0	1165	Blue
-36	1160	Blue2
296	1135	M2A
-9	1065	L16A
468	1018	L17
468	950	L18
342	934	L19
270	879	L20
72	877	L21
0	864	L22
-261	793	WG9
-76	747	LP5
-945	698	WG8
-513	698	WG8A
-207	690	CWGT
-301	643	CWGEx
-189	614	WG7
-459	614	WG7A
-432	570	LP6
-913	449	LP8
-828	403	WG6A
-954	421	WG6
-1199	363	LP9
-1210	363	LP9A
-1278	315	CWGF1
-1246	251	ST4
-1341	251	ST4A
-1350	196	CWGD
-1845	192	WG4A
-1737	190	LP10
-2097	152	CWGB
-1786	171	WG3
-1818	159	WG3A
-981	152	WG0

2002 (cont.)

-432	152	WG0A
-2241	136	CWGA
-1908	127	WG2
-1962	121	WG1

2003

628	1518	JGC1
402	1489	CJA1
485	1455	WPA1
372	1468	LP2
373	1421	WPA2
532	1423	DCP1
347	1384	LP4
334	1355	WPA3
462	1348	Extra
281	1317	JGC2
388	1291	WPA4
413	1278	WPA5
324	1266	L1
540	1192	?
571	1165	Blue
605	1160	Blue2
-216	1135	M2A
-369	1065	L16A
-360	1018	L17
-288	950	L18
-463	934	L19
-526	879	L20
-432	877	L21
-603	864	L22
-756	793	WG9
-1048	747	LP5
-913	698	WG8
-1278	690	CWGT
-1206	648	CWGS
-1134	643	CWGEx
-1287	614	WG7A
-1719	570	LP6
-1300	421	WG6
-1332	363	LP9A
-1381	251	ST4A
-1530	228	WG5
-1656	196	CWGD
-1606	192	WG4
-1683	190	LP10
-1638	190	LP10A
-2110	159	WG3A
-2191	159	WG3B
-1917	152	WG0B
-2340	136	CWGA
-1728	127	WG2
-1786	121	WG1

2004

324	1518	JGC1
283	1489	CJA1
290	1455	WPA1
225	1468	LP2
192	1421	WPA2
276	1423	DCP1
284	1384	LP4
242	1355	WPA3
258	1348	Extra
244	1317	JGC2
393	1292	WPA4
262	1278	WPA5
196	1266	L1
168	1192	?
211	1165	Blue
153	1160	Blue2
342	1070	L16A
252	1018	L17
162	950	L18
112	934	L19D
139	900	L20
81	900	L20A
9	877	L21
-319	869	L22

2004 (cont.)

-135	793	WG9
-252	750	LP5
-306	698	WG8
-450	690	CWGT
-252	648	CWGS
-522	643	CWGEx
-639	614	WG7A
-765	570	LP6
-1066	462	LP8
-1192	421	WG6
-1102	421	WG6A
-1066	383	JP4
-1152	378	JP3
-1242	378	JP5
-1089	372	LP9
-1156	359	JP2
-648	348	JP1
-1505	310	CWGF1
-1372	251	ST4
-1323	228	WG5
-1435	228	WG5A
-1134	211	CWGD
-1705	192	WG4
-1530	190	LP10A
-1588	190	LP10B
-1764	171	WG3B
-1710	152	WG0
-1917	136	CWGA
-1764	127	WG2
-1795	127	WG2A
-1620	121	WG1

2005

353	1518	JGC1
144	1489	CJA1
269	1455	WPA1
277	1468	LP2
196	1421	WPA2
298	1423	DCP1
226	1384	LP4
380	1355	WPA3
214	1348	Extra
188	1317	JGC2
156	1291	WPA4
170	1278	WPA5
-27	1266	L1
-252	1192	?
-333	1160	Blue2
-817	1135	M2A
-783	1065	L16A
-387	1018	L17
-747	950	L18
-1134	934	L19
-936	879	L20
-1170	877	L21
-1782	864	L22
-1755	793	WG9
-1962	698	WG8
-1836	690	CWGT
-2106	648	CWGS
-2106	643	CWGEx
-2362	421	WG6
-2997	196	CWGD
-2970	159	WG3A
-3636	136	CWGA
-3123	127	WG2

2006

422	1518	JGC1
206	1489	CJA1
186	1455	WPA1
316	1468	LP2
175	1421	WPA2
273	1423	DCP1
187	1384	LP4
266	1355	WPA3
307	1348	EXTRA
204	1317	JGC2

2006 (cont.)

200	1292	WPA4
204	1278	WPA5
266	1266	L1
246	1192	QMARK
270	1165	BLUE
175	1160	BLUE2
36	1120	M2A
135	1070	L16A
-72	1018	L17
-94	950	L18
45	934	L19D
-225	900	L20
-306	877	L21
-900	869	L22
-621	793	WG9
-540	793	WG9A
-540	750	LP5
-648	698	WG8
-486	690	CWGT
-706	648	CWGS
-594	643	CWGX
-756	614	WG7A
-1008	570	LP6
-1129	462	LP8
-1107	421	WG6
-1224	372	LP9
-1287	315	ST6
-1386	251	ST4
-1435	228	WG5
-1507	192	WG4
-1575	190	LP10A
-1984	171	WG3B
-1993	152	WG0
-2529	136	CWGA
-2277	127	WG2
-2232	121	WG1

2007

248	1521	JGC1
184	1492	CJA1
110	1458	WPA1
178	1467	LP2
72	1419	WPA2
191	1418	DCP1
148	1372	LP4
80	1348	WPA3
184	1329	EXTRA
111	1302	JGC2
100	1275	WPA4
113	1260	WPA5
97	1243	L1
-555	1171	QMARK
-749	1140	BLUE
-503	1139	BLUE2
-1100	1018	L16A
-1280	949	L17
-1030	892	L18
-1745	859	L19
-1785	843	L20
-2000	838	L21
-2510	839	L22
-2500	740	WG9
-2480	703	LP5
-2380	686	WG8
-2142	679	CWGT
-2007	620	CWGS
-2038	615	CWGX
-2560	587	WG7
-2770	568	LP6
-2835	490	LP8
-3110	422	WG6
-2480	398	LP9A
*-3220	196	WG4
*-3549	195	WG5
-3663	184	CWGD
*-3253	183	LP10
*-3630	168	WG3
-4644	132	CWGA
*-3862	127	WG1

2008

114	1521	JGC1
89	1492	CJA1
79	1458	WPA1
40	1467	LP2
12	1419	WPA2
108	1418	DCP1
91	1372	LP4
64	1348	WPA3
90	1329	EXTRA
59	1302	JGC2
84	1275	WPA4
115	126	WPA5
14	1243	L1
-73	1171	QMARK
-648	1140	BLUE
-651	1139	BLUE2
-1516	1060	L16A
-1116	949	L17
-1260	949	L17A
-1773	892	L18
-1471	906	L18A
-1642	880	L19
-1588	863	L20
-1777	851	L21A
-2038	745	WG9A
-2160	684	WG8A
-1782	667	CWGT
-2079	629	CWGS
-2169	625	CWGX
-2061	598	WG7A
-2290	575	LP6A
-2250	488	LP8A
-2142	423	WG6
-2196	398	LP9A
-2475	299	ST6
-1980	237	ST4
-2835	188	WG5
-2493	189	CWGD
-1827	184	WG4
-2682	186	LP10
-3055	157	WG3
-4770	120	CWGA
-3631	112	WG1

2009

176	1521	JGC1
156	1497	CJA1
172	1466	WPA1
173	1459	LP2
162	1414	WPA2
197	1411	DCP1
188	1381	LP4
173	1339	WPA3
241	1329	EXTRA
154	1300	JGC2
188	1273	WPA4
164	1260	WPA5
165	1238	L1
107	1228	MARK
-648	1140	BLUE
-651	1139	BLUE2
-954	1020	L16A
-981	1018	L16D
-873	1016	L16E
-913	966	L17A
-1084	906	L18A
-1287	859	L19
-1305	845	L20
-1332	836	L21A
-1449	703	LP5
-1476	680	WG8A
-1359	667	CWGT
-1620	621	CWGX
-1575	598	WG7A
-2767	575	LP6A
-2092	488	LP8A
-2133	423	WG6
-2119	382	LP9A
-2241	293	ST6

2009 (cont.)

-2317	237	ST4
-2610	188	WG5
-2376	177	CWGD
-2637	190	WG4
-2542	180	LP10
-2817	154	WG3
-3348	112	WG1

2010

431	1520	JGC1
250	1486	CJA1
255	1455	WPA1
276	1479	LP2
231	1449	WPA2
283	1441	DCP1
325	1273	WPA4
252	1261	WPA5
211	1228	L1
255	1160	QMARK
-54	1126	BLUE
-90	1129	BLUE2
-378	1043	L16A
-189	949	L17
-135	950	L17A
-445	890	L18A
-706	843	L20
-792	836	L21A
-1228	740	WG9A
-972	703	LP5
-720	679	CWGT
-1089	587	WG7A
-1170	575	LP6A
-1539	457	LP8A
-1579	408	WG6
-1795	382	LP9A
-1926	290	ST6
-1998	242	ST4
-2128	191	WG5
-1350	177	CWGD
-2205	190	WG4
-2124	180	LP10
-2569	154	WG3
-3006	114	WG1

2011

293	1520	JGC1
243	1486	CJA1
165	1455	WPA1
248	1479	LP2
-160	1449	WPA2
343	1441	DCP1
261	1364	LP4
156	1343	WPA3
-446	1329	EXTRA
-590	1308	JGC2
-417	1273	WPA4
-933	1261	WPA5
-936	1228	L1
-1248	1160	QMARK
-819	1126	BLUE
-603	1043	L16Z
-1791	950	L17
-1998	859	L18A
-2002	836	L20
-2430	680	LP5
-2412	679	CWGT
-2196	457	LP6A
-2259	382	WG6
-2808	298	LP9A
-3429	177	WG5
-3402	154	LP10
-3825	154	WG3
-4140	114	WG1

2012			2013			2014			2015		
199	1520	JGC1	215	1520	JGC1	138	1519	JGC1	119	1519	JGC1
213	1497	CJA1	184	1497	CJA1	162	1457	WPA1	190	1457	WPA1
-63	1447	WPA1	225	1447	WPA1	93	1480	CJA1	188	1480	CJA1
148	1459	LP2	185	1459	LP2	116	1415	WPA2	97	1415	WPA2
-162	1410	WPA2	175	1410	WPA2	122	1459	LP2	119	1459	LP2
-135	1411	DCP1	209	1411	DCP1	130	1411	DCP1	119	1411	DCP1
-549	1376	LP4	161	1376	LP4	107	1374	LP4	95	1374	LP4
99	1341	WPA3	136	1341	WPA3	144	1341	WPA3	147	1341	WPA3
-171	1324	EXTRA	246	1324	EXTRA	187	1324	EXTRA	91	1324	EXTRA
-432	1285	JGC2	130	1295	JGC2	106	1295	JGC2	79	1295	JGC2
-704	1265	WPA4	184	1265	WPA4	99	1265	WPA4	87	1265	WPA4
-387	1261	WPA5	184	1261	WPA5	98	1261	WPA5	28	1261	WPA5
-778	1238	L1	162	1238	L1	128	1238	L1	-315	1238	L1
-387	1228	QMARK	108	1228	QUERY	-306	1228	QMARK	-360	1228	QMARK
-837	1144	BLUE	140	1144	BLUE	-189	1170	BLUE2	-490	1170	BLUE2
-1305	1043	L16	50	1043	L16	-477	1041	L16A	-1116	1041	L16A
-1278	1043	L16A	150	1043	L16Z	-414	1041	L16Z	-1449	901	L18
-1363	1043	L16Z	120	901	L18A	-720	901	L18	-1350	866	L19
-1476	848	L17	200	872	L19	-841	866	L19	-1557	861	L20
-1701	859	L18A	0	856	L20	-1053	861	L20	-1471	747	WG9A
-1800	872	L19	-198	842	L21	-1075	747	WG9	-1737	702	WG8
-1746	836	L20	-112	770	WG9	-1120	726	LP5	-1764	668	CWGT
-1944	842	L21	-171	687	LP5	-940	702	WG8A	-1845	625	CWGEx
-2034	770	WG9	-103	680	WG8	-976	702	WG8	-1768	597	WG7
-2025	680	LP5	-117	679	CWGT	-1080	668	CWGT	-2151	556	LP6
-1782	680	WG8	-243	621	CWGX	-1224	625	CWGEx	-2133	482	LP8
-1755	679	CWGT	-270	591	WG7	-1134	597	WG7	-2038	394	WG6
-1989	621	CWGX	-328	457	LP6	-1575	556	LP6	-1926	367	LP9
-1971	575	WG7	-504	453	LP8	-1683	482	LP8	-2493	298	ST6
-2403	456	LP8	-531	394	WG6	-1435	394	WG6	-2016	242	ST4
-2412	382	WG6	-504	394	WG6A	-1453	367	LP9	-2560	195	WG5
-2331	368	LP9	-477	367	LP9	-1795	298	ST6	-2232	199	WG4
-2673	293	ST6	-562	367	LP9A	-1750	242	ST4A	-2574	176	ST2
-2619	191	ST4	-702	289	ST6	-2124	195	WG5	-2659	180	LP10
-2979	177	WG5	-787	289	ST6A	-1840	199	WG4	-3370	150	WG3
-2745	180	WG4	-765	191	ST4	-1876	176	ST2			
-2952	154	LP10	-787	191	ST4A	-2421	180	LP10			
-3096	142	WG3	-855	187	WG5	-2178	150	WG3			
-3636	107	WG1	-891	187	WG5A	-2884	122	WG1			
			-877	167	CWGD						
			-877	167	ST2						
			-882	193	WG4						
			-985	193	WG4A						
			-1143	170	LP10						
			-990	170	LP10A						
			-1296	142	WG3						
			-1593	107	WG1						

APPENDIX 3: dGPS AND TEMPERATURE DATA 2012-2015

A3 Figure 1. dGPS station located at the Lower station (~370 m a.s.l.), July 2014.

Dual-frequency GPS (dGPS) measurements were collected at White Glacier between 2012 and 2015 for the purposes of velocity measurement and comparison with earlier glacier dynamics studies conducted between 1960-1970. Details of the methods and findings of these earlier studies are available in Müller and Iken [1973] and Iken [1974]. Contemporary calculations of ice motion were acquired from differencing daily average positions at the Upper (~870 m a.s.l.), Middle (~580 m a.s.l.), and Lower (~370 m a.s.l.) dGPS stations at the same geographic locations of the earlier studies. The instrumentation and installation of the stations is shown in A3, Figure 1, and described in Chapter 4, Section 4.4.2, which includes details of the post-processing techniques using the Precise Point Positioning (PPP) tool provided by Natural Resources Canada: http://webapp.geod.nrcan.gc.ca/geod/tools-outils/ppp.php

The following Appendix provides tables of dGPS measurements of daily position, velocity, and temperature, as well as their associated errors for each station for a given year. The daily mean Easting (E), Northing (N), and Elevation (Z) is derived from the average of 24 hours of position measurements (collected on a 15 s sampling interval) from 00h00 to 23h59, such that the daily mean position is centered on noon (12h00) for a given day of year (DOY). The standard deviations of these E, N, and Z positions (noted as E_std, N_std, and Z_std) are provided and incorporate both instrument error and the displacement over the course of one day. The daily velocity down-glacier (Vx) is calculated from the slope of a linear regression through the down-glacier displacement and sample time. The associated error (Vx_err) is the root-mean square error incorporating the standard deviations of E and N. Daily mean temperatures (T) were calculated from hourly measurements by shielded HOBO-U23 temperature/relative humidity loggers. In instances where loggers failed or were not yet installed, T was modelled using daily temperature lapse-rates derived from two automatic weather stations at the glacier terminus and an upper nunatak. The final column in the tables provided (*) indicates whether the temperature values are based upon this model (1) or observation (2). In 2012 the middle dGPS was initially programmed to collect positions every 15 s for 1 hour between 12h00 and 13h00 local time daily. In this case, E, N, Z are calculated from the mean of 1 hour of observation, and similarly for their standard deviations. Vx is derived from the displacement between daily mean positions and therefore the first DOY with observations does not have corresponding Vx or Vx_err values. Coordinates are in NAD83 UTM zone 15N and elevations are given in the Canadian Geodetic Vertical Datum (CGVD28_HTv2.0).

Upper (Moraine) Profile: 2013

DOY	E(m)	N(m)	Z(m)	E_std(m)	N_std(m)	Z_std(m)	Vx(cm d^{-1})	Vx_err	T(C°)	*
119	544449.901	8825972.957	863.137	0.024	0.020	0.037	9.81	0.80	-17.0	2
120	544449.974	8825972.887	863.146	0.022	0.022	0.026	10.28	0.75	-16.1	2
121	544450.042	8825972.817	863.124	0.021	0.021	0.026	9.57	0.65	-8.5	2
122	544450.113	8825972.747	863.141	0.021	0.021	0.026	9.72	0.57	-13.8	2
123	544450.181	8825972.679	863.130	0.020	0.022	0.026	9.93	0.68	-19.9	2
124	544450.251	8825972.609	863.145	0.022	0.022	0.024	10.32	0.61	-21.2	2
125	544450.319	8825972.541	863.128	0.020	0.022	0.023	9.97	0.62	-22.3	2
126	544450.389	8825972.472	863.139	0.020	0.022	0.025	10.00	0.60	-19.8	2
127	544450.459	8825972.403	863.137	0.022	0.022	0.026	10.31	0.63	-18.5	2
128	544450.530	8825972.334	863.134	0.022	0.021	0.025	10.16	0.59	-23.3	2
129	544450.597	8825972.264	863.128	0.024	0.020	0.026	10.35	0.58	-24.2	2
130	544450.667	8825972.195	863.124	0.026	0.023	0.028	11.23	0.74	-21.0	2
131	544450.739	8825972.126	863.118	0.023	0.021	0.027	10.43	0.69	-20.2	2
132	544450.806	8825972.059	863.122	0.026	0.023	0.032	10.33	1.22	-18.9	2
133	544450.877	8825971.988	863.121	0.023	0.022	0.025	10.59	0.66	-19.5	2
134	544450.948	8825971.920	863.118	0.024	0.023	0.024	10.81	0.73	-18.6	2
135	544451.015	8825971.849	863.125	0.021	0.023	0.028	10.33	0.68	-17.5	2
136	544451.088	8825971.782	863.117	0.022	0.021	0.026	9.83	0.74	-13.2	2
137	544451.156	8825971.712	863.121	0.023	0.022	0.027	10.23	0.87	-9.2	2
138	544451.225	8825971.642	863.117	0.021	0.021	0.022	9.99	0.68	-7.4	2
139	544451.293	8825971.572	863.112	0.021	0.022	0.023	10.09	0.66	-10.4	2
140	544451.363	8825971.503	863.116	0.020	0.022	0.022	9.93	0.60	-12.0	2
141	544451.432	8825971.434	863.115	0.023	0.022	0.025	10.46	0.64	-10.3	2
142	544451.502	8825971.365	863.113	0.022	0.021	0.022	10.17	0.62	-9.9	2
143	544451.572	8825971.296	863.110	0.023	0.023	0.022	10.85	0.71	-9.2	2
144	544451.645	8825971.227	863.112	0.026	0.022	0.024	11.23	0.70	-10.8	2
145	544451.711	8825971.158	863.107	0.023	0.022	0.024	10.50	0.73	-7.0	2
146	544451.780	8825971.090	863.107	0.023	0.021	0.022	10.24	0.71	-12.2	2
147	544451.851	8825971.019	863.111	0.023	0.020	0.026	9.86	0.66	-5.2	1
148	544451.917	8825970.951	863.096	0.022	0.020	0.023	9.69	0.81	-6.1	1
149	544451.989	8825970.880	863.099	0.022	0.022	0.022	10.18	0.77	-5.6	1
150	544452.058	8825970.810	863.094	0.022	0.022	0.023	10.22	0.70	-6.6	1
151	544452.127	8825970.741	863.095	0.022	0.023	0.023	10.61	0.71	-4.7	1
152	544452.197	8825970.672	863.096	0.022	0.024	0.024	10.76	0.67	-6.5	1
153	544452.266	8825970.602	863.087	0.022	0.026	0.025	11.34	0.67	-7.8	1
154	544452.337	8825970.535	863.087	0.024	0.026	0.030	11.55	0.71	-8.4	1
155	544452.399	8825970.464	863.056	0.030	0.027	0.057	12.72	1.09	-11.4	1
156	544452.473	8825970.398	863.082	0.023	0.025	0.027	11.32	0.68	-12.8	1
157	544452.543	8825970.330	863.088	0.025	0.023	0.032	11.18	0.83	-8.4	1
158	544452.611	8825970.259	863.064	0.024	0.026	0.029	11.16	0.92	-2.3	1
159	544452.686	8825970.187	863.067	0.024	0.025	0.025	11.50	0.80	-4.0	1
160	544452.756	8825970.121	863.058	0.029	0.024	0.041	10.71	0.88	-5.9	1
161	544452.823	8825970.047	863.061	0.025	0.025	0.025	11.64	0.68	-4.5	1
162	544452.894	8825969.979	863.056	0.024	0.022	0.030	10.68	0.81	-2.5	1
163	544452.967	8825969.910	863.051	0.031	0.026	0.031	11.79	1.24	-1.0	1
164	544453.024	8825969.841	863.069	0.052	0.038	0.075	15.18	3.13	-0.4	1
165	544453.099	8825969.773	863.044	0.023	0.023	0.033	10.35	0.89	-1.1	1
166	544453.167	8825969.709	863.043	0.023	0.021	0.040	8.10	1.66	-2.9	1
167	544453.243	8825969.631	863.055	0.025	0.024	0.031	11.40	0.81	-3.3	1
168	544453.311	8825969.564	863.001	0.022	0.025	0.038	10.98	0.77	-5.0	1
169	544453.389	8825969.494	863.031	0.028	0.026	0.040	10.76	1.62	-2.6	1
170	544453.455	8825969.421	863.027	0.027	0.026	0.034	11.84	1.27	-2.4	1
171	544453.521	8825969.353	863.032	0.021	0.024	0.035	10.25	0.76	-1.8	1
172	544453.592	8825969.285	863.039	0.026	0.024	0.029	11.13	1.12	-3.2	1
173	544453.664	8825969.215	863.036	0.026	0.021	0.028	10.68	0.90	-2.5	1
174	544453.732	8825969.145	863.038	0.025	0.022	0.029	10.55	0.84	-3.6	1
175	544453.803	8825969.075	863.042	0.029	0.022	0.040	11.03	1.34	-4.9	1
176	544453.873	8825969.009	863.012	0.026	0.022	0.034	10.84	0.80	-5.3	1
177	544453.946	8825968.938	863.027	0.026	0.021	0.028	10.81	0.69	-5.7	1
178	544454.012	8825968.870	863.033	0.022	0.023	0.026	10.38	0.73	-3.7	1
179	544454.083	8825968.797	863.031	0.022	0.021	0.028	9.97	0.68	-1.2	1
180	544454.156	8825968.727	863.040	0.030	0.026	0.032	13.11	0.92	-2.5	1
181	544454.226	8825968.661	863.047	0.021	0.029	0.037	11.33	0.90	-3.4	1
182	544454.295	8825968.589	863.019	0.021	0.022	0.033	9.91	0.80	-5.5	1
183	544454.368	8825968.519	863.033	0.022	0.022	0.027	9.95	0.77	-0.7	1
184	544454.435	8825968.452	863.015	0.023	0.022	0.038	9.88	0.88	1.4	1
185	544454.507	8825968.380	863.021	0.026	0.021	0.027	10.75	0.89	1.2	1
186	544454.579	8825968.311	863.017	0.027	0.022	0.029	10.92	1.12	-1.1	1
187	544454.648	8825968.239	863.021	0.028	0.023	0.034	11.56	0.89	-0.0	1
188	544454.715	8825968.171	863.013	0.023	0.022	0.026	10.13	0.89	0.5	1
189	544454.784	8825968.101	863.007	0.024	0.021	0.026	10.06	0.78	1.5	1
190	544454.854	8825968.029	863.002	0.025	0.020	0.029	9.86	0.96	1.9	1
191	544454.926	8825967.959	863.004	0.030	0.022	0.029	11.16	1.03	2.0	1
192	544454.999	8825967.888	863.015	0.024	0.022	0.032	10.18	0.91	2.7	1
193	544455.067	8825967.822	863.014	0.026	0.019	0.033	10.15	0.86	0.2	1
194	544455.137	8825967.748	863.011	0.028	0.026	0.037	11.82	1.23	2.9	1
195	544455.206	8825967.683	863.011	0.019	0.022	0.034	8.99	0.98	2.0	1
196	544455.286	8825967.610	863.022	0.020	0.022	0.034	8.30	0.96	3.6	1
197	544455.353	8825967.537	863.023	0.023	0.023	0.027	10.69	0.81	5.7	1
198	544455.422	8825967.464	863.021	0.023	0.025	0.030	10.66	1.19	5.8	1
199	544455.501	8825967.397	863.017	0.025	0.022	0.031	10.40	0.99	5.9	1
200	544455.577	8825967.319	863.012	0.027	0.023	0.031	11.60	0.86	5.8	1
201	544455.655	8825967.235	863.018	0.027	0.025	0.026	12.18	0.78	5.9	1

Upper (Moraine) Profile: 2013 (continued)

DOY	E(m)	N(m)	Z(m)	E_std(m)	N_std(m)	Z_std(m)	Vx(cm d^{-1})	Vx_err	T(C°)	*
202	544455.733	8825967.151	863.025	0.026	0.025	0.027	11.59	0.77	5.6	1
203	544455.822	8825967.064	863.027	0.031	0.025	0.026	13.07	0.78	5.2	1
204	544455.922	8825966.969	863.024	0.033	0.028	0.026	14.30	0.85	3.6	1
205	544456.026	8825966.870	863.014	0.037	0.036	0.048	15.96	1.31	2.1	1
206	544456.134	8825966.781	863.016	0.030	0.026	0.037	13.18	0.82	-2.4	1
207	544456.218	8825966.697	862.990	0.026	0.023	0.026	11.43	0.85	-5.2	1
208	544456.302	8825966.622	862.986	0.020	0.023	0.035	9.73	0.97	-4.4	1
209	544456.377	8825966.549	862.984	0.024	0.021	0.026	10.08	0.76	-3.9	1
210	544456.453	8825966.474	862.986	0.022	0.020	0.024	9.52	0.65	-4.1	1
211	544456.530	8825966.397	862.983	0.021	0.021	0.024	9.72	0.63	-1.6	1
212	544456.605	8825966.322	862.975	0.023	0.020	0.023	9.78	0.62	0.8	1
213	544456.682	8825966.247	862.973	0.023	0.022	0.025	10.46	0.65	-0.5	1
214	544456.761	8825966.174	862.973	0.027	0.024	0.028	10.39	1.15	0.3	1
215	544456.830	8825966.099	862.967	0.024	0.020	0.026	10.30	0.65	0.5	1
216	544456.909	8825966.026	862.965	0.023	0.021	0.030	9.75	0.74	0.6	1
217	544456.997	8825965.940	862.974	0.037	0.035	0.034	16.96	0.82	3.4	1
218	544457.153	8825965.766	862.988	0.045	0.050	0.034	22.28	1.77	3.7	1
219	544457.297	8825965.639	862.992	0.038	0.035	0.042	16.97	1.04	1.5	1
220	544457.422	8825965.520	862.985	0.043	0.039	0.034	19.35	0.96	1.7	1
221	544457.528	8825965.408	862.996	0.033	0.018	0.037	10.75	1.20	1.5	1
222	544457.631	8825965.315	863.004	0.045	0.046	0.055	21.22	1.67	3.3	1
223	544457.819	8825965.156	862.994	0.053	0.037	0.039	21.37	1.15	2.4	1
224	544457.934	8825965.040	863.020	0.032	0.020	0.045	9.33	1.16	0.4	1
225	544458.039	8825964.964	862.977	0.035	0.030	0.032	14.69	1.23	-2.2	1
226	544458.131	8825964.881	862.966	0.025	0.024	0.032	11.29	0.65	-4.8	1
227	544458.225	8825964.796	862.943	0.037	0.028	0.031	14.02	1.30	-6.1	1
228	544458.303	8825964.727	862.937	0.029	0.024	0.036	12.29	0.86	-6.7	1
229	544458.379	8825964.660	862.930	0.029	0.021	0.035	5.78	1.75	-7.7	1
230	544458.459	8825964.562	862.938	0.032	0.021	0.054	11.26	0.81	-7.1	1
231	544458.540	8825964.490	862.942	0.026	0.022	0.026	11.21	0.75	-9.6	1
232	544458.617	8825964.414	862.939	0.024	0.021	0.025	10.75	0.65	-9.7	1
233	544458.690	8825964.337	862.940	0.024	0.023	0.026	10.82	0.64	-8.5	1
234	544458.771	8825964.253	862.943	0.033	0.023	0.048	7.99	2.19	-9.2	1
235	544458.845	8825964.189	862.938	0.024	0.021	0.024	9.97	0.81	-8.8	1
236	544458.917	8825964.116	862.922	0.022	0.024	0.035	10.05	0.84	-1.5	1
237	544458.997	8825964.037	862.941	0.027	0.023	0.024	11.55	0.88	-0.4	1
238	544459.065	8825963.965	862.934	0.022	0.029	0.032	7.61	1.54	-2.8	1
239	544459.143	8825963.886	862.926	0.025	0.024	0.037	10.14	0.93	-5.5	1
240	544459.216	8825963.814	862.937	0.026	0.025	0.030	9.89	1.35	-4.6	1
241	544459.294	8825963.742	862.924	0.024	0.024	0.030	10.69	0.94	-5.1	1
242	544459.371	8825963.670	862.929	0.025	0.024	0.026	11.56	0.71	-4.3	1
243	544459.446	8825963.598	862.922	0.024	0.023	0.029	10.62	0.80	-5.2	1
244	544459.517	8825963.526	862.916	0.022	0.021	0.026	9.84	0.79	-6.3	1
245	544459.593	8825963.446	862.920	0.023	0.023	0.026	10.39	0.88	-7.0	1
246	544459.671	8825963.377	862.908	0.021	0.021	0.029	9.63	0.71	-5.8	1
247	544459.744	8825963.304	862.906	0.023	0.022	0.027	10.66	0.61	-6.0	1
248	544459.815	8825963.233	862.919	0.027	0.023	0.044	11.52	0.87	-7.5	1
249	544459.893	8825963.158	862.902	0.026	0.021	0.026	10.65	0.67	-9.1	1
250	544459.967	8825963.084	862.903	0.023	0.023	0.031	10.56	0.65	-6.6	1
251	544460.045	8825963.016	862.903	0.022	0.021	0.031	9.48	0.72	-3.9	1
252	544460.115	8825962.937	862.909	0.021	0.024	0.025	10.06	0.89	-6.0	1
253	544460.191	8825962.868	862.901	0.031	0.038	0.050	12.24	2.55	-9.1	1
254	544460.263	8825962.790	862.904	0.023	0.023	0.037	9.90	0.89	-7.4	1
255	544460.337	8825962.719	862.891	0.017	0.024	0.030	8.98	0.86	-7.6	1
256	544460.415	8825962.647	862.895	0.022	0.021	0.027	9.73	0.80	-10.2	1
257	544460.486	8825962.574	862.891	0.021	0.024	0.028	10.32	0.71	-8.4	1
258	544460.560	8825962.502	862.893	0.021	0.022	0.025	10.25	0.60	-9.0	1
259	544460.634	8825962.432	862.885	0.021	0.023	0.027	9.91	0.90	-10.6	1
260	544460.705	8825962.356	862.882	0.023	0.027	0.045	10.04	1.41	-9.8	1
261	544460.781	8825962.283	862.884	0.026	0.022	0.031	10.62	0.88	-10.5	1
262	544460.854	8825962.211	862.882	0.022	0.024	0.025	10.72	0.81	-11.4	1
263	544460.930	8825962.139	862.883	0.022	0.022	0.024	10.35	0.74	-10.5	1
264	544461.004	8825962.067	862.886	0.022	0.024	0.024	10.67	0.81	-11.1	1
265	544461.077	8825961.995	862.881	0.025	0.026	0.033	10.98	1.13	-10.5	1
266	544461.153	8825961.924	862.881	0.022	0.023	0.025	10.42	0.80	-12.1	1
267	544461.229	8825961.854	862.873	0.022	0.019	0.027	9.26	0.89	-12.2	1
268	544461.302	8825961.771	862.881	0.032	0.024	0.049	9.97	2.02	-9.8	1
269	544461.373	8825961.708	862.878	0.029	0.026	0.033	11.67	1.56	-9.8	1
270	544461.448	8825961.638	862.877	0.022	0.019	0.025	9.13	0.82	-7.6	1
271	544461.523	8825961.560	862.891	0.032	0.030	0.038	11.36	2.03	-4.9	1
272	544461.593	8825961.492	862.873	0.022	0.025	0.034	10.21	0.98	-5.4	1
273	544461.670	8825961.418	862.867	0.021	0.024	0.027	10.18	0.81	-9.3	1
274	544461.741	8825961.346	862.860	0.021	0.023	0.028	10.13	0.81	-11.4	1
275	544461.817	8825961.271	862.853	0.021	0.024	0.025	10.07	0.85	-14.5	1
276	544461.890	8825961.192	862.859	0.035	0.024	0.042	10.84	1.86	-16.0	1
277	544461.967	8825961.127	862.857	0.024	0.025	0.028	10.88	0.99	-16.9	1

Upper (Moraine) Profile: 2014

DOY	E(m)	N(m)	Z(m)	E_std(m)	N_std(m)	Z_std(m)	Vx(cm d^{-1})	Vx_err	T(C°)	*
119	544477.008	8825946.409	862.410	0.024	0.021	0.024	10.78	0.61	-14.5	2
120	544477.078	8825946.341	862.407	0.023	0.020	0.027	10.04	0.76	-15.5	2
121	544477.154	8825946.271	862.405	0.027	0.021	0.024	11.32	0.72	-15.2	2
122	544477.231	8825946.202	862.398	0.025	0.023	0.026	10.78	0.96	-10.9	2
123	544477.295	8825946.131	862.401	0.022	0.022	0.027	10.06	0.87	-13.9	2
124	544477.366	8825946.059	862.403	0.024	0.024	0.033	10.06	1.39	-13.8	2
125	544477.434	8825945.997	862.402	0.023	0.025	0.034	5.55	1.64	-15.6	2
126	544477.507	8825945.917	862.413	0.028	0.019	0.049	9.16	0.82	-11.8	2
127	544477.580	8825945.851	862.417	0.021	0.023	0.030	10.06	0.92	-11.7	2
128	544477.651	8825945.782	862.424	0.022	0.022	0.025	10.03	0.78	-11.0	2
129	544477.726	8825945.711	862.407	0.023	0.023	0.026	10.70	0.74	-11.8	2
130	544477.800	8825945.639	862.389	0.027	0.025	0.052	11.27	1.09	-14.6	2
131	544477.873	8825945.567	862.396	0.024	0.023	0.021	11.20	0.54	-14.3	2
132	544477.946	8825945.500	862.403	0.024	0.027	0.033	11.56	0.97	-13.2	2
133	544478.017	8825945.427	862.392	0.024	0.023	0.023	10.93	0.75	-13.4	2
134	544478.089	8825945.358	862.393	0.024	0.023	0.023	11.06	0.70	-11.5	2
135	544478.160	8825945.287	862.384	0.025	0.022	0.024	10.98	0.65	-9.1	2
136	544478.233	8825945.217	862.387	0.025	0.021	0.022	10.73	0.68	-12.0	2
137	544478.306	8825945.148	862.380	0.025	0.022	0.027	11.10	0.71	-12.7	2
138	544478.376	8825945.076	862.375	0.025	0.022	0.025	11.16	0.65	-15.5	2
139	544478.451	8825945.004	862.383	0.027	0.023	0.023	11.75	0.68	-15.5	2
140	544478.517	8825944.934	862.386	0.029	0.024	0.033	12.12	0.82	-14.1	2
141	544478.605	8825944.862	862.376	0.042	0.033	0.030	14.75	1.64	-13.6	2
142	544478.663	8825944.796	862.373	0.026	0.023	0.042	10.86	0.99	-14.2	2
143	544478.737	8825944.725	862.373	0.022	0.022	0.023	10.33	0.59	-13.3	2
144	544478.809	8825944.653	862.378	0.023	0.023	0.023	10.88	0.61	-9.1	2
145	544478.883	8825944.584	862.376	0.023	0.022	0.026	10.69	0.62	-5.0	2
146	544478.954	8825944.509	862.369	0.027	0.024	0.029	11.42	1.02	-6.2	2
147	544479.025	8825944.441	862.364	0.025	0.025	0.022	11.72	0.65	-9.5	2
148	544479.097	8825944.373	862.350	0.025	0.021	0.026	10.41	0.88	-6.7	2
149	544479.167	8825944.300	862.359	0.028	0.023	0.028	11.87	0.71	-7.3	2
150	544479.242	8825944.229	862.353	0.024	0.024	0.022	11.22	0.65	-8.0	2
151	544479.312	8825944.160	862.359	0.023	0.023	0.023	10.73	0.65	-9.2	2
152	544479.385	8825944.091	862.344	0.024	0.022	0.025	10.62	0.77	-9.0	2
153	544479.454	8825944.022	862.367	0.021	0.022	0.029	10.10	0.78	-2.4	2
154	544479.531	8825943.949	862.343	0.024	0.022	0.026	10.56	0.72	0.6	2
155	544479.602	8825943.879	862.341	0.024	0.021	0.027	10.64	0.73	-0.2	2
156	544479.675	8825943.809	862.342	0.024	0.023	0.025	11.00	0.72	-0.6	2
157	544479.747	8825943.739	862.339	0.022	0.022	0.023	10.38	0.70	-0.7	2
158	544479.821	8825943.668	862.337	0.026	0.022	0.025	11.23	0.74	-5.1	2
159	544479.893	8825943.598	862.331	0.025	0.023	0.024	11.04	0.69	-6.6	2
160	544479.967	8825943.526	862.336	0.025	0.022	0.035	9.95	1.23	-6.7	2
161	544480.036	8825943.458	862.327	0.024	0.022	0.025	10.37	0.70	-5.5	2
162	544480.109	8825943.386	862.328	0.025	0.021	0.026	10.28	0.80	-3.9	2
163	544480.183	8825943.314	862.324	0.025	0.021	0.027	10.44	0.69	-4.4	2
164	544480.254	8825943.245	862.321	0.026	0.018	0.025	10.22	0.80	-1.9	2
165	544480.331	8825943.174	862.325	0.021	0.021	0.032	9.18	1.01	2.5	2
166	544480.399	8825943.103	862.317	0.025	0.020	0.025	10.31	0.70	-1.2	2
167	544480.471	8825943.033	862.315	0.024	0.021	0.025	10.50	0.72	-2.0	2
168	544480.542	8825942.963	862.325	0.024	0.020	0.062	7.74	1.62	-1.6	2
169	544480.620	8825942.897	862.305	0.030	0.018	0.033	8.84	1.74	-0.3	2
170	544480.679	8825942.808	862.309	0.051	0.029	0.076	14.44	2.92	1.2	2
171	544480.768	8825942.750	862.297	0.026	0.020	0.033	10.56	0.92	1.5	2
172	544480.835	8825942.674	862.305	0.021	0.025	0.033	10.30	0.87	2.7	2
173	544480.909	8825942.607	862.296	0.025	0.020	0.045	9.99	0.93	1.5	2
174	544480.985	8825942.535	862.284	0.025	0.020	0.029	9.37	1.21	-0.1	2
175	544481.046	8825942.470	862.288	0.018	0.027	0.033	6.58	1.34	-1.3	2
176	544481.120	8825942.390	862.291	0.038	0.020	0.073	9.23	2.50	1.7	2
177	544481.199	8825942.326	862.290	0.025	0.019	0.024	9.74	0.79	3.6	2
178	544481.276	8825942.253	862.291	0.030	0.020	0.029	11.23	1.07	3.9	2
179	544481.353	8825942.169	862.299	0.027	0.027	0.027	12.32	0.97	2.8	2
180	544481.443	8825942.078	862.303	0.031	0.024	0.031	12.68	0.90	3.1	2
181	544481.544	8825941.980	862.310	0.035	0.025	0.028	13.99	0.89	2.6	2
182	544481.655	8825941.874	862.314	0.037	0.031	0.028	16.16	0.76	3.7	2
183	544481.774	8825941.733	862.346	0.033	0.040	0.029	17.54	0.84	4.1	2
184	544481.919	8825941.600	862.337	0.046	0.037	0.027	19.99	1.06	3.2	2
185	544482.053	8825941.482	862.329	0.039	0.036	0.028	17.57	0.90	2.9	2
186	544482.178	8825941.371	862.314	0.037	0.031	0.031	15.48	1.11	4.2	2
187	544482.297	8825941.253	862.306	0.033	0.035	0.048	14.21	1.53	3.9	2
188	544482.433	8825941.119	862.331	0.057	0.038	0.054	17.59	3.10	3.4	2
189	544482.540	8825941.020	862.316	0.033	0.035	0.033	15.96	0.89	2.2	2
190	544482.664	8825940.899	862.320	0.036	0.043	0.033	18.68	0.84	2.1	2
191	544482.785	8825940.773	862.345	0.032	0.041	0.037	16.74	0.92	2.4	2
192	544482.899	8825940.639	862.376	0.033	0.033	0.030	15.46	0.69	3.1	1
193	544483.004	8825940.544	862.371	0.030	0.030	0.030	13.65	0.72	2.2	1
194	544483.103	8825940.458	862.352	0.030	0.021	0.027	11.40	0.76	1.8	1
195	544483.198	8825940.379	862.340	0.032	0.024	0.029	12.57	1.02	3.3	1
196	544483.305	8825940.268	862.347	0.033	0.031	0.033	13.96	1.30	3.9	1
197	544483.415	8825940.171	862.333	0.030	0.026	0.055	12.16	1.33	2.3	1
198	544483.517	8825940.078	862.327	0.027	0.023	0.029	11.16	0.96	1.6	1
199	544483.606	8825939.995	862.319	0.027	0.029	0.026	12.85	0.71	3.0	1
200	544483.714	8825939.887	862.325	0.030	0.032	0.027	14.30	0.96	3.8	1
201	544483.817	8825939.767	862.336	0.033	0.039	0.027	16.96	0.88	4.3	1

Upper (Moraine) Profile: 2014 (continued)

DOY	E(m)	N(m)	Z(m)	E_std(m)	N_std(m)	Z_std(m)	Vx(cm d^{-1})	Vx_err	T(C°)	*
202	544483.933	8825939.655	862.337	0.033	0.034	0.029	15.76	0.87	3.4	1
203	544484.037	8825939.571	862.320	0.030	0.018	0.031	10.62	0.86	1.6	1
204	544484.143	8825939.490	862.292	0.037	0.020	0.031	11.48	1.20	-3.5	1
205	544484.242	8825939.410	862.272	0.029	0.024	0.029	12.45	0.65	-1.3	1
206	544484.328	8825939.327	862.262	0.025	0.022	0.027	10.29	0.67	2.9	1
207	544484.414	8825939.244	862.259	0.029	0.023	0.027	11.58	0.74	1.2	1
208	544484.506	8825939.160	862.249	0.027	0.021	0.031	11.16	0.64	-0.7	1
209	544484.590	8825939.071	862.244	0.027	0.026	0.030	12.23	0.91	-0.8	1
210	544484.673	8825938.993	862.242	0.029	0.024	0.040	11.43	1.21	0.6	1
211	544484.753	8825938.919	862.234	0.025	0.025	0.024	11.63	0.69	2.4	1
212	544484.844	8825938.829	862.245	0.024	0.028	0.029	11.79	0.69	3.0	1
213	544484.957	8825938.717	862.243	0.035	0.027	0.031	14.56	0.78	3.7	1
214	544485.071	8825938.598	862.262	0.042	0.054	0.047	21.99	1.81	4.9	1
215	544485.233	8825938.461	862.228	0.039	0.039	0.026	18.56	0.70	0.5	1
216	544485.345	8825938.357	862.230	0.026	0.024	0.027	11.43	0.77	1.4	1
217	544485.432	8825938.280	862.211	0.027	0.024	0.026	11.97	0.83	2.6	1
218	544485.526	8825938.193	862.205	0.027	0.026	0.026	12.27	0.81	3.3	1
219	544485.632	8825938.097	862.211	0.036	0.031	0.026	16.21	0.74	4.4	1
220	544485.749	8825937.995	862.203	0.034	0.033	0.031	15.78	1.01	5.0	1
221	544485.864	8825937.894	862.198	0.033	0.032	0.035	14.95	1.34	5.2	1
222	544485.965	8825937.808	862.193	0.028	0.026	0.034	12.40	0.97	2.6	1
223	544486.054	8825937.727	862.179	0.029	0.026	0.025	12.87	0.63	0.7	1
224	544486.145	8825937.640	862.184	0.036	0.025	0.033	12.80	1.64	0.8	1
225	544486.229	8825937.565	862.173	0.025	0.026	0.027	11.54	0.85	2.6	1
226	544486.319	8825937.487	862.179	0.022	0.026	0.032	10.80	1.09	1.0	1
227	544486.397	8825937.406	862.167	0.025	0.025	0.025	11.58	0.65	-0.3	1
228	544486.482	8825937.331	862.151	0.023	0.025	0.028	10.99	0.87	0.4	1
229	544486.570	8825937.251	862.155	0.028	0.021	0.028	11.09	0.92	-0.2	1
230	544486.635	8825937.178	862.164	0.044	0.036	0.065	16.14	2.13	-1.4	1
231	544486.727	8825937.101	862.146	0.023	0.022	0.028	10.24	0.82	0.5	1
232	544486.805	8825937.021	862.152	0.025	0.019	0.034	9.59	0.91	1.5	1
233	544486.889	8825936.948	862.143	0.027	0.022	0.048	9.55	1.37	-0.7	1
234	544486.962	8825936.874	862.141	0.020	0.022	0.031	9.56	0.85	-2.8	1
235	544487.035	8825936.804	862.133	0.020	0.020	0.023	9.25	0.60	-2.5	1
236	544487.116	8825936.729	862.133	0.026	0.022	0.025	10.99	0.77	-1.1	1
237	544487.191	8825936.655	862.138	0.022	0.024	0.023	10.72	0.61	-0.9	1
238	544487.268	8825936.582	862.140	0.018	0.023	0.023	9.43	0.72	-0.8	1
239	544487.339	8825936.511	862.128	0.020	0.023	0.031	9.32	1.03	-4.2	1
240	544487.418	8825936.438	862.128	0.021	0.023	0.026	9.66	0.77	-2.5	1
241	544487.492	8825936.368	862.119	0.022	0.023	0.028	9.75	1.09	-0.8	1
242	544487.572	8825936.291	862.130	0.021	0.022	0.022	9.80	0.74	1.0	1
243	544487.648	8825936.217	862.126	0.023	0.028	0.029	11.23	0.98	0.9	1
244	544487.726	8825936.146	862.119	0.019	0.023	0.024	9.41	0.72	0.0	1
245	544487.800	8825936.071	862.120	0.018	0.023	0.022	9.20	0.87	-0.6	1
246	544487.878	8825935.997	862.122	0.022	0.022	0.023	10.10	0.66	-1.3	1
247	544487.950	8825935.924	862.123	0.018	0.024	0.030	9.34	0.87	-1.1	1
248	544488.025	8825935.853	862.114	0.019	0.022	0.028	9.25	0.72	-2.5	1
249	544488.102	8825935.780	862.112	0.020	0.021	0.023	9.29	0.73	-1.9	1
250	544488.176	8825935.708	862.110	0.021	0.024	0.023	10.34	0.82	-4.1	1
251	544488.252	8825935.637	862.122	0.018	0.025	0.036	9.29	1.15	-4.3	1
252	544488.326	8825935.563	862.098	0.021	0.027	0.027	10.75	1.21	-7.9	1
253	544488.405	8825935.490	862.102	0.022	0.023	0.024	10.51	0.96	-9.4	1
254	544488.478	8825935.418	862.098	0.019	0.024	0.023	9.51	1.00	-9.7	1
255	544488.554	8825935.345	862.099	0.023	0.024	0.026	10.63	0.91	-9.0	1
256	544488.634	8825935.271	862.077	0.024	0.023	0.032	10.59	0.95	-8.3	1
257	544488.707	8825935.197	862.087	0.023	0.028	0.039	11.04	1.29	-9.1	1
258	544488.782	8825935.128	862.089	0.022	0.024	0.026	10.39	0.96	-7.6	1
259	544488.858	8825935.057	862.088	0.022	0.023	0.023	9.69	1.06	-8.9	1
260	544488.931	8825934.985	862.088	0.020	0.023	0.022	9.57	0.98	-8.9	1
261	544489.005	8825934.914	862.086	0.016	0.023	0.024	8.52	1.04	-7.2	1
262	544489.088	8825934.841	862.088	0.017	0.026	0.025	9.26	0.97	-3.2	1
263	544489.158	8825934.768	862.078	0.020	0.027	0.025	10.86	0.74	-5.6	1
264	544489.233	8825934.695	862.085	0.024	0.024	0.025	11.00	0.74	-10.2	1
265	544489.305	8825934.624	862.078	0.022	0.023	0.028	10.48	0.75	-10.3	1
266	544489.379	8825934.552	862.074	0.023	0.026	0.023	11.14	0.85	-11.9	1
267	544489.457	8825934.482	862.065	0.020	0.025	0.028	10.34	0.75	-12.4	1
268	544489.531	8825934.406	862.070	0.024	0.024	0.025	11.08	0.83	-12.4	1
269	544489.607	8825934.334	862.069	0.024	0.025	0.028	11.03	0.96	-14.7	1
270	544489.682	8825934.263	862.067	0.023	0.023	0.024	10.51	0.87	-15.8	1
271	544489.756	8825934.191	862.064	0.024	0.025	0.024	10.94	1.01	-14.4	1
272	544489.834	8825934.117	862.064	0.027	0.028	0.027	12.10	1.10	-14.4	1
273	544489.905	8825934.050	862.058	0.026	0.025	0.027	11.06	1.14	-11.6	1
274	544489.993	8825933.970	862.053	0.024	0.025	0.028	11.02	0.73	-11.2	1
275	544490.065	8825933.895	862.055	0.023	0.022	0.025	11.66	1.09	-10.6	1
276	544490.136	8825933.827	862.055	0.021	0.022	0.026	10.90	0.86	-10.9	1

Upper (Moraine) Profile: 2015

DOY	E(m)	N(m)	Z(m)	E_std(m)	N_std(m)	Z_std(m)	Vx(cm d^{-1})	Vx_err	T(C°)	*
114	544504.950	8825921.528	860.774	0.023	0.022	0.022	10.70	0.58	-13.5	2
115	544505.019	8825921.459	860.781	0.020	0.021	0.027	9.22	0.82	-11.0	2
116	544505.097	8825921.387	860.781	0.023	0.020	0.025	10.01	0.71	-9.2	2
117	544505.167	8825921.319	860.777	0.025	0.023	0.026	11.10	0.64	-11.3	2
118	544505.241	8825921.250	860.771	0.025	0.021	0.024	10.76	0.53	-12.9	2
119	544505.313	8825921.180	860.769	0.024	0.021	0.024	10.72	0.65	-13.9	2
120	544505.384	8825921.110	860.764	0.025	0.022	0.025	11.23	0.60	-12.9	2
121	544505.456	8825921.042	860.765	0.024	0.023	0.026	10.79	0.64	-12.7	2
122	544505.529	8825920.972	860.758	0.026	0.022	0.025	11.33	0.68	-12.0	2
123	544505.601	8825920.903	860.754	0.026	0.021	0.027	11.04	0.69	-11.0	2
124	544505.674	8825920.832	860.753	0.024	0.022	0.025	10.89	0.56	-11.4	2
125	544505.746	8825920.766	860.751	0.022	0.022	0.025	10.24	0.78	-12.7	2
126	544505.820	8825920.692	860.748	0.025	0.022	0.026	10.98	0.67	-14.2	2
127	544505.893	8825920.625	860.749	0.026	0.021	0.024	11.11	0.69	-17.2	2
128	544505.965	8825920.554	860.742	0.024	0.022	0.025	10.88	0.65	-17.5	2
129	544506.039	8825920.484	860.742	0.026	0.023	0.025	11.28	0.83	-15.2	2
130	544506.111	8825920.415	860.751	0.025	0.025	0.033	11.55	0.85	-11.9	2
131	544506.175	8825920.346	860.735	0.035	0.029	0.057	13.12	1.97	-14.7	2
132	544506.256	8825920.274	860.736	0.027	0.024	0.024	11.95	0.73	-17.2	2
133	544506.328	8825920.206	860.733	0.023	0.025	0.024	11.22	0.64	-18.6	2
134	544506.401	8825920.132	860.724	0.027	0.025	0.032	11.98	0.75	-17.4	2
135	544506.475	8825920.064	860.709	0.026	0.029	0.029	12.76	0.81	-12.7	2
136	544506.547	8825919.995	860.730	0.023	0.024	0.025	11.15	0.76	-9.0	2
137	544506.618	8825919.927	860.732	0.023	0.023	0.027	10.68	0.83	-9.9	2
138	544506.694	8825919.858	860.720	0.027	0.021	0.032	10.93	1.04	-9.0	2
139	544506.764	8825919.789	860.719	0.026	0.023	0.031	11.27	0.84	-10.3	2
140	544506.836	8825919.718	860.725	0.025	0.022	0.031	10.92	0.75	-9.6	2
141	544506.910	8825919.649	860.704	0.026	0.022	0.024	11.12	0.79	-10.4	2
142	544506.982	8825919.579	860.702	0.025	0.023	0.029	11.07	0.68	-14.1	2
143	544507.056	8825919.504	860.692	0.027	0.026	0.028	12.33	0.83	-16.1	2
144	544507.129	8825919.437	860.688	0.025	0.025	0.025	11.33	0.80	-8.6	2
145	544507.202	8825919.370	860.680	0.023	0.019	0.033	9.12	1.19	-8.2	2
146	544507.272	8825919.298	860.692	0.030	0.023	0.032	12.35	0.92	-4.7	2
147	544507.348	8825919.226	860.685	0.026	0.023	0.025	11.35	0.76	-4.5	2
148	544507.422	8825919.158	860.697	0.025	0.023	0.030	11.12	0.69	-5.0	2
149	544507.489	8825919.091	860.683	0.029	0.028	0.029	12.36	1.53	-4.6	2
150	544507.565	8825919.018	860.680	0.025	0.022	0.026	10.80	0.79	-4.6	2
151	544507.639	8825918.950	860.679	0.026	0.022	0.029	11.00	0.87	-2.0	2
152	544507.708	8825918.879	860.672	0.028	0.024	0.025	11.69	1.19	-0.6	2
153	544507.782	8825918.805	860.673	0.025	0.022	0.025	11.02	0.65	-1.7	2
154	544507.853	8825918.740	860.671	0.031	0.027	0.024	12.66	1.43	-0.2	2
155	544507.931	8825918.666	860.668	0.027	0.021	0.023	11.11	0.65	-0.7	2
156	544508.007	8825918.596	860.669	0.028	0.022	0.023	11.63	0.71	-1.7	2
157	544508.081	8825918.528	860.668	0.030	0.025	0.028	11.93	1.41	-4.3	2
158	544508.159	8825918.455	860.668	0.029	0.022	0.031	11.34	1.12	-5.6	2
159	544508.228	8825918.381	860.666	0.028	0.024	0.031	11.66	0.83	-2.0	2
160	544508.308	8825918.311	860.662	0.026	0.021	0.025	10.82	0.97	0.3	2
161	544508.381	8825918.238	860.654	0.023	0.021	0.026	10.25	0.74	0.7	2
162	544508.456	8825918.166	860.647	0.024	0.023	0.030	10.95	0.80	-0.8	2
163	544508.530	8825918.095	860.646	0.025	0.022	0.024	10.72	0.83	0.2	2
164	544508.604	8825918.022	860.643	0.026	0.020	0.025	10.91	0.69	1.9	2
165	544508.683	8825917.954	860.629	0.027	0.021	0.028	11.02	0.86	2.4	2
166	544508.764	8825917.878	860.636	0.029	0.021	0.030	10.88	1.34	1.9	2
167	544508.838	8825917.802	860.633	0.028	0.023	0.025	12.09	0.73	0.8	2
168	544508.923	8825917.727	860.628	0.024	0.025	0.028	11.15	0.91	2.1	2
169	544509.010	8825917.641	860.627	0.029	0.023	0.028	11.73	1.05	1.9	2
170	544509.098	8825917.553	860.617	0.032	0.023	0.028	13.14	0.81	0.6	2
171	544509.187	8825917.469	860.608	0.029	0.023	0.023	12.27	0.70	0.8	2
172	544509.274	8825917.391	860.611	0.030	0.024	0.033	12.11	1.28	0.6	2
173	544509.357	8825917.306	860.603	0.028	0.025	0.025	12.44	0.89	1.5	2
174	544509.441	8825917.226	860.593	0.026	0.024	0.029	11.80	0.75	0.9	2
175	544509.527	8825917.148	860.602	0.028	0.023	0.031	11.55	0.98	2.1	2
176	544509.611	8825917.069	860.585	0.028	0.023	0.029	11.71	0.88	0.5	2
177	544509.693	8825916.991	860.588	0.029	0.022	0.025	11.64	0.99	0.6	2
178	544509.778	8825916.907	860.585	0.030	0.027	0.029	13.40	0.79	2.1	2
179	544509.880	8825916.814	860.577	0.033	0.026	0.026	14.03	0.88	3.8	2
180	544509.983	8825916.696	860.595	0.030	0.033	0.029	15.10	0.88	2.5	2
181	544510.076	8825916.596	860.615	0.033	0.030	0.052	14.61	1.12	2.3	2
182	544510.160	8825916.497	860.601	0.032	0.032	0.033	13.65	1.79	5.0	2
183	544510.278	8825916.398	860.600	0.037	0.028	0.024	15.41	0.84	2.5	2
184	544510.388	8825916.288	860.601	0.039	0.031	0.055	16.57	1.04	2.6	2
185	544510.523	8825916.168	860.580	0.041	0.040	0.025	19.15	0.80	3.7	2
186	544510.668	8825916.047	860.560	0.037	0.028	0.034	15.21	0.97	3.2	2
187	544510.789	8825915.936	860.567	0.031	0.038	0.053	16.06	0.97	5.0	2
188	544510.915	8825915.809	860.558	0.040	0.046	0.032	20.00	1.33	7.2	2
189	544511.057	8825915.677	860.562	0.037	0.044	0.028	19.28	0.69	7.5	2
190	544511.195	8825915.549	860.555	0.034	0.044	0.034	18.44	0.85	8.2	2
191	544511.318	8825915.421	860.563	0.030	0.037	0.027	15.97	0.70	6.9	2
192	544511.450	8825915.300	860.560	0.049	0.056	0.026	22.37	0.82	6.2	2
193	544511.626	8825915.116	860.586	0.044	0.045	0.028	21.29	1.08	7.0	2
194	544511.767	8825915.007	860.557	0.039	0.036	0.026	17.93	0.77	5.6	2
195	544511.895	8825914.900	860.531	0.036	0.035	0.027	17.01	0.73	4.9	2
196	544512.023	8825914.795	860.502	0.041	0.039	0.026	19.09	0.79	4.1	2

Upper (Moraine) Profile: 2015 (continued)

DOY	E(m)	N(m)	Z(m)	E_std(m)	N_std(m)	Z_std(m)	Vx(cm d^{-1})	Vx_err	T(C°)	*
197	544512.150	8825914.686	860.488	0.038	0.036	0.026	17.57	0.77	4.0	2
198	544512.270	8825914.576	860.484	0.040	0.037	0.028	18.13	0.95	3.9	2
199	544512.387	8825914.461	860.480	0.051	0.045	0.037	21.98	1.27	5.5	2
200	544512.515	8825914.357	860.464	0.032	0.027	0.033	13.94	1.00	4.6	2
201	544512.619	8825914.246	860.468	0.043	0.054	0.038	22.60	1.37	4.7	2
202	544512.769	8825914.119	860.461	0.037	0.037	0.026	17.36	0.85	5.0	2
203	544512.891	8825914.012	860.444	0.038	0.038	0.026	17.93	0.90	6.0	2
204	544513.013	8825913.906	860.436	0.040	0.039	0.027	18.60	1.07	5.9	2
205	544513.132	8825913.798	860.428	0.038	0.035	0.026	17.35	0.95	5.0	2
206	544513.247	8825913.696	860.416	0.035	0.038	0.027	17.25	0.88	4.9	2
207	544513.359	8825913.600	860.406	0.035	0.033	0.026	16.14	0.73	4.2	2
208	544513.466	8825913.509	860.400	0.032	0.025	0.030	13.39	0.77	4.2	2
209	544513.560	8825913.428	860.381	0.030	0.027	0.028	13.36	0.68	4.3	2
210	544513.659	8825913.321	860.394	0.040	0.047	0.027	20.59	1.25	4.1	2
211	544513.780	8825913.207	860.389	0.035	0.037	0.030	16.02	1.62	3.6	2
212	544513.887	8825913.122	860.376	0.029	0.024	0.033	12.46	0.78	0.7	2
213	544513.980	8825913.036	860.366	0.031	0.027	0.024	13.77	0.64	1.0	2
214	544514.069	8825912.957	860.362	0.024	0.021	0.035	9.97	0.83	2.5	2
215	544514.148	8825912.884	860.353	0.024	0.021	0.026	9.67	1.00	2.8	2
216	544514.215	8825912.804	860.362	0.023	0.028	0.068	7.87	2.13	1.8	2
217	544514.319	8825912.718	860.339	0.024	0.023	0.027	10.98	0.74	-0.5	2
218	544514.400	8825912.643	860.336	0.024	0.027	0.022	11.66	0.69	-4.0	2
219	544514.482	8825912.566	860.336	0.024	0.021	0.024	10.51	0.67	-2.9	2
220	544514.562	8825912.496	860.327	0.022	0.023	0.025	10.25	0.63	2.2	2
221	544514.640	8825912.424	860.324	0.024	0.027	0.027	11.11	0.96	1.6	2
222	544514.714	8825912.347	860.327	0.022	0.021	0.025	10.10	0.57	0.5	2
223	544514.796	8825912.273	860.325	0.022	0.023	0.025	10.57	0.56	1.5	2
224	544514.877	8825912.191	860.314	0.025	0.025	0.025	11.87	0.64	3.3	2
225	544514.966	8825912.107	860.312	0.026	0.024	0.023	11.80	0.72	2.2	2
226	544515.059	8825912.015	860.303	0.027	0.028	0.023	12.95	0.72	2.4	2
227	544515.155	8825911.917	860.299	0.033	0.036	0.047	15.11	1.53	2.5	2
228	544515.253	8825911.828	860.308	0.029	0.026	0.023	13.05	0.67	1.9	2
229	544515.339	8825911.744	860.300	0.023	0.024	0.026	10.63	0.85	1.5	2
230	544515.422	8825911.669	860.287	0.022	0.025	0.023	10.69	0.82	1.5	2

Middle (Wind) Profile: 2012

DOY	E(m)	N(m)	Z(m)	E_std(m)	N_std(m)	Z_std(m)	Vx(cm d^{-1})	Vx_err	T(C°)	*
129	545824.245	8823214.931	584.652	0.017	0.010	0.035	NaN	NaN	-16.6	1
130	545824.222	8823214.862	584.630	0.014	0.008	0.037	5.43	1.10	-12.5	1
131	545824.254	8823214.790	584.590	0.012	0.009	0.028	7.83	1.35	-11.4	1
132	545824.297	8823214.736	584.572	0.008	0.009	0.032	6.69	1.39	-8.9	1
133	545824.330	8823214.667	584.548	0.007	0.009	0.033	7.59	1.22	-6.7	1
134	545824.385	8823214.581	584.553	0.012	0.008	0.030	10.16	1.29	-6.7	1
135	545824.404	8823214.528	584.547	0.010	0.008	0.027	5.52	1.33	-5.6	1
136	545824.449	8823214.429	584.508	0.020	0.010	0.035	10.91	1.56	-6.3	1
137	545824.509	8823214.358	584.490	0.017	0.010	0.035	8.95	1.57	-6.5	1
138	545824.542	8823214.311	584.482	0.016	0.011	0.030	5.59	1.32	-9.1	1
139	545824.589	8823214.216	584.499	0.019	0.011	0.025	10.58	1.36	-9.3	1
140	545824.606	8823214.139	584.452	0.023	0.009	0.027	7.74	1.71	-8.8	1
141	545824.591	8823214.167	584.487	0.006	0.007	0.022	-3.12	1.61	-7.6	1
142	545824.643	8823214.096	584.457	0.006	0.006	0.021	8.58	1.02	-8.1	1
143	545824.665	8823214.042	584.445	0.004	0.009	0.020	5.85	1.05	-8.3	1
144	545824.694	8823213.990	584.389	0.004	0.009	0.025	5.92	1.18	-8.3	1
145	545824.700	8823213.935	584.466	0.005	0.011	0.026	5.31	1.24	-5.5	1
146	545824.666	8823213.903	584.504	0.007	0.014	0.028	1.53	1.46	-5.6	1
147	545824.763	8823213.748	584.536	0.016	0.009	0.026	18.10	1.29	-4.5	1
148	545824.728	8823213.780	584.533	0.011	0.009	0.033	-4.40	1.06	-5.4	1
149	545824.785	8823213.701	584.488	0.011	0.007	0.025	9.56	1.15	-2.6	1
150	545824.776	8823213.650	584.491	0.015	0.007	0.027	4.32	1.18	-1.2	1
151	545824.815	8823213.554	584.498	0.009	0.010	0.029	10.33	1.33	2.3	1
152	545824.845	8823213.462	584.517	0.009	0.007	0.031	9.62	1.23	-1.5	1
153	545824.868	8823213.393	584.517	0.008	0.007	0.035	7.30	1.03	-2.2	1
154	545824.869	8823213.331	584.517	0.008	0.009	0.034	5.71	1.14	1.6	1
155	545824.960	8823213.234	584.505	0.007	0.009	0.027	12.57	1.25	3.1	1
156	545824.985	8823213.166	584.489	0.008	0.014	0.022	7.16	1.60	0.2	1
157	545825.022	8823213.128	584.477	0.011	0.012	0.019	5.00	1.69	0.4	1
158	545825.057	8823213.050	584.491	0.009	0.011	0.023	8.51	1.41	0.6	1
159	545825.028	8823212.951	584.448	0.007	0.010	0.035	7.97	1.30	2.4	1
160	545825.160	8823212.947	584.458	0.010	0.013	0.031	5.68	1.44	3.7	1
161	545825.165	8823212.786	584.465	0.015	0.009	0.027	14.92	1.42	3.2	1
162	545825.185	8823212.666	584.482	0.012	0.010	0.029	11.78	1.41	3.2	1
163	545825.240	8823212.594	584.464	0.008	0.006	0.026	8.79	1.30	4.8	1
164	545825.297	8823212.480	584.478	0.011	0.007	0.027	12.81	0.98	5.9	1
165	545825.358	8823212.238	584.560	0.006	0.008	0.032	24.58	0.96	6.2	1
166	545825.422	8823212.047	584.569	0.008	0.015	0.037	20.06	1.40	5.3	1
167	545825.485	8823211.918	584.504	0.010	0.015	0.039	14.40	1.73	1.7	1
168	545825.586	8823211.834	584.483	0.009	0.009	0.025	11.69	1.37	1.0	1
169	545825.624	8823211.734	584.507	0.010	0.007	0.027	10.69	0.88	0.6	1
170	545825.676	8823211.670	584.483	0.011	0.005	0.026	7.97	0.79	1.9	1
171	545825.670	8823211.568	584.483	0.008	0.007	0.037	9.08	0.91	4.9	1

Middle (Wind) Profile: 2012 (continued)

DOY	E(m)	N(m)	Z(m)	E_std(m)	N_std(m)	Z_std(m)	Vx(cm d^{-1})	Vx_err	T(C°)	*
172	545825.721	8823211.427	584.495	0.014	0.009	0.027	14.92	1.15	4.4	1
173	545825.772	8823211.304	584.484	0.008	0.010	0.023	13.37	1.40	0.7	1
174	545825.848	8823211.258	584.465	0.016	0.009	0.025	7.21	1.31	-0.1	1
175	545825.889	8823211.127	584.464	0.008	0.007	0.025	13.69	1.02	-0.9	1
176	545825.954	8823211.029	584.463	0.007	0.009	0.021	11.60	1.17	1.0	1
177	545825.969	8823210.949	584.459	0.012	0.010	0.022	7.96	1.34	1.7	1
178	545826.055	8823210.835	584.509	0.013	0.010	0.019	13.77	1.52	5.3	1
179	545826.091	8823210.716	584.430	0.011	0.010	0.024	12.39	1.68	7.3	1
180	545826.173	8823210.489	584.504	0.005	0.007	0.029	24.13	1.39	10.9	1
181	545826.336	8823210.150	584.565	0.013	0.012	0.028	37.60	1.49	12.2	1
182	545826.459	8823209.857	584.526	0.010	0.008	0.031	31.73	1.62	12.0	1
183	545826.537	8823209.648	584.482	0.009	0.009	0.025	22.24	1.30	11.7	1
184	545826.679	8823209.472	584.480	0.006	0.006	0.021	21.85	1.07	10.1	1
185	545826.691	8823209.337	584.467	0.012	0.013	0.028	12.90	1.09	9.8	1
186	545826.772	8823209.221	584.445	0.005	0.010	0.019	13.85	1.27	9.0	1
187	545826.713	8823209.154	584.354	0.007	0.014	0.026	3.77	1.58	8.5	1
188	545826.926	8823208.981	584.420	0.009	0.008	0.017	24.38	1.47	10.0	1
189	545826.888	8823208.926	584.404	0.006	0.010	0.017	3.53	1.21	7.0	1
190	545826.928	8823208.805	584.399	0.007	0.006	0.018	12.70	1.17	4.8	1
191	545827.011	8823208.703	584.392	0.005	0.007	0.020	12.60	0.94	8.1	1
192	545827.025	8823208.584	584.384	0.008	0.008	0.021	11.45	1.16	7.4	1
193	545827.054	8823208.511	584.372	0.005	0.008	0.024	7.89	1.17	4.2	1
194	545827.072	8823208.468	584.335	0.009	0.010	0.024	4.67	1.03	6.0	1
195	545827.152	8823208.362	584.329	0.007	0.011	0.024	12.92	1.23	3.6	1
196	545827.166	8823208.303	584.296	0.009	0.010	0.028	6.00	1.27	4.8	1
197	545827.228	8823208.142	584.385	0.011	0.011	0.031	17.17	1.19	7.2	1
198	545827.283	8823208.097	584.311	0.010	0.009	0.019	6.38	1.14	7.6	1
199	545827.328	8823207.981	584.280	0.014	0.009	0.021	12.38	1.40	7.4	1
200	545827.395	8823207.909	584.300	0.009	0.007	0.019	9.33	1.34	8.9	1
201	545827.394	8823207.842	584.280	0.008	0.008	0.020	6.11	0.96	7.5	1
202	545827.426	8823207.719	584.315	0.005	0.008	0.023	12.52	0.99	2.7	1
203	545827.452	8823207.625	584.290	0.009	0.009	0.029	9.69	1.03	2.7	1
204	545827.517	8823207.559	584.292	0.005	0.006	0.020	8.57	0.97	1.6	1
205	545827.555	8823207.477	584.293	0.006	0.009	0.019	9.07	1.08	2.4	1
206	545827.581	8823207.395	584.284	0.006	0.007	0.026	8.53	1.15	0.8	1
207	545827.609	8823207.360	584.213	0.008	0.009	0.027	4.34	1.19	3.5	1
208	545827.621	8823207.239	584.254	0.007	0.008	0.025	11.63	1.24	4.7	1
209	545827.635	8823207.136	584.279	0.007	0.009	0.027	9.97	1.20	6.7	1
210	545827.761	8823206.896	584.425	0.010	0.008	0.026	26.97	1.20	6.3	1
211	545827.824	8823206.798	584.338	0.012	0.007	0.030	11.50	0.99	4.6	1
212	545827.882	8823206.725	584.289	0.010	0.007	0.025	9.04	0.87	5.4	1
213	545827.923	8823206.688	584.244	0.006	0.008	0.025	5.07	0.95	4.7	1
214	545827.958	8823206.579	584.217	0.011	0.009	0.031	11.34	1.14	6.5	1
215	545827.993	8823206.473	584.253	0.010	0.007	0.027	11.11	1.06	8.0	1
216	545828.052	8823206.384	584.237	0.011	0.009	0.032	10.52	1.11	8.8	1
217	545828.085	8823206.363	584.296	0.008	0.012	0.031	3.28	1.59	7.4	1
218	545828.084	8823206.198	584.253	0.011	0.008	0.034	15.10	1.59	7.2	1
219	545828.084	8823206.131	584.210	0.006	0.010	0.032	6.13	1.35	4.4	1
220	545828.128	8823206.064	584.208	0.008	0.011	0.027	7.90	1.34	2.4	1
221	545828.199	8823205.987	584.209	0.007	0.008	0.026	9.85	1.15	-0.9	1
222	545828.236	8823205.919	584.201	0.007	0.008	0.020	7.80	0.96	-1.6	1
223	545828.273	8823205.846	584.192	0.008	0.006	0.022	8.15	0.98	-2.5	1
224	545828.287	8823205.770	584.181	0.008	0.007	0.020	7.54	1.06	-2.8	1
225	545828.411	8823205.682	584.198	0.011	0.012	0.018	13.01	1.66	-2.0	1
226	545828.377	8823205.678	584.139	0.018	0.016	0.049	-0.99	1.85	-1.1	1
227	545828.401	8823205.552	584.163	0.012	0.007	0.022	12.51	1.33	-1.0	1
228	545828.406	8823205.449	584.237	0.005	0.009	0.023	9.64	1.13	-0.9	1
229	545828.415	8823205.385	584.226	0.005	0.007	0.022	6.19	1.15	2.4	1
230	545828.483	8823205.318	584.251	0.007	0.006	0.025	8.84	0.95	1.9	1
231	545828.514	8823205.278	584.210	0.005	0.005	0.020	4.94	0.78	-2.7	1
232	545828.548	8823205.210	584.190	0.004	0.005	0.020	7.56	0.67	0.3	1
233	545828.558	8823205.125	584.238	0.009	0.005	0.026	8.24	0.84	3.2	1
234	545828.578	8823205.095	584.197	0.005	0.006	0.026	3.57	0.89	4.6	1
235	545828.611	8823204.996	584.214	0.006	0.007	0.021	10.38	0.85	4.3	1
236	545828.666	8823204.897	584.239	0.007	0.009	0.034	11.22	1.04	5.0	1
237	545828.670	8823204.885	584.162	0.006	0.006	0.019	1.27	0.96	3.9	1
238	545828.684	8823204.850	584.172	0.008	0.005	0.020	3.77	0.71	2.7	1
239	545828.702	8823204.747	584.183	0.004	0.005	0.020	10.12	0.68	2.9	1
240	545828.741	8823204.679	584.182	0.004	0.005	0.020	7.83	0.66	2.8	1
241	545828.744	8823204.610	584.179	0.008	0.005	0.019	6.44	0.77	2.6	1
242	545828.804	8823204.513	584.166	0.006	0.006	0.023	11.28	0.76	1.8	1
243	545828.825	8823204.465	584.171	0.007	0.006	0.022	5.24	0.66	1.8	1
244	545828.865	8823204.399	584.193	0.006	0.006	0.024	7.61	0.78	1.3	1
245	545828.897	8823204.324	584.188	0.008	0.005	0.025	8.16	0.79	-0.4	1
246	545828.914	8823204.264	584.183	0.006	0.006	0.019	6.17	0.80	-1.9	1
247	545828.936	8823204.219	584.182	0.006	0.008	0.020	5.03	0.89	-3.8	1
248	545828.990	8823204.187	584.172	0.008	0.007	0.020	5.05	0.88	-2.7	1
249	545829.010	8823204.125	584.170	0.007	0.009	0.020	6.52	1.07	-3.7	1
250	545829.029	8823204.050	584.175	0.010	0.007	0.020	7.63	1.12	-3.7	1
251	545829.077	8823203.977	584.178	0.008	0.012	0.022	8.64	1.31	-1.8	1
252	545829.115	8823203.909	584.228	0.009	0.009	0.031	7.73	1.49	-2.0	1
253	545829.150	8823203.869	584.206	0.009	0.007	0.023	5.06	1.35	-1.0	1
254	545829.167	8823203.806	584.192	0.009	0.007	0.023	6.51	1.22	-0.6	1

Middle (Wind) Profile: 2012 (continued)

DOY	E(m)	N(m)	Z(m)	E_std(m)	N_std(m)	Z_std(m)	Vx(cm d^{-1})	Vx_err	T(C°)	*
255	545829.166	8823203.750	584.145	0.012	0.010	0.022	5.01	1.48	-4.4	1
256	545829.212	8823203.663	584.171	0.008	0.010	0.023	9.87	1.67	-5.7	1
257	545829.254	8823203.587	584.169	0.006	0.009	0.023	8.57	1.47	-4.9	1
258	545829.306	8823203.517	584.157	0.005	0.009	0.024	8.58	1.23	-5.1	1
259	545829.357	8823203.478	584.118	0.011	0.017	0.051	5.57	2.12	-6.0	1
260	545829.367	8823203.353	584.192	0.012	0.015	0.050	11.87	2.49	-5.1	1
261	545829.364	8823203.299	584.125	0.005	0.007	0.028	4.87	1.66	-2.3	1
262	545829.440	8823203.242	584.149	0.009	0.011	0.031	8.22	1.09	0.4	1
263	545829.453	8823203.180	584.135	0.008	0.009	0.029	6.19	1.12	0.7	1
264	545829.499	8823203.134	584.097	0.010	0.012	0.034	6.05	1.19	-2.8	1
265	545829.472	8823203.061	584.130	0.006	0.007	0.027	5.60	1.17	-6.7	1
266	545829.514	8823202.985	584.144	0.007	0.009	0.025	8.66	0.99	-6.6	1
267	545829.533	8823202.947	584.098	0.004	0.008	0.025	4.31	1.05	-4.9	1
268	545829.519	8823202.890	584.090	0.005	0.008	0.032	4.61	1.09	-3.6	1
269	545829.555	8823202.785	584.148	0.011	0.006	0.027	11.09	0.97	-3.5	1
270	545829.558	8823202.737	584.124	0.005	0.007	0.023	4.47	0.87	-4.4	1
271	545829.585	8823202.687	584.103	0.005	0.005	0.018	5.67	0.82	-6.3	1
272	545829.605	8823202.635	584.102	0.004	0.005	0.017	5.61	0.68	-6.3	1
273	545829.625	8823202.567	584.113	0.004	0.005	0.023	6.97	0.67	-6.9	1
274	545829.654	8823202.524	584.088	0.005	0.006	0.020	5.13	0.69	-8.4	1
275	545829.690	8823202.448	584.092	0.005	0.005	0.018	8.38	0.69	-9.9	1
276	545829.709	8823202.379	584.099	0.003	0.005	0.016	7.14	0.68	-10.4	1
277	545829.788	8823202.255	584.084	0.007	0.016	0.021	14.49	1.52	-13.6	1
278	545829.794	8823202.229	584.084	0.005	0.007	0.018	2.65	1.57	-14.8	1
279	545829.823	8823202.156	584.076	0.006	0.008	0.027	7.88	0.93	-14.1	1
280	545829.839	8823202.106	584.088	0.005	0.006	0.018	5.19	0.91	-13.5	1
281	545829.872	8823202.043	584.076	0.006	0.006	0.021	7.10	0.87	-16.7	1
282	545829.899	8823201.923	584.102	0.010	0.010	0.020	12.05	1.07	-17.6	1
283	545829.931	8823201.854	584.098	0.015	0.006	0.017	7.67	1.01	-19.6	1
284	545829.946	8823201.840	584.098	0.009	0.005	0.018	1.86	0.78	-21.0	1
285	545829.975	8823201.764	584.092	0.009	0.006	0.016	8.11	0.79	-21.6	1
286	545830.004	8823201.683	584.097	0.013	0.007	0.024	8.53	1.02	-15.0	1
287	545830.012	8823201.623	584.102	0.012	0.005	0.019	5.83	1.11	-10.2	1
288	545830.054	8823201.610	584.113	0.007	0.005	0.020	2.92	0.91	-10.2	1
289	545830.071	8823201.514	584.108	0.009	0.008	0.019	9.49	1.14	-10.0	1
290	545830.087	8823201.469	584.087	0.009	0.008	0.022	4.76	1.38	-10.4	1
291	545830.115	8823201.395	584.110	0.008	0.006	0.022	7.92	1.22	-8.4	1
292	545830.154	8823201.381	584.126	0.006	0.010	0.025	2.86	1.24	-5.1	1
293	545830.170	8823201.283	584.120	0.007	0.005	0.025	9.59	1.20	-15.9	1
294	545830.189	8823201.221	584.114	0.007	0.005	0.025	6.47	0.93	-16.3	1
295	545830.226	8823201.184	584.106	0.006	0.006	0.026	4.76	0.89	-17.9	1
296	545830.233	8823201.123	584.061	0.006	0.005	0.027	5.95	0.85	-18.6	1
297	545830.288	8823201.079	584.078	0.007	0.007	0.035	6.22	0.95	-13.3	1
298	545830.274	8823201.019	584.048	0.008	0.011	0.033	4.91	1.32	-12.3	1
299	545830.285	8823200.905	584.077	0.006	0.006	0.024	10.92	1.30	-16.6	1
300	545830.281	8823200.826	584.069	0.008	0.011	0.024	7.03	1.43	-22.1	1
301	545830.348	8823200.787	584.066	0.006	0.006	0.020	6.33	1.43	-24.3	1
302	545830.317	8823200.670	584.095	0.011	0.013	0.034	9.45	1.63	-25.5	1
303	545830.359	8823200.652	584.047	0.007	0.010	0.028	3.37	1.85	-21.9	1
304	545830.384	8823200.590	584.067	0.006	0.009	0.028	6.60	1.50	-23.8	1
305	545830.437	8823200.547	584.046	0.005	0.009	0.033	6.09	1.34	-22.0	1
306	545830.458	8823200.465	584.085	0.006	0.009	0.025	8.38	1.28	-22.0	1
307	545830.511	8823200.428	584.034	0.005	0.007	0.028	5.53	1.12	-20.0	1
308	545830.501	8823200.367	584.053	0.006	0.009	0.027	5.19	1.05	-23.4	1
309	545830.528	8823200.314	584.058	0.006	0.007	0.027	5.85	1.09	-24.4	1
310	545830.525	8823200.248	584.069	0.007	0.009	0.026	5.96	1.06	-28.0	1
311	545830.577	8823200.192	584.080	0.005	0.010	0.022	7.21	1.23	-25.5	1
312	545830.613	8823200.136	584.061	0.006	0.007	0.024	6.64	1.12	-24.8	1
313	545830.662	8823200.077	584.059	0.007	0.006	0.019	7.32	0.76	-25.1	1

Middle (Wind) Profile: 2013

DOY	E(m)	N(m)	Z(m)	E_std(m)	N_std(m)	Z_std(m)	Vx(cm d^{-1})	Vx_err	T(C°)	*
119	545833.428	8823191.825	582.538	0.020	0.018	0.042	5.92	1.20	-14.3	2
120	545833.453	8823191.768	582.551	0.009	0.020	0.029	6.62	0.86	-14.8	2
121	545833.479	8823191.708	582.540	0.012	0.018	0.025	5.95	0.79	-7.6	2
122	545833.506	8823191.649	582.531	0.008	0.017	0.025	5.85	0.62	-13.3	2
123	545833.527	8823191.589	582.551	0.013	0.019	0.039	6.22	0.92	-18.1	2
124	545833.556	8823191.528	582.540	0.011	0.020	0.024	7.12	0.62	-17.9	2
125	545833.581	8823191.469	582.536	0.009	0.020	0.022	6.92	0.66	-18.7	2
126	545833.607	8823191.410	582.537	0.009	0.020	0.023	6.83	0.69	-17.3	2
127	545833.633	8823191.349	582.536	0.011	0.021	0.032	7.15	0.98	-16.4	2
128	545833.660	8823191.290	582.534	0.011	0.018	0.024	6.71	0.59	-20.0	2
129	545833.684	8823191.230	582.525	0.010	0.019	0.025	7.01	0.63	-22.7	2
130	545833.711	8823191.171	582.520	0.012	0.020	0.025	7.19	0.70	-20.4	2
131	545833.735	8823191.111	582.524	0.010	0.019	0.027	6.69	0.80	-18.1	2
132	545833.761	8823191.050	582.527	0.010	0.019	0.024	6.71	0.71	-16.2	2
133	545833.788	8823190.991	582.524	0.011	0.020	0.024	6.93	0.78	-16.5	2
134	545833.814	8823190.931	582.517	0.014	0.023	0.031	7.57	1.10	-15.3	2
135	545833.840	8823190.872	582.525	0.011	0.020	0.025	7.02	0.66	-14.4	2
136	545833.868	8823190.813	582.525	0.012	0.020	0.024	6.80	0.71	-11.7	2

Middle (Wind) Profile: 2013 (continued)

DOY	E(m)	N(m)	Z(m)	E_std(m)	N_std(m)	Z_std(m)	Vx(cm d^{-1})	Vx_err	T(C°)	*
137	545833.893	8823190.754	582.528	0.011	0.020	0.025	6.66	0.77	-7.5	2
138	545833.916	8823190.695	582.518	0.010	0.018	0.024	6.22	0.78	-6.3	2
139	545833.942	8823190.636	582.526	0.013	0.020	0.035	6.23	1.23	-7.8	2
140	545833.968	8823190.573	582.526	0.010	0.021	0.022	7.26	0.74	-9.9	2
141	545833.992	8823190.513	582.527	0.011	0.021	0.022	7.20	0.69	-9.9	2
142	545834.020	8823190.454	582.524	0.010	0.018	0.022	6.12	0.72	-8.2	2
143	545834.044	8823190.393	582.525	0.012	0.021	0.021	7.53	0.70	-8.9	2
144	545834.074	8823190.334	582.525	0.013	0.020	0.025	7.36	0.69	-9.0	2
145	545834.097	8823190.275	582.522	0.011	0.018	0.022	6.48	0.66	-5.2	2
146	545834.122	8823190.215	582.521	0.011	0.019	0.022	6.82	0.70	-4.4	2
147	545834.149	8823190.155	582.526	0.011	0.018	0.024	6.64	0.69	-1.8	2
148	545834.173	8823190.090	582.517	0.015	0.024	0.029	7.55	1.46	-3.0	2
149	545834.199	8823190.034	582.516	0.012	0.020	0.021	7.00	0.76	-5.1	2
150	545834.225	8823189.975	582.511	0.011	0.020	0.022	7.04	0.76	-6.4	2
151	545834.251	8823189.913	582.512	0.013	0.020	0.023	7.27	0.76	-6.9	2
152	545834.276	8823189.855	582.514	0.012	0.021	0.023	7.72	0.63	-5.0	2
153	545834.300	8823189.794	582.511	0.012	0.024	0.025	8.39	0.71	-6.6	2
154	545834.328	8823189.735	582.516	0.011	0.022	0.030	7.83	0.65	-7.9	2
155	545834.350	8823189.676	582.498	0.014	0.023	0.033	8.28	0.75	-8.8	2
156	545834.378	8823189.617	582.508	0.012	0.022	0.031	7.69	0.72	-10.2	2
157	545834.404	8823189.560	582.516	0.014	0.022	0.030	7.48	1.03	-5.9	2
158	545834.434	8823189.497	582.488	0.016	0.024	0.028	8.07	1.15	0.1	2
159	545834.453	8823189.437	582.492	0.020	0.025	0.033	9.89	0.88	-2.6	2
160	545834.486	8823189.380	582.487	0.019	0.023	0.041	6.83	1.20	-2.8	2
161	545834.508	8823189.314	582.498	0.013	0.024	0.026	8.62	0.76	-1.1	2
162	545834.538	8823189.254	582.502	0.012	0.022	0.028	7.83	0.81	-2.1	2
163	545834.564	8823189.197	582.498	0.011	0.021	0.027	7.03	0.97	1.7	2
164	545834.584	8823189.133	582.497	0.041	0.034	0.052	8.34	2.97	-0.2	2
165	545834.613	8823189.074	582.507	0.013	0.024	0.030	8.30	0.71	1.4	2
166	545834.638	8823189.021	582.496	0.011	0.018	0.037	6.09	0.76	-0.2	2
167	545834.665	8823188.956	582.510	0.012	0.020	0.029	7.35	0.68	-1.7	2
168	545834.688	8823188.897	582.460	0.011	0.024	0.038	8.12	0.74	-2.8	2
169	545834.722	8823188.838	582.476	0.013	0.021	0.034	7.36	0.90	-0.9	2
170	545834.745	8823188.773	582.490	0.016	0.023	0.030	8.47	1.05	-0.5	2
171	545834.767	8823188.715	582.492	0.012	0.024	0.032	8.28	0.80	-1.2	2
172	545834.793	8823188.656	582.496	0.012	0.022	0.027	8.07	0.78	-0.5	2
173	545834.821	8823188.595	582.492	0.012	0.020	0.026	7.39	0.72	-0.5	2
174	545834.847	8823188.536	582.494	0.012	0.020	0.025	7.42	0.76	-0.8	2
175	545834.873	8823188.476	582.513	0.013	0.022	0.047	7.81	0.79	-2.5	2
176	545834.899	8823188.417	582.489	0.013	0.020	0.034	7.43	0.70	-3.4	2
177	545834.923	8823188.355	582.489	0.019	0.021	0.031	6.76	1.01	-5.2	2
178	545834.956	8823188.297	582.495	0.015	0.019	0.028	6.96	0.81	-1.4	2
179	545834.976	8823188.235	582.490	0.013	0.023	0.027	8.08	0.81	1.6	2
180	545835.001	8823188.175	582.501	0.013	0.022	0.032	7.89	0.72	-0.0	2
181	545835.029	8823188.114	582.489	0.011	0.025	0.043	8.42	0.76	-0.7	2
182	545835.056	8823188.050	582.474	0.013	0.019	0.032	6.20	0.88	-2.8	2
183	545835.083	8823187.991	582.487	0.010	0.020	0.025	6.90	0.66	1.9	2
184	545835.110	8823187.931	582.476	0.012	0.022	0.026	7.75	0.78	3.2	2
185	545835.139	8823187.871	582.471	0.014	0.022	0.028	7.92	0.84	2.5	2
186	545835.162	8823187.808	582.468	0.013	0.022	0.030	8.01	0.85	1.1	2
187	545835.190	8823187.748	582.466	0.014	0.019	0.029	7.11	0.80	1.7	2
188	545835.217	8823187.686	582.467	0.013	0.021	0.028	7.57	0.75	3.5	2
189	545835.243	8823187.621	582.470	0.013	0.021	0.026	7.54	0.81	3.0	2
190	545835.271	8823187.556	582.467	0.014	0.020	0.030	7.64	0.78	3.2	2
191	545835.298	8823187.493	582.458	0.014	0.021	0.032	7.52	0.75	3.6	2
192	545835.330	8823187.424	582.467	0.014	0.020	0.032	7.20	0.85	4.5	2
193	545835.359	8823187.362	582.469	0.016	0.021	0.030	7.56	0.88	3.4	2
194	545835.386	8823187.290	582.459	0.014	0.027	0.033	9.55	1.00	4.8	2
195	545835.418	8823187.226	582.450	0.011	0.022	0.028	7.60	0.83	4.1	2
196	545835.447	8823187.156	582.454	0.011	0.020	0.027	6.96	0.68	5.3	2
197	545835.481	8823187.080	582.450	0.012	0.024	0.025	8.36	0.85	5.4	2
198	545835.513	8823187.000	582.446	0.012	0.026	0.027	8.97	0.94	5.8	2
199	545835.552	8823186.930	582.441	0.015	0.023	0.029	8.06	1.02	4.6	2
200	545835.585	8823186.856	582.426	0.017	0.033	0.056	7.23	2.67	6.7	2
201	545835.618	8823186.767	582.437	0.015	0.023	0.028	8.64	0.84	4.4	2
202	545835.654	8823186.689	582.433	0.014	0.024	0.025	8.85	0.74	5.1	2
203	545835.691	8823186.598	582.437	0.016	0.028	0.025	10.73	0.72	5.5	2
204	545835.753	8823186.439	582.470	0.030	0.071	0.037	26.04	1.34	4.6	2
205	545835.826	8823186.244	582.516	0.023	0.051	0.034	18.75	1.00	3.1	2
206	545835.888	8823186.123	582.512	0.018	0.024	0.031	9.11	0.94	-0.3	2
207	545835.926	8823186.039	582.475	0.014	0.023	0.024	8.23	0.97	-3.0	2
208	545835.962	8823185.961	582.472	0.011	0.023	0.022	8.37	0.57	-2.3	2
209	545835.999	8823185.887	582.458	0.016	0.022	0.024	8.06	0.90	-1.0	2
210	545836.031	8823185.812	582.462	0.013	0.020	0.023	7.71	0.60	-1.7	2
211	545836.065	8823185.735	582.461	0.011	0.021	0.024	7.52	0.64	-0.8	2
212	545836.099	8823185.661	582.456	0.019	0.018	0.026	6.73	1.23	-1.2	2
213	545836.136	8823185.575	582.458	0.039	0.026	0.045	6.08	2.43	1.2	2
214	545836.163	8823185.506	582.458	0.012	0.022	0.026	8.12	0.64	1.9	2
215	545836.195	8823185.431	582.458	0.014	0.020	0.025	7.63	0.64	1.4	2
216	545836.233	8823185.351	582.460	0.015	0.020	0.027	7.57	0.64	1.4	2
217	545836.279	8823185.247	582.466	0.027	0.054	0.031	19.80	1.55	3.0	2
218	545836.403	8823184.929	582.563	0.037	0.076	0.040	28.00	2.10	3.1	2
219	545836.494	8823184.727	582.576	0.029	0.043	0.031	17.10	1.22	2.9	2

Middle (Wind) Profile: 2013 (continued)

DOY	E(m)	N(m)	Z(m)	E_std(m)	N_std(m)	Z_std(m)	Vx(cm d^{-1})	Vx_err	T(C°)	*
220	545836.558	8823184.614	582.540	0.024	0.023	0.030	9.37	1.04	2.0	2
221	545836.607	8823184.529	582.500	0.017	0.021	0.036	7.60	0.89	2.1	2
222	545836.670	8823184.374	582.540	0.038	0.093	0.063	32.57	3.15	3.2	2
223	545836.790	8823184.099	582.564	0.028	0.029	0.043	11.93	1.26	1.4	2
224	545836.840	8823184.017	582.513	0.026	0.022	0.044	6.30	1.51	-0.3	2
225	545836.885	8823183.933	582.477	0.016	0.024	0.031	9.37	0.74	-1.9	2
226	545836.922	8823183.855	582.466	0.013	0.023	0.030	8.16	0.77	-2.9	2
227	545836.960	8823183.775	582.454	0.014	0.020	0.030	7.49	0.73	-3.8	2
228	545836.991	8823183.699	582.425	0.015	0.022	0.024	8.00	0.91	-5.4	2
229	545837.023	8823183.623	582.452	0.014	0.022	0.022	8.15	0.79	-6.0	2
230	545837.057	8823183.550	582.434	0.014	0.022	0.030	8.01	0.75	-5.5	2
231	545837.087	8823183.474	582.440	0.013	0.020	0.025	7.33	0.66	-7.5	2
232	545837.118	8823183.401	582.435	0.012	0.018	0.026	6.85	0.61	-8.3	2
233	545837.147	8823183.327	582.435	0.013	0.022	0.024	7.95	0.69	-7.0	2
234	545837.187	8823183.254	582.446	0.031	0.023	0.090	4.97	2.38	-7.5	2
235	545837.211	8823183.190	582.426	0.014	0.019	0.023	6.70	0.79	-8.8	2
236	545837.237	8823183.113	582.441	0.013	0.024	0.035	7.78	0.93	-0.1	2
237	545837.274	8823183.045	582.441	0.016	0.021	0.023	8.12	0.86	0.9	2
238	545837.308	8823182.973	582.439	0.017	0.024	0.026	9.03	0.87	-1.6	2
239	545837.332	8823182.906	582.428	0.012	0.024	0.025	8.26	0.83	-3.2	2
240	545837.358	8823182.834	582.437	0.021	0.023	0.029	6.80	1.29	-3.1	2
241	545837.392	8823182.768	582.427	0.014	0.021	0.027	7.39	0.89	-3.2	2
242	545837.423	8823182.701	582.429	0.011	0.022	0.024	7.53	0.72	-4.5	2
243	545837.453	8823182.632	582.430	0.013	0.020	0.026	7.13	0.75	-6.8	2
244	545837.478	8823182.567	582.423	0.012	0.020	0.025	6.71	0.77	-5.7	2
245	545837.511	8823182.491	582.429	0.015	0.021	0.024	7.14	0.94	-4.2	2
246	545837.542	8823182.424	582.426	0.016	0.020	0.029	7.09	0.87	-4.4	2
247	545837.572	8823182.356	582.410	0.019	0.020	0.030	6.92	1.27	-4.9	2
248	545837.598	8823182.295	582.420	0.015	0.017	0.028	5.43	0.91	-8.0	2
249	545837.629	8823182.221	582.420	0.016	0.018	0.025	6.80	0.69	-10.4	2
250	545837.659	8823182.155	582.410	0.013	0.018	0.026	6.58	0.72	-4.8	2
251	545837.689	8823182.085	582.411	0.010	0.021	0.027	6.75	0.82	-1.7	2
252	545837.720	8823182.019	582.415	0.010	0.019	0.023	6.65	0.71	-2.9	2
253	545837.747	8823181.950	582.412	0.012	0.024	0.025	7.58	0.96	-3.9	2
254	545837.783	8823181.885	582.413	0.021	0.018	0.033	6.30	1.18	-3.4	2
255	545837.806	8823181.813	582.411	0.010	0.025	0.026	8.02	0.80	-5.9	2
256	545837.837	8823181.744	582.411	0.009	0.021	0.025	7.36	0.67	-7.2	2
257	545837.866	8823181.676	582.408	0.009	0.023	0.025	7.81	0.74	-7.9	2
258	545837.895	8823181.612	582.403	0.012	0.019	0.030	6.32	0.71	-9.2	2
259	545837.923	8823181.542	582.402	0.010	0.024	0.024	8.31	0.69	-5.9	2
260	545837.949	8823181.472	582.405	0.018	0.027	0.043	7.56	1.58	-5.7	2
261	545837.984	8823181.406	582.408	0.011	0.022	0.023	7.83	0.67	-9.2	2
262	545838.012	8823181.338	582.407	0.011	0.023	0.024	8.15	0.74	-10.2	2
263	545838.043	8823181.270	582.408	0.011	0.021	0.022	7.56	0.63	-9.3	2
264	545838.072	8823181.203	582.410	0.012	0.023	0.023	8.17	0.72	-11.2	2
265	545838.102	8823181.137	582.410	0.011	0.023	0.024	8.11	0.71	-10.1	2
266	545838.136	8823181.070	582.401	0.014	0.021	0.031	7.80	0.71	-11.1	2
267	545838.164	8823181.004	582.398	0.010	0.018	0.027	5.98	0.83	-13.9	2
268	545838.192	8823180.925	582.404	0.024	0.023	0.049	6.68	1.72	-12.1	2
269	545838.219	8823180.866	582.402	0.010	0.021	0.028	7.39	0.64	-10.7	2
270	545838.249	8823180.801	582.403	0.009	0.019	0.026	6.50	0.67	-7.2	2

Middle (Wind) Profile: 2014

DOY	E(m)	N(m)	Z(m)	E_std(m)	N_std(m)	Z_std(m)	Vx(cm d^{-1})	Vx_err	T(C°)	*
116	545844.342	8823166.853	582.220	0.011	0.021	0.025	7.23	0.77	-11.3	2
117	545844.369	8823166.788	582.222	0.012	0.019	0.024	6.68	0.77	-12.4	2
118	545844.397	8823166.725	582.227	0.012	0.019	0.024	6.84	0.66	-13.1	2
119	545844.422	8823166.658	582.222	0.011	0.020	0.024	7.00	0.76	-11.4	2
120	545844.459	8823166.599	582.210	0.032	0.021	0.057	5.52	1.42	-12.6	2
121	545844.480	8823166.530	582.220	0.012	0.021	0.022	7.13	0.88	-13.2	2
122	545844.512	8823166.466	582.215	0.014	0.020	0.025	6.93	1.06	-9.3	2
123	545844.536	8823166.402	582.222	0.011	0.020	0.026	6.92	0.72	-13.5	2
124	545844.559	8823166.366	582.233	0.006	0.006	0.028	1.98	0.54	-13.1	2
125	545844.585	8823166.274	582.202	0.036	0.036	0.038	2.94	3.13	-13.0	2
126	545844.618	8823166.206	582.232	0.020	0.019	0.049	4.68	1.31	-9.5	2
127	545844.647	8823166.147	582.230	0.012	0.020	0.027	6.74	0.85	-9.9	2
128	545844.671	8823166.104	582.238	0.007	0.007	0.024	2.78	0.71	-8.9	2
191	545845.046	8823163.708	581.346	0.304	0.486	0.136	-	-	4.5	2
192	545845.024	8823163.722	581.333	0.018	0.033	0.030	12.04	0.73	3.0	2
193	545845.074	8823163.616	581.325	0.017	0.032	0.030	11.70	0.72	3.2	2
194	545845.124	8823163.521	581.302	0.019	0.022	0.029	8.13	0.69	2.6	2
195	545845.170	8823163.429	581.291	0.024	0.030	0.026	11.52	0.72	5.6	2
196	545845.230	8823163.282	581.291	0.023	0.046	0.027	16.67	1.00	6.9	2
197	545845.286	8823163.151	581.303	0.023	0.024	0.059	7.49	1.52	5.0	2
198	545845.334	8823163.049	581.292	0.015	0.029	0.028	10.62	0.71	2.4	2
199	545845.377	8823162.959	581.282	0.013	0.029	0.030	10.08	0.82	4.0	2
200	545845.424	8823162.856	581.284	0.014	0.027	0.031	9.67	0.79	4.8	2
201	545845.471	8823162.755	581.282	0.017	0.034	0.026	12.28	0.88	4.9	2
202	545845.519	8823162.649	581.280	0.017	0.028	0.031	10.25	0.73	4.5	2

Middle (Wind) Profile: 2015

DOY	E(m)	N(m)	Z(m)	E_std(m)	N_std(m)	Z_std(m)	Vx(cm d^{-1})	Vx_err	T(C°)	*
114	545854.158	8823143.151	581.099	0.011	0.020	0.019	7.25	0.64	-10.4	2
115	545854.185	8823143.085	581.113	0.013	0.023	0.027	8.04	0.91	-10.0	2
116	545854.217	8823143.015	581.149	0.012	0.020	0.024	7.20	0.69	-10.3	2
117	545854.245	8823142.951	581.152	0.013	0.021	0.025	7.57	0.76	-13.7	2
118	545854.274	8823142.888	581.149	0.013	0.020	0.024	7.46	0.73	-15.2	2
119	545854.303	8823142.822	581.149	0.012	0.022	0.024	7.82	0.72	-16.5	2
120	545854.331	8823142.759	581.147	0.012	0.022	0.027	7.60	0.87	-16.1	2
121	545854.357	8823142.696	581.149	0.012	0.021	0.027	7.04	0.94	-15.4	2
122	545854.388	8823142.630	581.146	0.013	0.021	0.025	7.77	0.74	-14.5	2
123	545854.409	8823142.561	581.140	0.020	0.030	0.040	8.87	1.17	-14.7	2
124	545854.443	8823142.502	581.144	0.013	0.023	0.025	8.37	0.82	-12.9	2
125	545854.473	8823142.439	581.144	0.012	0.022	0.024	7.66	0.79	-14.4	2
126	545854.501	8823142.373	581.140	0.012	0.021	0.030	7.66	0.84	-16.5	2
127	545854.531	8823142.310	581.145	0.014	0.020	0.024	7.70	0.80	-17.1	2
128	545854.559	8823142.245	581.143	0.012	0.021	0.024	7.61	0.79	-17.5	2
129	545854.589	8823142.180	581.142	0.014	0.021	0.023	7.56	0.75	-15.8	2
130	545854.617	8823142.115	581.152	0.013	0.023	0.029	8.29	0.82	-12.5	2
131	545854.635	8823142.052	581.142	0.031	0.032	0.053	10.64	2.41	-15.0	2
132	545854.677	8823141.991	581.145	0.026	0.029	0.046	8.09	1.95	-15.1	2
133	545854.703	8823141.925	581.137	0.011	0.024	0.024	8.27	0.78	-16.4	2
134	545854.730	8823141.858	581.126	0.012	0.022	0.027	7.92	0.70	-15.1	2
135	545854.759	8823141.794	581.130	0.014	0.025	0.032	9.04	0.81	-12.4	2
136	545854.788	8823141.731	581.147	0.013	0.022	0.026	8.27	0.78	-9.4	2
137	545854.814	8823141.666	581.144	0.011	0.021	0.026	7.40	0.78	-8.8	2
138	545854.848	8823141.603	581.139	0.015	0.021	0.030	7.37	1.12	-7.2	2
139	545854.875	8823141.538	581.135	0.012	0.023	0.027	8.17	0.72	-8.6	2
140	545854.902	8823141.474	581.148	0.013	0.021	0.030	7.79	0.77	-7.6	2
141	545854.930	8823141.409	581.132	0.013	0.023	0.026	8.51	0.74	-8.8	2
142	545854.960	8823141.347	581.120	0.012	0.021	0.031	7.35	0.79	-12.9	2
143	545854.987	8823141.279	581.126	0.013	0.022	0.027	8.11	0.66	-13.9	2
144	545855.017	8823141.213	581.127	0.012	0.022	0.026	7.88	0.72	-6.4	2
145	545855.042	8823141.150	581.126	0.011	0.023	0.026	8.11	0.80	-6.7	2
146	545855.074	8823141.086	581.130	0.014	0.024	0.027	8.46	0.94	-3.0	2
147	545855.105	8823141.021	581.129	0.013	0.023	0.026	8.15	0.89	-2.8	2
148	545855.131	8823140.958	581.129	0.016	0.023	0.030	8.18	1.17	-3.5	2
149	545855.157	8823140.892	581.133	0.012	0.023	0.026	8.09	0.85	-2.3	2
150	545855.187	8823140.828	581.130	0.011	0.023	0.026	8.28	0.65	-1.3	2
151	545855.217	8823140.763	581.133	0.013	0.023	0.025	8.49	0.66	0.3	2
152	545855.244	8823140.699	581.124	0.012	0.021	0.025	7.82	0.67	0.8	2
153	545855.271	8823140.631	581.127	0.013	0.021	0.025	8.02	0.64	-0.9	2
154	545855.302	8823140.568	581.128	0.014	0.022	0.024	8.27	0.65	1.8	2
155	545855.333	8823140.503	581.125	0.014	0.021	0.025	7.91	0.69	0.8	2
156	545855.362	8823140.438	581.129	0.016	0.022	0.024	8.58	0.72	-0.7	2
157	545855.392	8823140.370	581.130	0.014	0.021	0.023	7.62	0.78	-2.4	2
158	545855.420	8823140.307	581.131	0.014	0.019	0.029	6.21	1.10	-3.8	2
159	545855.451	8823140.232	581.137	0.015	0.024	0.032	8.93	0.72	-0.7	2
160	545855.482	8823140.170	581.132	0.014	0.021	0.025	7.25	1.03	1.6	2
161	545855.512	8823140.099	581.129	0.010	0.021	0.025	7.62	0.68	1.2	2
162	545855.541	8823140.034	581.125	0.012	0.021	0.026	7.69	0.75	0.6	2
163	545855.570	8823139.965	581.127	0.014	0.023	0.025	8.50	0.83	1.1	2
164	545855.601	8823139.897	581.121	0.014	0.023	0.027	8.34	0.80	2.6	2
165	545855.632	8823139.830	581.117	0.014	0.023	0.029	8.62	0.88	4.0	2
166	545855.671	8823139.751	581.118	0.016	0.025	0.027	9.29	0.92	3.2	2
167	545855.705	8823139.667	581.124	0.018	0.027	0.028	10.30	0.75	2.5	2
168	545855.746	8823139.576	581.123	0.017	0.030	0.027	10.62	0.83	4.1	2
169	545855.795	8823139.465	581.128	0.019	0.038	0.028	13.97	1.18	2.7	2
170	545855.837	8823139.345	581.127	0.022	0.036	0.030	13.79	0.94	2.1	2
171	545855.891	8823139.229	581.121	0.021	0.037	0.024	14.29	0.66	2.5	2
172	545855.949	8823139.093	581.155	0.023	0.040	0.029	15.46	0.90	3.0	2
173	545855.994	8823138.980	581.185	0.022	0.033	0.030	12.54	1.09	3.1	2
174	545856.043	8823138.874	581.180	0.019	0.032	0.028	12.04	0.91	2.5	2
175	545856.091	8823138.774	581.179	0.018	0.030	0.030	11.58	0.75	3.2	2
176	545856.137	8823138.677	581.172	0.016	0.027	0.026	10.22	0.68	1.2	2
177	545856.179	8823138.586	581.176	0.017	0.029	0.024	10.84	0.86	3.0	2
178	545856.231	8823138.484	581.180	0.022	0.030	0.028	11.88	1.05	3.4	2
179	545856.301	8823138.339	581.176	0.049	0.039	0.075	11.32	3.36	5.6	2
180	545856.356	8823138.197	581.180	0.024	0.048	0.026	18.13	0.80	3.7	2
181	545856.422	8823138.032	581.230	0.026	0.040	0.027	15.82	0.94	2.5	2
182	545856.478	8823137.904	581.216	0.026	0.043	0.032	15.50	1.77	4.9	2
183	545856.553	8823137.750	581.239	0.028	0.048	0.025	18.72	0.93	3.5	2
184	545856.622	8823137.591	581.250	0.034	0.049	0.038	19.21	1.37	3.5	2
185	545856.696	8823137.423	581.263	0.034	0.065	0.028	24.70	1.52	5.4	2
186	545856.805	8823137.169	581.293	0.032	0.034	0.047	14.24	1.35	4.9	2
187	545856.883	8823137.056	581.247	0.022	0.042	0.030	15.30	1.19	6.7	2
188	545856.955	8823136.898	581.260	0.028	0.061	0.027	22.75	1.08	8.1	2
189	545857.029	8823136.737	581.268	0.025	0.044	0.027	16.65	1.16	8.1	2
190	545857.099	8823136.608	581.261	0.022	0.032	0.031	12.75	0.93	9.3	2
191	545857.158	8823136.501	581.224	0.020	0.036	0.027	13.90	0.73	7.7	2
192	545857.218	8823136.372	581.225	0.024	0.055	0.026	19.51	1.70	7.4	2
193	545857.296	8823136.208	581.221	0.020	0.036	0.024	13.62	0.80	8.1	2
194	545857.356	8823136.096	581.213	0.029	0.041	0.025	15.97	1.39	7.2	2
195	545857.400	8823136.003	581.190	0.024	0.045	0.059	15.79	1.80	7.2	2
196	545857.449	8823135.890	581.183	0.021	0.033	0.024	12.88	0.77	6.0	2

Middle (Wind) Profile: 2015 (continued)

DOY	E(m)	N(m)	Z(m)	E_std(m)	N_std(m)	Z_std(m)	Vx(cm d^{-1})	Vx_err	T(C°)	*
197	545857.498	8823135.791	581.173	0.019	0.029	0.024	11.15	0.75	6.3	2
198	545857.541	8823135.698	581.165	0.018	0.028	0.022	10.82	0.68	5.8	2
199	545857.583	8823135.602	581.163	0.019	0.028	0.024	11.06	0.64	7.0	2
200	545857.629	8823135.501	581.161	0.018	0.031	0.027	11.51	0.97	6.4	2
201	545857.670	8823135.411	581.155	0.019	0.032	0.025	12.02	0.80	6.2	2
202	545857.719	8823135.309	581.159	0.019	0.028	0.024	10.77	0.73	6.8	2
203	545857.765	8823135.219	581.157	0.018	0.027	0.047	9.39	1.33	7.0	2
204	545857.805	8823135.124	581.153	0.016	0.027	0.024	10.47	0.74	7.1	2
205	545857.846	8823135.028	581.151	0.018	0.028	0.023	10.80	0.73	7.1	2
206	545857.887	8823134.933	581.129	0.020	0.031	0.078	10.60	1.42	7.0	2
207	545857.930	8823134.843	581.143	0.018	0.025	0.048	8.65	1.44	6.5	2
208	545857.977	8823134.759	581.150	0.023	0.022	0.042	9.15	0.95	6.0	2
209	545858.015	8823134.673	581.135	0.017	0.025	0.027	9.72	0.76	5.1	2
210	545858.054	8823134.577	581.138	0.017	0.033	0.032	12.21	0.73	6.0	2
211	545858.095	8823134.489	581.131	0.014	0.029	0.035	10.25	0.88	5.1	2
212	545858.143	8823134.398	581.125	0.022	0.022	0.026	8.57	1.17	1.4	2
213	545858.178	8823134.309	581.126	0.019	0.027	0.028	10.48	0.88	3.8	2
214	545858.221	8823134.225	581.123	0.014	0.020	0.032	7.39	0.82	4.5	2
215	545858.249	8823134.152	581.129	0.016	0.021	0.041	6.27	1.50	5.0	2
216	545858.285	8823134.066	581.135	0.023	0.031	0.050	6.27	2.25	3.7	2
217	545858.337	8823133.972	581.115	0.013	0.023	0.025	8.36	0.72	0.0	2
218	545858.374	8823133.892	581.119	0.013	0.026	0.025	8.71	1.05	-1.3	2
219	545858.411	8823133.815	581.112	0.011	0.022	0.023	7.77	0.66	-0.8	2
220	545858.447	8823133.741	581.104	0.012	0.022	0.022	7.82	0.86	2.6	2
221	545858.482	8823133.671	581.104	0.012	0.022	0.025	7.87	0.74	2.1	2
222	545858.512	8823133.592	581.110	0.011	0.023	0.023	8.22	0.57	2.4	2
223	545858.552	8823133.515	581.119	0.021	0.026	0.041	8.23	1.35	3.6	2
224	545858.583	8823133.422	581.108	0.013	0.029	0.025	9.82	1.00	5.6	2
225	545858.630	8823133.311	581.115	0.016	0.032	0.023	11.73	0.71	5.0	2
226	545858.683	8823133.186	581.113	0.021	0.040	0.024	15.00	0.95	5.5	2
227	545858.747	8823133.036	581.137	0.019	0.047	0.028	16.82	1.15	5.1	2
228	545858.808	8823132.899	581.159	0.018	0.034	0.024	12.82	0.82	4.3	2
229	545858.854	8823132.805	581.143	0.013	0.021	0.026	7.40	0.93	3.4	2
230	545858.891	8823132.732	581.133	0.015	0.023	0.023	8.25	0.90	2.8	2
231	545858.927	8823132.660	581.126	0.010	0.023	0.025	7.63	0.86	1.8	2
232	545858.963	8823132.586	581.115	0.011	0.021	0.024	7.21	0.85	2.6	2
233	545858.987	8823132.529	581.111	0.008	0.018	0.023	4.98	1.13	1.8	2
234	545859.020	8823132.462	581.108	0.022	0.022	0.032	7.44	1.51	1.1	2
235	545859.051	8823132.388	581.110	0.011	0.024	0.025	7.48	1.19	-0.7	2
236	545859.078	8823132.319	581.117	0.013	0.030	0.045	7.76	1.69	-0.8	2
237	545859.115	8823132.250	581.108	0.011	0.023	0.022	7.62	0.94	-1.2	2
238	545859.146	8823132.182	581.113	0.011	0.020	0.022	6.90	0.82	-0.0	2
239	545859.177	8823132.112	581.117	0.011	0.023	0.021	7.89	0.84	-0.5	2
240	545859.201	8823132.036	581.112	0.027	0.035	0.031	8.24	2.51	-0.8	2
241	545859.240	8823131.972	581.114	0.011	0.021	0.022	7.22	0.80	-2.2	2
242	545859.272	8823131.903	581.116	0.011	0.021	0.022	7.11	0.89	-1.6	2
243	545859.298	8823131.836	581.114	0.010	0.022	0.022	7.07	1.14	0.1	2
244	545859.334	8823131.768	581.110	0.014	0.023	0.028	7.63	1.29	1.4	2
245	545859.361	8823131.697	581.115	0.013	0.021	0.028	7.02	1.18	-1.4	2
246	545859.390	8823131.635	581.115	0.009	0.020	0.025	6.19	1.00	-1.6	2
247	545859.421	8823131.567	581.119	0.011	0.021	0.023	6.85	1.03	-2.6	2
248	545859.450	8823131.505	581.109	0.010	0.021	0.026	6.33	1.20	-3.9	2
249	545859.474	8823131.438	581.112	0.026	0.025	0.043	7.57	2.07	-6.1	2
250	545859.515	8823131.367	581.116	0.011	0.019	0.023	6.52	0.69	-4.9	2
251	545859.541	8823131.299	581.112	0.008	0.021	0.023	6.48	1.01	-7.6	2
252	545859.572	8823131.226	581.115	0.009	0.022	0.020	7.51	0.84	-3.7	2
253	545859.597	8823131.159	581.102	0.034	0.036	0.055	9.93	2.75	-2.6	2
254	545859.634	8823131.091	581.110	0.013	0.021	0.032	6.78	1.09	-6.1	2
255	545859.667	8823131.024	581.107	0.011	0.020	0.020	7.26	0.77	-6.7	2
256	545859.694	8823130.960	581.114	0.012	0.020	0.021	7.20	0.74	-7.1	2
257	545859.727	8823130.893	581.116	0.014	0.018	0.032	5.94	1.19	-5.9	2
258	545859.750	8823130.823	581.114	0.010	0.024	0.022	7.54	1.23	-4.1	2
259	545859.786	8823130.756	581.114	0.015	0.021	0.030	5.90	1.23	-10.4	2
260	545859.812	8823130.694	581.107	0.010	0.022	0.019	6.96	0.99	-7.4	2
261	545859.842	8823130.621	581.110	0.009	0.021	0.020	6.71	0.98	-9.9	2

Lower (Anniversary) Profile: 2013

DOY	E(m)	N(m)	Z(m)	E_std(m)	N_std(m)	Z_std(m)	Vx(cm d^{-1})	Vx_err	T(C°)	*
196	546987.986	8821382.147	375.514	0.013	0.039	0.035	12.39	1.49	6.9	1
197	546988.026	8821382.021	375.507	0.013	0.035	0.029	12.18	0.96	8.0	1
198	546988.054	8821381.908	375.500	0.013	0.035	0.030	11.60	1.27	7.3	1
199	546988.093	8821381.804	375.501	0.017	0.029	0.031	10.55	0.93	6.4	1
200	546988.126	8821381.686	375.497	0.020	0.037	0.032	13.11	1.13	7.2	1
201	546988.161	8821381.571	375.493	0.017	0.028	0.029	10.12	0.79	7.1	1
202	546988.191	8821381.470	375.490	0.015	0.035	0.030	12.10	0.98	-	2
203	546988.227	8821381.367	375.487	0.015	0.031	0.031	10.87	0.91	6.2	2
204	546988.262	8821381.259	375.479	0.015	0.049	0.032	16.51	1.69	5.2	2
205	546988.300	8821381.118	375.479	0.021	0.030	0.037	10.13	1.29	4.9	2
206	546988.338	8821381.032	375.479	0.017	0.016	0.031	4.07	1.20	1.2	2
207	546988.354	8821380.961	375.445	0.012	0.020	0.044	5.85	1.11	-1.3	2

Lower (Anniversary) Profile: 2013 (continued)

DOY	E(m)	N(m)	Z(m)	E_std(m)	N_std(m)	Z_std(m)	Vx(cm d^{-1})	Vx_err	T(C°)	*
208	546988.384	8821380.899	375.435	0.009	0.018	0.029	4.77	0.96	-1.1	2
209	546988.407	8821380.829	375.426	0.014	0.028	0.026	9.58	0.97	-1.0	2
210	546988.429	8821380.747	375.420	0.010	0.015	0.027	4.25	0.81	-1.0	2
211	546988.447	8821380.693	375.413	0.011	0.016	0.025	4.37	0.89	0.2	2
212	546988.464	8821380.642	375.408	0.010	0.013	0.027	4.05	0.66	0.5	2
213	546988.485	8821380.589	375.406	0.011	0.017	0.027	5.47	0.71	1.3	2
214	546988.511	8821380.528	375.410	0.014	0.020	0.029	6.64	0.90	1.7	2
215	546988.530	8821380.459	375.399	0.011	0.021	0.026	6.94	0.76	0.7	2
216	546988.555	8821380.381	375.399	0.011	0.020	0.028	6.59	0.69	2.0	2
217	546988.604	8821380.235	375.416	0.025	0.083	0.030	29.40	1.21	4.0	2
218	546988.673	8821379.934	375.436	0.031	0.068	0.033	24.74	1.50	3.8	2
219	546988.744	8821379.738	375.421	0.022	0.037	0.034	14.00	0.98	3.2	2
220	546988.791	8821379.638	375.392	0.021	0.017	0.029	6.47	0.85	1.8	2
221	546988.827	8821379.570	375.353	0.023	0.024	0.059	4.63	2.13	2.5	2
222	546988.868	8821379.452	375.392	0.023	0.063	0.039	21.80	1.59	4.2	2
223	546988.944	8821379.201	375.391	0.026	0.032	0.041	11.68	1.61	1.6	2
224	546988.984	8821379.130	375.352	0.020	0.014	0.040	4.12	1.10	0.0	2
225	546989.014	8821379.067	375.318	0.011	0.020	0.032	7.11	0.66	-0.6	2
226	546989.033	8821379.006	375.318	0.009	0.018	0.029	5.40	0.77	-2.2	2
227	546989.057	8821378.944	375.313	0.008	0.016	0.034	5.26	0.66	-2.8	2
228	546989.074	8821378.896	375.291	0.009	0.017	0.029	5.40	0.75	-4.1	2
229	546989.093	8821378.840	375.303	0.009	0.016	0.024	5.44	0.65	-4.9	2
230	546989.112	8821378.790	375.292	0.009	0.016	0.031	5.04	0.77	-4.0	2
231	546989.124	8821378.735	375.290	0.010	0.016	0.025	4.82	0.85	-6.4	2
232	546989.151	8821378.681	375.274	0.018	0.016	0.036	6.34	0.76	-6.8	2
233	546989.161	8821378.633	375.282	0.009	0.020	0.026	6.63	0.80	-5.7	2
234	546989.176	8821378.583	375.276	0.024	0.021	0.051	6.09	1.67	-6.3	2
235	546989.198	8821378.536	375.278	0.008	0.016	0.024	4.63	0.77	-8.0	2
236	546989.210	8821378.483	375.280	0.009	0.020	0.036	5.22	1.22	0.6	2
237	546989.236	8821378.435	375.278	0.012	0.017	0.025	4.59	1.21	2.2	2
238	546989.255	8821378.386	375.275	0.012	0.018	0.029	6.46	0.87	-2.6	2
239	546989.265	8821378.340	375.264	0.007	0.019	0.028	5.94	0.79	-4.6	2
240	546989.283	8821378.286	375.271	0.011	0.024	0.031	6.03	1.58	-3.4	2
241	546989.300	8821378.247	375.260	0.007	0.017	0.030	5.02	0.82	-4.4	2
242	546989.317	8821378.200	375.262	0.008	0.017	0.028	5.15	0.76	-4.9	2
243	546989.335	8821378.154	375.262	0.008	0.015	0.026	4.93	0.72	-6.1	2
244	546989.347	8821378.109	375.255	0.009	0.017	0.028	4.83	0.79	-5.0	2
245	546989.366	8821378.058	375.257	0.009	0.016	0.025	4.64	0.79	-2.9	2
246	546989.383	8821378.012	375.260	0.009	0.016	0.028	4.73	0.78	-2.3	2
247	546989.400	8821377.969	375.249	0.007	0.016	0.026	4.93	0.69	-3.3	2
248	546989.414	8821377.923	375.250	0.008	0.016	0.027	5.08	0.82	-6.7	2
249	546989.434	8821377.879	375.247	0.008	0.018	0.029	4.99	0.92	-8.3	2
250	546989.446	8821377.831	375.243	0.007	0.015	0.029	4.11	0.97	-5.4	2
251	546989.464	8821377.785	375.243	0.008	0.018	0.029	4.68	0.98	0.2	2
252	546989.480	8821377.740	375.243	0.007	0.018	0.026	4.80	1.03	-0.8	2
253	546989.488	8821377.696	375.242	0.028	0.034	0.073	6.24	2.93	-2.1	2
254	546989.512	8821377.655	375.230	0.017	0.018	0.034	3.97	1.22	-1.4	2
255	546989.529	8821377.602	375.235	0.007	0.018	0.029	4.78	0.87	-3.3	2
256	546989.547	8821377.556	375.236	0.008	0.016	0.028	4.67	0.87	-5.0	2
257	546989.562	8821377.511	375.231	0.007	0.018	0.027	5.47	0.77	-5.8	2
258	546989.578	8821377.467	375.232	0.006	0.017	0.026	5.27	0.79	-7.8	2
259	546989.594	8821377.421	375.228	0.007	0.018	0.026	5.66	0.79	-7.4	2
260	546989.611	8821377.376	375.233	0.007	0.019	0.029	5.57	0.88	-5.5	2
261	546989.628	8821377.331	375.231	0.007	0.019	0.025	5.66	0.84	-8.3	2
262	546989.642	8821377.285	375.229	0.008	0.019	0.026	5.92	0.85	-9.1	2
263	546989.660	8821377.241	375.229	0.007	0.017	0.024	5.18	0.77	-7.9	2
264	546989.676	8821377.196	375.231	0.009	0.019	0.025	6.15	0.83	-11.9	2
265	546989.693	8821377.153	375.230	0.009	0.019	0.026	5.98	0.78	-9.4	2
266	546989.710	8821377.108	375.225	0.009	0.018	0.026	5.55	0.80	-11.7	2
267	546989.726	8821377.063	375.220	0.008	0.017	0.027	4.97	0.74	-13.4	2
268	546989.742	8821377.016	375.222	0.008	0.019	0.025	6.07	0.72	-11.3	2
269	546989.757	8821376.973	375.220	0.010	0.017	0.028	5.43	0.75	-10.9	2
270	546989.774	8821376.930	375.218	0.010	0.016	0.027	4.56	0.73	-5.9	2
271	546989.799	8821376.885	375.220	0.017	0.020	0.026	6.08	1.28	-6.4	2
272	546989.792	8821376.841	375.221	0.032	0.030	0.042	9.59	1.59	-8.5	2

Lower (Anniversary) Profile: 2014

DOY	E(m)	N(m)	Z(m)	E_std(m)	N_std(m)	Z_std(m)	Vx(cm d^{-1})	Vx_err	T(C°)	*
113	546992.977	8821368.015	374.949	0.010	0.015	0.031	5.10	0.72	-15.4	2
114	546992.993	8821367.975	374.954	0.010	0.016	0.027	5.30	0.73	-14.9	2
115	546993.005	8821367.929	374.956	0.013	0.019	0.029	6.41	0.82	-10.8	2
116	546993.021	8821367.892	374.954	0.008	0.017	0.025	5.74	0.65	-9.5	2
117	546993.036	8821367.851	374.951	0.008	0.014	0.023	4.81	0.61	-11.9	2
118	546993.052	8821367.811	374.952	0.010	0.014	0.026	4.75	0.61	-12.7	2
119	546993.065	8821367.768	374.947	0.009	0.014	0.024	4.58	0.65	-9.2	2
120	546993.087	8821367.731	374.933	0.029	0.016	0.054	3.68	1.13	-11.5	2
121	546993.093	8821367.685	374.945	0.009	0.015	0.023	5.11	0.62	-11.3	2
122	546993.111	8821367.644	374.943	0.011	0.015	0.026	5.23	0.74	-10.2	2
123	546993.124	8821367.603	374.942	0.009	0.013	0.026	4.34	0.58	-14.9	2
124	546993.128	8821367.557	374.948	0.036	0.022	0.034	5.11	0.97	-14.6	2

Lower (Anniversary) Profile: 2014 (continued)

DOY	E(m)	N(m)	Z(m)	E_std(m)	N_std(m)	Z_std(m)	Vx(cm d^{-1})	Vx_err	T(C°)	*
125	546993.165	8821367.528	374.934	0.028	0.021	0.043	1.99	2.24	-11.0	2
126	546993.168	8821367.478	374.948	0.008	0.014	0.027	4.43	0.74	-8.9	2
127	546993.184	8821367.439	374.946	0.008	0.015	0.025	4.72	0.66	-9.8	2
128	546993.196	8821367.398	374.949	0.009	0.015	0.022	4.41	0.76	-9.0	2
129	546993.213	8821367.356	374.935	0.009	0.015	0.022	4.98	0.64	-8.0	2
130	546993.229	8821367.313	374.938	0.010	0.015	0.021	5.18	0.59	-10.2	2
131	546993.245	8821367.269	374.936	0.010	0.016	0.020	5.39	0.60	-12.1	2
132	546993.262	8821367.230	374.945	0.012	0.019	0.035	6.24	0.91	-11.6	2
133	546993.274	8821367.186	374.937	0.011	0.015	0.021	5.52	0.63	-13.7	2
134	546993.289	8821367.145	374.942	0.011	0.016	0.024	5.89	0.63	-10.8	2
135	546993.303	8821367.104	374.923	0.010	0.015	0.024	5.26	0.66	-6.8	2
136	546993.319	8821367.062	374.928	0.011	0.014	0.021	4.88	0.61	-7.7	2
137	546993.333	8821367.021	374.928	0.010	0.015	0.020	5.41	0.67	-10.5	2
138	546993.347	8821366.978	374.934	0.011	0.015	0.020	5.43	0.59	-10.8	2
139	546993.362	8821366.934	374.931	0.013	0.018	0.021	6.26	0.70	-10.3	2
140	546993.371	8821366.898	374.940	0.024	0.022	0.053	7.19	1.24	-8.9	2
141	546993.395	8821366.856	374.929	0.011	0.014	0.022	4.36	0.93	-10.6	2
142	546993.404	8821366.813	374.932	0.013	0.016	0.030	5.38	0.93	-10.0	2
143	546993.421	8821366.770	374.930	0.009	0.016	0.022	5.48	0.70	-10.0	2
144	546993.435	8821366.732	374.929	0.010	0.018	0.027	4.66	1.34	-5.1	2
145	546993.453	8821366.684	374.932	0.011	0.018	0.027	6.35	0.77	-2.8	2
146	546993.462	8821366.646	374.927	0.013	0.020	0.030	6.44	1.06	-3.0	2
147	546993.479	8821366.602	374.921	0.010	0.017	0.025	6.02	0.67	-6.2	2
148	546993.490	8821366.554	374.914	0.014	0.022	0.030	5.78	1.24	-3.1	2
149	546993.509	8821366.517	374.920	0.012	0.015	0.025	5.43	0.62	-3.5	2
150	546993.519	8821366.465	374.925	0.022	0.034	0.064	7.83	1.77	-5.0	2
151	546993.538	8821366.434	374.917	0.010	0.015	0.023	4.89	0.73	-6.1	2
152	546993.551	8821366.394	374.915	0.009	0.014	0.022	4.82	0.70	-5.5	2
153	546993.562	8821366.351	374.922	0.013	0.019	0.034	5.60	1.29	-1.0	2
154	546993.584	8821366.307	374.913	0.011	0.017	0.026	5.44	0.92	1.8	2
155	546993.599	8821366.267	374.908	0.010	0.015	0.027	5.04	0.75	1.9	2
156	546993.616	8821366.224	374.910	0.010	0.016	0.026	5.49	0.79	2.0	2
157	546993.629	8821366.183	374.907	0.009	0.015	0.024	5.19	0.70	-0.1	2
158	546993.644	8821366.139	374.910	0.010	0.014	0.023	5.10	0.68	-5.2	2
159	546993.659	8821366.098	374.904	0.011	0.016	0.023	5.34	0.72	-5.5	2
160	546993.675	8821366.054	374.903	0.010	0.015	0.022	5.24	0.67	-4.5	2
161	546993.689	8821366.014	374.903	0.011	0.015	0.024	5.29	0.70	-3.6	2
162	546993.705	8821365.972	374.903	0.012	0.014	0.026	4.90	0.76	-3.3	2
163	546993.720	8821365.928	374.903	0.013	0.014	0.027	4.79	0.81	-3.4	2
164	546993.732	8821365.886	374.903	0.013	0.014	0.027	4.76	0.71	-1.5	2
165	546993.751	8821365.842	374.905	0.010	0.014	0.030	3.85	0.96	1.3	2
166	546993.763	8821365.801	374.896	0.012	0.013	0.024	4.42	0.69	-0.3	2
167	546993.778	8821365.758	374.898	0.011	0.016	0.023	5.20	0.81	-1.9	2
168	546993.788	8821365.715	374.900	0.013	0.012	0.030	3.47	0.92	-0.6	2
169	546993.805	8821365.668	374.901	0.010	0.016	0.028	5.20	0.89	3.8	2
170	546993.826	8821365.624	374.900	0.020	0.021	0.040	5.53	1.72	4.7	2
171	546993.839	8821365.587	374.881	0.011	0.013	0.035	3.93	0.98	3.4	2
172	546993.854	8821365.552	374.888	0.020	0.015	0.036	2.43	1.18	6.1	2
173	546993.876	8821365.509	374.889	0.017	0.018	0.053	1.87	1.45	4.1	2
174	546993.886	8821365.457	374.881	0.015	0.017	0.031	4.77	1.14	3.2	2
175	546993.898	8821365.412	374.883	0.013	0.013	0.027	4.29	0.72	2.9	2
176	546993.910	8821365.365	374.897	0.009	0.016	0.028	5.11	0.71	4.1	2
177	546993.938	8821365.298	374.897	0.019	0.034	0.035	12.48	1.08	5.2	2
178	546993.973	8821365.165	374.927	0.016	0.039	0.028	13.85	0.78	6.9	2
179	546994.018	8821365.004	374.927	0.020	0.050	0.027	17.98	0.99	5.7	2
180	546994.063	8821364.840	374.922	0.019	0.037	0.025	13.89	0.62	4.8	2
181	546994.106	8821364.701	374.928	0.021	0.035	0.027	12.97	0.81	0.7	2
182	546994.152	8821364.577	374.912	0.016	0.028	0.028	10.09	0.83	2.4	2
183	546994.207	8821364.436	374.916	0.023	0.054	0.027	19.79	1.07	5.1	2
184	546994.262	8821364.280	374.908	0.020	0.053	0.028	18.78	1.35	5.9	2
185	546994.321	8821364.106	374.905	0.021	0.046	0.027	16.13	1.18	6.2	2
186	546994.369	8821363.969	374.894	0.022	0.033	0.039	11.47	1.27	3.9	2
187	546994.416	8821363.854	374.885	0.017	0.041	0.031	13.78	1.50	8.4	2
188	546994.455	8821363.745	374.873	0.014	0.024	0.029	8.49	0.79	7.0	2
189	546994.487	8821363.653	374.850	0.014	0.032	0.031	10.56	1.07	4.2	2
190	546994.522	8821363.564	374.838	0.014	0.034	0.027	11.94	0.84	4.8	2
191	546994.552	8821363.456	374.851	0.010	0.042	0.031	13.24	1.23	5.9	2
192	546994.561	8821363.353	374.862	0.015	0.021	0.029	7.44	0.74	4.2	2
193	546994.586	8821363.278	374.855	0.013	0.023	0.034	7.83	0.95	3.1	2
194	546994.615	8821363.202	374.847	0.017	0.020	0.031	7.85	0.82	2.9	2
195	546994.642	8821363.130	374.837	0.021	0.025	0.030	9.37	1.08	7.8	2
196	546994.675	8821363.041	374.840	0.023	0.029	0.029	10.80	1.30	8.6	2
197	546994.698	8821362.961	374.839	0.018	0.020	0.031	7.59	0.99	7.0	2
198	546994.724	8821362.894	374.825	0.015	0.019	0.031	6.85	0.97	2.8	2
199	546994.745	8821362.835	374.820	0.013	0.021	0.029	7.15	0.81	4.5	2
200	546994.776	8821362.753	374.814	0.011	0.019	0.029	6.02	0.93	6.6	1
201	546994.804	8821362.682	374.811	0.013	0.022	0.026	7.56	0.97	6.6	1
202	546994.829	8821362.612	374.808	0.015	0.020	0.033	7.06	1.02	5.7	1
203	546994.851	8821362.548	374.797	0.015	0.017	0.029	5.53	1.03	4.3	1
204	546994.868	8821362.486	374.782	0.022	0.019	0.036	5.40	1.44	-0.5	1
205	546994.894	8821362.419	374.780	0.013	0.021	0.028	7.44	0.72	1.3	1
206	546994.917	8821362.357	374.771	0.014	0.020	0.027	6.72	0.80	5.3	1
207	546994.943	8821362.292	374.768	0.013	0.020	0.029	6.27	1.01	3.3	1

Lower (Anniversary) Profile: 2014 (continued)

DOY	E(m)	N(m)	Z(m)	E_std(m)	N_std(m)	Z_std(m)	Vx(cm d^{-1})	Vx_err	T(C°)	*
208	546994.965	8821362.218	374.759	0.027	0.026	0.032	6.49	1.65	1.6	1
209	546994.994	8821362.149	374.759	0.018	0.016	0.038	4.38	1.23	1.7	1
210	546995.009	8821362.099	374.743	0.020	0.018	0.030	3.08	1.31	2.5	1
211	546995.040	8821362.025	374.750	0.018	0.024	0.035	6.13	1.51	4.9	1
212	546995.058	8821361.954	374.756	0.010	0.021	0.043	6.43	1.06	6.4	1
213	546995.087	8821361.879	374.740	0.011	0.017	0.030	5.58	0.81	6.8	1
214	546995.110	8821361.796	374.751	0.034	0.026	0.082	7.60	2.11	7.6	1
215	546995.146	8821361.691	374.753	0.010	0.026	0.028	8.23	1.28	4.4	1
216	546995.172	8821361.629	374.752	0.011	0.021	0.032	6.99	0.89	5.0	1
217	546995.196	8821361.558	374.735	0.011	0.021	0.027	6.75	0.99	6.4	1
218	546995.221	8821361.486	374.727	0.012	0.019	0.031	6.48	0.86	7.1	1
219	546995.255	8821361.424	374.733	0.013	0.027	0.029	9.61	0.89	8.0	1
220	546995.279	8821361.348	374.729	0.013	0.028	0.041	9.77	0.78	8.5	1
221	546995.305	8821361.271	374.714	0.016	0.028	0.041	9.75	1.04	8.6	1
222	546995.339	8821361.204	374.715	0.018	0.029	0.038	8.32	1.67	5.9	1
223	546995.357	8821361.136	374.713	0.011	0.022	0.027	7.45	0.83	4.4	1
224	546995.376	8821361.072	374.714	0.013	0.021	0.027	6.72	0.95	4.7	1
225	546995.399	8821361.007	374.711	0.009	0.020	0.028	6.19	1.01	6.1	1
226	546995.421	8821360.943	374.712	0.009	0.018	0.026	6.00	0.75	3.6	1
227	546995.442	8821360.883	374.697	0.012	0.021	0.034	6.42	0.96	2.0	1
228	546995.469	8821360.822	374.687	0.014	0.022	0.031	6.45	1.07	3.4	1
229	546995.484	8821360.763	374.685	0.017	0.020	0.037	4.49	1.49	1.4	1
230	546995.507	8821360.702	374.687	0.007	0.016	0.030	4.71	0.72	0.9	1
231	546995.525	8821360.646	374.676	0.008	0.020	0.038	5.96	0.99	4.3	1
232	546995.548	8821360.587	374.681	0.009	0.016	0.035	3.77	1.08	4.6	1
233	546995.570	8821360.529	374.672	0.019	0.022	0.044	5.83	1.56	2.1	1
234	546995.583	8821360.485	374.664	0.007	0.017	0.028	4.97	0.74	-0.2	1
235	546995.599	8821360.435	374.654	0.008	0.016	0.025	4.41	0.78	-0.3	1
236	546995.619	8821360.383	374.660	0.009	0.016	0.026	4.96	0.84	1.0	1
237	546995.635	8821360.335	374.658	0.007	0.017	0.025	5.06	0.80	0.5	1
238	546995.651	8821360.289	374.656	0.007	0.015	0.024	4.08	0.77	1.3	1
239	546995.667	8821360.241	374.644	0.008	0.014	0.025	3.18	1.02	-1.2	1
240	546995.683	8821360.193	374.649	0.007	0.016	0.023	4.37	0.81	-0.3	1
241	546995.701	8821360.143	374.652	0.008	0.017	0.027	3.79	1.21	1.4	1
242	546995.722	8821360.092	374.658	0.013	0.019	0.033	5.14	1.31	2.8	1
243	546995.735	8821360.048	374.646	0.007	0.015	0.029	4.24	0.90	2.4	1
244	546995.751	8821359.994	374.632	0.017	0.017	0.074	3.81	1.51	1.1	1
245	546995.767	8821359.944	374.640	0.018	0.037	0.068	7.00	2.82	-0.5	1
246	546995.786	8821359.905	374.640	0.009	0.017	0.028	4.49	0.96	0.1	1
247	546995.799	8821359.858	374.639	0.008	0.017	0.027	4.82	0.81	1.6	1
248	546995.819	8821359.813	374.632	0.008	0.013	0.028	3.63	0.74	-0.6	1
249	546995.858	8821359.765	374.625	0.053	0.038	0.091	3.84	2.88	-0.3	1
250	546995.847	8821359.719	374.623	0.016	0.023	0.034	6.44	1.40	-2.4	1
251	546995.868	8821359.670	374.642	0.008	0.018	0.035	4.37	1.15	-2.2	1
252	546995.881	8821359.624	374.626	0.007	0.018	0.028	5.12	1.00	-4.5	1
253	546995.899	8821359.575	374.621	0.009	0.018	0.022	4.81	1.08	-6.7	1
254	546995.917	8821359.529	374.623	0.008	0.016	0.022	4.25	1.02	-7.9	1
255	546995.931	8821359.481	374.607	0.010	0.018	0.028	5.41	1.01	-5.6	1
256	546995.951	8821359.433	374.604	0.010	0.017	0.028	4.84	1.03	-4.5	1
257	546995.966	8821359.384	374.620	0.013	0.019	0.035	5.30	1.12	-5.6	1
258	546995.986	8821359.344	374.607	0.010	0.020	0.033	5.26	1.00	-5.5	1
259	546996.005	8821359.299	374.599	0.011	0.016	0.037	4.84	0.96	-6.3	1
260	546996.016	8821359.253	374.607	0.009	0.016	0.024	4.48	0.77	-6.4	1
262	546996.047	8821359.146	374.616	0.010	0.016	0.026	5.91	1.13	0.3	1
263	546996.063	8821359.112	374.606	0.008	0.018	0.024	5.52	0.79	-3.8	1
264	546996.079	8821359.066	374.609	0.009	0.017	0.025	5.01	0.87	-9.1	1
265	546996.093	8821359.018	374.605	0.010	0.017	0.032	4.64	1.07	-9.1	1

Lower (Anniversary) Profile: 2015

DOY	E(m)	N(m)	Z(m)	E_std(m)	N_std(m)	Z_std(m)	Vx(cm d^{-1})	Vx_err	T(C°)	*
116	546998.452	8821349.241	371.974	0.010	0.014	0.030	4.32	0.85	-9.8	2
117	546998.466	8821349.201	371.978	0.012	0.015	0.027	4.99	0.87	-11.8	2
118	546998.483	8821349.162	371.974	0.010	0.013	0.026	4.60	0.72	-12.7	2
119	546998.496	8821349.121	371.971	0.011	0.015	0.026	5.04	0.85	-13.4	2
120	546998.511	8821349.085	371.975	0.013	0.020	0.029	4.80	1.58	-13.7	2
121	546998.522	8821349.041	371.973	0.009	0.014	0.031	4.77	0.75	-13.0	2
122	546998.538	8821349.000	371.965	0.011	0.014	0.027	4.95	0.73	-11.9	2
123	546998.553	8821348.958	371.965	0.012	0.014	0.027	5.04	0.75	-13.2	2
124	546998.567	8821348.918	371.967	0.010	0.015	0.027	5.08	0.72	-13.5	2
125	546998.581	8821348.877	371.966	0.007	0.014	0.026	4.54	0.69	-13.7	2
126	546998.594	8821348.835	371.960	0.009	0.014	0.028	4.26	0.80	-17.8	2
127	546998.610	8821348.796	371.962	0.011	0.013	0.028	4.43	0.74	-16.6	2
128	546998.625	8821348.756	371.958	0.010	0.013	0.026	4.48	0.70	-16.2	2
129	546998.639	8821348.715	371.958	0.011	0.013	0.026	4.15	0.76	-16.4	2
130	546998.652	8821348.673	371.966	0.011	0.015	0.029	4.92	0.89	-12.8	2
131	546998.665	8821348.633	371.960	0.009	0.014	0.027	4.42	0.72	-15.2	2
132	546998.686	8821348.595	371.957	0.029	0.024	0.049	4.33	2.09	-13.1	2
133	546998.696	8821348.551	371.951	0.009	0.018	0.024	5.73	0.90	-14.7	2
134	546998.710	8821348.508	371.942	0.010	0.017	0.027	5.39	0.81	-14.2	2
135	546998.723	8821348.467	371.940	0.014	0.016	0.037	5.13	0.96	-13.6	2

Lower (Anniversary) Profile: 2015 (continued)

DOY	E(m)	N(m)	Z(m)	E_std(m)	N_std(m)	Z_std(m)	Vx(cm d^{-1})	Vx_err	T(C°)	*
136	546998.740	8821348.427	371.957	0.009	0.014	0.027	4.77	0.73	-11.1	2
137	546998.752	8821348.387	371.957	0.009	0.014	0.030	4.18	0.81	-8.9	2
138	546998.769	8821348.347	371.947	0.010	0.013	0.031	4.29	0.75	-6.9	2
139	546998.786	8821348.305	371.941	0.010	0.014	0.028	4.78	0.77	-8.1	2
140	546998.797	8821348.265	371.952	0.010	0.015	0.030	4.72	0.74	-7.7	2
141	546998.812	8821348.223	371.934	0.010	0.015	0.026	5.16	0.78	-7.4	2
142	546998.829	8821348.181	371.924	0.011	0.018	0.042	5.67	0.98	-13.4	2
143	546998.840	8821348.139	371.931	0.010	0.017	0.029	5.54	0.83	-12.3	2
144	546998.856	8821348.096	371.929	0.010	0.017	0.027	5.44	0.81	-5.4	2
145	546998.870	8821348.056	371.922	0.008	0.018	0.031	4.93	1.05	-5.5	2
146	546998.884	8821348.016	371.927	0.012	0.017	0.027	5.61	0.95	-2.5	2
147	546998.900	8821347.973	371.922	0.010	0.016	0.029	5.23	0.87	-2.3	2
148	546998.915	8821347.933	371.929	0.009	0.015	0.030	4.87	0.76	-4.2	2
149	546998.924	8821347.893	371.926	0.009	0.015	0.027	4.74	0.83	-3.0	2
150	546998.940	8821347.852	371.919	0.013	0.015	0.029	4.94	0.86	-1.4	2
151	546998.955	8821347.809	371.916	0.012	0.016	0.025	5.31	0.83	1.9	2
152	546998.969	8821347.768	371.916	0.012	0.016	0.028	5.48	0.79	2.3	2
153	546998.983	8821347.722	371.925	0.012	0.019	0.031	5.98	1.09	-1.1	2
154	546999.013	8821347.678	371.917	0.035	0.027	0.065	5.10	2.58	0.3	2
155	546999.014	8821347.643	371.917	0.011	0.014	0.027	4.90	0.72	-0.8	2
156	546999.028	8821347.601	371.915	0.011	0.014	0.026	4.96	0.69	-1.9	2
157	546999.043	8821347.561	371.919	0.010	0.013	0.023	4.27	0.65	-2.0	2
158	546999.055	8821347.520	371.916	0.010	0.013	0.029	3.14	0.89	-2.5	2
159	546999.074	8821347.472	371.916	0.011	0.015	0.030	4.92	0.90	0.0	2
160	546999.089	8821347.434	371.910	0.010	0.013	0.029	4.05	0.81	1.8	2
161	546999.103	8821347.389	371.904	0.008	0.013	0.028	4.10	0.71	0.7	2
162	546999.120	8821347.347	371.902	0.009	0.013	0.028	4.29	0.65	0.6	2
163	546999.135	8821347.303	371.900	0.010	0.014	0.026	4.96	0.70	0.7	2
164	546999.150	8821347.258	371.897	0.012	0.014	0.027	4.93	0.75	2.3	2
165	546999.168	8821347.214	371.899	0.015	0.016	0.030	5.79	0.91	4.7	2
166	546999.194	8821347.153	371.915	0.015	0.017	0.030	6.15	0.79	4.5	2
167	546999.214	8821347.094	371.916	0.014	0.021	0.029	7.61	0.69	3.6	2
168	546999.238	8821347.025	371.904	0.012	0.022	0.029	7.47	0.71	4.7	2
169	546999.274	8821346.911	371.905	0.020	0.038	0.036	13.46	1.18	2.1	2
170	546999.299	8821346.773	371.925	0.033	0.038	0.033	13.60	2.08	2.4	2
171	546999.337	8821346.674	371.909	0.016	0.027	0.038	9.51	1.11	2.9	2
172	546999.371	8821346.579	371.919	0.017	0.028	0.032	10.27	1.06	4.1	2
173	546999.397	8821346.489	371.920	0.014	0.027	0.032	9.94	0.81	4.9	2
174	546999.429	8821346.391	371.909	0.017	0.029	0.036	10.40	1.01	4.1	2
175	546999.460	8821346.302	371.915	0.013	0.025	0.034	9.22	0.71	4.7	2
176	546999.489	8821346.216	371.903	0.012	0.021	0.028	7.52	0.72	2.0	2
177	546999.515	8821346.145	371.897	0.012	0.022	0.027	7.68	0.85	4.6	2
178	546999.550	8821346.043	371.909	0.015	0.036	0.040	12.99	0.73	6.6	2
179	546999.593	8821345.893	371.912	0.021	0.051	0.032	18.47	1.14	7.3	2
180	546999.647	8821345.744	371.913	0.018	0.025	0.032	9.80	0.71	4.9	2
181	546999.685	8821345.640	371.895	0.016	0.043	0.026	15.57	0.84	4.1	2
182	546999.719	8821345.515	371.889	0.019	0.039	0.033	13.39	1.43	7.1	2
183	546999.770	8821345.400	371.886	0.028	0.020	0.035	7.27	1.38	6.0	2
184	546999.793	8821345.269	371.874	0.033	0.036	0.062	13.70	1.33	5.4	2
185	546999.856	8821345.128	371.892	0.026	0.060	0.032	21.62	1.47	7.2	2
186	546999.922	8821344.902	371.882	0.026	0.054	0.048	18.45	2.37	7.0	2
187	546999.973	8821344.790	371.864	0.014	0.031	0.056	10.66	1.14	8.9	2
188	547000.012	8821344.680	371.846	0.017	0.041	0.032	14.57	1.18	10.7	2
189	547000.048	8821344.570	371.839	0.013	0.030	0.026	10.55	0.98	10.7	2
190	547000.076	8821344.475	371.820	0.018	0.030	0.031	10.74	0.93	12.4	2
191	547000.110	8821344.394	371.798	0.012	0.026	0.027	9.19	0.67	9.7	2
192	547000.142	8821344.307	371.786	0.012	0.027	0.027	9.60	0.69	9.9	2
193	547000.173	8821344.217	371.777	0.013	0.024	0.025	8.68	0.75	11.4	2
194	547000.202	8821344.132	371.760	0.014	0.028	0.024	10.33	0.71	10.7	2
195	547000.223	8821344.051	371.745	0.012	0.026	0.028	9.06	0.71	9.2	2
196	547000.251	8821343.971	371.722	0.014	0.028	0.025	10.08	0.83	9.2	2
197	547000.277	8821343.873	371.712	0.011	0.034	0.028	11.70	0.92	7.2	2
198	547000.304	8821343.787	371.697	0.018	0.025	0.029	8.83	1.22	6.6	2
199	547000.319	8821343.714	371.689	0.018	0.024	0.031	8.28	0.97	7.3	2
200	547000.355	8821343.628	371.687	0.015	0.029	0.033	10.24	1.07	7.8	2
201	547000.380	8821343.548	371.657	0.020	0.027	0.047	9.16	1.02	6.8	2
202	547000.409	8821343.470	371.658	0.012	0.023	0.025	8.03	0.64	8.0	2
203	547000.437	8821343.386	371.637	0.011	0.025	0.026	8.78	0.67	10.3	2
204	547000.460	8821343.309	371.627	0.012	0.024	0.027	8.67	0.71	8.7	2
205	547000.485	8821343.231	371.616	0.013	0.024	0.025	8.66	0.69	8.7	2
206	547000.511	8821343.154	371.598	0.010	0.029	0.024	10.09	0.77	8.9	2
207	547000.537	8821343.074	371.584	0.010	0.026	0.025	8.94	0.85	8.2	2
208	547000.568	8821342.994	371.571	0.020	0.020	0.039	7.26	0.90	5.8	2
209	547000.590	8821342.920	371.555	0.011	0.023	0.028	7.92	0.74	6.0	2
210	547000.614	8821342.840	371.544	0.010	0.027	0.025	9.23	0.65	7.2	2
211	547000.639	8821342.754	371.525	0.011	0.026	0.026	9.25	0.77	6.0	2
212	547000.669	8821342.672	371.502	0.025	0.023	0.071	7.14	1.59	1.7	2
213	547000.692	8821342.602	371.504	0.013	0.025	0.024	8.98	0.75	4.8	2
214	547000.723	8821342.522	371.491	0.014	0.023	0.027	8.50	0.80	6.2	2
215	547000.744	8821342.452	371.484	0.014	0.020	0.029	6.59	0.90	6.2	2
216	547000.772	8821342.376	371.486	0.013	0.028	0.038	8.34	1.39	5.1	2
217	547000.794	8821342.300	371.456	0.008	0.021	0.026	7.21	0.71	0.6	2
218	547000.820	8821342.237	371.446	0.014	0.019	0.026	6.25	0.83	-0.6	2

Lower (Anniversary) Profile: 2015 (continued)

DOY	E(m)	N(m)	Z(m)	E_std(m)	N_std(m)	Z_std(m)	Vx(cm d^{-1})	Vx_err	T(C°)	*
219	547000.836	8821342.170	371.438	0.008	0.021	0.025	7.01	0.66	0.5	2
220	547000.858	8821342.114	371.433	0.011	0.020	0.030	6.68	0.84	1.8	2
221	547000.874	8821342.056	371.412	0.020	0.024	0.031	6.07	1.52	2.2	2
222	547000.905	8821341.987	371.423	0.009	0.021	0.025	6.73	0.92	1.4	2
223	547000.934	8821341.923	371.434	0.018	0.024	0.038	7.28	1.38	4.1	2
224	547000.955	8821341.844	371.423	0.011	0.030	0.035	9.49	1.26	6.2	2
225	547000.982	8821341.754	371.426	0.012	0.023	0.037	7.62	0.97	6.8	2
226	547001.008	8821341.670	371.411	0.012	0.030	0.024	10.54	1.03	6.3	2
227	547001.035	8821341.580	371.411	0.010	0.027	0.026	8.90	0.95	6.5	2
228	547001.068	8821341.511	371.411	0.009	0.026	0.024	8.58	0.95	5.8	2
229	547001.086	8821341.442	371.400	0.008	0.020	0.026	6.03	0.95	1.8	2
230	547001.114	8821341.384	371.402	0.009	0.018	0.026	5.08	1.01	1.2	2
231	547001.129	8821341.327	371.386	0.012	0.017	0.040	5.46	0.89	1.8	2
232	547001.152	8821341.269	371.381	0.009	0.018	0.025	5.64	0.89	3.3	2
233	547001.170	8821341.216	371.368	0.008	0.018	0.034	5.75	0.78	2.5	2
234	547001.195	8821341.160	371.370	0.027	0.022	0.042	6.69	1.47	1.5	2
235	547001.215	8821341.113	371.361	0.019	0.023	0.046	4.78	1.80	0.1	2
236	547001.229	8821341.053	371.365	0.011	0.019	0.025	5.77	0.90	0.1	2
237	547001.247	8821341.001	371.361	0.010	0.018	0.024	5.61	0.73	-0.5	2
238	547001.263	8821340.952	371.362	0.010	0.018	0.024	5.43	0.88	1.6	2
239	547001.281	8821340.903	371.363	0.009	0.018	0.023	5.70	0.77	0.8	2
240	547001.293	8821340.851	371.354	0.015	0.026	0.028	6.04	1.61	1.3	2
241	547001.316	8821340.806	371.354	0.007	0.017	0.025	5.37	0.86	-0.7	2
242	547001.325	8821340.757	371.351	0.017	0.024	0.025	5.20	1.70	-0.2	2
243	547001.347	8821340.710	371.346	0.007	0.016	0.025	4.65	0.89	0.4	2
244	547001.368	8821340.660	371.348	0.011	0.020	0.028	6.23	1.12	3.1	2
245	547001.381	8821340.614	371.346	0.010	0.018	0.025	5.70	0.88	0.1	2
246	547001.397	8821340.568	371.343	0.015	0.019	0.046	4.66	1.36	0.1	2
247	547001.415	8821340.521	371.342	0.009	0.015	0.024	4.69	0.81	-1.4	2
248	547001.427	8821340.484	371.332	0.010	0.015	0.030	4.25	0.89	-2.7	2
249	547001.447	8821340.438	371.330	0.011	0.012	0.027	2.54	1.04	-4.9	2
250	547001.464	8821340.388	371.340	0.017	0.023	0.035	6.60	1.21	-3.8	2
251	547001.480	8821340.337	371.333	0.009	0.018	0.021	5.51	0.80	-5.5	2
252	547001.499	8821340.294	371.331	0.011	0.023	0.026	6.47	1.08	-2.1	2
253	547001.504	8821340.244	371.322	0.031	0.028	0.047	6.88	1.82	-1.3	2
254	547001.530	8821340.195	371.330	0.010	0.016	0.024	5.13	0.80	-4.2	2
255	547001.545	8821340.152	371.318	0.008	0.019	0.023	5.28	1.04	-5.9	2
256	547001.560	8821340.106	371.315	0.010	0.015	0.047	4.18	1.07	-5.5	2
257	547001.574	8821340.063	371.329	0.017	0.018	0.039	5.70	1.04	-4.4	2
258	547001.592	8821340.016	371.318	0.009	0.015	0.021	5.27	0.64	-3.6	2
259	547001.600	8821339.970	371.314	0.014	0.017	0.032	4.71	0.89	-9.3	2
260	547001.622	8821339.927	371.306	0.009	0.018	0.022	5.01	0.91	-6.3	2
261	547001.636	8821339.878	371.312	0.008	0.015	0.022	3.85	0.94	-8.4	2
262	547001.655	8821339.846	371.309	0.009	0.016	0.033	-1.95	1.63	-9.1	2
263	547001.671	8821339.780	371.303	0.008	0.012	0.022	4.75	0.78	-10.0	2
264	547001.685	8821339.735	371.310	0.012	0.021	0.035	5.05	1.71	-11.4	2
265	547001.704	8821339.699	371.301	0.008	0.018	0.024	5.46	0.90	-10.5	2
266	547001.722	8821339.647	371.306	0.017	0.023	0.029	7.53	1.30	-8.4	2
267	547001.741	8821339.601	371.315	0.019	0.014	0.031	4.49	1.36	-9.9	2